Doctoral theses at NTNU, 2021:229

Steffen Loen Sunde

Numerical and experimental fretting fatigue with application to engineering design

Doctoral thesis

NTNU
Norwegian University of Science and Technology
Thesis for the Degree of Philosophiae Doctor
Faculty of Engineering
Department of Mechanical and Industrial Engineering

NTNU
Norwegian University of Science and Technology

Steffen Loen Sunde

Numerical and experimental fretting fatigue with application to engineering design

Thesis for the Degree of Philosophiae Doctor

Trondheim, June 2021

Norwegian University of Science and Technology
Faculty of Engineering
Department of Mechanical and Industrial Engineering

NTNU
Norwegian University of
Science and Technology

NTNU
Norwegian University of Science and Technology

Thesis for the Degree of Philosophiae Doctor

Faculty of Engineering
Department of Mechanical and Industrial Engineering

ISBN 978-82-326-6612-6 (printed ver.)
ISBN 978-82-326-5195-5 (electronic ver.)
ISSN 1503-8181 (printed ver.)
ISSN 2703-8084 (online ver.)

Doctoral theses at NTNU, 2021:229

Printed by NTNU Grafisk senter

Preface

This Ph.D. thesis is submitted for partial fulfilment of the requirements for the degree of philosophiae doctor at Norwegian University of Science and Technology (NTNU), Trondheim Norway. The work of this doctoral project was carried out at the Departement of Mechanical and Industrial Engineering with supervision from Prof. Bjørn Haugen and Prof. Filippo Berto. The project benefited from a fellowship awarded gratefully by the Departement of Mechanical and Industrial Engineering at NTNU.

Steffen Loen Sunde
Bergen, March 2021

Acknowledgements

Finishing this project would not have been possible without the help of colleagues, friends and family. Working on a Ph.D. project can be a frustrating exercise where progress certainly is a non-linear function of time.

First and foremost I would like to express my sincere gratitude to my supervisors on this project. Firstly, to Professor Bjørn Haugen, his impressive knowledge, insights and intuition was invaluable. Thank you for patiently enduring many weird ideas and sidetracks. I would also like to sincerely thank my co-supervisor Professor Filippo Berto. His experience and expertise in the field was crucial for progress.

Thank you Professor Torgeir Welo for providing the opportunity to start this project.

A lot of time was spent during this project in the workshop and I am grateful for all the help I've given by Carl-Magnus Midtbø, Børge Holen, Jan Magnus Ferstad and other highly skilled engineers in the workshop.

Thanks to all the great colleagues at the department, Emil André Valaker, Javad Ravazi, Klas Solberg, Luigi Mario Viespoli, Lise Sandnes, André Böhme, Cristian Torrez Rodriguez, Erik Sæter, Abedin Gagani, Daniele Di Candia and all the other great people at the Department of Mechanical and Industrial Engineering. I am also grateful to my colleagues at Bergen Engines.

It's important for me to thank Ane for putting up with my excessive workhours! Thank you for keeping me sane throughout this time. Finally, I'd like to thank my parents and family for the never-ending support.

Abstract

Fretting is a term covering a wide array of physical phenomena. When contacting bodies vibrate, relative slip between the bodies cause surface damage including wear and plasticity and cracks. Partially stuck contacts with high stress gradients produce micro-cracks at the surface which may propagate and cause fretting fatigue failure. Grossly sliding contacts, however, are often dominated by increasing wear and loss of material.

Fretting have long been an interest to researchers in tribology and material sciences and continues to be a relevant phenomenon in engineering practice. Numerous theories and methodologies are applied to fretting problems, but engineering approaches are often simpler than those found in academia. In this thesis, fretting fatigue is investigated both numerically and experimentally with special attention to engineering applications. It is recognised that recent academic advancements in understanding and modelling capabilities represent opportunities for the practicing engineer facing fretting problems.

In this thesis, traditional modelling using Finite Elements is used to solve fretting contacts. Critical plane post-processing is used to investigate fretting cracking behaviour. Some new experimental test rigs were developed to produce experimental results. Finally, simple, lumped-mass models were used to investigate friction dynamics related to fretting contacts.

Keywords: fretting, fatigue, numerical, experimental, friction dynamics

Table of Contents

List of Figures

Chapter 1

Introduction

1.1 Motivations and goals

There is an ever increasing demand of efficiency in the manufacturing industry. Engineers are faced with the the challenging task of designing reliable and performant machine components with high material utilisation. The machine components have increasingly complex geometries, are subjected to high cyclic loads and thorough analysis is required to ensure long-lasting components. Moreover, such components are often part of a larger, complex machinery with numerous interacting parts. Design and production becomes an iterative process; the complete system is not finished until all components concurrently comply with the design criteria. This iterative production can in fact be very complex when non-linear damaging effects are encountered. Early predictive capabilities become increasingly important; efficient identification of problem areas can accelerate the iterative design process and avoid expensive late stage repairs.

Moving contacting parts are examples of non-linearity and exist everywhere: bolted joints, press-fits, bearings etc. Surface damage and fatigue life reduction caused by fretting in contacts are sometimes extremely difficult to predict. Due to the complexity of the mechanisms involved, gross simplifications are often made and combined with full-scale testing. Full-scale testing is usually more costly than performing computer-aided predictions. Increasing knowledge of the mechanisms involved and with modern computational power and better prediction methodologies, fretting fatigue can be avoided at an early design stage greatly reducing costs.

Although fretting have been studied for over a century, its effects to fatigue components are still elusive. Fretting fatigue damage is known to be influenced by a large set of factors and its synthesis is almost chaotic in nature. For engineering applications, detailed analysis of all the parameters involved is impossible and compromises must be made. Simplified methods are preferred, but neglecting important features of the problem at hand may cause surprises. Ceaseless research into fretting fatigue generate increasing knowledge and im-

proved predictive capabilities but some features of fretting contacts are still not completely understood, particularly related to micro-geometry the dynamics of the contact friction.

The gap between industry and academic approaches are in many cases considerable. Whereas in industry, simple holistic methods are applied to complex situations, the opposite is often the case in academia: complex models are applied to simple lab specimens subjected to simple loads.

The main goals of this thesis can be divided into three parts: Theoretical, numerical and experimental. A solid theoretical foundation is important understand the complexities involved in fretting fatigue and is key to form relevant intuitions. Numerical predictive tools applicable to a wide range of industrial settings is the ultimate goal. It can be argued that physical testing may be less important if the predictive capabilities are good. Physical testing is still important in fretting as large variations in physical behaviour are found. Moreover, validation of numerical methodologies is essential.

1.1.1 Research objectives

The ultimate goal of any research project is to advance current knowledge and to provide concrete contributions to the field. Fretting and fretting fatigue are topics touching upon several different fields each of which with long traditions. Contributing to such a complex field with many great researchers is not an easy task.

The objective of this project is twofold. Firstly, there is a need for increased knowledge and understanding of the mechanisms involved in fretting fatigue which needs to be physically tested. Secondly, developing predictive methodologies are important for engineers to holistically assess fatigue problems for the given component. A collaboration with the industry engineers is especially fruitful due to the opportunity to assess real-world problems, and to shorten the gap between the industrial methods and current research.

In this project, fretting is investigated both numerically and experimentally, in an attempt to answer how certain features of contact affect the fretting behaviour. Of particular interest is how complex loads and dynamic friction affects fretting contact and its fatigue behaviour. New physical testing capabilities are devised to provide experimental data and numerical models are developed to correlate predictions with experiments. Together, they provide a capacity for detailed parameter studies and further work. Finally, the numerical methodologies herein devised are useful for supplementing engineering dynamics analyses.

1.2 Industrial context

Contacting metallic components are used throughout engineering. Often, these components are subjected to severe cyclic loads, causing fretting-initiated cracks to greatly reduce fatigue life. Fretting problems have been studied for over a century now, and continues to be highly relevant to many fields of mechanical

engineering. However, fretting fatigue remains rather specific, and in fact many engineering students are unknown to its existence. Compared to plain fatigue, fretting can reduce the component life by up to an order of magnitude [1] and for engineers neglecting to address these effects, the consequences can be severe.

Industry problems are related to different fretting phenomena, including wear and fatigue. Fretting wear can cause problems to press-fits and bearings where material removal destroy tight tolerances. Fretting fatigue cause fatigue components to crack and fail prematurely. Metal fatigue assessments of real components remain complex due to uncertainties in microstructure and load histories. For vibrating components in contact, relative movement (slip) cause abrasive wear and micro-cracks to form at the surface. In many cases the components are also subjected to bulk fatigue loads, cause fretting-initiated cracks to propagate. This is known as fretting fatigue. Fretting fatigue is complex due to the many interrelated factors; surface friction and roughness, material microstructure, loading and contact geometry are among the most important ones [2]. Fretting is also known for its dependency on very small-scale effects, with contact *partial slip* and severe *stress gradients* at the surface.

The very intricate nature of fretting fatigue cause it to be an interesting topic to researchers, but a headache for engineers. Although numerous relevant parameters for fretting fatigue have been studied during the last century, many industrial situations remain unclear. Engineers are often concerned with large geometries and varying operation conditions which makes fretting fatigue difficult to predict and expensive to test. Many complex numerical tools to analyse fretting have been proposed in the literature, but in industry simplified "black box" methods are often used. Hence, in many cases there is a considerable gap between the scientific approaches and the simple methods used in industry.

A classical industrial application is the dovetail joint used in turbine engines. The turbine blades are attached to the engine rotor using a dovetail or fir-tree joint causing high axial loads and relative motion between the blade and the rotor in harsh conditions with high temperatures. This application initiated many fretting test campaigns and gained much interest among researchers and engineers. A somewhat related case is the fretting occurring between piston engine valves and valve seats: thermal gradients in the cylinder heads distort the valve seats causing non-uniform contact pressures [3]. Piston engines are especially disposed to fretting problems as they have many highly loaded moving parts, bolted joints and press-fits [4].

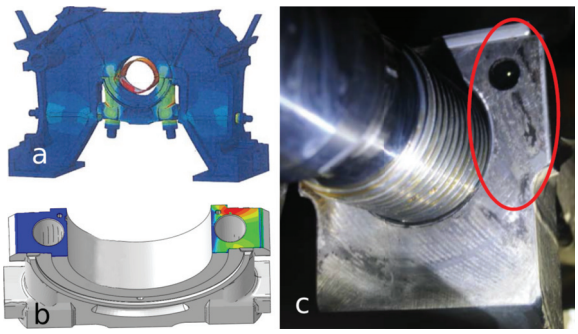

Figure 1.1: Fretting in a main bearing cap in marine diesel engine after some tens of thousands of running hours.

The experience with fretting fatigue in medium-speed piston engines sparked the interest for this project. More specifically, certain features of fretting were especially relevant to address for engines experiencing complex load cycles: fretting fatigue crack initiation and how the friction properties affect contact behaviour. Ultimately, the goal is to improve the efficacy of analysis and early-stage predictive capabilities, mitigating the need for full-scale testing and thus reducing production costs.

1.3 Thesis outline

Previous Sections described difficulties related to fretting and fretting fatigue. This thesis presents project work aiming to contribute to both industrial and academic methodologies through a collection of scientific publications. Relevant theory and supplementary analyses are included in the dissertation for improved consistency.

The thesis can be divided into two main parts: experimental and numerical. Experimental fretting fatigue test rigs were developed and put to use. The numerical part is twofold: *Quantitative* analyses of fretting fatigue cracking behaviour and lives using multiaxial fatigue criteria and *qualitative* analyses of frictional behaviour with non-linear lumped-parameter models.

The following list presents a general outline of the thesis.

Chapter 1 Presents a context for the project work and the accompanying scientific publications. Difficulties with fretting are described and both academic and industrial interests in the topics are briefly outlined.

Chapter 2 Describes methodologies related to Finite Element analyses and fretting fatigue cracking behaviour. Theoretical foundations and some relevant historical background is included for completeness.

Chapter 3 Describes experimental work conducted to investigate fretting fatigue. The development of new testing facilities is described and challenges therein. Experimental data are compared with numerical predictions and some recommendations are given for further experimental work.

Chapter 4 Presents discrete lumped-parameter models used to simulate dynamic properties of frictional contacts. The simulations provide insights into rich dynamic response and may be used to inform the Finite Element analyses.

Chapter 5 Presents concluding remarks and recommendations for further work.

Appendix Contains the scientific publications related to this Ph.D. project thus far. A number of expositions used throughout the project that are potentially useful for the reader is also included.

1.4 List of contributions

This thesis includes four scientific papers on the topics related to this project and fretting fatigue in general. These publications can be found in full in the appendices but a brief summary of the contributions will be presented in this section. All publications were written by Steffen L. Sunde, with the supervision from Bjørn Haugen and Filippo Berto.

1.4.1 Paper I

A review paper seeking to collect and review recent developments within the field of fretting fatigue. The field have grown large and numerous papers are published on fretting fatigue every year. Therefore, review papers are occasionally very beneficial to gather recent progress. The paper has a focus on developments relevant for engineers. More specifically, critical plane methods, notch analogies and crack analogies are highlighted as potential useful tools for the practicing engineer.

Predicting fretting fatigue in engineering design
S.L. Sunde, F. Berto, B. Haugen
International Journal of Fatigue, Volume 117, December 2018, Pages 314-326
`https://doi.org/10.1016/j.ijfatigue.2018.08.028`

1.4.2 Paper II

Shear stress-based critical plane criteria are popular amongst engineers and researchers alike. In this paper, the efficiency of such criteria are addressed and potential improvements are presented. More specifically, the critical plane search space is discretised using triangular cells and adaptively refined. Details of implementation and choice of programming language were also investigated. Not surprisingly, compiled language (C++) were found to be around two orders of magnitude faster than interpreted language (Python). The adaptive refinement technique was found to be efficient and accurate, but at a cost of implementation complexity. Ordinary brute force methods are usually adequate but triangular elements nonetheless discretise the search space more uniformly than regular angular increments.

Efficient implementation of critical plane for 3D stress histories using triangular elements
S.L. Sunde, B. Haugen, F. Berto
International Journal of Fatigue, Volume 134, May 2020, 105448
https://doi.org/10.1016/j.ijfatigue.2019.105448

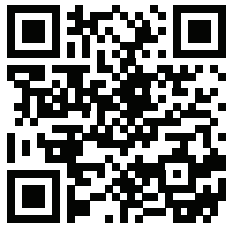

1.4.3 Paper III

A short communications describing the state of fretting fatigue assessments in the industry of medium-speed reciprocating engines. Here, large and complex machine components are subjected to non-proportional load histories. Engine dynamics are usually solved using condensed multi-body models that provide the loading conditions for subsequent fretting analyses using Finite Element Methods. Fretting analyses are usually conducted using simple Ruiz-like parameters combined with industry experience. There is an obvious potential for more elaborate analysis at different stages in the development process with the available time and information at each stage. Critical plane methods are also used, but usually at a later stage in the design process due to efficiency and little information available.

Fretting in medium-speed reciprocating engines - Comments on practices and opportunities
S.L. Sunde, F. Berto, B. Haugen
Material Design & Processing Communications, 2020; e201
https://doi.org/10.1002/mdp2.201

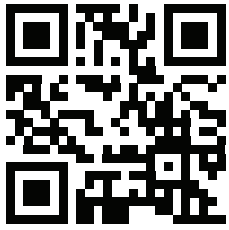

1.4.4 Paper IV

The development of a new test rig is demonstrated and put to use. The test rig is based on the dovetail joint and the many test fixtures found in literature on such joints. The fixture is simple, but allow for testing with a variety of different conditions. Inserted contact pads provide a simple means to test different contact geometries, material combinations and surface treatments. Enclosing the lower fixture gripping bracket should permit testing in submerged conditions. The usual disadvantage of the dovetail test configuration is that there is less control over contact conditions; this is also the primary drawback of this test fixture. However, using a multiaxial fatigue machine, the torsional actuator can be used as an additional source of excitation to the specimens. The test rig is demonstrated with a simple test program with Ti-6Al-4V specimens. The

tests were simulated using Finite Element Methods and post-processed using critical plane methods with Theory of Critical Distances. It was found that very simple analyses using bulk material properties and assumptions made for the coefficient of friction could predict the cracking direction and life within a certain accuracy. The fixture is concluded to be useful for further experimental work.

Experimental and numerical fretting fatigue using a new test fixture
S.L. Sunde, B. Haugen, F. Berto
International Journal of Fatigue, Volume 143, February 2021, 106011
https://doi.org/10.1016/j.ijfatigue.2020.106011

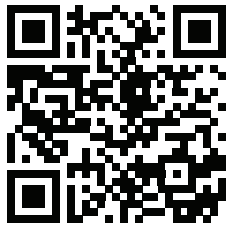

1.5 List of presentations

(I) S.L. Sunde, F. Berto, B. Haugen, S.K. Eidsvik, Experiences with fretting fatigue n medium speed reciprocating engines, 14th International Conference on Fracture (ICF14), Rhodes, Greece (July 2017).

(II) S.L. Sunde, B. Haugen, F. Berto, Fretting fatigue tests using multiaxial fatigue rig, ESIS 2nd International Conference on Structural Integrity and Durability (ICSID), Dubrovnik, Croatia (October 2018)

Chapter 2

Numerical fretting fatigue

This is the most important chapter of the thesis. A considerable amount of work have been put into numerically simulating fretting fatigue. Being able to calculate and predict fretting fatigue is an important goal for engineers as physical testing is not always possible in the time frame given. Thus, early predictions can cause considerable cost-savings and avoid unnecessary design iterations. The finite element methods are already well known for practicing engineers and form the basis for solving fretting contacts in this project. Continuum mechanics and contact mechanics are used to determine the stresses and strains occurring in sliding contacts assuming smooth surfaces and isotropic materials.

2.1 Contact Mechanics

As fretting and fretting fatigue are phenomena that occur in contact problems, the advantages of understanding contact mechanics are clear. Most real fretting contacts are too complex to be analysed using analytical methods, and numerical discretisations and computer solutions are necessary. Nonetheless, an understanding in basic contact mechanics gives key insight into fretting behaviour. The equations demonstrated in this section are used throughout relevant research as well as in this thesis. Analytic models are appropriate for engineering situations with rolling contact; roller bearings, gear meshing, cam-rollers etc. However, analytic sliding contact is more involved, as will be demonstrated in this section. The use of Finite Element Methods is addressed in section 2.5. In the following, the basics of contact elasticity and frictional contact relevant for the fretting are covered.

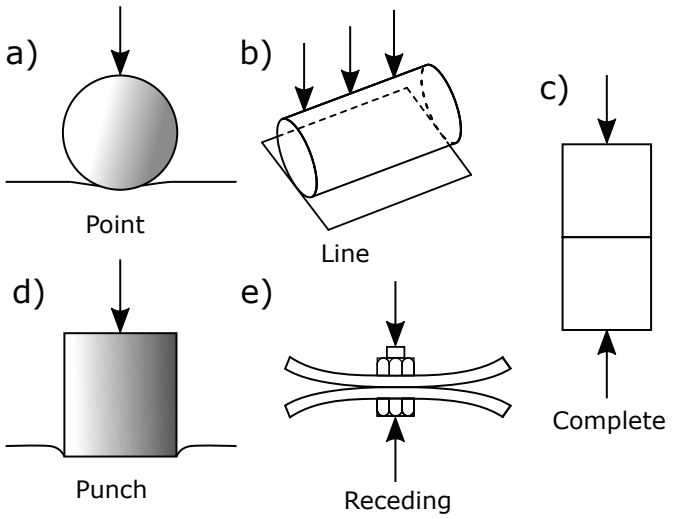

Figure 2.1: Different classes of contact with fundamentally different behaviour.

As early as in the late 1800, researchers started mathematically describing contact. Hertz [5] derived relations for simple frictionless contacts in the 1880s, which later formed the foundation for a whole separate field of contact that can be called Hertzian theory. Hertz analysed the stresses occurring in cylinders and spheres in frictionless contact and derived simple closed-form solutions that are still used in engineering. Later, these models were extended to include the effects adhesion.

Contact can be divided into several types that behave in fundamentally different manner. One of the most relevant classifications is whether the contact is *complete* or *incomplete*. Contact problems where at least one contacting surfaces is convex are incomplete contact. In these configurations contact area increase with increasing pressure and the contacting bodies have a common surface tangent at the edge of contact, see e.g. point contact (a) in Figure 2.1. In complete contact however, the contact area is independent of the pressure, see type c and d in.

Half-plane (two-dimensional half-space) is the theoretical idea of the entire two-dimensional plane being divided into two. Many contact theories assume one of the contacting bodies to be described as a half-plane, i.e. having semi-infinite dimensions. This assumption of half-plane theory holds to a reasonable degree when contact is small compared with the dimensions of the real body.

When two bodies are pressed against each other, material particles at the surfaces are displaced both in normal and in tangential direction. If the bodies are *elastically similar*, the tangential displacements are the same for the two bodies for a pure normal force and no slip occurs. Hence, contact is independent of the friction and no tangential traction occurs. In this *uncoupled* solution, Hertz pressure profile are still valid under the influence of tangential load. For

elastically dissimilar bodies however, slip occurs due to pure normal force and the tangential and normal solutions are therefore *coupled*. Most real fretting contacts are elastically dissimilar to some degree but uncoupled solutions are often used as approximations. See e.g. Nowell [6] and Hills et al. [7] for analyses on coupled solutions for cylindrical contact with tangential loads.

The contact between cylinder and half-plane is given special treatment here. This contact is essentially a specialisation of cylinder-cylinder contact where one of the cylinders have infinite radius. This case is demonstrated in Figure 2.1b. Similar (Hertzian) line contact was used in the experimental campaign in Paper III and forms the pressure profiles studied numerically in paper V, see section 4.

Due to the work of Hertz [5], the parabolic pressure profile $p(x)$ from a cylinder pressed onto a half-plane can be expressed as

$$p(x) = p_0 \sqrt{1 - \frac{x}{a}^2} \tag{2.1}$$

where x is positional coordinate with origin in the contact center, p_0 is the peak pressure and a is the contact half-width, see figure 2.2. The peak pressure is obtained by

$$p_0 = \frac{2P}{\pi a} \tag{2.2}$$

where P is the contact force. Lastly, the contact half-width is obtained by

$$a = \sqrt{\frac{2PE^*}{\pi R}} \tag{2.3}$$

Where the composite elasticity E^* is given for plane strain conditions for similar materials by

$$E* = \frac{4(1-\mu^2)}{E} \tag{2.4}$$

Where μ is the material Poisson's ratio and E is the Young's modulus.

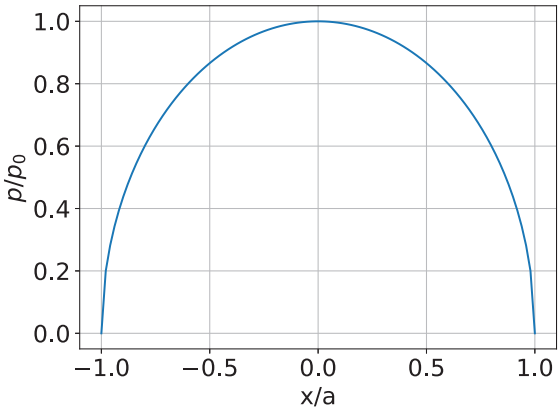

Figure 2.2: Normalised Hertz (line) pressure profile

For more literature on closed-form solutions, readers are referred to literature on contact mechanics [8, 7].

A fundamentally different type of contact is the sharp-edge contact as shown for the complete types in Figure 2.1d. Here, the contacting bodies do not have a common surface tangent at the edges and so the resulting contact pressure is *singular*. Notionally sharp-edged contacts are usually avoided in engineering practice, but can in practice be seen e.g. in bolted joints.

2.2 Sliding contact

Frictional contact problems with shear loads are much more involved, and most analyses relies on half-plane theory. When a tangential force is applied to the contacting bodies, shear tractions act across the two surfaces opposite in direction but equal in magnitude. Relative motion (slip) between the surfaces dissipate energy. Friction is clearly one of the most important factors affecting fretting fatigue as the shear tractions cause strong subsurface stress gradients and due to friction work causing surface wear. The relationship between slip amplitude and fretting behaviour have been debated in literature for decades [9]. The friction properties of a contact depends on numerous parameters and is not a function of the material combination only. In many cases though friction stress q is assumed to depend on the material combination through the coefficient of friction μ (COF) and limited by

$$|q(x, y)| = \mu p(x, y) \tag{2.5}$$

where $q(x, y)$ is the shear traction at the position (x, y), μ is the coefficient of friction and $p(x, y) > 0$ is the pressure. Note that the form of equation (2.5) is local, i.e. the values are functions of position. When a shear load Q is applied to the bodies, two possible situations occur; if the load exceeds the shear limit, the

bodies will globally slide against each other. For any lower shear load however, the contact is in a state where some parts of the contact area remains stuck whilst others slide. The latter state is known as partial slip and is especially critically in fretting fatigue causing high shear stress gradients.

The analysis of partial slip usually starts with Cattaneo [10] and Mindlin [11] who independently derived relationships describing the case of partial slip for elastically similar convex contact.

Consider cylinder-on-plane contact as shown in Figure 2.1b with its pressure profile being described in equation 2.1. When a tangential force Q is subsequently applied to the cylinder, parts of the contact surfaces will start to slip. As long as the tangential force is less than the limiting value of static friction, i.e. $Q < \mu P$, the contact will be in *partial slip*. More specifically, as the pressure as seen in Figure 2.2 vanishes at the contact edges, sliding will in theory initiate at the edges even for vanishingly small shear force. As the force increases so does the amount of area in slip, usually denoted c. This is illustrated in Figure 2.3

She slip size is found by assuming the partial slip shear stress profile $q(x)$ to be a perturbation of the fully sliding solution [7],

$$q(x) = \mu P + q'(x) = \mu p_0 \sqrt{1 - \frac{x}{a}^2} + q'(x) \tag{2.6}$$

where $q'(x)$ is the correcting term active in the slip zones ($a > |x| > c$). By integrating the shear over the contact the extent of the stick zone may be expressed as

$$\frac{c}{a} = \sqrt{1 - \left|\frac{Q}{\mu P}\right|} \tag{2.7}$$

This is a very important relation in analytical fretting fatigue. For details of its derivation, reader is referred to e.g. [7]. The shear profile resulting from equation (2.7) can be seen in Figure 2.3 for different values of coefficient of friction.

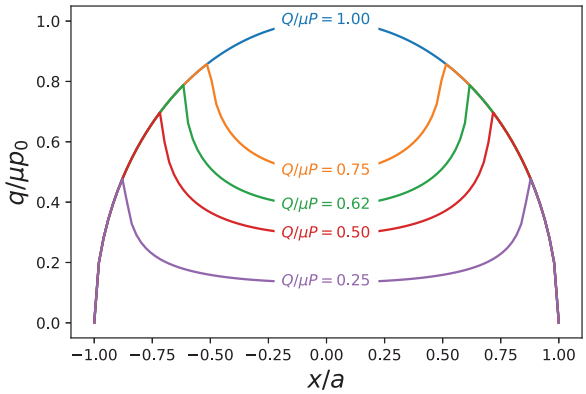

Figure 2.3: Normalised shear stress for partial slip conditions for cylinder-on-plane contact.

The partial slip conditions described by equation (2.7) is only for monotonically shear loading. As fretting fatigue is subjected to cyclic tangential force $\pm Q$ however, the shear stress can be describes as varying between this expression on either side of the extremes [7]. The shear distribution becomes dependent on the load history.

The cyclic loading experienced during fretting fatigue reverses the sliding direction for each cycle. As the tangential force reverses direction, the contact area instantly sticks. Further reduction in shear loading cause reverse slip to occur at the contact edges. A new slip zone $c' < |x| \leq a$ occurs and an additional correction term is needed to applied to the shear distribution. This is given by

$$q''(x) = 2\mu p_0 \frac{c'}{a} \sqrt{1 - \frac{x}{c'}^2} \tag{2.8}$$

where the factor 2 is to cancel out the previous correction. A similar shear evolution is found when analysing Hertzian contact with varying normal load, as was the case in Paper IV (See Appendix A.4). As the normal and shear traction vary proportionally in the dovetail configuration, the stick boundaries move considerably during the load sequence, se Section 2.5.2.

In-depth analytical treatments of frictional contacts is out of scope in this thesis. For more in-depth theories on analytical sliding contacts, the reader is encouraged to read book on fretting fatigue by Hills and Nowell (1993) [7] and more recent extensions to Cattaneo-Mindlin. Jäger [12] and Ciavarella [13] independently found that the Cattaneo-Mindlin method applied to *any* contact problem for which half-plane theory applied. This meant that general partial slip conditions could be analysed for contacts using the shear correction methods. Thus, many types of contact could be analysed without resolving to numerical discretisation.

Thus far, contact between two bodies have only been addressed on a macroscopic level, i.e. neglecting the fact that real surfaces are rough. The assumption of smooth surfaces is a valid assumption in many cases of engineering design. Contacting bodies are usually machined with high precision, ground and or polished and the effects of roughness diminishes compared to the stresses determined by macroscopic geometry. The initial surface roughness do however play an important role for the friction properties and gross slip wear rates [14]. For studies on fretting fatigue including the effects of surface roughness, see e.g. Yue and Wahab [15].

Closed forms solutions described in this section only apply to convex (complete) contacts. Flat or sharp-edged contacts (see Figure 2.1) have singularities that need special treatment. Sharp-edge contact do sometimes occur in engineering applications and these behave fundamentally different from the rounded contact for which closed-form equations exist. Much fretting research have studied sharp-edge contact and the stress concentrations occurring at the contact edges. Its similarity to the singular stress fields surrounding crack tips have caused tools developed in the field of fracture mechanics to be applied, see Section 2.4. As fretting cracks are usually found at the edges of contact where its nucleation and early growth are dominated by the severe stress gradient, analysing the Sackfield et al. [16] introduced asymptotic methods to characterise the edge of contacts. The application of asymptotic matching is an exciting method to analyse the stress fields surrounding sharp edges in fretting contacts. See e.g. [16, 17]. Semi-analytical methods are also used on fretting contacts [18, 19].

2.3 Fretting contacts

Due to friction, relative sliding motions will cause damage to the contacting surfaces. The nature of this damage and indeed its severity depends on numerous factors, where one of the most cited factor is the sliding amplitude. The dependence of fretting on sliding amplitude was early recognised, though the mechanisms behind it have been debated. A classical graphical demonstration of this dependence was given in the seminal paper by Vingsbo and Söderberg in 1988 [20], where fretting fatigue life was plotted with a non-monotonic U-shaped curve with displacement amplitude, see Figure 2.4. Here, fretting wear is seen to monotonically increase. A similarly shaped relation was given by Waterhouse [21], but with life plotted as a function *slip* amplitude.

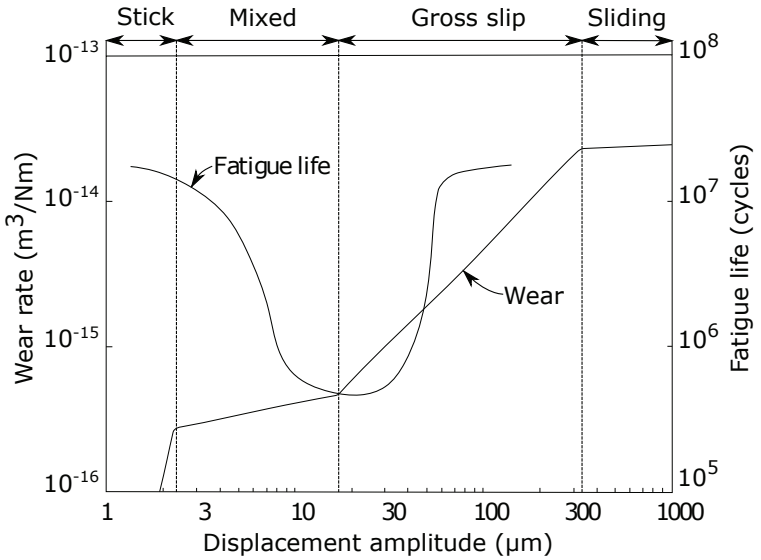

Figure 2.4: Relating the slip amplitude to fretting regime, as demonstrated by Vingsbo and Söderberg [20]

Fatigue life is seen to decline as the slip amplitude increases whereas wear increases. This motivated fretting behaviour to be divided into different *regimes* depending on the mechanisms involved. For very small values of slip, the contacting bodies are generally stuck, acting almost as one body with edge cracks. As mentioned in section 2.1, cylindrical contact will experience local slip at the edges when loaded tangentially, even for the smallest shear force. Similarly, spherical (point) contacts experience an annulus of slip. In real contact, rough surfaces experience local slip on asperity levels. Hence, some slip is inevitable, and real contacts often fall into the partial slip or mixed regimes, rather than being fully stuck. At low values of displacement amplitude, most fretting contacts are in partial slip. In this regime, increasing shearing stress (thus also slip amplitude), causes the stress singularity at the slip boundary to grow. At the trailing edge of contact, increasingly favorable conditions for surface crack initiation. As the sliding amplitude increases, contact enters the mixed stick regime, where fatigue damage is greatly reduced but wear is still modest.

Interestingly, the fatigue life increases as the sliding amplitude is further increased, moving into the gross slip regime. When the shearing force surpasses the frictional limit, contacting bodies will slide nominally and hence, the shear stress singularities are reduced. As the sliding amplitude increases, so does the frictional work (wear) which promote debris formation and particle ejection. This can increase fatigue life by improving the contact conformity and by removing initiated cracks before they are allowed to propagate.

Indeed, there have been many misinterpretations of the dependence of fretting on slip amplitude. As noted by Pearson and Shipway [9], the strong rela-

tion between fretting sliding amplitude and wear coefficient is often caused by a negligent of differentiate far-field displacement from the near-contact sliding. Additionally, the researchers point to a threshold duration for fretting wear to occur. There are a number of factors that can cause so-called *false fretting*, where relative motion is accommodated, resulting in less surface slip [22]. Recent research shows a much less clear relation between the slip amplitude and wear coefficient, and in some cases actually *independency* is suggested [9].

Perhaps the most important contribution in the aforementioned paper by Vingsbo and Söderberg was the introduction of the concept of "fretting maps". Today, characterising fretting behaviour and material response using different graphical tools, i.e. maps is in many ways a sub-field of fretting in itself. A fretting map is, simply put, a visualization of certain fretting variables of interest to distinguish the different regimes and identifying the critical values of said variables. For more information about recent development in fretting maps, readers are referred to [23].

It is clear that tribological mechanisms plays an important role for the fretting damage modes. Although for nominally stuck contacts, frictional work is limited and surface stress gradients are severe. Hence, in many such cases surface fatigue crack formation dominates the problem and wear can be neglected [24]. Nonetheless, some amount of micro-slip do occur, and local fretting damage is governed by factors such as surface hardness and roughness as well as loading and material microstructure. Particle detachment starts as soon as the bodies slide against each other but for fretting fatigue applications in the stick and mixed regime, particle detachment and ejection are limited. As the slip amplitudes increase, so does wear and particle detachment. In some cases, particles forms a third body, protecting the first bodies, in others, hard particles cause abrasive wear to the contact. Especially for hard coatings, entrapped debris can form such abrasive particles when detached from the first bodies. Other effects that can play important roles are surface oxidation, work hardening, micro-plasticity, surface residual stresses etc.

2.4 Fretting fatigue

Microscopic material damage starts to accumulate immediately upon fretting loading and is a continuous process during cyclic loading. If the loads are high enough, accumulated damage will eventually have formed a defect that may be called a crack. The initiated cracks are microscopic in size and their behaviour is therefore strongly influenced by local geometry, material microstructure, defects and surface roughness. Hence, modelling the process of crack initiation is very difficult and empirical methods are used.

In plain fatigue, cracks usually initiate at surface flaws (e.g. micro-cracks from the machining process) but can also initiate at internal material voids, pre-existing flaws or inclusions. For smooth specimens, microscopic plastic slip can drive an accumulation of dislocations along persistent slip bands [7] which subsequently develops into cracks. For the case of fretting fatigue, crack initia-

tion is usually caused by the presence of high tensile stresses at the surfaces by the stick-slip boundary (see Section 2.2). These tensile stresses frequently form multiple micro-cracks at the surfaces, some of which will continue to grow whilst others might self-arrest. Once a crack have grown large enough, its behaviour is dominated by the stress raisers from the crack tip itself. In this case it may be classified as being in the *propagation* phase.

Numerical models of fretting crack initiation are often decoupled from the crack growth stage. A popular methodology to model the initiation phase is using multiaxial fatigue criteria and critical plane methods, see Section 2.7. Continuum Damage Mechanics (CDM) uses damage evolution laws directly in the constitutive equations, see e.g. [25, 26, 27, 28].

There is no rigorous definition that separates the initiation and propagation phases of a crack. An initiated defect is sometimes heuristically defined to be the smallest detectable crack, which is of course not unambiguous as it depends on the method with which the cracks are detected. A more appropriate definition can be derived from fracture mechanics; as the crack becomes larger than one or two grain sizes, its behaviour will be increasingly dominated by the crack tip singularity, and it may be described by fracture mechanics regime. Thus, initiation is the duration of damage accumulation until its subsequent behaviour can be described by fracture mechanics. It is clear that for a crack on the same scale as microstructure features, the assumption of isotropic material will not hold.

Williams [29] analysed in 1950s the state of stress surrounding singularities and demonstrated the stress at the tip of a crack (in polar coordinates) to be *square-root singular* with the distance r from the crack tip, see Figure 2.5. The spatial variation of stress depends upon whether the load is normal, in-plane shear or out-of-plane shear stress and the strength of the singularities are characterised using the mode I, II and III *stress intensity factors* (SIF), K_I, K_{II} and K_{III} respectively.

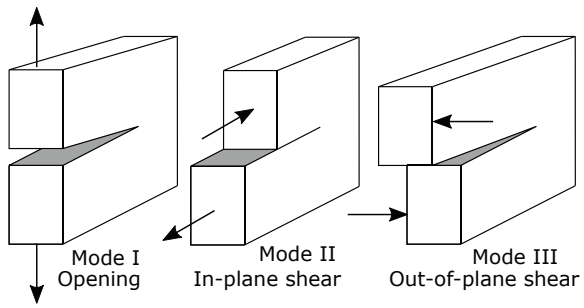

Figure 2.5: Three modes of crack loading.

The crack tip stress fields are aptly described using a polar (or cylindrical) coordinates as shown in Figure 2.6.

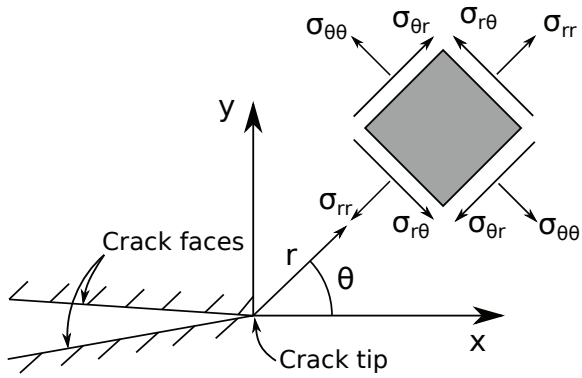

Figure 2.6: Crack tip stresses in polar coordinate system

The state of stress near the crack tip may consequently be expressed as a combination of the three modes,

$$\sigma_{ij}(r,\theta) = \frac{1}{\sqrt{2\pi r}}\left(K_I f_{ij}^I(\theta) + K_{II} f_{ij}^{II}(\theta) + K_{III} f_{ij}^{III}\right) \tag{2.9}$$

where $\sigma_{ij}(r,\theta)$ is the stress tensor at the position (r,θ). The functions $f_ij(\theta)$ are functions describing the angular variation of the stress field, while it is clear that the the stress intensity factors determines the strength of the field. Indeed as one approaches the crack tip $x \to 0$, the stress grow infinitely large. Turning the preceding equations around, stress intensity factors can be calculated numerically using e.g. finite element method. The stress intensity factors are subsequently used with a suitable criteria for crack propagation and direction [26]. Consider for simplicity the SIF

$$K = Y\sigma\sqrt{\pi a} \tag{2.10}$$

where Y is the geometrical correction, e.g. accounting for the fact that spatial dimensions are in fact not infinite. The driving force for crack propagation is the *range* of stress intensity factor given by

$$\Delta K = K_{max} - K_{min} \tag{2.11}$$

Using the stress intensity factor range, crack propagation can conveniently be divided into the following three stages [7].

Stage I Once a crack is "initiated", its early growth is often dominated by Mode II, i.e. driven by shear loading the accompanying plasticity.

Stage II As the crack becomes microscopically large, the crack tip stresses will dominate its growth in Mode I.

Stage III At some point, the crack will have grown so large that the reduced cross-section area of the component are unable to carry the load and the crack growth rate accelerates until failure.

These stages are visualized in Figure 2.7 where crack growth rate da/dN is plotted as a function of the stress intensity factor range in a log-log scale.

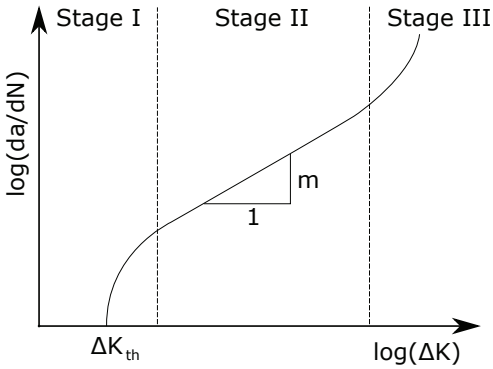

Figure 2.7: Three stages of crack growth

Stage II is often called the Paris region due to the linear, predictable nature of the crack growth rate. This linear relation for da/dN is expressed by the Paris' equation,

$$\frac{da}{dN} = A(\Delta K)^m \tag{2.12}$$

where ΔK is the Mode I stress intensity range and A and m are material parameters.

Equation (2.12) is used in fretting fatigue analyses when crack growth represents a considerable portion of the total fretting life. Recall that initiation mechanisms should be treated. The Paris equation is often used when investigating fretting fatigue cracking behaviour by subtracting the crack growth phase from the total cracking life [30]. The material parameters are often found in literature and material textbooks. Note however that in practice, growth rate and orientation may depend on mixed-mode features, load ratio and other factors [26]. These aspects are not treated here. The relations derived here are also important in *crack arrest methods* in fretting, see Section 2.4.1

A simple definition of crack path is obtained by assuming the crack to grow in Mode I, consequently utilising the mixed-mode SIF expressions to calculate the crack orientation: finding the orientation for which K_{II} is minimized [31]. There are however numerous different criteria to define crack path and in fretting fatigue, see e.g. [32, 26].

The application of linear elastic fracture mechanics to cracks relies on neglecting (minimising) the effects of plasticity. Some local plasticity will always occur at the crack tip, but in many cases the extent of this plastic process zone is small; the surrounding stress field is elastic and the stress intensity factors

applies. The plastic zone can be expressed by

$$r_p = \frac{1}{3\pi}\left(\frac{K_I}{\sigma_y}\right)^2 \tag{2.13}$$

where r_p is the radius of the plastic zone and σ_y is the yield strength of the material. This is following Irwin's plastic zone definition assuming Von Mises' yield and Mode I loading in plain strain [7].

The above separation of crack into stages is a simplification since mixed-mode effects are omitted. The stress fields found under fretting contact are multiaxial and early fretting crack growth are most likely affected by mixed-mode effects and crack closure effects. Once a crack have grown out of the influence of contact stresses, crack growth is determined by the bulk loading and is essentially a plain fatigue crack propagation problem. Hence, fretting really only affects Stage I and a portion of stage II [33].

The theories of linear elastic fracture mechanics demonstrated in this brief overview are relevant for fretting fatigue not only due to the characterisation of crack propagation. An equivalence between the square-root singular stress fields at crack tips (recall equation (2.9)) and the stresses from sharp-edge fretting contacts. This equivalence was noted by Giannakopoulos et al. [34] and sparked a interest amongst researchers in *crack analogies*. Similarly, the conditions of small-scale yielding is usually assumed. Mugadu et al.[35] used more general asymptotic stress matching to characterise fretting fatigue stress fields, later applied to incomplete contacts [17]. Asymptotic methods to fretting fatigue is not the focus of this thesis but it is acknowledged that these tools can be appropriate tools in many engineering contexts. Asymptotic methods are useful for fretting fatigue because it provides means for characterising the most detrimental fields (surrounding the contact edges) from which cracks nucleate, circumventing the need to analyse the entire contact. Thus, the local stress fields may be matched with those in experiments and as such be used to quantify fretting fatigue strength.

2.4.1 Crack arrest

Self-arrested fretting cracks are often found in engineering applications [36, 37]. As illustrated in Figure 2.7, the power law breaks down in stage I where the cracks are short. The existence of a threshold condition for which cracks do not grow is often assumed and can be used as fretting fatigue threshold conditions. In many contacts, the stress gradient is so severe that micro-cracks form at the surface, but quickly grow out of the highly stressed material and hence potentially self-arrest. Fretting cracks are frequently seen to be initiated from the trailing edge of contact, and grow in shear mode obliquely under the fretting contact where compressive stresses can cause the crack to close [38]. If the crack is fully closed before reaching stage II, it will arrest.

Short crack methodologies have been applied to fretting fatigue to find threshold conditions. Plotting the threshold stress intensity factor as a function

of crack length, the threshold regimes for crack arrest can be found. The well-known diagram of Kitagawa-Takahashi (K-T) is an example of such a diagram used on fretting fatigue [36]. Other transition curves used are El-Haddad [39], and Bazant curves [40].

2.4.2 Fretting fatigue stress histories

Fretting fatigue initiation and early crack growth is complicated by the fact that the stress fields under contact in general are multiaxial. Due to the non-linearity of contact, most stress variations are also non-proportional even for proportionally applied loads. This means that the stress tensors have components that individually change throughout the load history. If all the oscillating stress components are in-phase, the principal direction of the stress is constant, and the load is classified as proportional. In non-proportional loading, however, the stress components change in a non-proportional fashion, and the principal direction of stress rotates. Consequently, the orientation of the material plane experiencing the most damaging stress is not known *a priori*. In non-proportional loading, the material may experience additional hardening due to non-planar slip bands, which can greatly reduce the fatigue life [41]. Sensitivity to non-proportional loading varies from material to material, depending on its microstructure, hardness etc. [42]. Many steels have been found to experience non-proportional hardening, while e.g. aluminium alloys are less affected [43]. In general, non-proportional loading is known to be at least as damaging as proportional loading, and should be accounted into the fatigue model [44]. This suggests that fatigue damage accumulates on different material planes independently, and that critical plane models are physically ground. Section 2.7 discusses the application of critical plane which was used in Paper IV (see Appendix A.4) to predict fretting fatigue initiation life.

When fatigue assessments are to be made in terms of life predictions, damaging load cycles have to be identified and properly accounted for. For variable amplitude load histories, this require cycle counting algorithms to identify the load reversals. Uniaxial and equivalent stress (e.g. von Mises) histories have only one dimension and therefore permit cycle counting using traditional *Rainflow counting* [45] but multiaxial stress histories cause some problems. Since non-proportional load histories can have stress components with individual reversals, counting is non-trivial. Attempts to perform multiaxial cycle counting have been made by applying Rainflow counting on each projected material plane [46]. Other methodologies executes the counting on *relative quantities* of the stress invariants. Wang and Brown [47] performed counting on the relative von Mises strains to overcome the problem of load sign loss in the stress invariants. Meggiolaro and de Castro [48] proposed a modification to avoid the largest load range to be missed. Anes et al. [49] proposed a "stress scale factor" between the shear and axial stresses to which counting was made. In most fretting fatigue experiments, cycle counting is avoided since the load histories are simple. In engineering practice however, complex load histories are often encountered and care must be taken to correctly identify all relevant damaging events. Susmel

and Taylor [50] counted on the equivalent (resolved) shear stress on the material plane experiencing the largest variance of the counting variable. Proper cycle counting is especially important in fretting fatigue crack initiation when equivalent stresses are calculated in the candidate plane, see Section 2.7. In CDM models, damage evolution models are usually incorporated directly into the FE solver.

It has already been described how fretting contacts cause severe stress gradients. Such stress raisers clearly affect the fretting fatigue performance, but the exact consequences for the crack initiation and growth is complicated, as the stress field variations becomes very non-uniform. For fatigue assessments dealing with stress raisers, such as in fretting contact, the gradient is seen to greatly affect fretting cracks [51, 52]. In such cases local (hot spot) methods becomes over-conservative and averaging techniques are often used, e.g. using the Theory of Critical Distances [50, 53]. The next section addresses the use of such averaging methodologies in the presence of stress raisers.

2.4.3 Theory of Critical Distances

It is well-known in fatigue that utilising the peak values from stress raisers can cause gross over-estimation of fatigue damage. If one assumes that the physical processes that initiate and drive a crack is relevant over a material volume of certain size, one would expects individual discrete point stresses to not necessarily fully determine material damage. In this view, fatigue damage should be evaluated over a spatial dimension. The size of this dimension is expected to be related to the material and its fatigue properties [54, 55], but is more recently also related to the the stress raiser itself, see e.g. [56, 24]. The effect of stress gradients on fatigue life has long been researched in the field of notch fatigue, but researchers have found the methods to work well for the stress raisers in fretting contacts as well, making the fretting crack initiation analysis to be amenable to the tools developed by notch fatigue. Figure 2.8 demonstrates this symbiosis.

Giannakopoulos et al. [34] pointed out the quantitative equivalence between stress concentrations from sharp-edge contacts and notches, coining the term "crack analogue" for fretting fatigue. Although the stress gradient in fretting case is usually much more severe than in the case of notches, the analogy is clear and quite useful. For more on such notch analogies see e.g. Nowell and Dini [57] and Ciavarella [58].

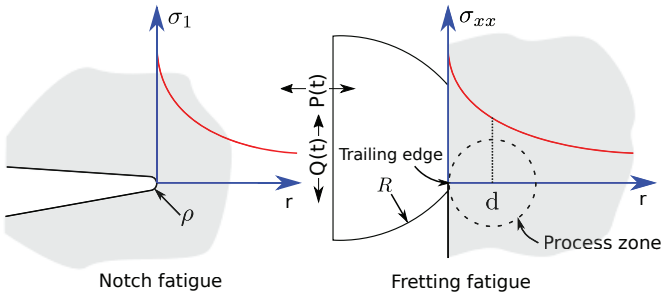

Figure 2.8: Comparing notch fatigue evaluation with fretting fatigue at a distance or averaged over a volume.

The *local* hot-spot fatigue analysis will in some cases act as reassuring conservatism to the practicing engineer, but in many other cases, depending on the severity of the stress raisers, cause expensive designs. *Non-local* analysis methods have been proposed to handle the stress raisers and the resulting size effects. In notch fatigue, the Method of Critical Distances [59, 54] considers various forms of averaging schemes; in the point method, fatigue is evaluated at a single point evaluated at some critical distance from the peak (hot-spot). The Line method averages the values over a line and the area/volume methods uses the averaged stress over a certain area/volume of material. The point method can simply be expressed as

$$\sigma_{\mathit{eff}} = \sigma(r = d) \tag{2.14}$$

whereas averaging schemes can be written as

$$\sigma_{\mathit{eff}} = \frac{1}{|\Omega|} \int_{\Omega} \sigma(\mathbf{r}) d\mathbf{r} \tag{2.15}$$

where the averaging domain Ω can be a line, area or volume.

A common method to determine the static length scale L is by considering the size of the process zone to be related to material fatigue limit as

$$L = \frac{1}{\pi} \left(\frac{\Delta K_{th}}{\Delta \sigma_0} \right) \tag{2.16}$$

where K_{th} is the threshold stress intensity factor and $\Delta\sigma_0$ is the uniaxial fatigue limit. This length can be recognized as the transition length from short cracks to long cracks [39]. The shape and size of this spatial dimension is somewhat arbitrary but it is recognized that non-propagating cracks are confined to a process zone of such size.

In Paper III (see Appendix A.3), both volume method and point method was used in an attempt to predict fretting life for a series of dovetail fretting specimens. See Section 3. Here, the critical distance was averaged over the line along the cracking direction under fretting, i.e. slightly oblique.

2.5 Finite element modeling

The finite element method is a family of mathematical tools to solve partial differential equations (PDE). During the last few decades the Finite Element Method (FEM) has become very accessible to engineers and researchers and is now considered by many to be the primary tool to solve fretting contact stresses and strains. Most practical contacts can be solved using commercial FEM software packages and sometimes even using open source libraries. Some common commercial packages are Abaqus, Ansys, NX-NASTRAN, which usually are freely available for students. Examples of popular open source libraries are deal.ii [60] FEniCS [61] and GetFEM++ [62] amongst many others. Although many open source alternatives are quite advanced, its usage in engineering practice is often limited and commercial packages dominate. Additionally, contact algorithms are considered advanced features that are more developed and readily available in commercial software. In this thesis Abaqus is used extensively to solve fretting contacts. Relevant examples can be seen in Section 2.5.1 and Paper IV (see Appendix A.4). A drawback with the increasing availability and simplification of FEM is the many potential pitfalls involved: Mistakes can be easily made and difficult to investigate. This is certainly the case when it comes to frictional contacts. In this section, the application of FEM to solve fretting fatigue is briefly discussed.

The main idea behind the finite element method is given in its name. Instead of solving the PDE over the entire continuous domain, the domain is divided into a finite number of discrete elements. Using the weak (integral) form of the equations and a set of chosen *test functions*, the discrete equation system is solved for the unknown field variables. For linear systems, solution methods consist mainly of matrix operations. The solutions are approximations by definition but discretisation error vanishes for increasingly refined element grids. Highly refined mesh is especially important in areas where the field variables have large spatial variations, which is indeed the case for fretting contacts. See e.g. 2.15.

Contact introduces nonlinear constraints to the discrete equations and is therefore only suitably solved using nonlinear solvers. These solvers perform additional contact iterations to find converged solutions. For three-dimensional models the additional iteration steps can be very expensive computationally, depending on the details of contact algorithms.

In practice, solving FE contact problems involve many algorithmic options, and its often a trade-off between accuracy and computational cost. When two bodies come into contact, forces are transferred between the two surfaces both in normal and tangential directions. However, as the contact area itself is unknown, special algorithms are necessary to determine which nodes that come into contact. Usually, the surfaces that *might* come into contact are assigned contact elements prior to the analysis. The contact solver will track the elements during the analysis, detect contact and iterate on the solution. For fretting problems, such "surface-to-surface" definition is most relevant.

Real contacting bodies do not penetrate each other and the contact solver

can enforce this condition ("hard contact") by using *Lagrange* multipliers. This method causes additional unknowns to the equation systems which can be costly for large models. Normal conditions are alternatively solved using a penalty stiffness. A small amount of penetration is then allowed but is controlled by the normal stiffness. A high penalty parameter cause small penetration (error) but can make the stiffness matrix ill-conditioned and cause difficulties for the contact solver. Values for penalty parameter are often chosen based on the stiffnesses of the first bodies, but in practice some experience and trial-and-error is common. In case of fretting contact, hard contact is frequently used [63, 15] but in many cases penalty stiffness solutions are sufficiently accurate [64].

Lagrange multipliers are also used to solve tangential constraints and is often chosen for problems where slip resolution is important, like in fretting fatigue. By using multipliers accurate slip values are enforced and proper slip conditions can be found, again at the cost of additional unknowns. Convergence problems can also occur as oscillations in stick/slip status and may require additional solver iterations. On the other hand, using penalty stiffness in the tangential direction, a small amount of elastic slip is allowed before slip occurs. This formulations is much simpler and can greatly improve solution cost. However, as accurate slip solutions are important in fretting fatigue, care must be taken in the choice of penalty parameters. Some FE software packages (e.g. Abaqus and ANSYS) offer *augmented Lagrange* methods as compromise, in which zero penetration solution is found through a series of penalty iterations. For frictional sliding, the tangent (solution) stiffness matrix becomes unsymmetric [65] and require special matrix solution methods. Figure 2.13 shows a comparison of penalty stiffness and Lagrange multiplier method for a fretting problem.

Traditionally, linear element types have been preferred to discretise contact geometry. Numerical problems can occur for higher-order elements having mid-side nodes. However, some software packages offer specialised higher-order element formulations that is suitable for contact problems and in some cases are actually preferred as they can more accurately describe surface curvature and subsurface stress gradients. The analyst should in general consult with the manual of the FE solver in question for details. In fretting problems, element meshes are often refined to a degree where linear elements are accurate enough.

In this thesis, FE software is used extensively to solve fretting contacts, in 3D and 2D. Paper IV A.4 demonstrates the application on of FEM to develop a test-rig and was used to simulate and predict fretting fatigue for a set of dovetail specimens.

2.5.1 A fretting example

Abaqus/Standard is a general-purpose finite element software package known for its ability to solve contact problems and is used in many fretting studies in literature [66, 24, 67]. The contact solver in Abaqus is advanced and offer many solution methods, and correspondingly, its use is complex and offer many potential traps. In this section, the application of Abaqus/standard is discussed for a classical fretting problem. Consider the contact problem shown in Figure

2.9. This example will be used as a demonstrator in the following sections with critical plane post-processing. See Araùjo and Nowell [51] for experimental results related to this configuration.

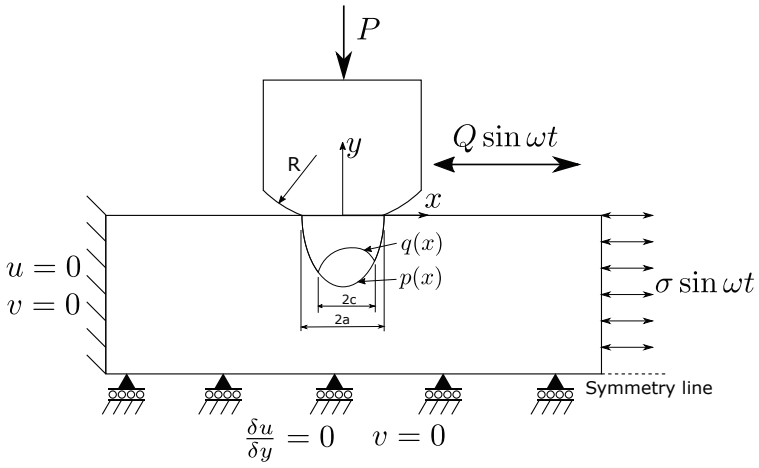

Figure 2.9: Simple two-dimensional finite element model of fretting fatigue specimen.

The classical contact configuration with a constant pad pressure P and monotonically increasing shear force $Q < \mu P$, often referred to as the Cattaneo-Mindlin configuration and was discussed in section 2.2). Here, sinusoidal shear force and in-phase fatigue load are applied to the contact. As the peak shear force transferred between the pad and specimen is lower than the friction limit the contact will be to be in partial slip causing a high shear stress at the stick-slip interface. Sliding occurs in one plane and a two-dimensional model is appropriate, in this case plane strain. Here, a distinction will be made between fretting fatigue case and *plain fretting* case; the former being loaded in both fretting shear and fatigue, the latter only in fretting shear ($\sigma = 0$). Figure 2.10 show a comparison of the surface tractions and slip for the plain fretting case and fretting fatigue ($\sigma = 280$ MPa).

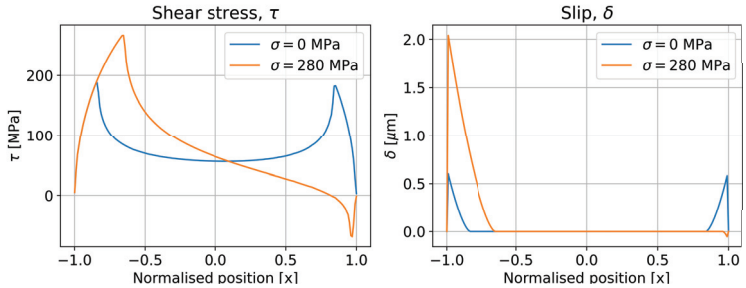

Figure 2.10: Comparing shear stress and slip for plain fretting vs fretting fatigue.

Symmetry is seen in shear stress and slip for the plain fretting case, somewhat equating the trailing and leading edges in terms of fretting damage. In fretting fatigue case it is clear how the trailing edge experience more severe shear stress due to the additional straining from the fatigue loading. The Hertzian (line) contact profile with large contact radius R cause the problem to be well-behaving with no sharp corners if the surface elements are sufficiently small. Due to the resulting stress gradients and local sliding on the micro-scale, a highly refined mesh is necessary. It is not uncommon with element sizes in fretting studies to be in the ranges of $10 - 50\mu m$ and even down to $2 - 5\mu m$ [68]. See Figure 2.11 and Figure 2.12 for mesh convergence analysis of plain fretting and fretting fatigue case respectively.

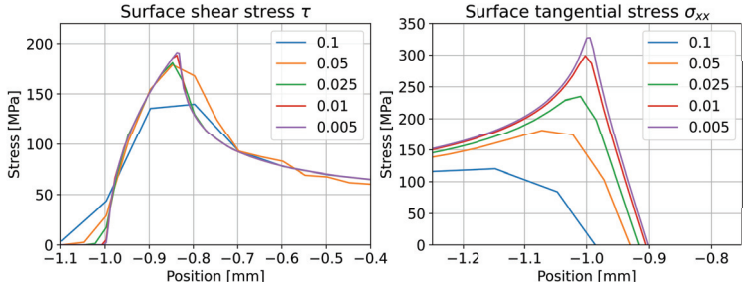

Figure 2.11: Contact convergence for plain fretting contact stresses at peak shear load.

As can be seen in Figure 2.11, peak shear stresses at the trailing edge of contact are found to converge for relatively coarse meshes. The tangential stress σ_{xx} at the trailing edge stick-slip boundary is singular and increases for as the mesh is refined.

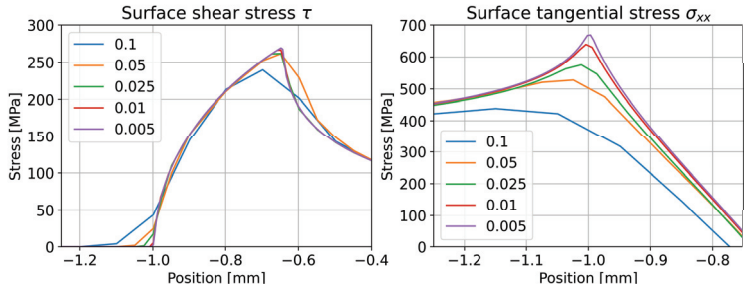

Figure 2.12: Contact convergence for fretting fatigue with bulk fatigue load $\sigma = 280$ MPa

The mesh refinement analysis of the fretting fatigue case have similar characteristics. Accurate shear stresses are found at the trailing edge for elements sizes of $5\mu m$ or finer. The tangential stress however require fine mesh to not underestimate the fretting crack initiation conditions.

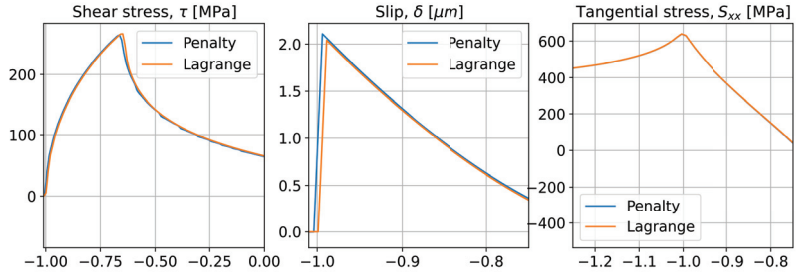

Figure 2.13: Difference between penalty stiffness and Lagrangian multipliers. Notice how the contact shear stresses are the same, but allowing a small amount of elastic slip (here $5\mu m$), cause non-conservative results for the surface stress σ_{xx}.

Surface quantities like shear stress and slip do not describe fretting damage alone. In most fatigue analyses, empirical combinations of stresses and strains are assumed to initiate and propagate fatigue crack. This require a post-processing analysis where the temporal field variations is accounted for. Section 2.7 demonstrates the use of critical plane methods to determine fretting fatigue cracking behaviour by using subsurface stress histories. In the following Section the analysis of the relevant substrate field values is demonstrated.

Figure 2.14 compares fretting stress cycle at trailing edge of contact and in the substrate. Notice the quite proportional nature of the stress cycles at these points. It is clear that very high tensile stress amplitudes occur at the trailing edge of contact dominates the stress tensor. promotes initiation of surface cracks.

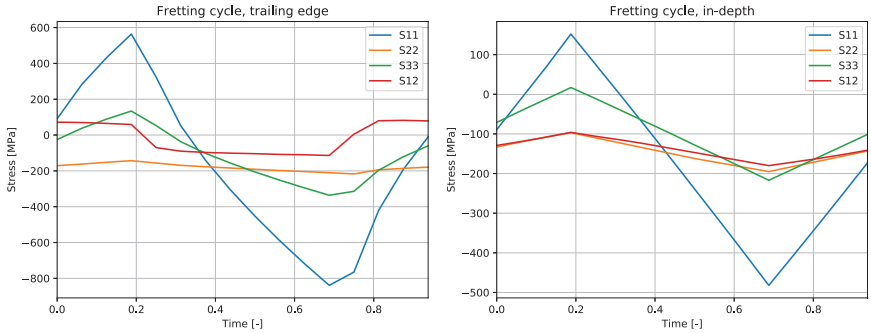

Figure 2.14: Fretting fatigue stress cycle at trailing edge $(-1.03, 0.0)$ and in-depth $(-1.1, -0.5)$

The subsurface stress field can be used to estimate the severity of fretting contact loads. Figure 2.15 indicates material damage in terms of deviatoric stresses (Von Mises equivalent stress). Not surprisingly, values are high but also localized to the contact vicinity in the plain fretting case. For the fretting fatigue case the bulk stresses are strong enough for fretting-initiated cracks to propagate.

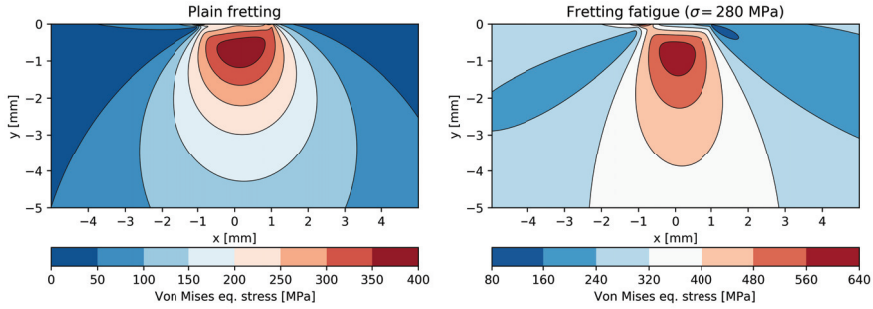

Figure 2.15: Subsurface Von Mises equivalent stresses for plain fretting and fretting fatigue. Von Mises stresses indicate material shear damage.

Evaluating subsurface von Mises equivalent stresses from quasi-static FE solutions can give valuable insights into the severity of contact, but the non-proportional stress histories resulting from fretting contact (see section 2.4.2) usually require more elaborate analysis through post-process analysis. See section 2.6 for fretting assessments made using surface quantities. In section 2.7 critical plane post-processing methodologies are discussed.

2.5.2 Dovetail joint

A large amount of research has been carried out on fretting fatigue in dovetail joints [69, 70, 71, 72, 67, 73]. Consider the aircraft turbine blades attached to the rotor by a dovetail joint. Due to the centrifugal forces acting on the blade, sliding contact occurs between the blade and the rotor, causing fretting fatigue. Additional aerodynamic and mechanical vibrations may also apply. Contact in the dovetail joint is usually flat and rounded (see Section 2.1), but in Paper IV Hertzian contact profile was used as shown in Figure 2.16. The choice of Hertzian contact geometry was made to allow for closed form equations to apply.

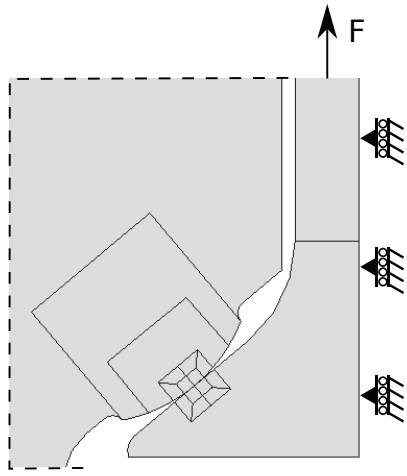

Figure 2.16: Dovetail geometry used in Paper IV.

Figure 2.16 demonstrates how geometry was partitioned to allow for a very steep variation in element sizes. For details around this, see Paper IV in Appendix A.4. In publication, FEM was used to analyse a series of experiments made on titanium specimens. See Section 3.2 for general aspects of experimental testing. The dovetail configuration differs from the Cattaneo-Mindlin case as the normal and shear loading both vary with time in a proportional manner. In many cases, a single load is applied to the dovetail joint, providing both normal, tangential and bulk loading. In terms of finite element analysis, this configuration present some additional numerical complexities, compared with fretting contacts with constant pressure. As contact pressure and shearing act simultaneously, slip amplitudes are often longer compared with the classical case discussed in Section 2.5.1. The contact shear evolution demonstrated in Figure 2.17 summarises the contact situation for the dovetail configuration.

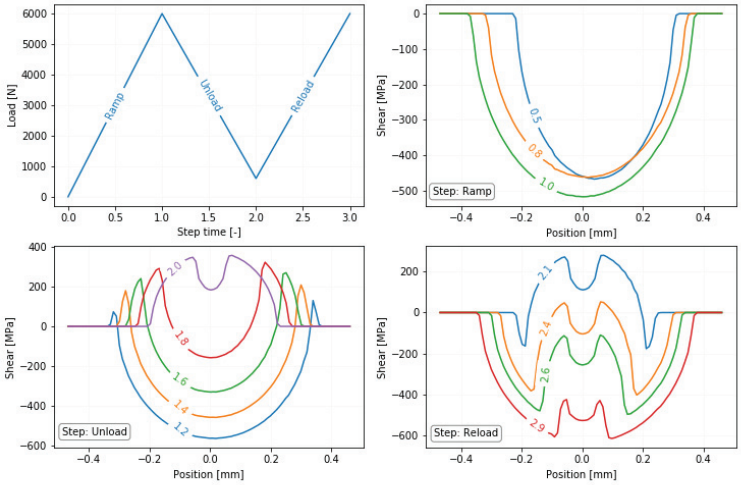

Figure 2.17: Traction evolution on dovetail joint where pressure and tangential force both vary with the axial load.

The stick-slip history seen in Figure 2.17 shows how the stick-slip boundary moves significantly during the fretting cycle as both tangential and normal loads vary in-phase for the dovetail specimens. Surface fatigue damage can therefore be assumed to be smeared over a larger area, potentially increasing cracking life. For more on this fretting configuration, see Paper IV.

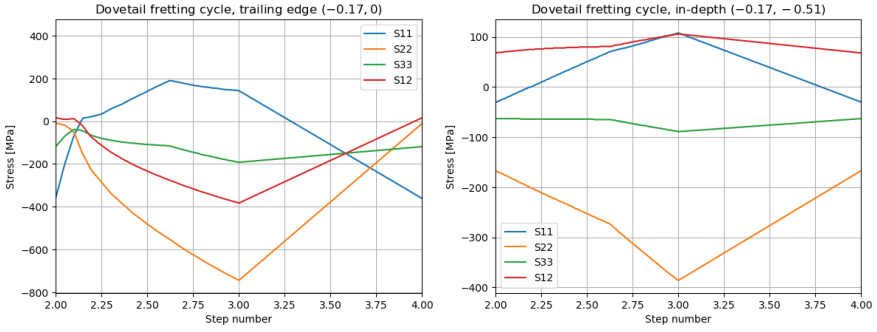

Figure 2.18: Dovetail fretting cycle demonstrated for critical point at trailing edge, and in-depth.

Figure 2.18 demonstrates the fretting stress cycles for two selected specimen

material points: the critical point at the trailing edge and at a distance of approximately 0.5 mm inward. When compared with the corresponding stress cycle in Figure 2.14, it is clear that the dovetail case experience much more non-proportional stress variations. As mentioned in Section 2.4.2, non-proportional loads may have significant effect on fatigue properties and must be included in the damage model. For more on the analysis of the dovetail geometry, see Paper IV in Appendix A.4.

2.5.3 Three-dimensional fretting analysis

Most finite element fretting analyses in this thesis use two-dimensional discretisations. Although instantaneous slip occurs in a plane, real contacts experience some transverse strain due to Poisson's ratio. Moreover, for 3D load histories, some contacts can hypothetically experience sliding in multiple directions during a cycle. For fretting experiments and many cases of real contacts, sliding action occurs in a single dimension, and its solution with respect to stresses and strains can be approximated using two-dimensional plane strain or plane stress analysis. Kim and Mall [74] investigated the differences between three-dimensional and two-dimensional models for cylindrical (Hertzian) and flat and rounded contact. Edge-effects were found to be negligible and that a plane strain analysis provided accurate results.

3D finite element contact solutions are *considerably* more expensive computationally as the fretting area already require a very fine mesh. Additional efforts are often required to mesh the geometry, sometimes requiring the contacting bodies to have perfectly aligning elements. Indeed, most experimental setups and academic studies consider sliding in one single plane. But in mechanical engineering practice, complicated load histories can cause slip histories to require three-dimensional analysis. In Paper III, such circumstances were discussed in the case of medium-speed reciprocating engines. In piston engines, gas forces and inertia forces act in different directions and at multiple frequencies. Slip may occur in more than one plane during an engine cycle. In this industry, complex FEM models are simplified using methods of condensations; millions of degrees of freedom are condensed to *super-elements* with a very small subset of important degrees of freedom. The condensed models are used to simulate the relevant dynamics of the engine and the resulting forces are applied to simplified (local) contact models to analyse the fretting cycles.

Other sub-modelling techniques have proven necessary in order to isolate the fretting contact problem. Sub-modelling techniques are often incorporated into the finite element software package. Another and more recent technique was used by Montebello et al. [75, 76]. Here, the velocity field surrounding the strong fretting stress gradient is partitioned by using intensity factors, much like the stress intensity factors in fracture mechanics (See Section 2.4). The key idea with using velocity field though, is that since velocity is an extensive parameter, it can capture the nonlinear nature of the contact.

2.6 Fretting-specific parameters

Preceding sections considered the application of finite element method to solve fretting contacts and it was declared that quantifying fretting fatigue damage using quasi-static stresses and strains alone is unsatisfactory. As such, FE solutions serve a purpose as qualitative analysis but for quantitative fretting analyses temporal variations must be considered. Hence, post-processing steps are usually required. Several fretting-specific parameters have been proposed to characterise fretting behaviour and many of these are commonly used in engineering practice [77, 78].

The seminal papers by Ruiz et al. [69, 79] were among the first to suggest the use of fretting specific energy-based parameters. They studied fretting in aircraft turbine blades and suggested using the shear stress work on the contact interfaces to quantify fretting damage. Analyses were made in two-dimensional models and several two-dimensional parameters were suggested, one for fretting surface damage (wear) and one for fretting crack initiation. Intensity of the surface damage was suggested to be governed by the frictional work ($\tau\delta$).

In an attempt to quantify fretting *fatigue*, a parameter was obtained by multiplying the shear work with the surface tangential stress, thus

$$k = \sigma_t \tau \delta \tag{2.17}$$

where k is the "second Ruiz fretting parameter", henceforth called fretting fatigue damage parameter (FFDP). σ_t is the stress component acting parallel to the contact surface, τ is the shear stress and δ is the slip distance.

In numerical analyses consisting of several time steps, the FFDP is computed by integrating the shear work over the fretting cycle $t \in [0, T]$ and multiplied by the largest tangential stress during that cycle.

$$k = \sigma_1 \cdot W = \sigma_1 \int \boldsymbol{\tau} \cdot d\boldsymbol{s} = \sigma_1 \int_0^T \boldsymbol{\tau} \cdot \dot{\boldsymbol{s}} dt \tag{2.18}$$

where $\boldsymbol{\tau}$ is the shear stress vector and $\boldsymbol{s}$ is the slip vector. Tangential stress σ_t is here swapped with *maximum principal stress* σ_1 to overcome the unidimensional nature of the original Ruiz parameter. Numerically, the shear work can be calculated using the midpoint rule as

$$W = \sum_{n=1}^{N} \frac{\boldsymbol{\tau}_{n-1} + \boldsymbol{\tau}_n}{2} \cdot (\boldsymbol{s}_n - \boldsymbol{s}_{n-1}) \tag{2.19}$$

Where $n \in [1, N]$ is the discrete time step. Note however, the lack of physical interpretation of the FFDP. It is simply an empirical, "composite" parameter obtained by multiplying the surface damage (via shear work) with the crack driving force (via the normal stress). Nowell and Hills [1], found (2.17) to correlate with fretting cracks and that there seems to be a threshold value.

In Figure 2.19 the FFD parameter is plotted for a series of dovetail specimens tested in the published article IV, See Appendix A.3. Leading and trailing edges

are highlighted as critical areas, but a quantitative assessment of the values is difficult without relevant data for comparisons.

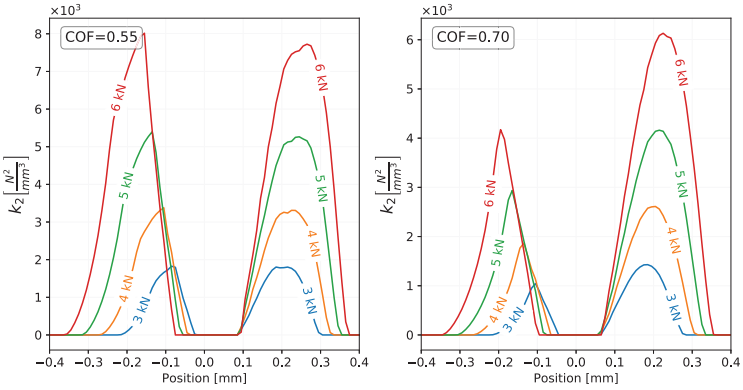

Figure 2.19: Ruiz FFD parameter. The left and right peaks in each plot are the leading and trailing edges, respectively.

Vidner et al. [80] recently suggested using the frictional power instead of work. They also suggested extensions to the Ruiz parameter where critical plane-based parameters to be used in place of maximum principal stress. Other fretting-specific parameters are e.g. "fretting related damage" parameter (FRD) [81].

$$FRD = \alpha + \beta\sqrt{\frac{Q}{fP}} \tag{2.20}$$

The FRD parameter was related to the plain fatigue methods as a knock-down factor to determine the number of cycles to failure and thus making full use of already existing plain fatigue data. Q is the sliding force, P is the normal load, f coefficient of friction α and β are fitting coefficients.

Although the fretting-specific parameters discussed in this section are simple and approachable, their physical interpretations are lacking. Its reasonable to assume that fretting damage is a function of shear work or power but the complex mechanics of fretting crack initiation and early growth are not adequately described using only surface quantities. In this thesis critical plane methods were found superior to surface parameters in terms of characterising fretting fatigue cracking behaviour and life estimations. These methods are described in the following section.

2.7 Critical Plane Analysis

Previous sections were concerned with analysing fretting fatigue severity by evaluating quasi-static finite element solutions and empirical fretting-specific parameters. To quantify fatigue lives is, however, an involved task that require more advanced analysis. In many fields of engineering, safe-life design principles are applied and the overall safety against fretting is objective of the fretting analysis. Although the Ruiz parameters, when combined with experience may give such insights wrt. fretting damage, their robustness are limited. Moreover, life predictions are very useful for component fatigue design and to meaningfully determine service intervals. More physically valid descriptions are always desired as they help reasoning about the mechanisms involved. In this section the application of critical plane methodology is described to predict fretting fatigue crack initiation lives and orientation.

The main numerical difficulty related to quantitative fatigue analysis of fretting contact is how to handle the highly localised non-proportional stress variations (see section 2.4). Inherent uncertainty is always present, related to variability in microstructure and surface roughness. Hence, any numerical prediction is only an approximation and scatter will certainly be present in the results. Critical plane analyses is by many researchers the preferred method to quantify fatigue damage for multiaxial stress histories. It has long been acknowledged that fatigue damage manifests itself in material planes with certain preferential orientations, depending on the loading and material. Critical plane methods in general calculates the fatigue damage on a large number of such *candidate* material planes in search for the most critical one. In theory there exist infinitely many candidate planes for each material point and a discrete selection must be made. Furthermore, the critical plane search is usually performed for a large set of material points, often generated by the finite element method (see Section 2.5). The potentially large computational cost of critical plane methods is clear: The critical plane criteria is evaluated for a large number of plane orientations for each material point. For densely meshed geometries like in fretting fatigue, this results in a time consuming analysis.

Much research have focused on improving the efficiency, accuracy and unambiguity of critical plane methods and Paper II (See Appendix A.2) investigated and demonstrated some relevant aspects of a numerical implementation. A framework for efficiently calculating critical plane orientation and damage was developed for the general case of three-dimensional stress histories. The details of these methods and the application to fretting fatigue are demonstrated in this section.

2.7.1 Multiaxial fatigue criteria

Numerous different fatigue criteria and methodologies have been proposed throughout the history and the application of some criteria was reviewed in paper I, see Appendix A.1. See also Navaro et al. [82] and Bhatti and Wahab [83] for an overview. Most commonly applied to fretting fatigue problems are the classi-

cal Smith-Watson-Topper [84], Fatemi-Socie [85] and Findley [86] parameters. More recent parameters having success is the Modified Wöhler Curve Method [87] and Carpinteri-Spagnoli criterion [88, 89] amongst others.

One of the most classical fatigue criteria is the Smith-Watson-Topper [84] parameter based on tensile strain and mean stress. This criterion is commonly used on materials cracks are Mode I-dominated and often for low-cycle fatigue. In its critical plane form it can be expressed as

$$SWT = \sigma_{max} \frac{\Delta\epsilon_1}{2} \tag{2.21}$$

where σ_{max} is the maximum normal stress and $\Delta\epsilon_1$ is the principal strain range. Extensions to the SWT parameter have been proposed that accounts for shear mechanisms, making it more suitable for shear-failing materials [90]. As tensile stresses are known to form micro-cracks at the fretting contact boundaries, SWT parameter could be applicable to many relevant fretting problems.

Most numerical efforts to quantify fretting fatigue damage in this project rely on the Findley parameter (FP). In its simple form it can be expressed as

$$FP = \tau_a + k\sigma_{max} \tag{2.22}$$

where τ_a is equivalent shear stress acting in the candidate plane, k is a material parameter and σ_{max} is the maximum normal stress on the same plane during the stress cycle. The parameter k can be interpreted as a measure of sensitivity to *opening mode* effects on the shear cracks. k is therefore often lower for shear dominated (ductile materials) than for brittle materials. Socie [91] propose to use $0.1-0.2$ for ductile materials, but in Paper IV (see Appendix A.4), $k = 0.35$ was found to work well for Ti-6Al-4V dovetail fretting specimens. Kallmeyer et al. [92] found 0.35 to give best correlation with uni-axial and bi-axial data for Ti-6Al-4V.

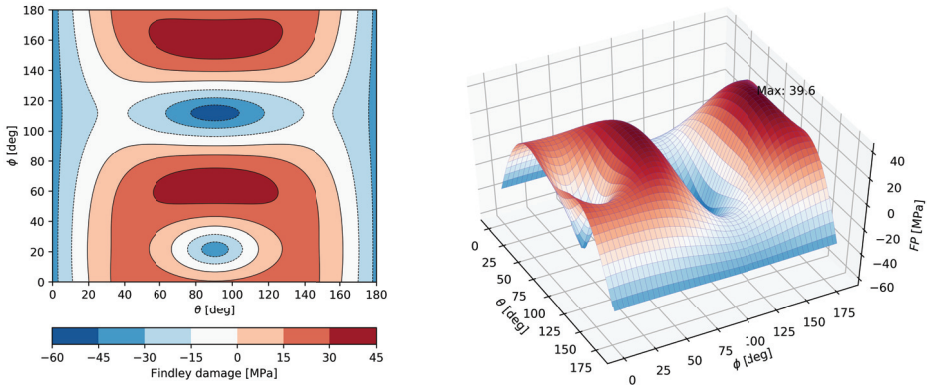

Figure 2.20: Findley fatigue damage parameter as a function of candidate plane orientation

In Figure 2.20 the Findley parameter in Equation (2.22) is visualised for the single material point in contact center of problem described in section 2.5.1. Negative values are the result of compressive normal stresses and hence, fatigue life in these orientations are infinite. Notice the symmetry in the damage surfaces; this is a result of the two-dimensional FE discretisation.

2.7.2 Resolved shear stress amplitude

As demonstrated in (2.22), the Findley parameter rely on a scalar value shear amplitude. It was described in section 2.4 how fatigue cracks in ductile metals are often initiated by shear mechanisms. Many shear-based fatigue criteria have been proposed, some of which were reviewed in Paper I. Shear-based criteria share a common difficulty in terms of implementation; as the shear stress (or strain) history in the candidate plane is a set of *vectors*, some heuristic is needed to obtain a *equivalent shear stress (or strain) amplitude*. Therefore, the SWT parameter is simpler in its implementation because all the quantities in (2.21) are directed along the candidate plane normal. Methods to compute the equivalent shear stress amplitude is a research field on it own and many different methodologies have been used, see e.g. [93] for a discussion on measures of equivalent shear stress amplitudes, uniqueness and quantification of non-proportionality.

Load history for a material point is represented by a discrete set of Cauchy stress tensors $\boldsymbol{T}$ represented in the standard basis by the matrix

$$\boldsymbol{T} = \begin{bmatrix} \sigma_{xx} & \sigma_{xy} & \sigma_{xz} \\ \sigma_{xy} & \sigma_{yy} & \sigma_{yz} \\ \sigma_{xz} & \sigma_{yz} & \sigma_{zz} \end{bmatrix} \tag{2.23}$$

i.e. with six independent components which in general can be its own function of time.

The stress tensor describes the stress state in a small point (continuum) and by the *Cauchy stress theorem*, the stresses acting on an arbitrary material plane through this point can be found by

$$\boldsymbol{t} = \boldsymbol{T} \cdot \boldsymbol{n} \tag{2.24}$$

where $\boldsymbol{t}$ is the stress traction acting on the material plane. The sequence of traction vectors acting on the candidate plane obtained from the load history can be thought to describe a three-dimensional object. To find the resolved shear stress amplitude acting on the material plane, this object is projected onto the plane π with its own coordinate system $\boldsymbol{e}_i$. A two-dimensional polygon is obtained, from which the shear stress amplitude can be calculated.

The third axis $\boldsymbol{e}_3$ of the candidate plane coordinate system is in the plane normal direction, but the other two axes are not given and can be chosen rather arbitrarily as long as they are mutually perpendicular. Convention used here is to choose $\boldsymbol{e}_1$ by cyclic permutation of the largest component of the normal vector, as demonstrated in Algorithm 1.

Following enclosure demonstrates the convention used to determine candidate plane coordinate system.

Algorithm 1 Determining a suitable coordinate system in candidate plane

procedure InPlaneCsys($\boldsymbol{n} \in \mathbb{R}^3$)
  $\boldsymbol{n} \leftarrow \frac{1}{\|\boldsymbol{n}\|}\boldsymbol{n}$ ▷ Ensure normal vector has unit length

  $n_x = |\boldsymbol{n}[0]|$
  $n_y = |\boldsymbol{n}[1]|$
  $n_z = |\boldsymbol{n}[2]|$

  if $n_x \geq n_y$ and $n_x \geq n_z$ **then**
    $\boldsymbol{e}_x = (0, 1, 0)$
  else if $n_y \geq n_x$ and $n_y \geq n_z$ **then**
    $\boldsymbol{e}_x = (0, 0, 1)$
  else
    $\boldsymbol{e}_x = (1, 0, 0)$

  $\boldsymbol{e}_x \leftarrow \boldsymbol{e} + \boldsymbol{e}_x^T\boldsymbol{n} \cdot \boldsymbol{n}$ ▷ Add out-of-plane directions
  $\boldsymbol{e}_x \leftarrow \frac{1}{\|\boldsymbol{e}_x\|}\boldsymbol{e}_x$ ▷ Renormalise
  $\boldsymbol{e}_y = \boldsymbol{n} \times \boldsymbol{e}_x$

  return $[\boldsymbol{e}_x, \quad \boldsymbol{e}_y, \quad \boldsymbol{n}]$

The simple algorithm demonstrated above uniquely defines an in-plane coordinate system (change of basis) that is used to calculate the shear stress history in the candidate plane.

2.7.3 A brief note about algorithm complexity

Critical plane computations rely on a number of algorithms. In case of large models with many material points to be evaluated for fatigue, the computational cost of these algorithms matter. Some relevant algorithms were discussed in Paper II. In this section, the discussion is expanded and a brief description of algorithm complexity is included for completeness.

Big-O notation is a way of classifying the efficiency of an algorithm and is often used to describe time and space (memory) usage. E.g. a time complexity of $O(n)$ means that the algorithm scales linearly in time with the size n of the input. However, this does not necessarily mean that the input is only visited once; the notation is *asymptotic* and describes the limiting behaviour as the input parameters goes to infinity. As an example, consider the algorithm for the convex hull described on the following section. The time complexity of the sorting step is $O(n \log n)$. After sorting, the shear stress history is traversed twice, once from each end, which is linear in time $O(n)$. The total time is then $O(n \log n) + 2 \cdot O(n)$, but using asymptotic notation, the converging time

complexity is bounded by the largest component, thus the convex hull is also $O(n \log n)$. Many relevant algorithms have polynomial time complexity and brute force methods are often $O(n^2)$ or $O(n!)$ but in some cases more optimal algorithms in $O(n \log n)$ exist. It is common in research to focus on the asymptotic behaviour and dropping constants. However, in practice, constants do matter and for practical cases, the actual implementation should be profiled to validate the efficiency.

In many cases of fatigue analysis, the number of time steps to be evaluated are relatively few for each damaging load cycle. However, in non-proportional histories increased temporal resolution are necessary to fully describe the damaging cycles. Examples of relevant engineering problems were discussed in Paper III. In four stroke piston engines, the major load cycle consist of 720 crank degrees and may contain several loads. These are often simulated using crank steps of 10-20 crank degrees [77]. Note though that for non-proportional variable-amplitude load histories, cycle counting may be necessary. Bottom line is: Efficiency of the critical plane analysis is not known until time profiles of the real implementations are inspected. Engineering FE-models often have high number of material points to be analysed and the running time of critical plane analyses becomes important.

2.7.4 Convex Hull

The convex hull (CH) of a set of two-dimensional points is the smallest polygon containing all points (see Figure 2.21). This mathematical object can be shown to be unique for the given set of points and is proven useful in several aspects of fatigue analysis. When calculating stress vectors in the candidate plane, CH is shown to contain all the points used to affecting the resolved shear stress (see Sections 2.7.5 and 2.7.6). Hence, the CH can be used to reduce the number of history points and accelerate the fatigue evaluation. In Figure 2.23 this concept is demonstrated for the fretting fatigue case described in the previous sections. Some points are seen to be discarded without affecting the equivalent shear stress amplitudes.

A number of algorithms are found to compute the convex hull efficiently, e.g. "Graham Scan" has time-complexity $O(n \log n)$ where n is the number of time steps. As the idea behind CH in this context is to reduce the number of points used in the determination the resolved shear stress, without lack of generality. The exact loss of generality depends on the definition of shear stress amplitude but it can be shown to not affect the result for MRH and MCC (See section 2.7.5 and 2.7.6 respectively). The practical effectiveness depends on the implementation but the theoretical effectiveness is also limited to the complexity of the subsequent resolved shear stress step. By computing the convex hull before brute-forcing MCC, potentially great computational effort can be saved. The actual amount of time saved depends also on the load history as only interior points are removed. For a proportional shear stress history, all points in the candidate plane are co-linear and only the two extreme points are necessary. However, for a 90 degree out-of-phase loading, the shear path is a

circle and the convex hull actually contains all the original points. For many practical load cases, a majority of the points lie *inside* the CH and hence do not contribute to the resolved shear amplitude defined by shape-enclosing methods. In these cases the convex hull can be used to reduce the accelerate the next steps in the fatigue evaluation.

The $O(nlogn)$ algorithm by Graham [94] is described in pseudo-code in Algorithm 2. Example implementations are included in the appendices. Note that these examples are simple for the case of brevity and in many cases more stable and efficient implementations are available through third-party libraries (see Section 2.8). For Python, the convex hull algorithm is available through the *ConvexHull* class available in SciPy library [95].

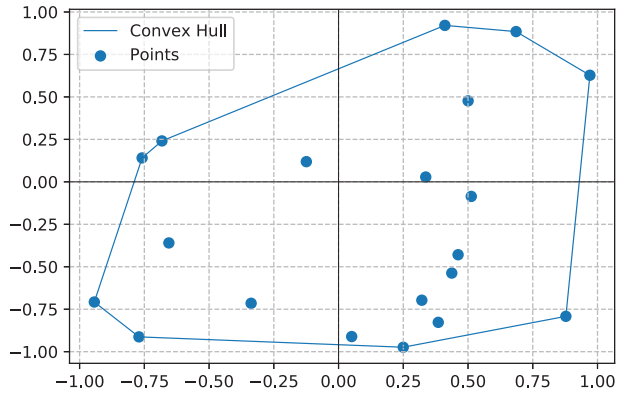

Figure 2.21: Two-dimensional convex hull

As the convex hull is only an intermediate step in calculating the equivalent shear stress, it is strictly not necessary. It may however speed up the critical plane analysis in many cases. In paper II the efficiency of the convex hull was investigated for the use on many relevant fatigue loading histories.

2.7.5 Minimum Circumscribed Circle

The Minimum Circumscribed Circle (MCC) was one of the first proposed definitions for the resolved shear stress [96]. This two-dimensional geometric object fully enclose the shear stress path and is unique. The problem with MCC is its inability to distinguish between proportional and non-proportional paths. It is recognized that fatigue behaviours of materials are different for proportional and non-proportional load [97]. However, the MCC predicts the same amplitude value for a straight line than for a circle with the line as its diameter. Ellipses have been proposed as a means of addressing this deficiency [46].

Algorithm 2 Algorithm for computing Convex Hull

```
1:  procedure ConvexHull(P = [p(x, y)] ∈ ℝ²)                ▷ Graham Scan
2:      P ← sort(P)                                  ▷ Sort points lexicographically.
3:      U = [p_0, p_1]                               ▷ Upper half of the convex hull.
4:      for p ∈ P do                                          ▷ Traverse points.
5:          i = 0
6:          while |U| ≥ i do                ▷ Check against points on hull thus far.
7:              if Turn(U_{-1}, U_{-2}, p) is Clockwise then
8:                  i ← i + 1
9:              else
10:                 Remove U_{-j}
11:         Append p to U

12:     L = [p_{-1}, p_{-2}]                         ▷ Lower half of the convex hull.
13:     for p ∈ [p_{-3}, ...p_0] do                   ▷ Traverse reversed point list.
14:         i = 0
15:         while |L| ≥ i do                ▷ Check against points on hull thus far.
16:             if Turn(L_{-1}, L_{-2}, p) is Clockwise then
17:                 i ← i + 1
18:             else
19:                 Remove L_{-j}
20:         Append p to L

21:     L ← L[1..−1]              ▷ Discard overlapping endpoints in L and U.
22:     return U + L                                  ▷ Return the joined hull halves
```

For this circle, the center and radius can be interpreted as mean and amplitude shear stress, respectively. A great benefit of the MCC is that it is unique for a given set of input points and hence, results in unambiguous values for mean shear stress and resolved shear stress amplitude. Note however that the Findley criterion in Equation (2.22) is independent on mean shear. Computing the MCC efficiently, however, is not straight-forward. An exhaustive (brute-force) search algorithm is trivial to implement by leveraging the fact that the circle passes through two or three points. Thus, MCC is found simply by checking all possible circles consisting of two or three points separately [98] and chooses the smallest one that contains all other points. This results in a very large number of visited circles to and quickly becomes very computationally demanding for large problem sizes even for short histories.

The task of computing MCC can be formulated as a convex quadratic programming (QP) problem with one linear constraint for each input point [99]. The problem can be written as

$$\begin{aligned} \min_{x,y,z} \quad & \{x^2 + y^2 + z\} \\ \text{s.t.} \quad & 2x\tau_{u,i} + 2x\tau v, i + z \geq \tau_{u,i}^2 + \tau_{v,i}^2 \end{aligned} \tag{2.25}$$

where the three optimisation variables x, y, z are the x-coordinate, y-coordinate and squared radius respectively. Finding the optimal solution is easy using existing quadratic program solvers which are available in many commercial software packages, but also using free open-source libraries. An implementation in Python using the open source library *cvxpy* [100] is included in the appendices and can be similarly solved using C++ libraries like CGAL [101]. Details of solving quadratic programs are outside the scope if this thesis, but the interested reader are referred to textbooks like [102]. See also Bernasconi and Papadopoulos [103] for a discussion on effective means of computing the minimum circumscribed circle, including iterative methods.

In figure 2.22 three different methods for computing the MCC are compared. The inefficiency of the brute force method is clear for problem sizes larger than 10 points. By using the convex hull, problem size is reduced. Note that this comparison is made for pseudo-random points where the number of interior points is higher than for most shear histories. An important point to make is that if the shear history have many interior points, proper cycle counting algorithms should be used so that all damaging cycles are accounted for. The actual computational benefit from CH is as described above dependent on the distribution of points in the candidate plane. This also explains the irregular nature of the brute force method in Figure 2.22. In this thesis, the convex hull was used extensively to speed up the process. Some of the observations made for real load histories are demonstrated in Paper II.

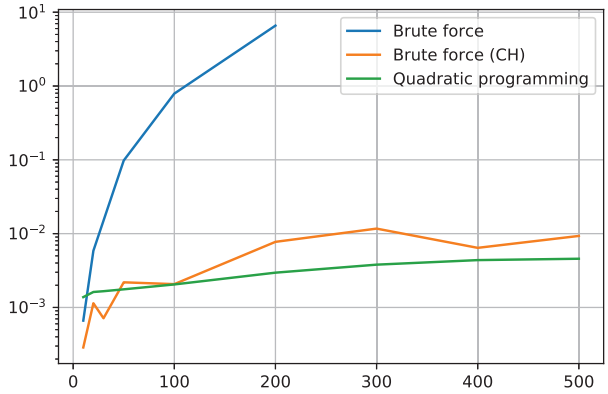

Figure 2.22: Comparing computational time for three different algorithms computing MCC. Comparisons were made with Intel Xeon W3680 (3.3 GHz) using naive Python (see Appendix A.5).

Example implementations of the convex hull is shown in appendix A.5 for completeness. Due to the fact that MCC do not properly account for non-proportionality in the shear stress history, other alternative definitions of the shear stress amplitude was sought.

2.7.6 Maximum Rectangular Hull

Instead of enclosing the shear stress history in a circle, Araùjo et al. [104] proposed using a rectangle with maximised diagonal, correspondingly predicting a larger resolved shear amplitude for a non-proportional load compared with the proportional. This is demonstrated on a candidate plane for the fretting fatigue case demonstrated in previous section and visualized in Figure 2.23.

The definition of the maximum rectangular hull (MRH) can be written as

$$\tau_a = \max_{\omega} \sqrt{a_1^2(\omega) + a_2^2(\omega)}, \quad 0 \leq \omega \leq \pi/2 \tag{2.26}$$

where the sides of the rectangle a_1 and a_2 are given by

$$a_i(\omega) = \frac{1}{2}\left[\max_t \tau_i(\omega, t) - \min_t \tau_i(\omega, t)\right], \quad i = 1, 2 \tag{2.27}$$

The definition of MRH in Equation (2.26) can be interpreted as the rectangle found by rotating the shear path for a number of orientations $\omega \in [0, \pi/2]$, maximising its bi-directional projection. The equivalent shear stress amplitude is then half of the diagonal of the MRH. The mean shear stress can be the geometrical center of the square.

Note that the maximum rectangular hull algorithm is linear in the number of points, but with a potentially high constant related to the number of rotations ω checked. If, for instance, one degree increments were considered for ω, the running time is $O(90 \cdot n)$. However, the original authors [51] found that only five to ten rotations were necessary. In Paper II, MRH was used extensively on real load histories and the accuracy was discussed. MRH was also used to compute fretting fatigue life for a set of Ti-6Al-4V dovetail specimens in Paper IV (see Section 3.2.

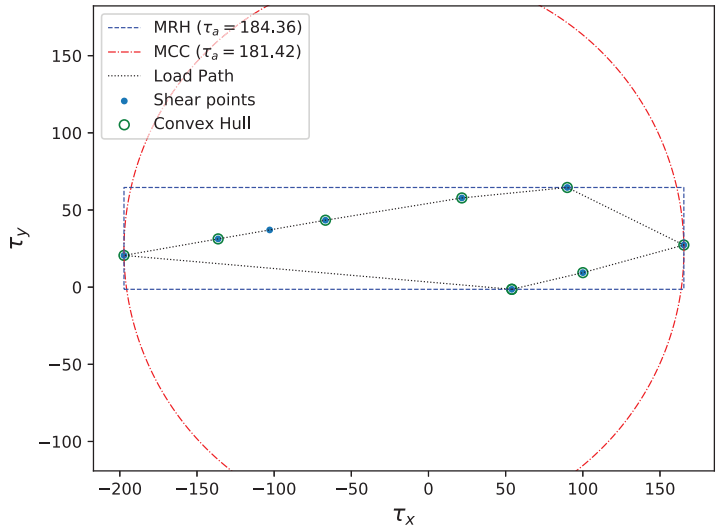

Figure 2.23: Convex hull, minimum circumscribed circle and maximum rectangular hull for the shear stress path in a candidate plane.

Figure 2.23 summarises the calculation of equivalent shear stress for fatigue evaluation. Here, the candidate plane of $(45, 45)$ is investigated for the hot-spot found for the fretting fatigue case demonstrated in previous section. Notice how the MRH algorithm predicts slightly higher resolved shear stress compared with MCC due to the non-proportional shear loading path. Notice also how the convex hull in this case only removes one single point for being co-linear with the adjacent points. It is clear that by adjusting appropriate tolerances for co-linearity, more points could be excluded. This is typical for many fretting fatigue shear paths.

2.7.7 Angular search space discretisation

To compute the critical plane for a material point and a given load history, generally all possible planes passing through the point needs to be investigated.

As there is theoretically infinitely many possible candidate plane orientations, the search space needs to be discretised. Different discretisation strategies are possible and some were reviewed in Paper II. In this Paper, an iterative selection scheme was proposed, using triangular elements that facilitate local search space refinement. In this section, some of these methods are discussed.

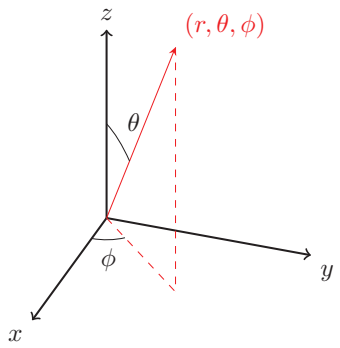

Figure 2.24: Spherical coordinate system

Consider a spherical coordinate system centered in this material point and following ISO 80000-2:2009 convention. The three coordinates (r, θ, ϕ) is used to denote the radial distance, polar angle and azimuthal angle, respectively. Figure 2.24 shows how the spherical coordinate system relates to the Cartesian coordinates (x, y, z).

$$r = \sqrt{x^2 + y^2 + z^2} \tag{2.28a}$$

$$\theta = arctan\frac{\sqrt{x^2 + y^2}}{z} \tag{2.28b}$$

$$\phi = arctan\frac{y}{x} \tag{2.28c}$$

The orientation of a material plane running through the origin can be described by either the two rotations θ and ϕ or by its unit normal vector. Results are here expressed in angle orientations, but the numerical implementations favors the normal vector as it is used directly in the linear algebra equations for the shear projection (see Algorithm 1). The components of the plane normal vector are found by

$$x = r\sin\theta\cos\phi \tag{2.29a}$$

$$y = r\sin\theta\sin\phi \tag{2.29b}$$

$$z = r\cos\theta \tag{2.29c}$$

In most cases a pre-determined set of angles $\theta, \phi \in [0^o, 180^o]$ are used to define the critical plane search space, divided e.g. by angular increments of

1^o. However, note that this space can halved by acknowledging the fact that a plane flipped by rotating it 180 degrees is the same plane. The search space for material plane orientations can be thought of as a unit hemisphere.

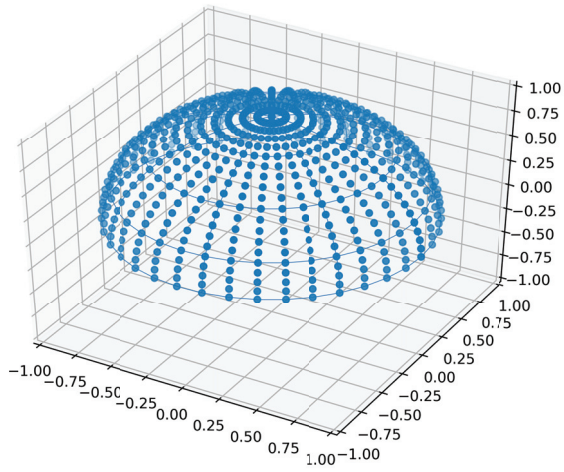

Figure 2.25: Rectangular discretisation of critical plane search space

Figure 2.25 clearly demonstrates how the rectangular discretisation cause an uneven distribution of plane orientations. While the rectangular choice makes sense for a flat surface, the hemisphere will have a high density around and lower around the equator. Rectangular grid was used to produce the damage surface shown in Figure 2.20 and works well for such visualisation. However, uneven distribution can inaccurately represent the damages for material planes along the equator if a coarse mesh is chosen. Moreover, choosing a fine such mesh produces an unnecessarily fine mesh at the poles.

Alternatively, the hemisphere can be discretised using triangular elements as shown in Figure 2.26. This produces a more homogeneous search space discretisation [105, 99]. Triangular cells are also trivially partitioned into smaller triangular elements, permitting a discretisation to be refined, even locally. This opens possibilities to adaptively refine the search space. Paper II found in appendix A.2 describes an implementation of such adaptive refinement scheme, albeit naive. It is shown find the critical plane accurately for a smaller number of candidate planes.

The very naive adaptive scheme was shown in paper II. is demonstrated in Figure 2.26. Here, a pre-determined coarse set of triangles was first calculated and triangles was recursively refined based on the local damage. Slight computational advantage was shown by comparing load histories found in the literature and by computing a large number of pseudo-random load histories.

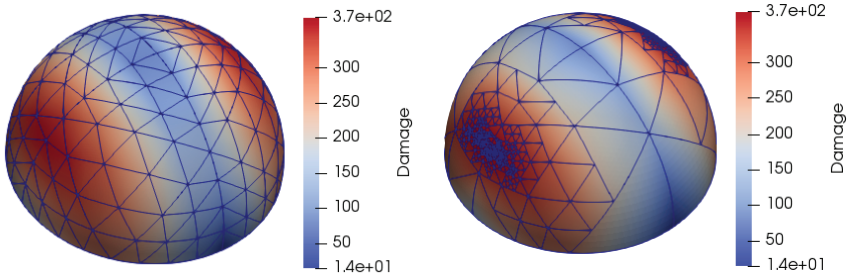

Figure 2.26: Findley fatigue damage at hot-spot, comparing a brute-force approach with a naive adaptive refinement.

2.7.8 Application to fretting

In this section, the use of critical plane method is demonstrated on fretting contact. More specifically, Findley parameter is applied to the plain fretting and fretting fatigue case which were solved using FEM in section 2.5.

Figure 2.27 demonstrates the Findley parameter for the material point situated at trailing edge, and for the material point at 0.5 mm depth from trailing edge. Symmetries are clear and peak damages found at $\theta = 90^o$. The trailing edge point shows two almost-equally damaging peaks both serving as potentially cracking directions.

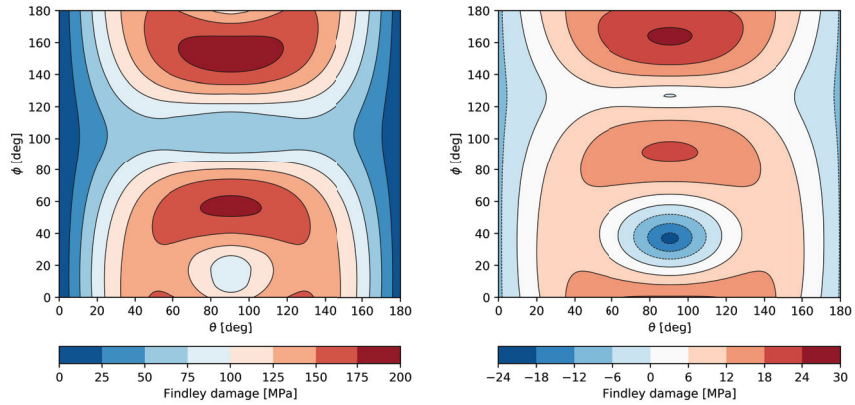

Figure 2.27: Subsurface Findley damage ($k = 0.1$) for the plain fretting case described in section 2.5. Left figure is at the surface trailing edge and right is at 0.5 mm depth from said point.

Similar visualisation is made for the fretting fatigue case and shown in Figure 2.28. Both points are now considerably stressed, with contours being qualitatively very similar. Cracking is now increasingly probable along material points

with aligning critical directions.

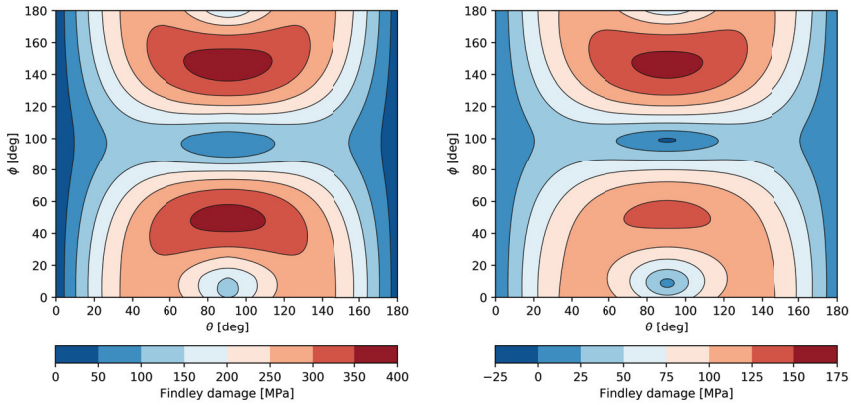

Figure 2.28: Subsurface Findley damage ($k = 0.1$) for the fretting fatigue case described in section 2.5. Left figure is at the surface trailing edge and right is at 0.5 mm depth from said point.

Figure 2.29 visualises the subsurface scalar field representing Findley damage for the plain fretting case. Since shear is cycled between $\pm Q$, the damage field is quite symmetrical to the contact center. Damage is highly localised to the close-surface area at the "trailing" and "leading" edges of contact. Bulk fatigue damage is low and for any surface-initiated crack, propagation until failure is not expected.

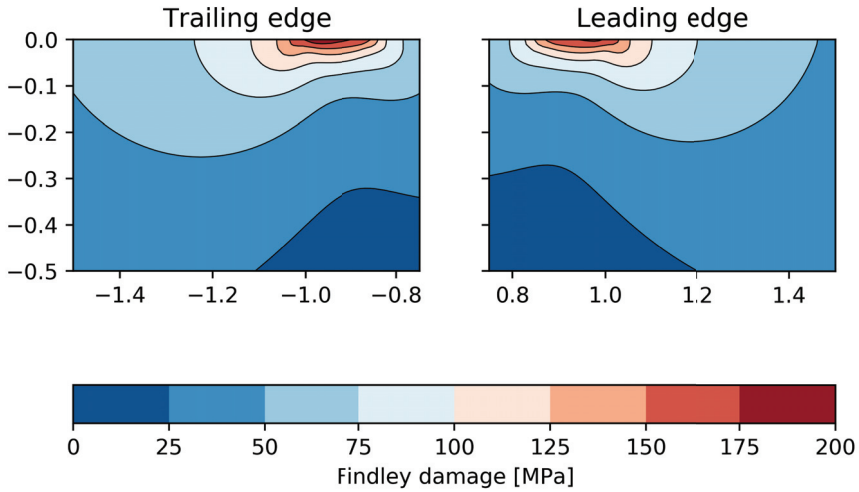

Figure 2.29: Findley damage parameter ($k = 0.1$) for fretting contact () without bulk fatigue loading.

In the case of fretting fatigue (Figure 2.30) however, damage is more localised around the trailing edge of contact. Subsurface fatigue loads are severe enough to potentially propagate fretting-initiated cracks to failure.

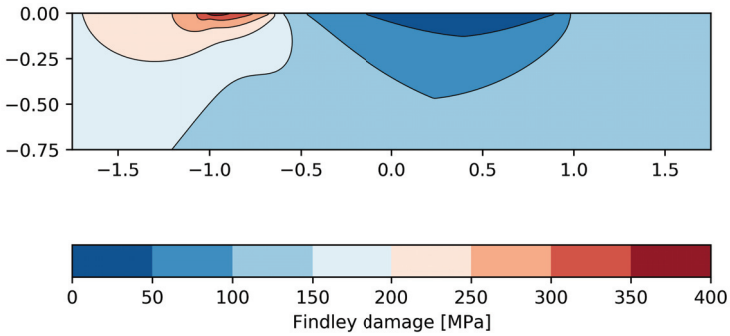

Figure 2.30: Fretting fatigue case Findley ($k = 0.1$)

2.7.9 Dovetail fretting fatigue

In paper IV, Findley critical plane parameter was used to calculate fretting fatigue crack initiation in dovetail experimental tests. Good agreement was found when used in combination with averaging schemes from the Theory of Critical Distances (see Section 2.4.3. As described in Section 2.5.2, normal and shearing tractions oscilate in-phase and cause the slip to vary over the contact surface.

Crack initiation mechanisms are smeared over an area. This is demonstrated in Figure 2.31 where Findley damage parameter is plotted for the specimen substrate. Very localised damage is found, as expected. By subsequent averaging, the Findley parameter was used to predict initiation life using Basquin's equations, See Paper IV in Appendix A.4.

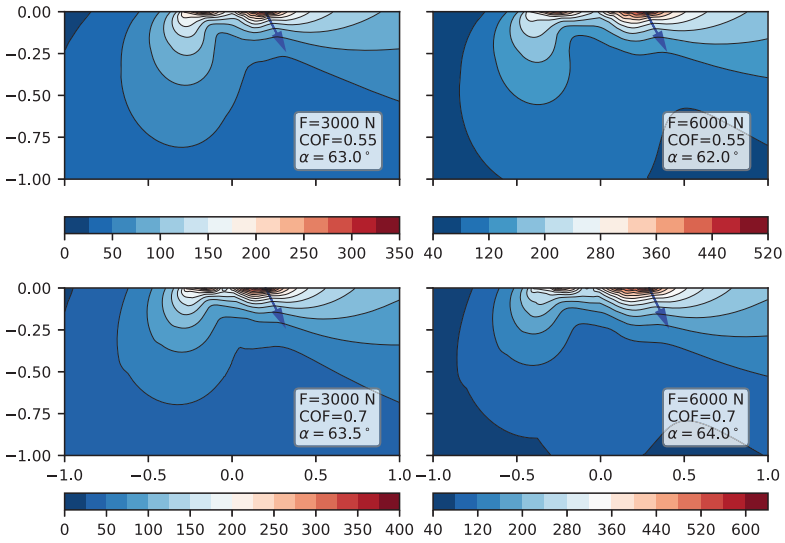

Figure 2.31: Subsurface Findley damage parameter with hot-spot cracking direction indicated by arrow.

2.8 Choice of programming languages

The choice of programming language and implementation plays an important role in numerical analysis and is therefore honored with a brief section here. During this thesis, mainly *C++* and *Python* were used, but also *Fortran* and the relatively young language *Rust*. These languages have different strengths and weaknesses with respect to numerical fatigue analysis and they are outlined in the following.

Python is one of the most obvious choices for mechanical engineers. It is an easy to use scripting/programming language that does not require separate compilation steps. Library support in Python is excellent, the numerical libraries *numpy* and *SciPy* provide efficient array operations with linear algebra and other relevant algorithms. The plotting library *matplotlib* provide visualisation tools and is used extensively for plotting in this thesis, see e.g. 2.21

and 2.20. Python is also very explicitly written, making it easy to read and understand. An example of this is shown in Appendix A.5 where convex hull is implemented in Python. Notice how similar it is to the pseudo-code presented in Algorithm 2. Since memory management is handled internally, a large burden is hidden from the user. This is why Python is an excellent scripting language for such numerical work, particularly in prototype stages. However, Python may be slow for CPU-intensive work compared to compiled languages. In critical plane analyses, Python using numpy libraries was found to be up to two orders of magnitude slower than compiled languages. This difference was lowered to approximately one order of magnitude by using so-called "Just-in-time" (JIT) compilation. By using JIT libraries, Python code is compiled to machine code making use of e.g. CPU vector operations, and even opens up for parallelisation. See e.g. *Numba* library.

In this thesis C++ was predominantly used for the CPU-intensive work that is critical plane analysis. Advanced C++ compilers are able to optimise many of the operations. Using the vast *Boost*-libries and Eigen3 for linear algebra, C++ is an especially powerful language for numerical calculations. Multi-threading is also fairly accessible using e.g. *OpenMP*. These libraries were used to implement efficient critical plane analyses in Paper II (See Appendix A.2). However, C++ is very large and complex language which can be difficult to use and easy to make errors. Convex hull algorithm is for demonstration shown in appendix A.5. Rust is a relatively new programming language that have grown in popularity among researchers [106]. Rust is a low-level compiled language like C++ but with additional mechanisms for handling memory, thereby reducing the potential for bugs especially in multi-threading situations. High-level functional abstractions and excellent tooling support (e.g. package manager and build tools) are some of the reasons for its popularity as an alternative for C++.

Many computational steps in critical plane analyses are trivially computed in parallel. For a given computational task, this means in practice that little work is required to separate the workload into multiple parallel tasks and this is the case when each parallel tasks have little or no inter-dependencies. In paper II, parallelisation was used on brute-force implementations of critical plane. where the search space was simply divided on a number of CPU threads. Each thread found its critical plane candidate, from which the global critical plane was found by comparing each threads maximum. On large, industrial models it may more make sense to parallelise on each material point. Adaptive scheme was found to offer only a slight improvement to efficiency. This is partly due to the brute-force methods to benefit from improved caching for more predictable code for the modern CPU. Note that the implementations in this thesis are by few means fully optimised and the efficiency and timing are only indicative.

Chapter 3

Experimental fretting fatigue

One does not simply study fretting fatigue without conducting any physical experiments. Experimental data and observations are essential in the field of fretting due to the complex and diverse mechanisms involved. Consequently, performing fretting fatigue tests is important for this thesis to be of any significant value. Due to the initial lack of fretting fatigue testing facilities, a considerable amount of resources were put into devising new experimental capabilities. These efforts will be summarised in this chapter. First, a brief review of the test methods used in the literature is presented in the following section for context.

3.1 Historical overview

Academic interest in fretting fatigue started with reports from plain fatigue tests with wear and fatigue cracks occurred at the specimen gripping joints [107]. One of the first test programs specifically aimed at surveying fretting was by Tomlinson [108] in 1927, however focusing on surface oxidation and wear. In a later study published in 1939 Tomlinson et al. [109], the authors wrote in the introduction "it is considered by some engineers that fatigue failures may be initiated by fretting effects, although it has to be admitted that there is no strong evidence either for or against this view". Moreover, the researchers reported the important observation relating cyclic slip with surface damage and that the repeated straining of contact surfaces could represent "some special type of fatigue action".

Warlow-Davies et al. [110] published in 1941 results from a study where fatigue specimens were first subjected to fretting corrosion on a separate machine. Surface damage was introduced to the cylindrical specimens by by attached clamps. Later fretting fatigue test configurations by other researchers applied the fatigue loads simultaneously with fretting contact using loading rings. Nish-

ioka and Hirakawa [111] applied cyclic bending to a cantilever beam while fretting the surface with a pad ("shoe") connected to two eccentric wheels from which the phase and relative magnitude between fatigue loading and slip could be controlled. Contact pressure was applied using a "proving ring" measured using strain gauges.

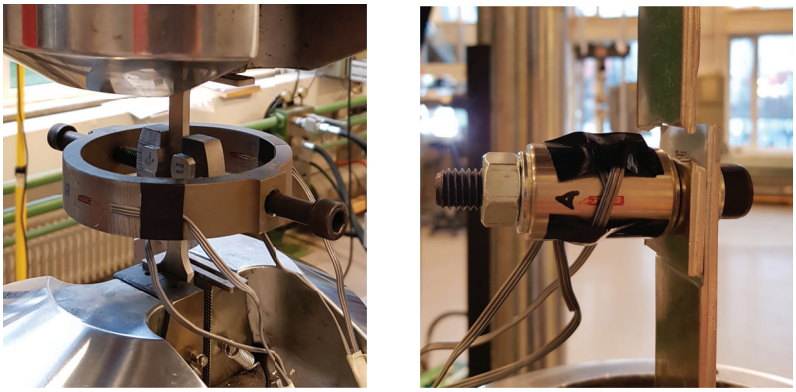

Figure 3.1: Clamping ring and lap-joint fretting fatigue tests used in this project.

Clamping mechanisms similar to the metal ring used by Nishioka and Hirakawa became a popular device for applying fretting contact to fatigue specimens. Correspondingly axially loaded fatigue samples were fretted by proving rings, either using "bridge-type" or by some pad which was retained from moving along with the surface strain. This way, both bulk fatigue loading and surface fretting is applied using a single, linear actuator. Early adoptions often made use of rotating motors with eccentric wheels to convert to oscillating motion [111]. However, with the industrialisation of axial fatigue machines, using the already established test facilities of plain fatigue introduced an opportunity to easily perform fretting fatigue tests with additional clamping devices.

A vast number of different methods and test were devised throughout the twentieth century and in 1992 there was an attempt to start standardisation of the fretting fatigue test [112]. However, there is still no accepted generic standard [113]. The more recent ASTM E2789 standard [114] from 2015 provides only guidelines and general requirements for conducting a fretting fatigue test program. While it provides definitions and terminology for testing, it does not make suggestions toward specific test setups.

Hills and Nowell summarized in 2009 [115] the most important features with fretting fatigue testing. They argue that the standardisation of fretting fatigue test geometries will make it easier to compare different sets of results, but standardisation may also restrict the *diversity* of test results and hence make them somewhat less helpful for understanding fretting fatigue as a whole.

Early fretting fatigue tests made use of single-actuator machines where pads, usually of bridge type, were clamped onto the specimen using proving rings

[116]. The clamping force is therefore constant as long as the wear was negligible. The Japanese standard *JSME S 015-2002* uses this test configuration [113]. More advanced, bi-axial test rigs permit the bulk fatigue load to be controlled independently from the contact loading. Early fretting tests at Oxford University used the fretting bridge on dogbone specimen, but during the end of 60s, they developed a test rig using Hertzian contact and electromagnetic resonance to generate the shear forces [117]. With this, the contact stresses, slip and displacements were controlled and these tests had a high degree of repeatability. Additional generelisations were made that permitted independent control of shear and bulk forces in the specimen. This was also tested for complete contacts with a self-aligning property avoiding rotation of the shear forces. The new arrangement have three independent actuators for the normal, shearing and bulk loads.

Figure 3.1 shows one of the test-rigs used in the prototyping stage in this project using clamping ring. Strain gauges are attached to the outer and inner surface of the clamping ring and are used to control the clamping force in the bolts. The strain gauge readings were first calibrated by loading the ring in a load cell. A designated jig was manufactured to simplify the assembly of the specimens as symmetrically as possible. The proving ring was not supported by other means than the contact pads, which unfortunately cause some inertia forces to affect the fretting contact. Nonetheless, the test rig prototype was used on a batch of aluminium samples and fretting initiated fatigue cracks were found. *In-situ* strain gauge readings allows for clamping force to be monitored during test. As expected, large scatter is found in the load-life plot due to the easily misaligned clamping arrangement. For the next iterations of this test, the mass of the ring is to be reduced and alternatively with additional supports, see e.g. Sabsabi et al. [118].

Another simple test fixture, is the plate lap-joint. When designing such joints, engineers often rely on standards like Eurocode 3. The bolted connection is designed to carry loads in shear and fatigue action and fretting can affect the area surrounding the bolts, greatly reducing fatigue resistance [28]. If clamping forces are high enough, the the joining plates can "recede" and circular partial-slip situation may surround the bolt vicinity. Clamping load is applied to the bolt by using a torque wrench with pre-determined torque. The losses in the bolt while tightening however cause the real clamping force to be unknown. Consequently, axial strain gauges are attached to the sleeve from which the clamping force can be calculated, see Figure 3.1. Nevertheless, such plate joints enable very accessible means for fretting fatigue experimental observations. The lap-joint shown in Figure 3.1 was developed and calibrated, but no experimental test campaigns are included here. It is argued that such tests are very suitable for educational purposes in mechanical engineering to provide testing experience and increase fretting fatigue awareness.

3.2 Dovetail joint

Driven by the development of aircraft turbine engines, much research have focused on fretting fatigue in turbine blade dovetail joints, see Figure 3.2. In these applications, mass is to be minimised whilst pursuing reliable operations in exceptionally harsh conditions. Turbine blades are attached to a rotating disk using dovetail or fir-tree joints. The joints are subjected to low-cycle fatigue loading due to centrifugal forces from engine start-up and high-cycle fatigue loading owing to mechanical and aerodynamic-induced vibrations. These loads cause microscopic relative sliding motion between the dovetail and the rotating disk, producing fretting damage. Failures by fretting fatigue was not uncommon [119].

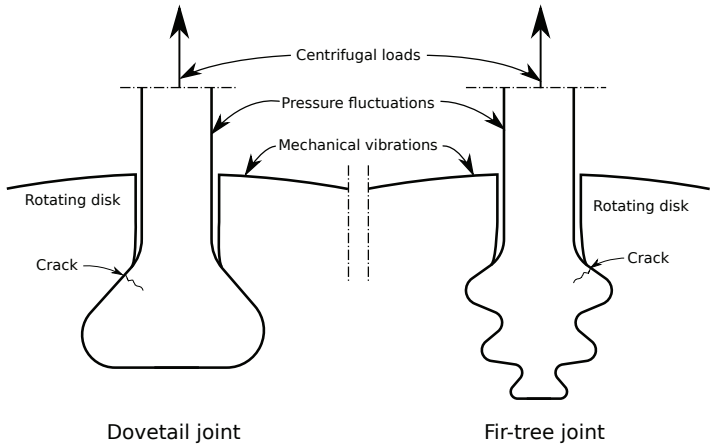

Figure 3.2: Two different mechanical joints to attach turbine blades: dovetail and fir-tree.

In Paper IV (see Appendix A.4) a new test rig based on the dovetail joint was developed and demonstrated with a set of Grade 5 titanium alloy specimens. The main idea behind adopting the dovetail arrangement here, is that a relatively simple test rig is obtained that can be readily mounted in most fatigue machines. Many dovetail-based fretting fatigue test rigs have been demonstrated in the literature, see e.g. [69, 67, 71, 120, 121, 122]. The original dovetail testing arrangements were generally used to replicate the fretting action in real turbine dovetail joints, but has become a popular test rig to produce fretting fatigue test results for more general use; comparing material combinations, load levels, palliatives etc. The main novelty of the test rig demonstrated in Paper IV is the idea of testing two specimens at the same time and using a torsional actuator to provide the secondary source of vibration. This way, mechanical vibrations can be simulated in addition to the axial centrifugal load.

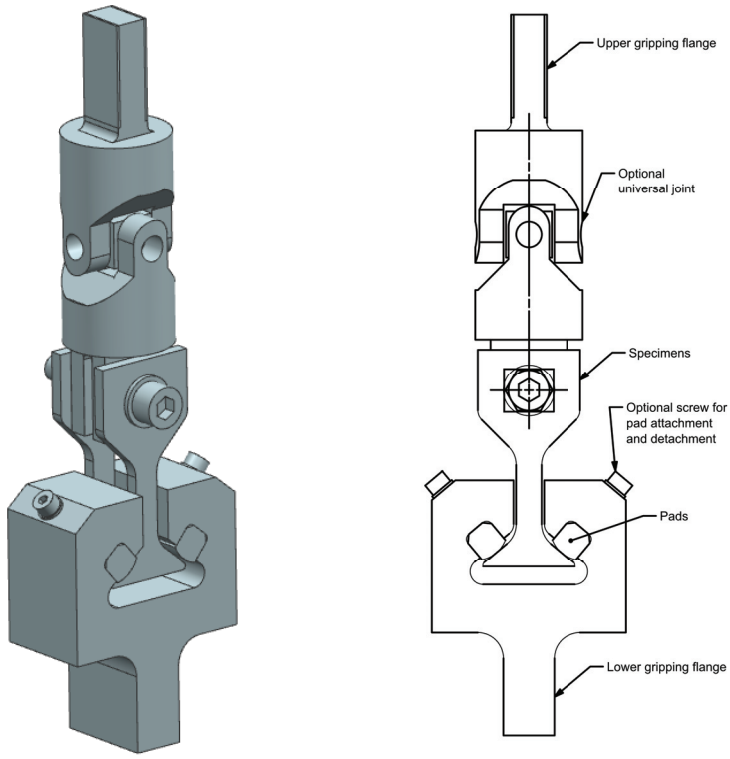

Figure 3.3: Dovetail arrangement used as test fixture in Paper III.

The demonstration of the dovetail test rig in Paper IV made use of a uniaxial fatigue machine, applying axial loads to a single specimen at a time. Load and displacement were monitored during testing and a very simple stopping criterion was employed based on the continuously monitored displacement. Tests were stopped if a jump was detected in the displacement signal. Note that this displacement includes the stretching on the rig itself and therefore includes the universal joint (See Figure 3.3). A subset of specimens were additionally equipped with strain gauges on both sides in order to more accurately record specimen behaviour during the test (see Figure 3.4). High frequency recording of load, displacement and strain gauge data for both sides were stored for post-processing and analysis.

Figure 3.4: Titanium specimen with strain gauges attached to both flanks on the dovetail specimen

Test rig was used on a complete series of 6082 aluminium and Ti-6Al-4V titanium alloys, two commonly used materials in fretting fatigue testing literature. The titanium alloy results were documented in Paper IV and correlated with predictions using finite element analyses. However, the aluminium results are not published yet. Aluminium and titanium alloy specimens were geometrically similar and some aluminium samples failed due to regular fatigue in the neck fillet instead of fretting fatigue. Here, it was found to be necessary to place 1 mm shims behind the aluminium fretting pads, see Figure 3.5. This "spacer" cause the contact to move upwards on the dovetail specimens, reducing the bending stress in the neck. Specimens were also milled at the bottom to slightly increase the bulk stress for fretting fatigue crack propagation.

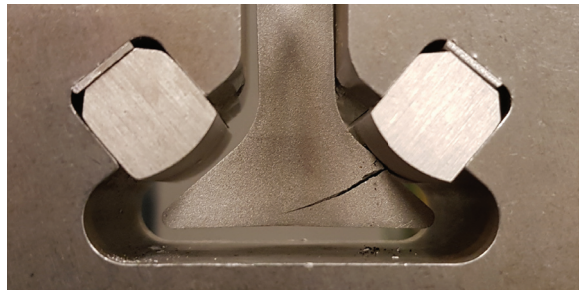

Figure 3.5: Aluminium dovetail specimen

All titanium specimens however failed by fretting fatigue, except two run-outs. Titanium specimens were inspected after failure using Scanning Electron Microscope (SEM) and light microscope. Figure 3.6 demonstrates how a fatigue crack initiated at the fretted area and propagated obliquely under fretting contact. For more SEM pictures, see Paper IV in Appendix A.4.

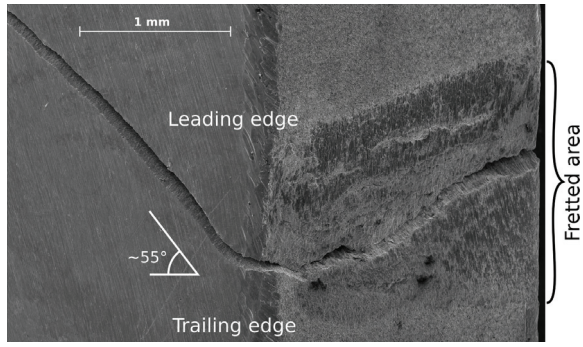

Figure 3.6: Scanning electron microscope of titanium specimen with *ad-hoc* spacers.

A digital camera attached to the light microscope was used to document the crack paths. High-resolution microscope images were obtained by an automated stitching process using Python and the open source framework libraries provided by OpenCV [123].

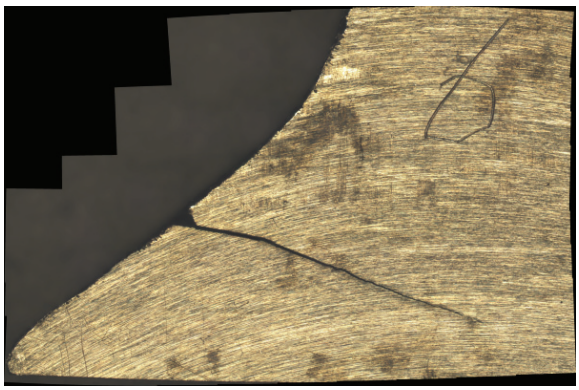

Figure 3.7: Stitched "high-resolution" microscope image.

Life predictions were made using the numerical framework demonstrated in Paper II. For details of the numerical work, see Section 2.7. Findley critical plane parameter with $k = 0.35$ was found to work well with Theory of Critical Distance (see Section 2.4.3). However, it is stressed that the results obtained are accompanied with a considerable amount of uncertainty: most notably is the EDM-wiring process that produces irregular surfaces with small, melted drops and micro-cracks. Fatigue crack initiation is dominated by macro-geometry of contact. The details of material microstructure are also not fully defined although its manufacturing process is known. Lastly, coefficient of friction is only assumed based on literature and not measured explicitly. Material plasticity was only seen in very small amount related to rubbing of surface asperities during the first few cycles and was therefore neglected in the analyses. For softer material, sharper-edge contact or higher loads, a plastic material model could be necessary. It is concluded that the simple study shown in Paper IV demonstrates the usefulness of the dovetail test configuration and its potential for more detailed fretting fatigue studies that are planned.

3.3 Clamping ring test

A variant of the bridge-type fretting fatigue test was build during this project as mentioned in Section 3.1. Using a proving ring, fretting contact is easily applied to "dogbone" specimens as shown in figure 3.8. The proving ring was manufactured using water jet and threads were subsequently applied for the clamping bolts. A specialised gripper bracket was made to permit the re-use of clamping pads from the dovetail test program which was described in the previous section, this bracket is shown in the following figure.

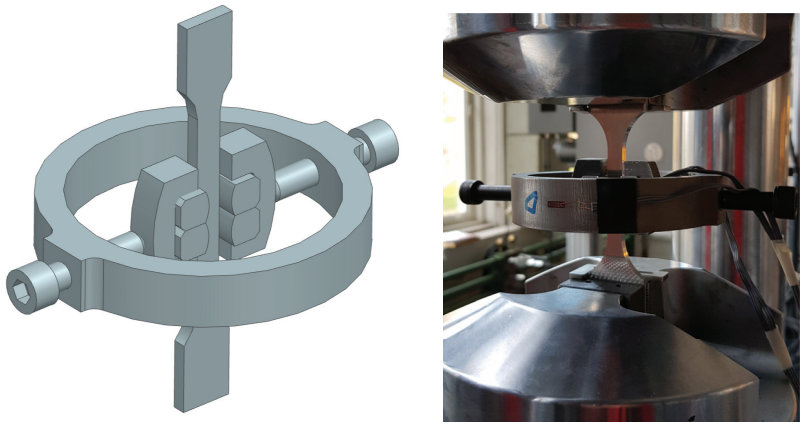

Figure 3.8: Clamping ring dogbone fretting fatigue test

Strain gauges were attached to the clamping ring to monitor the clamping loads. The clamping load was calibrated with a load cell; a series of known forces was applied to the bolts and strains in the proving ring was recorded. A series of aluminium specimens was tested and the load-life results are shown in figure 3.9. Note however that this test program was only an early-stage prototype and that the data is not particularly useful.

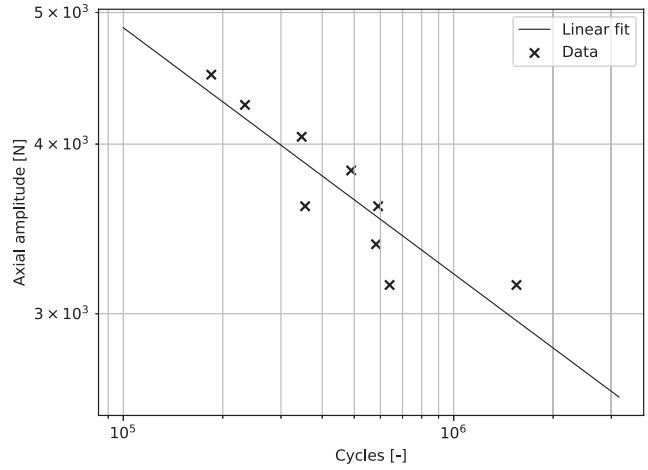

Figure 3.9: Life versus load for prototype dogbone specimens in aluminium. Considerable scatter is largely related to alignment difficulties.

The prototype test rig demonstrated in this section is very simple and ap-

proachable but has some inherent problems. Firstly, the weight of the rig itself cause unsymmetrical loads to the specimens tested. Mass of this ring should be minimised to ensure good dynamical behaviour and to permit higher testing frequencies. Secondly, the fixture consist of many loose parts which makes it difficult to assemble and load the specimens symmetrically. A special jig was used to facilitate this process but results still demonstrated considerable scatter as shown in Figure 3.9. Additional support to the clamping ring and pad bracket will improve the assembly procedure. Axial load cells should also be added to the bolts may provide better contact pressure recordings.

Chapter 4

Friction dynamics simulation

As friction is one of the most important parameters in fretting contact, it is given special attention in this chapter. More specifically is this chapter aimed at numerically exploring simple friction models for lumped-mass systems related to fretting. Non-linear effects due to friction cause quite simple discrete models to display rich dynamic behaviour and reproduce well-known physical properties of frictional contacts.

4.1 Friction modelling

Most fretting analyses use Amontons-Coulomb friction laws where the sliding resistance is assumed to be proportional only to the normal load through the coefficient of friction (COF), see Equation 2.5. This formulation is adequate for many engineering applications. COF are often obtained from tabulated data and chosen based on the relevant material combination. The actual friction however, is a *systems* parameter and depends on loads, contact geometry, environment (e.g. humidity, temperature) and many others [124].

Friction is clearly one of the chief parameters influencing fretting behavior as its determines the amount of slip and the substrate stress gradients coming from contact tractions. In Section 2.5.1, it was discussed how fretting behaviour strongly depends on the friction properties of the contact and some simple analytical expressions were shown in Section 2.1. Fretting contacts were historically described to attain one of three different sliding regimes: stick regime, partial slip, and gross sliding. In a "stuck" contact, bulk sliding is retained across the contact area but in reality, microscopic slip can, and most likely will, occur locally. Hence, a more appropriate way of separating the sliding regimes is partial slip, mixed stick-slip and gross slip [125, 89].

Friction properties in fretting wear and fretting fatigue are known to display temporal variations. Since the contacting surfaces experience surface modifica-

tions through wear and plasticity, this is to some degree expected. Complete fretting contacts are seen to sometimes experience *frictional shakedown* where the frictional slip eventually vanishes and the contact reaches a fully adhered steady state [126, 127, 128]. These shakedown phenomena have been compared with Melan's theory for plasticity [129].

Coulomb friction applies strictly only globally to contacts in gross sliding but through the work of Hertz [5], Cattaneo [10], Mindlin [130], Ciavarella [13] and Jäger [12] partial slip problems can be analysed analytically for certain smooth elastic contacts. See section 2.1. General frictional elastic contacts are usually solved using finite element methods and in Section 2.5 it was discussed how the non-linearity of frictional contacts are solved using such numerical methods. Nevertheless, most fretting analyses using numerical or analytical methods are static or quasi-static, neglecting inertia effects.

A number of deviations from Coulomb friction have also been found related to the dynamics of the system. Most well-known is perhaps the Stribeck effect [131], where even for dry contacts, the friction force experience a negative slope with respect to the relative sliding velocity, see Figure 4.1. A number of *velocity-weakening* friction models have been proposed to capture this effect, see e.g. [132]. The negative slope in velocity-weakening friction models are known to produce friction instabilities leading to self-excited vibrations with very rich dynamic response and chaotic solutions.

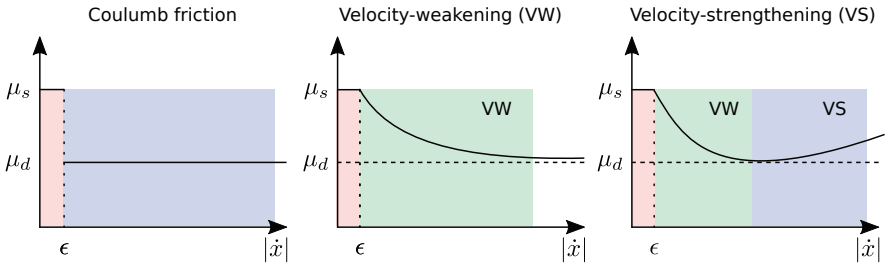

Figure 4.1: Three different friction functions.

A large body of research exist on friction dynamics using simple discrete models [133, 124]. Self-excited vibrations are found in robotic applications causing undesirable motion. The irregular and chaotic motions produced by stick-slip instabilities have been simulated numerically using single degree of freedom lumped-mass models, see e.g. Popp al.[134]. Unstable friction response have also been found to cause brake squeel [135] and seismic events [136]. The classical Burridge-Knopoff (BK) model [137] was introduced as early as 1967 to numerically study earthquake dynamics. The BK model consists of a one-dimensional chain of spring-connected masses on a slow-moving friction surface. Since the introduction in the sixties, many researchers have used similar models to reproduce various frictional response, see e.g. [136, 138, 135]. Such models have also been used to analyse applications where friction is deliberately intro-

duced to fretting contacts as a means of damping external vibrations. Sanliturk et al. [139] used a set of spring-dampers in parallel to analyse friction dampers in turbine blade assemblies. For an overview of friction models across different fields see Berger (2002) [124].

Research on the effects of rate-and-state dependent friction models in reciprocating motion is limited. Mulvihill et al. [140] found non-Coulomb features for gross sliding to relate to wear-scar interactions. Shalapko and Tarasova [141] analysed surface-layer effects in fretting fatigue using a two-degree of freedom system subjected to reciprocating motion and found their model to produce chaotic solutions. Thøgersen et al. [142] analysed frictional contact using distributions of micro-junctions and found the macroscale sliding to depend on relative velocity.

A natural question that arises is whether a static friction model is sufficient to model the frictional behaviour in fretting contacts. Another interesting question is whether simple lumped-parameter models can simulate surface interactions relevant for fretting contacts. Stick-slip is mainly a low-velocity phenomena where the negative slope of the friction curve is steep. As gross slip fretting contact is subjected to a sinusoidal shear force (or displacement), the velocity too cycle harmonically and moves through a wide range of velocities. However, as the fretting strokes are small for many cases of fretting, instabilities are usually suppressed. Nonetheless, single degree of freedom systems have been shown to produce interesting dynamics and to represent various friction phenomena numerically. They can give valuable insights into stick-slip behaviour and various velocity effects. In Section 4.2 a single DOF model is used to analyse reciprocating fretting motion. Partially stuck contacts found in many fretting applications obviously needs more than one DOF to represent the spatial variations. In Section 4.3 one-dimensional chains of blocks are used to investigate dynamic behaviour of Hertzian fretting contacts. These models have similarities with the Burridge-Knopoff models but are ascribed reciprocating motion and varying (Hertzian) contact profiles. This chapter demonstrates part of a project to model the complex dynamic friction interactions and to study the effects of time-varying (state-dependent) friction of fretting contacts.

4.2 One-dimensional friction model

Reciprocating fretting contact is analysed using a one-dimensional single degree of freedom (SDOF) lumped-mass model as shown in Figure 4.2. It was described in previous section that rich dynamics can be found even for SDOF models due non-linear rate-dependent friction functions, which are demonstrated in this Section. The SDOF model will be used to investigate parameters related to fretting contact but more importantly form the basis for multi-degree of freedom (MDOF) model demonstrated in Section 4.10.

Consider the single block with mass m, suspended by a linear spring with stiffness k and viscous damper with damping coefficient c. The block is pressed onto a friction surface ("belt") with pressure p and coefficient of friction μ.

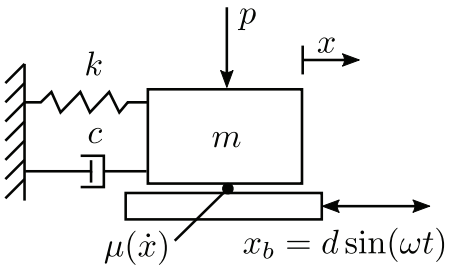

Figure 4.2: Discrete friction system for a single degree of freedom. A constant pressure P presses the block onto a rigid belt causing a shear force transmitted from the belt through coefficient of friction μ.

The equation of motion for this single degree of freedom system is

$$m\ddot{x} + c\dot{x} + kx = f_\mu(v_{rel}) \tag{4.1}$$

where x is the spatial displacement of the block. Dots denote derivative with respect to time t, i.e. $\dot{x}$ and $\ddot{x}$ is the velocity and acceleration of the block, respectively. The right hand side f_μ is the friction force which depends on the relative velocity between the block and belt, $v_{rel} = \dot{x} - v_b$.

The belt is prescribed a harmonic oscillation by

$$x_b(t) = d\sin(\omega t) \tag{4.2a}$$
$$v_b(t) = \omega d\cos(\omega t) \tag{4.2b}$$
$$a_b(t) = -\omega^2 d\sin(\omega t) \tag{4.2c}$$

where $\omega = 2\pi f$ is the angular velocity, f is the forcing frequency and d is the displacement amplitude ("fretting stroke"). A constant pressure p is exerted on the block, causing friction between the block and the belt. The shear force depends on the coefficient of friction (COF) μ, which in turn is a function of relative velocity. Denoting the COF at a given time as

$$\mu = \begin{cases} \mu_s & \text{for} \quad v_{rel} = 0 \\ \mu_d(v_{rel}) & \text{for} \quad v_{rel} \neq 0 \end{cases} \tag{4.3}$$

where μ_s is the static COF and μ_d i is the dynamic, rate-dependent coefficient of friction (See Figure 4.1). Following from (4.3), the friction force is only piecewise continuous. The stick force is limited by the friction limit and is always opposite in direction with respect to the relative velocity. The friction limit is $\mu_s p$ and the friction force may thus be described by

$$f_\mu = \begin{cases} min(\mu_s p, |F_a|) \cdot sgn(F_s) & \text{for } v_{rel} = 0 \\ \mu(v_r, t)p \cdot sgn(v_r) & \text{for } v_{rel} \neq 0 \end{cases} \tag{4.4}$$

where F_a is the force required to accelerate the mass with the belt and $F_s = kx$ is the spring force (see Figure 4.4) and sgn is the signum function expressed as

$$sgn(\alpha) = \begin{cases} 1 & \text{for } \alpha \geq 0 \\ -1 & \text{for } \alpha < 0 \end{cases} \tag{4.5}$$

where α in this case is a dummy variable.
A simple velocity-weakening friction law is used here,

$$\mu_d(v_{rel}) = \mu_k + \frac{\mu_s - \mu_k}{1 + \delta|v_{rel}|} \tag{4.6}$$

where δ is a coefficient describing the slope of the friction as seen in Figure 4.3. Note that there is a number of different rate-dependent friction models used in literature and this was chosen for its simplicity. See Berger (2002) [124] for an overview over other models.

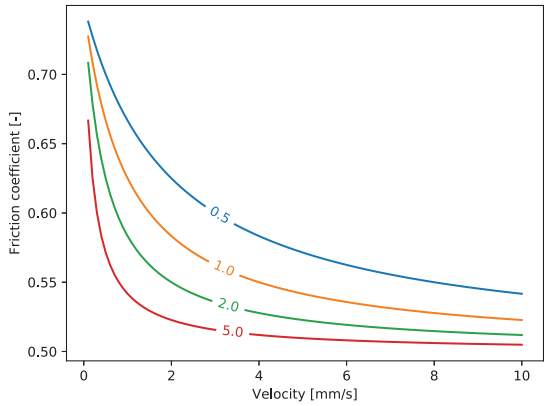

Figure 4.3: Friction curve for various values of scaling δ. Here $\mu_s = 0.75$ and $\mu_k = 0.5$

Physical quantities are specified instead of normalising the equations. The spring stiffness may be derived from the material constants and beam equations,

$$k = \frac{EA}{L}, \quad m = \rho AL \tag{4.7}$$

but for simplicity, the following quantities will be assumed for the remainder of this text: $m = 0.05$, $k = 10^5$, $\mu_s = 0.75$, $\mu_k = 0.50$ unless otherwise specified.

4.2.1 Damping

Equation (4.1) describes a forced harmonic oscillator with dissipation. For harmonically forced mechanical systems with sufficient dissipation, solution relaxes down to a steady state. Damping factor c controls the amount of dissipation of the system and this parameter is in reality difficult to quantify physically [143]. For fretting contacts, dissipation may be related to heat-generation from material straining and contact interaction, plastic work, sound etc. Here, linear velocity-dependent (viscous) damping force is assumed. From the characteristic polynomial of Equation (4.1), the *critical damping* for the system can be obtained and damping values are expressed as ratio of this critical value. Assuming for now purely stiffness-proportional damping, the damping ratio ξ can be expressed as

$$\xi = \frac{1}{2}\beta\omega \tag{4.8}$$

where β is the stiffness proportional damping factor and ω is the target frequency in radians. In engineering practice, appropriate damping ratios are often found to be $\xi = 0.01 - 0.1$ for a given target frequency [143]. The SDOF system has only one natural frequency ($\omega_n = \sqrt{(k/m)}$) and is forced with frequency ω. For most physical quantities relevant for fretting, forcing frequency is considerably lower than the natural frequencies of the system. It is clear from (4.8) that frequencies are damped differently for a given β. More on this is discussed for the multiple-degree of freedom system discussed in section 4.3

4.2.2 Results

The equation of motion (4.1) is integrated using the classical fourth order Runge-Kutta method (RK4). Details of the integration scheme is given in appendix A.9 for reference. The second order differential system is first rewritten as system of first-order equations and time is included in the state vector $\mathbb{u}$ for simplicity. The state vector and its tangent ("Jacobian") can then be written in vector form as

$$\mathbb{u} = \begin{bmatrix} u \\ \dot{u} \\ t \end{bmatrix} \quad \dot{\mathbb{u}} = \begin{bmatrix} \dot{x}_i \\ \ddot{x}_i \\ \dot{t} \end{bmatrix} = \begin{bmatrix} \dot{x}_i \\ \frac{1}{m_i}(F_s - F_r) \\ 1 \end{bmatrix} \tag{4.9}$$

Due to the transition between stick and slip states, the slope of the solution is only piece-wise continuous. To handle this in the temporal integration, one can either use a smoothing function or by "switching" the equation system [144]. Using a smoothing function cause the tangent to be continuous but results in very stiff equation near the transition. Such stiff differential equations may be difficult to integrate, often requiring a scheme with adaptive time-stepping. Using the switch model however, the tangent is calculated based on the current state of the block (stick vs slip). A "stick-band" is centered around the zero-velocity point, with a width of ϵ, see Figure 4.1. ϵ is here chosen to be 10^{-4}.

Time steps are usually chosen to be very small (10^{-7}) to minimise errors when transition between stick and slip, but also to avoid numerical instabilities if the time stepper would happen to fall in-between stick and slip.

Flowchart for the switching algorithm for the solution tangent is shown in Figure 4.4

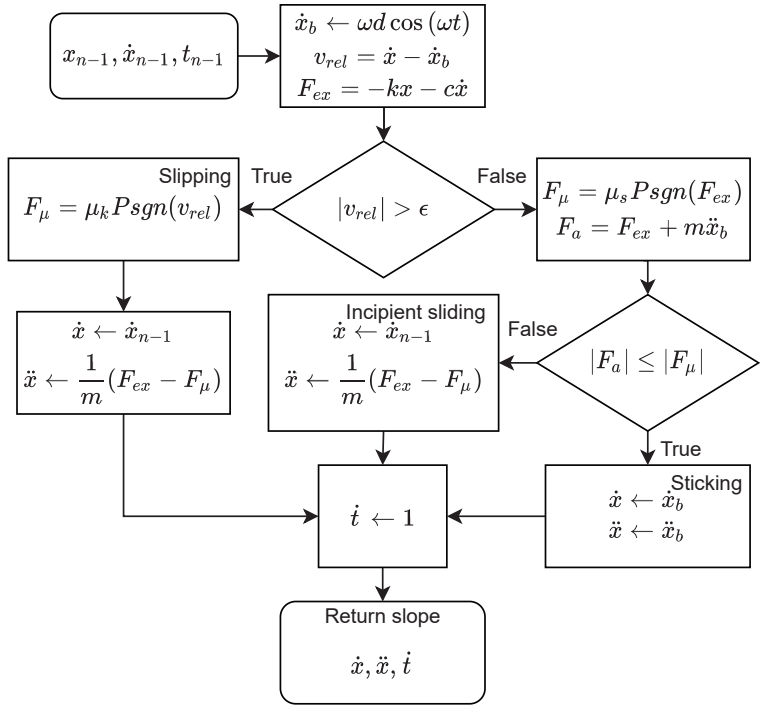

Figure 4.4: Flowchart for calculating the slope of the SDOF system

The phase space of the system described in Equation (4.1) is three-dimensional. Solution trajectories are visualised in Figure 4.5. The trajectory is demonstrated in (projected) two-dimensional and three-dimensional phase space. For some chaotic and irregular solutions, these visualisations are difficult to interpret as they appear to be random (see Figure 4.9). For some of these solutions, the three-dimensional phase space can be projected onto a two-dimensional phase space by taking intersections transversely to the trajectory flow. By recording long series of intersections with this plane, underlying dynamics can sometimes be appear in the projection plane. The periodic flow intersections with a specified plane is then recorded, known by *Poincaré map* after Henri Poincaré [145]. These visualisations are very popular tools in dynamic modelling and chaos theory and may be appropriate for some (rare) weakly dissipated friction system trajectories.

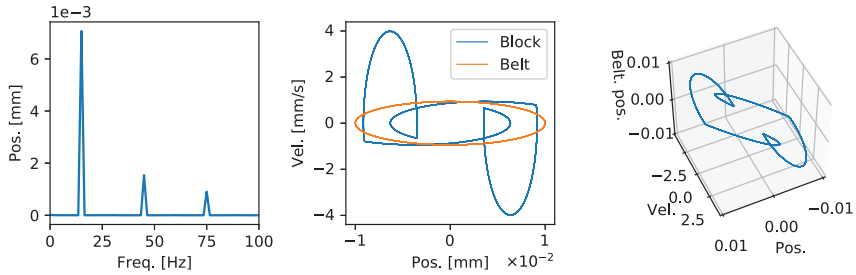

Figure 4.5: Example frequency and phase space for a weakly dissipated fretting contact in gross slip

Figure 4.5 demonstrates how the forcing frequency dominates the block behaviour mainly through first order (15 Hz) but also through third and fifth order (harmonics). The projected two-dimensional phase space show how the block have multiple attractors and velocity jumps as the belt change direction.

When friction force is large enough to resist shearing forces exerted to the block at outer limits of fretting stroke, block will adhere throughout fretting cycle. Thus after a small transient, depending on dissipation, block steady state solution will remain in stick. In this chapter, transient states are simply discarded as the steady-state behaviour usually define fretting damage. Sliding and sticking solutions are illustrated in Figure 4.6.

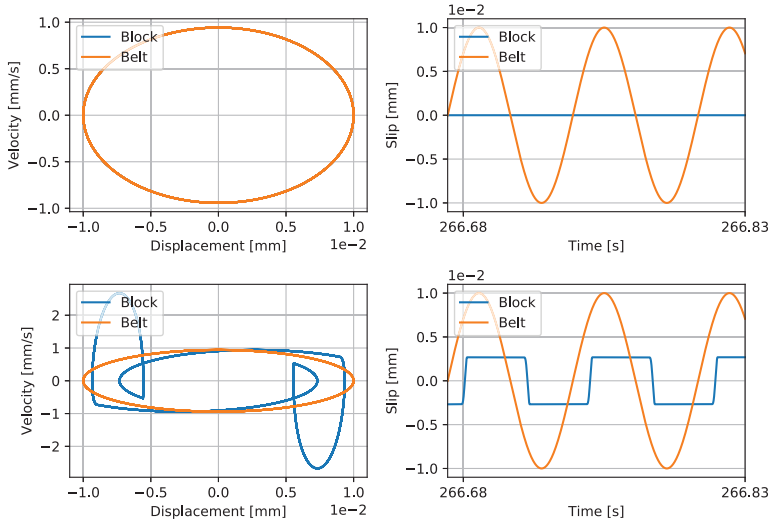

Figure 4.6: Comparing stick solution with slipping for single degree of freedom. Pressures are $P = 1500$ and $P = 1200$ for sticking and slipping solution respectively. Forcing frequency is $15Hz$, $\delta = 1$, $\xi = 0.05$.

As expected, solution is found to be very sensitive to the amount of dissipation: damping is found to suppress stick-slip behaviour. Chaotic solutions are not found for any relevant amounts of dissipation. The strong dependence on dissipation highlights the need to experimentally verify model and physical parameters before any qualitative analyses are to be hoped for. Figure 4.7 demonstrates how velocity jumps are suppressed by dissipation, but the slip amplitudes are only slightly affected by the damping ratio.

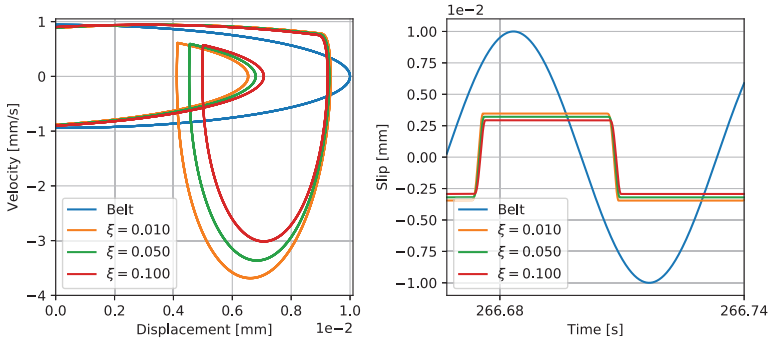

Figure 4.7: Solution for different values of damping ratio

Velocity of the block is also affected by the slope of the friction function (see Figure 4.3). For steep gradients, larger velocity jumps and slip amplitudes are found.

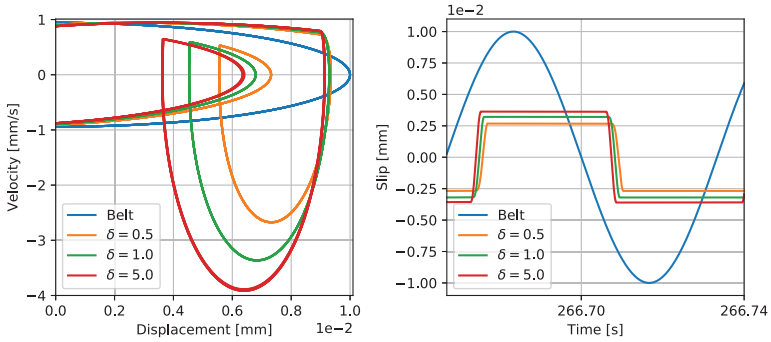

Figure 4.8: Solution for different values of friction slope δ

Irregular motion can be seen for very weakly dissipated systems. Apparent chaotic solutions are characterised by irregular trajectories in phase space and noise in the frequency space. Often, very little damping is needed to suppress chaotic behaviour. In dissipated systems chaos only occurs for rare combinations where the periodic bifurcations provide enough irregularity for the solution to diverge. Note that a common signature of chaotic behaviour is exponentially diverging of two initially close states. This phenomenon is not considered here.

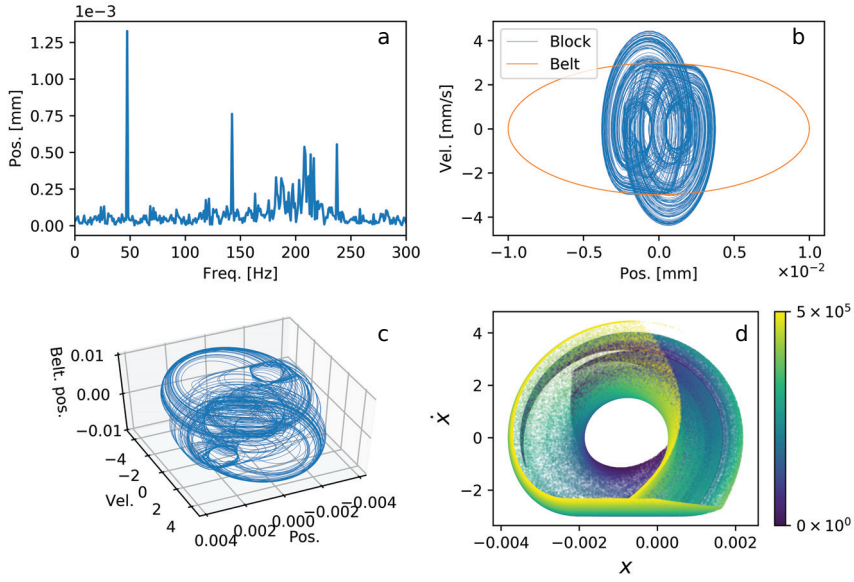

Figure 4.9: Apparent chaotic solution for weakly dissipated system at higher frequency ($\xi = 0.1\%$, $f \approx 47.46$ Hz, $\delta = 0.5$).

Figure 4.9 shows an example of apparent chaotic solution for weak dissipation and higher loading frequency. The frequency content of the pad displacement is broad-banded but dominated by the forcing frequency and its higher harmonics. In Figure 4.9*d*, intersections are taken at $x_b = 0$ to form a Poincaré map. Although the dimensionality of the state space in this visualisation is reduced by one, it is still difficult to interpret. Note however that such projections are not necessarily well-defined in the case of piece-wise continuous equations as in (4.1).

4.3 Multi-degree of freedom system

Attention is now turned to the frictional chain models similar to the Burridge-Knopoff-like systems. The idea is to obtain macroscopic fretting dynamical behaviour from a small scale ("micro"-model). The system described in Section 4.2 is therefore extended to N blocks forming a one-dimensional frictional chain as shown in Figure 4.10. The remainder of this section will for simplicity only consider $N = 100$.

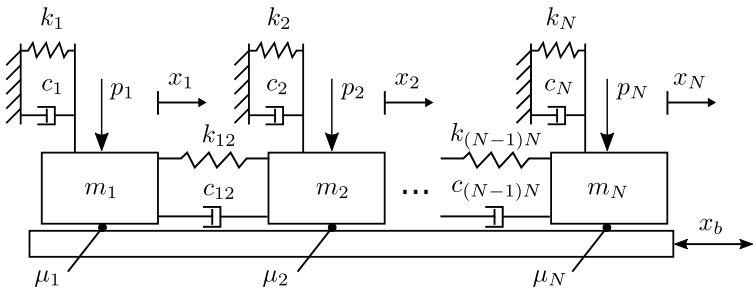

Figure 4.10: One dimensional friction chain with N degrees of freedom

The equation of motion for block i becomes

$$\begin{aligned} m\ddot{x}_i = &- k_i x - c_i \dot{x} \\ &- k_{(i-1)i}(x_i - x_{i-1}) - c_{(i-1)i}(\dot{x}_i - \dot{x}_{i-1}) \\ &- k_{i(i+1)}(x_i - x_{i+1})) - c_{i(i+1)}(\dot{x}_i - \dot{x}_{i+1}) \\ &+ F_{\mu,i} \end{aligned} \tag{4.10}$$

where $F_{\mu,i}$ is the friction force for block i which in general is a function of both velocity and state history. Rate dependency accounts for velocity-weakening (Stribeck-effects) and history-dependency can be used to model e.g. the friction evolution seen in fretting experiments. The pressures p_i can be used to ascribe spatially varying pressure. Here, Hertzian pressure profile will be used, see Equation (2.1), but with a small number of free blocks on each end of the chain.

For simplicity, in the following all intermediate springs will be ascribed the same stiffness k and spring to ground is $k_i = k/N$. All blocks will also have the same mass $m_i = m/N$. This system will have a series of broadly spaced natural frequencies, where the first natural mode corresponds to all blocks oscillating synchronously. The first natural frequency (in Hz) is hence

$$f_0 = \frac{1}{2\pi}\sqrt{\frac{k_i}{m_i}} \tag{4.11}$$

the highest natural mode of the system corresponds to all masses oscillating in opposite phase, i.e. having the natural frequency f_N (in Hz)

$$f_N = \frac{1}{2\pi}\sqrt{\frac{4 \cdot k_{12} + k_1}{m}} \tag{4.12}$$

Since mass and stiffness are scaled with respect to the SDOF model, first natural frequency is the same for this as in the previous section. The highest frequency will however increase with the number of blocks as springs in series should amount to the same overall stiffness, see Equation (4.7). This may cause problems for systems where N is large as the critical time step may become quite small.

4.3.1 Damping

In engineering practice Rayleigh damping factors are often chosen based on two (usually natural) *target frequencies*. As described in section 4.2.1, Rayleigh damping affects frequencies differently. The damping can be assumed to be a linear combination of mass and stiffness properties of the system. By assuming a linear damping relation, natural modes of the system remain uncoupled. This is numerically convenient but the physical reasoning is not always clear. Nonetheless, mass-proportional damping can be viewed as viscous damping which may result from fluid interactions at the surfaces. Stiffness-proportional damping may be thought to model dissipation from the material strain work. Consider the damping matrix $\boldsymbol{C}$ written as

$$\boldsymbol{C} = \alpha \boldsymbol{M} + \beta \boldsymbol{K} \tag{4.13}$$

where α and β are the Rayleigh damping coefficients related to mass and stiffness respectively. $\boldsymbol{M}$ and $\boldsymbol{K}$ are the mass and stiffness matrices. Matrix representations of these relations is convenient, but recall that explicit integration is used here and matrices are avoided in the solution. Similarly to SDOF demonstrated in Section 4.2, damping may be expressed as a ratio of critical damping. By entering Equation (4.13) into the characteristic equation of motion (4.1), the damping ratio for a given frequency f may be obtained by

$$\xi_f = \frac{\alpha}{2\omega_i} + \frac{\beta\omega_i}{2} \tag{4.14}$$

where ω_f is the target frequency in radians. There are two particularly important frequencies related to the frictional chain demonstrated in this section. That is the first natural frequency and the forcing frequency. As described in previous section, natural frequencies of the friction chain will span a wide spectre of frequencies which are higher than fretting forcing frequency. This means that forcing frequency and natural frequencies will receive different amounts of damping. For simplicity, damping is still assumed to be stiffness-proportional and thus only one target frequency is needed. For the remainder, damping ratios will be given wrt. the forcing frequency ξ_f or first natural frequency ξ_n. Ascribing an amount of damping ξ_nn the forcing frequency will be very lightly damped.

As dissipation is most likely affected by several different frequencies, some low-frequency (mass-proportional) damping is most likely appropriate, see Figure 4.16. Equation (4.14) can be rewritten to obtain the damping factors by

$$\begin{aligned} \alpha &= \frac{2\omega_1\omega_2}{\omega_2^2 - \omega_1^2}\left(\omega_2\xi_1 - \omega_1\xi_2\right) \\ \beta &= \frac{2}{\omega_2^2 - \omega_1^2}\left(\omega_2\xi_2 - \omega_1\xi_1\right) \end{aligned} \tag{4.15}$$

where ω_1 and ω_2 are the target frequencies and ξ_1 and ξ_2 are the corresponding frequencies. In practice these are often chosen to be $1-5\%$ of e.g. first and

third natural frequencies, but should in general be measured experimentally.

4.3.2 Results

In the following, MDOF model (Figure 4.10) will be simulated for a whole range of different parameters. Most interestingly here will be the general and qualitative solutions, demonstrating how different parameters affect the model and the resulting behaviour. However, it is stressed once again that no quantitative physical results are unavailable and that the models remain theoretical until a thorough experiment and calibration effort is made.

Hertzian contact pressure profile (see Equation (2.1)) is assigned to the model, but keeping five free blocks at each end. Pressures p in this section is referred as the peak pressure on center block. Forcing frequency is 15 Hz and fretting stroke amplitude is $d = 0.01$ mm.

Figure 4.11 show how higher contact pressure cause center blocks to stick whilst the contact edges experience minute relative sliding with the belt. For low contact pressure, contact enters gross sliding regime. In this regime shear forces cause all blocks to slide, revealing how the center block abruptly alters between sticking and slipping state. Local slip events are also evident for the outer blocks as oscillations in slip almost following the belt.

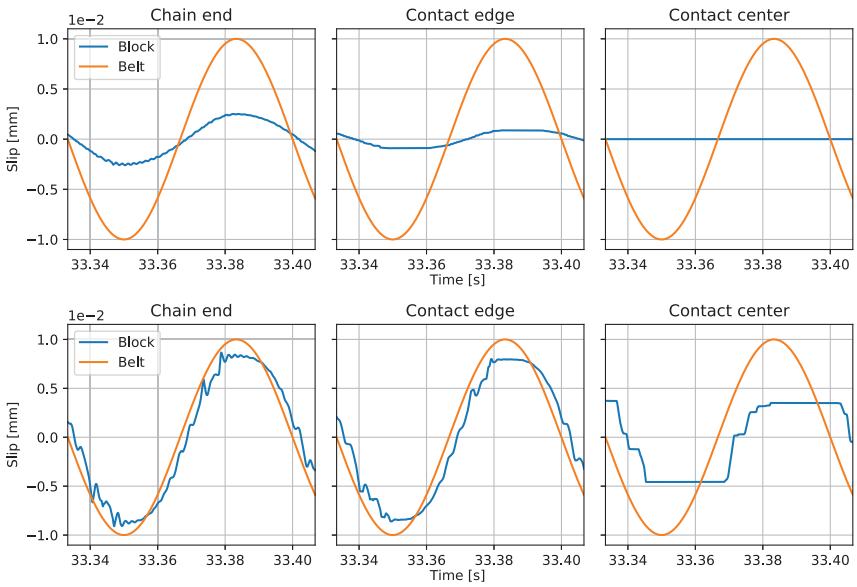

Figure 4.11: Different degrees of freedom for partial stick and gross slip regimes. Demonstrating difference between nominally stuck contact and gross sliding. Upper row: Partial stick solution for $p = 100$, lower row: gross slip for $p = 10$.

Hysteresis loops ("fretting cycles") are calculated by integrating the shear

force over contact and plotting as a function of belt displacement. An example is shown in Figure 4.12. For higher contact pressures, only a small subset of blocks slide, thus having the state of partial slip. Very local slip events at the contact edges cause small oscillations in the contact shear. The hysteresis area may be thought to represent the frictional work. The gross slip regime dissipates more friction energy which is related to increased fretting wear and lower cracking probability due to smaller peak shear stress.

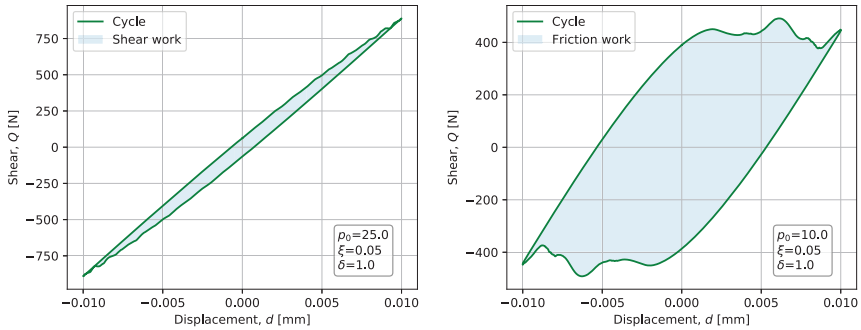

Figure 4.12: Comparing partial slip with grossly sliding hysteresis.

Quite irregular motion is seen for the gross sliding fretting loops, and they are perhaps more suitably studied using statistical analysis. Figure 4.13 demonstrates the fretting loop for a contact in gross slip. Small local slip-events are seen to cause oscillations at the end points

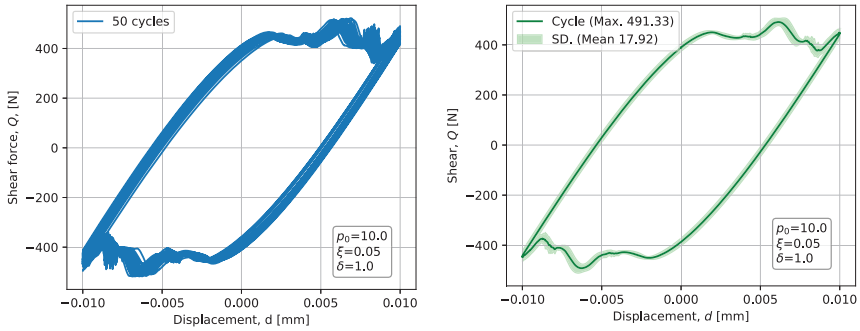

Figure 4.13: Simulating 50 fretting cycles and corresponding mean and standard deviation plot.

The macroscopic behaviour of the contact is found to be insignificantly affected by the slope δ of the friction function. Peak shear values are found to

vary only slightly but for steep friction function, the fretting loop is seen to be smoother.

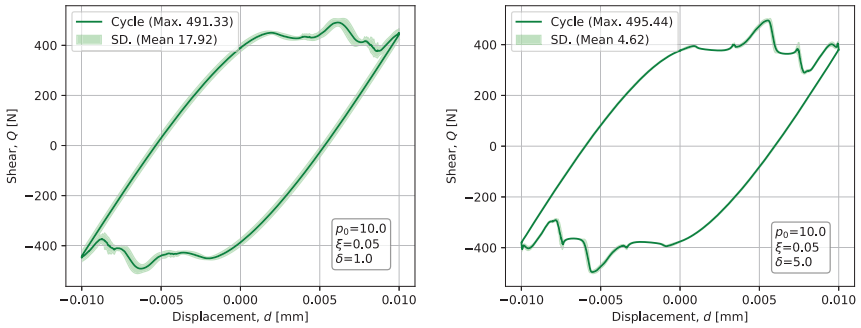

Figure 4.14: Comparing hysteresis loop for different values of friction slope δ. Less cyclic variation is seen for steeper friction slope.

For increasing stiffness-proportional damping, hysteresis loop becomes decreasingly irregular as seen in Figure 4.15. However, far out oscillations are increasingly abrupt which is most likely unphysical.

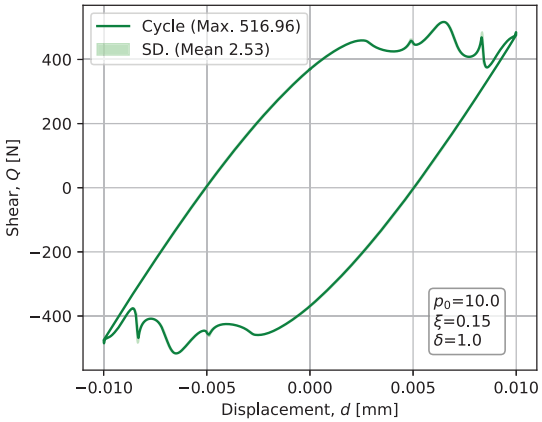

Figure 4.15: Fretting loop for higher values of stiffness-proportional damping. As blocks start to slip, block slip events cause oscillations in the shear force.

Figure 4.16 demonstrates hysteresis for the Hertzian fretting contact for both mass- and stiffness-proportional damping. The unphysical oscillations at the end points are suppressed, leading to a smooth hysteresis loop. Here, first natural frequency is damped with 1% and last natural frequency damped 5%.

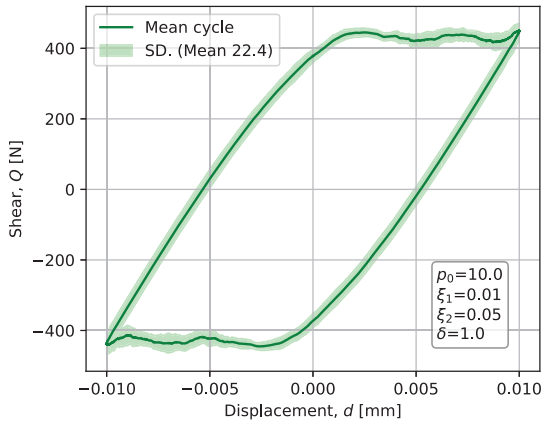

Figure 4.16: Fretting loop for system with both mass and stiffness proportional damping.

Spatial and temporal variations in coefficient of friction is permitted by having one extra degree of freedom per block. A friction evolution law is added to the system tangent and each block will have its own (small) variation in friction properties. Fretting contacts are known to experience increasing coefficient of friction during operation. This increase may be described by surface alterations (oxide layers wearing off, increasing conformity etc.) and wear debris interaction [146].

Consider for simplicity the friction evolution "laws",

$$\dot{\mu}_i = \gamma \Delta t (x_i - x_b) \tag{4.16a}$$

$$\dot{\mu}_i = \gamma \Delta t \tau (x_i - x_b) \tag{4.16b}$$

where γ is a constant describing evolve rate and τ is the shear force. Figure 4.17 demonstrates an accelerated example where the five different hysteresis are recorded throughout a fretting load history with $p = 10$ and evolve rate $\gamma = 1$. COF is seen to stabilize for central parts of the contact whilst contact edges continue to slide against the belt.

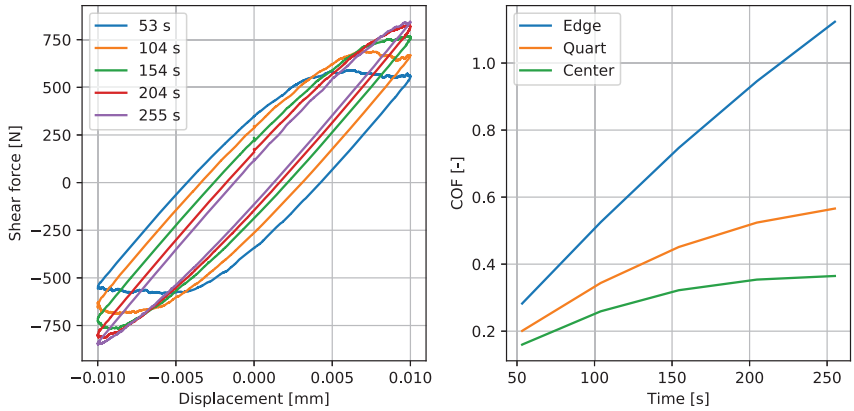

Figure 4.17: Fretting hysteresis loop with accelerated friction evolution law based on slip.

Figure 4.18 demonstrates an accelerated hysteresis loop evolution where the friction evolution law is based on shear work, rather than slip.

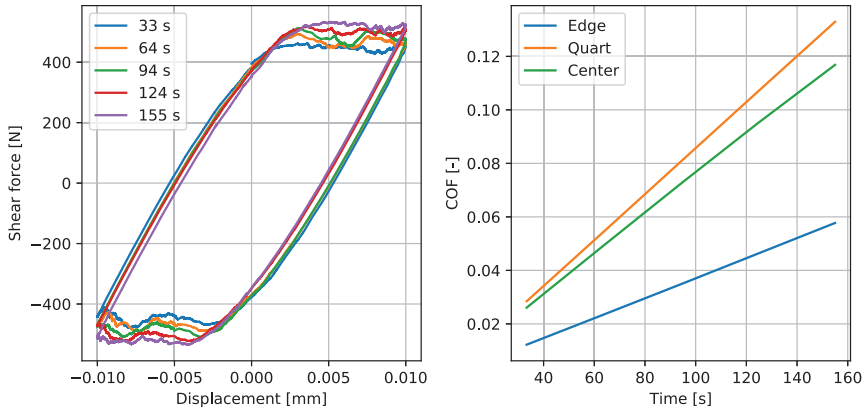

Figure 4.18: Fretting hysteresis loop with accelerated friction evolution law based on shear work.

Different evolution is seen for work-evolving coefficient and slip-evolving coefficient. The friction evolution laws demonstrated are very simplistic but provide interesting insights into both fretting behaviour. More complex evolution laws will be used in further work.

4.4 Discussion

In this chapter, steady-state frictional systems were investigated using discrete lumped-mass models. Nonlinear friction functions are shown to produce quite rich dynamics even for simple one-degree of freedom systems. It is recognised that friction plays an important role in the behaviour of fretting systems and it is the goal of these studies to qualitatively analyse the dynamic friction and its influence on fretting contacts. Obviously, experimental testing and calibration needs to be performed before any quantitative analyses can be made. Experimental verification of these friction simulations are not included in this thesis but is envisioned for further work. Numerical modelling of friction dynamics is also an ongoing research interest and is expected to continue through academic papers.

The mathematical tools from chaos theory and dynamic modelling in general provide very interesting and useful tools, some of which were demonstrated in this chapter. It is argued that studying dynamic friction behaviour using phase space diagrams, first return maps, bifurcation diagrams and, potentially, Lyapunov exponents can provide valuable insights into the behaviour of fretting contacts. Chaotic solutions was not found for the reciprocating fretting contacts for any physically relevant amount of damping. Chaos is generally rare for such dissipated systems, but may exist as threshold states depending on dissipation, system stiffness, forcing properties etc. Nonetheless, dependency on the physical parameters highlight the advantages of using statistical methods to analyse fretting contacts. Frequency methods are also useful in these models to analyse the frequency content and periodicity in the response.

The classical fourth-order Runge-Kutta integration scheme was used and found to be sufficiently accurate for steady state simulations. However, very short time steps are used to avoid inaccuracies related to the stick-slip transitions. Hence, implicit integration methods are currently not practical. Adaptive time stepping integrators may be useful, especially for the SDF system.

The numerical modelling and simulation of dynamic friction using the simple models demonstrated here continues to be a topic of great interest and will be subject to further research. Experimental work should also be conducted in order to further unite these methods with real fretting contacts. Furthermore, it is of interest in further work to investigate random rough surfaces and through parameter studies through Monte-Carlo simulations.

Chapter 5

Conclusions

In this project, a holistic approach to study fretting fatigue is undertaken. Fretting and fretting fatigue is inherently complex and intertwined problems. During the last century, numerous of parameters have been discussed to have an effect on fretting fatigue and numerous theories have been proposed. Similarly, the field is also represented by a very diverse set of analysis methodologies. A comprehensive study on fretting is therefore difficult. A holistic approach will in many cases mean addressing a problem for a large number of relevant factors and leaving out the non-important ones. The exact choice of which effects and parameters to include in the model often depend on the application. This project was initiated based on experience with varied fretting behaviour in the context of medium-speed piston engines. In this field, large geometries are subjected to complex fretting load histories causing problems sometimes dominated by fretting wear and sometimes dominated by fretting fatigue. The main goal of this project is to improve the prediction capabilities of fretting problems and to provide facilities to conduct relevant experimental work. Crack initiation prediction is of particular interest as fatigue failures are especially critical. Friction is also given special treatment as dynamic friction cause uncertainty to the mechanical joint behaviour.

This report was divided into four parts, each of which will be concluded in the following.

5.1 Numerical

The numerical work on fretting fatigue is the primary part of this thesis. The Ruiz parameters are used in many engineering practices and when combined with experience and recorded data, these can provide indications and estimates that inform design decisions early in the project. However, the lack of physical interpretation is a problem and there are obvious limits to the accuracy of interpolating the recorded data. Such parameters can predict fretting wear to some degree, but quantifying fretting initiation of cracks usually require more

advanced analysis.

Fretting fatigue is popularly addressed using critical plane methods. It is generally accepted that fatigue cracks initiate and grow in certain preferential material planes determined primarily by the material properties and loading. Section 2.7 reviewed the numerical aspects of implementing critical plane methodologies to fretting fatigue. Especially critical is managing the size and gradient effects occurring under fretting contact, and the use of Theory of Critical Distance was investigated in Paper IV, see Appendix A.4. For critical plane methods to be suitable for engineering projects, accuracy and efficiency is important. Paper II considered various ways of accelerating the critical plane analysis. Critical plane analyses are mainly used to predict fretting fatigue *initiation* and in some cases fracture mechanics methodologies must be applied to properly model the subsequent crack growth. This has not been a focus of this thesis, but remains part the work to be continued; it is recognised that more research is needed into the separation of initiation and propagation stages.

The choice of fatigue criterion probably needs some justification. The shear stress-based criteria was proposed by Findley [86] in the fifties and many more advanced criteria have been proposed since then, see Section 2.7.1. However, although simple in its form, the Findley criteria should be able to capture shear-based crack initiation and early growth as seen in many engineering metals. The use of fatigue criterion is not the main aim of this thesis, but the methods demonstrated here should be straight-forward to apply to many other criteria. Work is continuing with the application of other parameters, e.g. Carpinteri, see e.g. [88, 89].

The choice of suitable programming languages was an important part of the numerical work in this thesis. Python and C++ were used predominately, but also the newer language Rust. While Python is the obvious choice for prototyping, C++ was preferred for CPU-intensive critical plane algorithms, using multi-threading support through OpenMP and linear algebra using Eigen3. The recent programming language Rust provide a memory-safe alternative to C++ and is growing in popularity for scientific applications. Some code demonstrators in Python and C++ are included in the appendices that highlights the relevant benefits for each language.

5.2 Experimental

Experimental work is important in fretting projects. Fretting observations reported in academic literature and industrial practice are varied. The dovetail fixture demonstrated in Section 3.2 permit testing at a variety of testing conditions. Although testing can be performed at different loads, its usage is clearly limited compared with the bi-axial test rigs used in detailed fretting fatigue experimental campaigns.

Most of the experimental work conducted in this thesis is considered prototyping. Developing new fretting fatigue test capabilities require resources and time. Fretting fatigue test machines are also inherently complicated and devel-

oping new test machines should include intermediate steps. Ultimately, the goal of experimental testing is to be able to control many of the relevant parameters independently, such as contact tractions, fatigue load, material combinations etc. Controlling traction loads and fatigue loads independently require several actuators and fretting-specific machines are usually built [117]. Work is initiated during this project to build such a multi-actuator fretting fatigue test machine, but realisations of these plans were deprioritised in favour of the intermediate development steps that would produce test results faster. Future work includes building the more advanced test machines and inaugurate new students in the continuing experimental work.

The proving ring and lap-joint tests are examples of very accessible test setups which have both been demonstrated numerous times in research literature. Section 3 demonstrated the use of such tests during this in preliminary test programs. The results of these tests are not published yet and probably never will, but the tests nonetheless represented necessary exploratory experimental work and intermediate steps in developing useful test programs. These types of test rigs are quite limited, especially in terms of fretting loads. Usually, contact pressure is constant (and to some degree unknown due to bolt friction etc.) and shear forces are in-phase with the fatigue loads. Hence, these tests do not satisfy the interest in investigating loading effects. However, they do represent excellent opportunity for graduate students to do simple fretting tests. This is important because it is suggested here that the focus on contact mechanics and fretting fatigue in graduate mechanical engineering topics are to some degree neglected.

The dovetail fretting fatigue test demonstrated in Section 3.2 was developed with diversity and simplicity in mind. These two issues are in many ways conflicted since adopting possibilities of diversity, usually comes at the cost of complexity or lack of accuracy, hence, this fixture is a compromise. The dovetail joint fretting test is perhaps the most used configuration in the field, being simple and more importantly, it is related to concrete problems reported in the engineering field. Some additions were made to the fixture to make it more flexible. Firstly, allowing interchangeable contact pads enables different materials to be tested as demonstrated by many authors previously. Secondly, by allowing two specimens being tested at the same time, the rotating actuator in a multiaxial fatigue machine can be used to introduce a secondary source of vibration to the specimens. Paper IV demonstrates the use of this test configuration on a set of Ti-6Al-4V alloy specimens with cylindrical (Hertzian) contact geometry loaded axially.

Materials worked with during this project were mostly aluminium (6082) and Ti-6Al-4V. These materials were chosen simply because they are accessible and due to the existing fretting fatigue experimental data. Validation of the test methods used in this project preferred similar material. Also of further work is to extend the experimental work to materials used in the industry as described in paper III. Here it is suggested that the experimental data on cast irons are lacking. Fretting fatigue performance of cast iron alloys are relevant in the industry of heavy-duty machinery and interesting due to the self-lubricating

property of the graphite in cast iron.

It is acknowledged that especially fretting fatigue is a phenomenon concerned with the material and its microstructure. Material and fractography is perhaps given disproportional amount of attention in this thesis but more detailed material studies are part of the ongoing plans.

5.3 Friction simulations

Part four of this thesis was concerned with the dynamics of friction contacts. It is well-known that friction is one of the most important parameters in fretting contacts and it is not fully established how the dynamics of the contact affects the behaviour of the fretting system.

Discrete spring-block systems have been used for decades to analyse the non-linear dynamics due to friction. In Section 4 one-dimensional frictional chains were used to simulate friction dynamics in fretting contacts. The models were not ascribed particularly accurate and fretting-related physical properties, but are used to qualitatively study frictional behaviour of gross slip and mixed regime contacts for Hertzian contact profiles. The single degree of freedom oscillator with velocity-weakening friction law was found to suppress chaotic dynamics when appropriate amounts of damping is introduced. Using these models, rate- and state-dependent friction can be simulated to inform the dynamic behaviour of fretting contacts.

Bibliography

[1] D. Nowell and D.A. Hills. "Crack initiation criteria in fretting fatigue". In: *Wear* 136.2 (Mar. 1990), pp. 329–343. DOI: 10.1016/0043-1648(90)90155-4.

[2] J. A. Collins. "Fretting-Fatigue Damage-Factor Determination". In: *Journal of Engineering for Industry* 87.3 (June 1965), pp. 298–302. DOI: 10.1115/1.3670822. URL: http://manufacturingscience.asmedigitalcollection.asme.org/article.aspx?articleid=1439192.

[3] D. Kesavan et al. "High temperature fretting wear prediction of exhaust valve material". In: *Tribology International* 100 (2016). 42nd Leeds-Lyon Symposium on Tribology- Surfaces and Interfaces: Mysteries at Different Scales, pp. 280–286. ISSN: 0301-679X. DOI: https://doi.org/10.1016/j.triboint.2016.02.011. URL: https://www.sciencedirect.com/science/article/pii/S0301679X16000967.

[4] Steffen Loen Sunde, Filippo Berto, and Bjørn Haugen. "Fretting in medium-speed reciprocating engines—Comments on practices and opportunities". In: *Material Design & Processing Communications* n/a.n/a (). e201 MDPC-2020-038.R1, e201. DOI: https://doi.org/10.1002/mdp2.201. eprint: https://onlinelibrary.wiley.com/doi/pdf/10.1002/mdp2.201. URL: https://onlinelibrary.wiley.com/doi/abs/10.1002/mdp2.201.

[5] Heinrich Hertz. "Ueber die Berührung fester elastischer Körper." ger. In: *Journal für die reine und angewandte Mathematik* 92 (1882), pp. 156–171. URL: http://eudml.org/doc/148490.

[6] D. Nowell, D.A. Hills, and A. Sackfield. "Contact of dissimilar elastic cylinders under normal and tangential loading". In: *Journal of the Mechanics and Physics of Solids* 36.1 (1988), pp. 59–75. ISSN: 0022-5096. DOI: https://doi.org/10.1016/0022-5096(88)90020-8. URL: https://www.sciencedirect.com/science/article/pii/0022509688900208.

[7] D. A. Hills and D. Nowell. *Mechanics of Fretting Fatique*. Springer Netherlands, 1994. DOI: 10.1007/978-94-015-8281-0.

[8] K.L. Johnson. *Contact Mechanics*. Cambridge University Press, 1985. ISBN: 978-0-521-34796-9.

[9] S.R. Pearson and P.H. Shipway. "Is the wear coefficient dependent upon slip amplitude in fretting? Vingsbo and Söderberg revisited". In: *Wear* 330-331 (May 2015), pp. 93–102. DOI: 10.1016/j.wear.2014.11.005.

[10] Cs Cattaneo. "Sul contatto di due corpi elastici: distribuzione locale degli sforzi". In: *Rend. Accad. Naz. Lincei* 27.6 (1938), pp. 342–348.

[11] R.D. Mindlin and H. Deresiewicz. "Elastic spheres in contact under varying oblique forces". In: *Journal of Applied Mechanics* 20 (1953), pp. 327–344.

[12] J. Jäger. "A New Principle in Contact Mechanics". In: *Journal of Tribology* 120.4 (1998), pp. 677–684. DOI: 10.1115/1.2833765.

[13] Michele Ciavarella. "The generalized Cattaneo partial slip plane contact problem. I—Theory". In: *International Journal of Solids and Structures* 35.18 (1998), pp. 2349–2362. ISSN: 0020-7683. DOI: https://doi.org/10.1016/S0020-7683(97)00154-6. URL: http://www.sciencedirect.com/science/article/pii/S0020768397001546.

[14] Krzysztof Kubiak, T.W. Liskiewicz, and T.G. Mathia. "Surface morphology in engineering applications: Influence of roughness on sliding and wear in dry fretting". In: *Tribology International* 44.11 (Nov. 2011), pp. 1427–1432. DOI: 10.1016/j.triboint.2011.04.020. URL: http://eprints.hud.ac.uk/id/eprint/21591/.

[15] Tongyan Yue and Magd Abdel Wahab. "Roughness Effects on Fretting Fatigue". In: *Journal of Physics: Conference Series* 843 (May 2017), p. 012056. DOI: 10.1088/1742-6596/843/1/012056. URL: https://doi.org/10.1088/1742-6596/843/1/012056.

[16] A. Sackfield et al. "The application of asymptotic solutions to characterising the process zone in almost complete frictionless contacts". In: *Journal of the Mechanics and Physics of Solids* 51.7 (July 2003), pp. 1333–1346. DOI: 10.1016/s0022-5096(03)00020-6.

[17] Daniele Dini and David A. Hills. "Bounded asymptotic solutions for incomplete contacts in partial slip". In: *International Journal of Solids and Structures* 41.24-25 (Dec. 2004), pp. 7049–7062. DOI: 10.1016/j.ijsolstr.2004.05.058.

[18] Stefan Björklund and Sören Andersson. "A numerical method for real elastic contacts subjected to normal and tangential loading". In: *Wear* 179.1 (1994), pp. 117–122. ISSN: 0043-1648. DOI: https://doi.org/10.1016/0043-1648(94)90228-3. URL: https://www.sciencedirect.com/science/article/pii/0043164894902283.

[19] Qingbing Dong et al. "Fretting Contact of Layered Materials with Vertical Cracks Near Surfaces". In: *International Journal of Mechanical Sciences* (2021), p. 106361. ISSN: 0020-7403. DOI: https://doi.org/10.1016/j.ijmecsci.2021.106361. URL: https://www.sciencedirect.com/science/article/pii/S0020740321000965.

[20] Olof Vingsbo and Staffan Söderberg. "On fretting maps". In: *Wear* 126.2 (Nov. 1988), pp. 131–147. DOI: 10.1016/0043-1648(88)90134-2.

[21] R B Waterhouse and A J Trowsdale. "Residual stress and surface roughness in fretting fatigue". In: *Journal of Physics D: Applied Physics* 25.1A (Jan. 1992), A236–A239. DOI: 10.1088/0022-3727/25/1a/036.

[22] Y. Berthier, L. Vincent, and M. Godet. "Fretting fatigue and fretting wear". In: *Tribology International* 22.4 (Aug. 1989), pp. 235–242. DOI: 10.1016/0301-679x(89)90081-9.

[23] Z.R. Zhou et al. "Progress in fretting maps". In: *Tribology International* 39.10 (Oct. 2006), pp. 1068–1073. DOI: 10.1016/j.triboint.2006.02.001.

[24] J.A. Araújo et al. "Life prediction in multiaxial high cycle fretting fatigue". In: *International Journal of Fatigue* 134 (May 2020), p. 105504. DOI: 10.1016/j.ijfatigue.2020.105504.

[25] T. Zhang, P.E. McHugh, and S.B. Leen. "Finite element implementation of multiaxial continuum damage mechanics for plain and fretting fatigue". In: *International Journal of Fatigue* 44 (Nov. 2012), pp. 260–272. DOI: 10.1016/j.ijfatigue.2012.04.011.

[26] Reza Hojjati-Talemi et al. "Prediction of fretting fatigue crack initiation and propagation lifetime for cylindrical contact configuration". In: *Tribology International* 76 (2014). Proceedings of the Seventh International Symposium on Fretting Fatigue, pp. 73–91. ISSN: 0301-679X. DOI: https://doi.org/10.1016/j.triboint.2014.02.017. URL: https://www.sciencedirect.com/science/article/pii/S0301679X14000796.

[27] Reza Hojjati-Talemi, Magd Abdel Wahab, and Patrick De Baets. "Finite element simulation of phase difference effects on fretting fatigue crack nucleation behaviour". In: *Proceedings of the Institution of Mechanical Engineers, Part J: Journal of Engineering Tribology* 228.4 (2014), pp. 470–479. DOI: 10.1177/1350650113517092. eprint: https://doi.org/10.1177/1350650113517092. URL: https://doi.org/10.1177/1350650113517092.

[28] A. Ferjaoui et al. "Prediction of fretting fatigue crack initiation in double lap bolted joint using Continuum Damage Mechanics". In: *International Journal of Fatigue* 73 (2015), pp. 66–76. ISSN: 0142-1123. DOI: https://doi.org/10.1016/j.ijfatigue.2014.11.012. URL: https://www.sciencedirect.com/science/article/pii/S0142112314003004.

[29] M.L. Williams. "On the Stress Distribution at the Base of a Stationary Crack". In: 24 (Jan. 1957), pp. 109–114.

[30] Christopher D Lykins, Shankar Mall, and Vinod Jain. "An evaluation of parameters for predicting fretting fatigue crack initiation". In: *International Journal of Fatigue* 22.8 (2000), pp. 703–716. ISSN: 0142-1123. DOI: https://doi.org/10.1016/S0142-1123(00)00036-0. URL: http://www.sciencedirect.com/science/article/pii/S0142112300000360.

[31] Marcelo Avelar Antunes et al. “Stress intensity factor solutions for fretting fatigue using stress gradient factor”. In: *Engineering Fracture Mechanics* 186 (Dec. 2017), pp. 331–346. DOI: 10.1016/j.engfracmech.2017.10.031.

[32] Kwai S. Chan et al. In: *International Journal of Fracture* 112.4 (2001), pp. 299–330. DOI: 10.1023/a:1013507425050.

[33] S. Faanes. “Inclined cracks in fretting fatigue”. In: *Engineering Fracture Mechanics* 52.1 (Sept. 1995), pp. 71–82. DOI: 10.1016/0013-7944(94)00331-b.

[34] A.E. Giannakopoulos, T.C. Lindley, and S. Suresh. “Aspects of equivalence between contact mechanics and fracture mechanics: theoretical connections and a life-prediction methodology for fretting-fatigue”. In: *Acta Materialia* 46.9 (1998), pp. 2955–2968. ISSN: 1359-6454. DOI: http://dx.doi.org/10.1016/S1359-6454(98)00011-1. URL: http://www.sciencedirect.com/science/article/pii/S1359645498000111.

[35] A Mugadu, D.A Hills, and D Nowell. “Modifications to a fretting-fatigue testing apparatus based upon an analysis of contact stresses at complete and nearly complete contacts”. In: *Wear* 252.5-6 (Mar. 2002), pp. 475–483. DOI: 10.1016/s0043-1648(02)00007-8.

[36] J. A. Araújo and D Nowell. “Analysis of pad size effects in fretting fatigue using short crack arrest methodologies”. In: *International Journal of Fatigue* 21.9 (1999), pp. 947–956. ISSN: 0142-1123. DOI: https://doi.org/10.1016/S0142-1123(99)00077-8. URL: http://www.sciencedirect.com/science/article/pii/S0142112399000778.

[37] Mattia Pujatti, Mitja Suhadolc, and Daniel Piculin. “Fretting-initiated Fatigue in Large Bore Engines Connecting Rods”. In: *Procedia Engineering* 74 (2014), pp. 356–359. DOI: 10.1016/j.proeng.2014.06.279.

[38] Nitikorn Noraphaiphipaksa et al. “Fretting-contact-induced crack opening/closure behaviour in fretting fatigue”. In: *International Journal of Fatigue* 88 (July 2016), pp. 185–196. DOI: 10.1016/j.ijfatigue.2016.03.029.

[39] M. H. El Haddad, K. N. Smith, and T. H. Topper. “Fatigue Crack Propagation of Short Cracks”. In: *Journal of Engineering Materials and Technology* 101.1 (1979), p. 42. DOI: 10.1115/1.3443647.

[40] Raphael Araújo Cardoso et al. “An enrichment-based approach for the simulation of fretting problems”. In: *Computational Mechanics* (May 2018). DOI: 10.1007/s00466-018-1577-6.

[41] Marco Antonio Meggiolaro, Jaime Tupiassú Pinho de Castro, and Hao Wu. “On the use of tensor paths to estimate the nonproportionality factor of multiaxial stress or strain histories under free-surface conditions”. In: *Acta Mechanica* 227.11 (Dec. 2015), pp. 3087–3100. DOI: 10.1007/s00707-015-1543-8.

[42] Nima Shamsaei and Ali Fatemi. "Effect of microstructure and hardness on non-proportional cyclic hardening coefficient and predictions". In: *Materials Science and Engineering: A* 527.12 (May 2010), pp. 3015–3024. DOI: 10.1016/j.msea.2010.01.056.

[43] D. Socie. "Critical Plane Approaches for Multiaxial Fatigue Damage Assessment". In: *Advances in Multiaxial Fatigue*. ASTM International, 1993, pp. 7–7–30. DOI: 10.1520/stp24793s.

[44] I Papadopoulos. "A comparative study of multiaxial high-cycle fatigue criteria for metals". In: *International Journal of Fatigue* 19.3 (Mar. 1997), pp. 219–235. DOI: 10.1016/s0142-1123(96)00064-3.

[45] M. Matsuishi and T. Endo. "Fatigue of metals subjected to varying stress-fatigue lives under random loading". In: *Proc. Kyushu District Meeting, JSEM* (1968).

[46] Vitor Anes et al. "New cycle counting method for multiaxial fatigue". In: *International Journal of Fatigue* 67 (Oct. 2014), pp. 78–94. DOI: 10.1016/j.ijfatigue.2014.02.010.

[47] C. H. Wang and M. W. Brown. "Life Prediction Techniques for Variable Amplitude Multiaxial Fatigue—Part 1: Theories". In: *Journal of Engineering Materials and Technology* 118.3 (1996), p. 367. DOI: 10.1115/1.2806821.

[48] Marco Antonio Meggiolaro and Jaime Tupiassú Pinho de Castro. "An improved multiaxial rainflow algorithm for non-proportional stress or strain histories - Part I: Enclosing surface methods". In: *International Journal of Fatigue* 42 (Sept. 2012), pp. 217–226. DOI: 10.1016/j.ijfatigue.2011.10.014.

[49] V. Anes et al. "New approach for analysis of complex multiaxial loading paths". In: *International Journal of Fatigue* 62 (May 2014), pp. 21–33. DOI: 10.1016/j.ijfatigue.2013.05.004.

[50] Luca Susmel and David Taylor. "A critical distance/plane method to estimate finite life of notched components under variable amplitude uniaxial/multiaxial fatigue loading". In: *International Journal of Fatigue* 38 (May 2012), pp. 7–24. DOI: 10.1016/j.ijfatigue.2011.11.015.

[51] J. A. Araújo and D Nowell. "The effect of rapidly varying contact stress fields on fretting fatigue". In: *International Journal of Fatigue* 24.7 (2002), pp. 763–775. ISSN: 0142-1123. DOI: https://doi.org/10.1016/S0142-1123(01)00191-8.

[52] S. Fouvry, P. Kapsa, and L. Vincent. "Multiaxial fatigue analysis of fretting contact taking into account the size effect". In: *The 2nd International Symposium on Fretting Fatigue: Current Technology and Practices*. 2 1367. 2000, pp. 167–182. URL: https://www.scopus.com/inward/record.uri?eid=2-s2.0-0033907120&partnerID=40&md5=daa22afdedbdf5a3ecc8bfdda3ea9cb2.

[53] V.S.R. Adriano et al. "The influence of the fatigue process zone size on fatigue life estimations performed on aluminum wires containing geometric discontinuities using the Theory of Critical Distances". In: *Theoretical and Applied Fracture Mechanics* 97 (Oct. 2018), pp. 265–278. DOI: 10.1016/j.tafmec.2018.09.002.

[54] David Taylor. *The Theory of Critical Distances*. Elsevier, 2007. DOI: 10.1016/b978-0-08-044478-9.x5000-5.

[55] J. A. Araújo et al. "On the use of the Theory of Critical Distances and the Modified Wöhler Curve Method to estimate fretting fatigue strength of cylindrical contacts". In: *International Journal of Fatigue* 29.1 (2007), pp. 95–107. ISSN: 0142-1123. DOI: https://doi.org/10.1016/j.ijfatigue.2006.02.041. URL: http://www.sciencedirect.com/science/article/pii/S0142112306000776.

[56] S. Fouvry, H. Gallien, and B. Berthel. "From uni- to multi-axial fretting-fatigue crack nucleation: Development of a stress-gradient-dependent critical distance approach". In: *International Journal of Fatigue* 62 (2014). 9th Fatigue Damage of Structural Materials Conference, pp. 194–209. ISSN: 0142-1123. DOI: https://doi.org/10.1016/j.ijfatigue.2013.05.016. URL: http://www.sciencedirect.com/science/article/pii/S0142112313001655.

[57] D. Nowell and D. Dini. "Stress gradient effects in fretting fatigue". In: *Tribology International* 36.2 (2003). Fretting Fatigue, pp. 71–78. ISSN: 0301-679X. DOI: https://doi.org/10.1016/S0301-679X(02)00134-2. URL: http://www.sciencedirect.com/science/article/pii/S0301679X02001342.

[58] M. Ciavarella and G. Macina. "A note on the crack analogue model for fretting fatigue". In: *International Journal of Solids and Structures* 40.4 (Feb. 2003), pp. 807–825. DOI: 10.1016/s0020-7683(02)00652-2.

[59] H. Neuber. *Theory of notch stresses*. Springer, 1958.

[60] Daniel Arndt et al. "The deal.II finite element library: Design, features, and insights". In: *Computers & Mathematics with Applications* 81 (2021), pp. 407–422. ISSN: 0898-1221. DOI: 10.1016/j.camwa.2020.02.022. URL: https://arxiv.org/abs/1910.13247.

[61] Anders Logg. "Automating the Finite Element Method". In: *Archives of Computational Methods in Engineering* 14.2 (2007), pp. 93–138. DOI: 10.1007/s11831-007-9003-9.

[62] Yves Renard and Konstantinos Poulios. "GetFEM: Automated FE Modeling of Multiphysics Problems Based on a Generic Weak Form Language". In: *ACM Transactions on Mathematical Software* 47.1 (Jan. 2021), pp. 1–31. DOI: 10.1145/3412849.

[63] Yazhou Xu, Zhen Sun, and Yuqing Zhang. "Experimental and Numerical Investigations of Fretting Fatigue Behavior for Steel Q235 Single-Lap Bolted Joints". In: *Advances in Materials Science and Engineering* 2016 (2016), pp. 1–10. DOI: 10.1155/2016/6375131.

[64] Janne Juoksukangas. "Modelling and Experimental Analysis of Fretting Fatigue in Complete and Bolted Contacts". PhD thesis. Tampere University of Technology, 2017.

[65] Nam-Ho Kim. *Introduction to Nonlinear Finite Element Analysis*. Springer US, 2015. DOI: 10.1007/978-1-4419-1746-1.

[66] J. Ding et al. "Finite element simulation of fretting wear-fatigue interaction in spline couplings". In: *Tribology - Materials, Surfaces & Interfaces* 2.1 (Mar. 2008), pp. 10–24. DOI: 10.1179/175158308x320791.

[67] R. Rajasekaran and D. Nowell. "Fretting fatigue in dovetail blade roots: Experiment and analysis". In: *Tribology International* 39.10 (Oct. 2006), pp. 1277–1285. DOI: 10.1016/j.triboint.2006.02.044.

[68] Kyvia Pereira et al. "On the Convergence of Stresses in Fretting Fatigue". In: *Materials* 9.8 (July 2016), p. 639. DOI: 10.3390/ma9080639.

[69] C. Ruiz, P. H. B. Boddington, and K. C. Chen. "An investigation of fatigue and fretting in a dovetail joint". In: *Experimental Mechanics* 24.3 (1984), pp. 208–217. ISSN: 1741-2765. DOI: 10.1007/BF02323167. URL: http://dx.doi.org/10.1007/BF02323167.

[70] M Ciavarella and G Demelio. "A review of analytical aspects of fretting fatigue, with extension to damage parameters, and application to dovetail joints". In: *International Journal of Solids and Structures* 38.10 (2001), pp. 1791–1811. ISSN: 0020-7683. DOI: https://doi.org/10.1016/S0020-7683(00)00136-0. URL: http://www.sciencedirect.com/science/article/pii/S0020768300001360.

[71] B. P. Conner and T. Nicholas. "Using a Dovetail Fixture to Study Fretting Fatigue and Fretting Palliatives". In: *Journal of Engineering Materials and Technology* 128.2 (2006), p. 133. DOI: 10.1115/1.2172272.

[72] P.J. Golden and J.R. Calcaterra. "A fracture mechanics life prediction methodology applied to dovetail fretting". In: *Tribology International* 39.10 (Oct. 2006), pp. 1172–1180. DOI: 10.1016/j.triboint.2006.02.006.

[73] Liang Shi et al. "An investigation of fretting fatigue in a circular arc dovetail assembly". In: *International Journal of Fatigue* 82 (Jan. 2016), pp. 226–237. DOI: 10.1016/j.ijfatigue.2015.07.025.

[74] Heung Soo Kim and Shankar Mall. "Investigation into three-dimensional effects of finite contact width on fretting fatigue". In: *Finite Elements in Analysis and Design* 41.11 (2005), pp. 1140–1159. ISSN: 0168-874X. DOI: https://doi.org/10.1016/j.finel.2005.02.001. URL: https://www.sciencedirect.com/science/article/pii/S0168874X05000156.

[75] Claudio Montebello. "Analysis of the stress gradient effect in Fretting-Fatigue through a description based on nonlocal intensity factors". Theses. Université Paris-Saclay, Nov. 2015. URL: https://tel.archives-ouvertes.fr/tel-01238905.

[76] C. Montebello et al. "Analysis of the stress gradient effect in fretting-fatigue through nonlocal intensity factors". In: *International Journal of Fatigue* 82 (Jan. 2016), pp. 188–198. DOI: 10.1016/j.ijfatigue.2015.02.009.

[77] Jung Ho Son et al. "Fretting damage prediction of connecting rod of marine diesel engine". In: *Journal of Mechanical Science and Technology* 25.2 (Feb. 2011), pp. 441–447. DOI: 10.1007/s12206-010-1206-6.

[78] A. Strozzi et al. "A repertoire of failures in connecting rods for internal combustion engines, and indications on traditional and advanced design methods". In: *Engineering Failure Analysis* 60 (Feb. 2016), pp. 20–39. DOI: 10.1016/j.engfailanal.2015.11.034.

[79] Ruiz C and Chen KC. "Life assessment of dovetail joints between blades and disks in aero-engines". In: *Proc of Int Conf on Fatigue: Fatigue of Engineering Materials and Structures, Inst of Mech Eng, 187–194* (1986).

[80] J. Vidner and E. Leidich. "Enhanced Ruiz criterion for the evaluation of crack initiation in contact subjected to fretting fatigue". In: *International Journal of Fatigue* 29.9-11 (Sept. 2007), pp. 2040–2049. DOI: 10.1016/j.ijfatigue.2007.02.010.

[81] Xin Li, Zhengxing Zuo, and Wenjie Qin. "A fretting related damage parameter for fretting fatigue life prediction". In: *International Journal of Fatigue* 73.Supplement C (2015), pp. 110–118. ISSN: 0142-1123. DOI: https://doi.org/10.1016/j.ijfatigue.2014.12.003. URL: http://www.sciencedirect.com/science/article/pii/S0142112314003144.

[82] C. Navarro, S. Muñoz, and J. Domínguez. "On the use of multiaxial fatigue criteria for fretting fatigue life assessment". In: *International Journal of Fatigue* 30.1 (Jan. 2008), pp. 32–44. DOI: 10.1016/j.ijfatigue.2007.02.018.

[83] Nadeem Ali Bhatti and Magd Abdel Wahab. "A numerical investigation on critical plane orientation and initiation lifetimes in fretting fatigue under out of phase loading conditions". In: *Tribology International* 115 (2017), pp. 307–318. ISSN: 0301-679X. DOI: https://doi.org/10.1016/j.triboint.2017.05.036. URL: http://www.sciencedirect.com/science/article/pii/S0301679X17302839.

[84] K.N. Smith, P. Watson, and T.H. Topper. "Stress- strain function for the fatigue of metals". In: *J Mater* 5.4 (1970). cited By 1301, pp. 767–778. URL: https://www.scopus.com/inward/record.uri?eid=2-s2.0-0014890104&partnerID=40&md5=9381f9c5e7de03987a62416d0faf5ea7.

[85] Ali Fatemi and Darrell F. Socie. "A critical plane approach to multiaxial fatigue damage including out-of-phase loading". In: *Fatigue & Fracture of Engineering Materials and Structures* 11.3 (Mar. 1988), pp. 149–165. DOI: 10.1111/j.1460-2695.1988.tb01169.x.

[86] W. Nicholas Findley. *A theory for the effect of mean stress on fatigue of metals under combined torsion and axial load or bending*. Engineering Materials Research Laboratory, Division of Engineering, Brown University, 1958.

[87] L. Susmel and P. Lazzarin. "A biparametric Wöhler curve for high cycle multiaxial fatigue assessment". In: *Fatigue & Fracture of Engineering Materials & Structures* 25.1 (Jan. 2002), pp. 63–78. ISSN: 1460-2695. DOI: 10.1046/j.1460-2695.2002.00462.x. URL: http:https://doi.org/10.1046/j.1460-2695.2002.00462.x.

[88] Andrea Carpinteri and Andrea Spagnoli. "Multiaxial high-cycle fatigue criterion for hard metals". In: *International Journal of Fatigue* 23.2 (2001), pp. 135–145. ISSN: 0142-1123. DOI: https://doi.org/10.1016/S0142-1123(00)00075-X. URL: http://www.sciencedirect.com/science/article/pii/S014211230000075X.

[89] Sabrina Vantadori et al. "Early fretting crack orientation by using the critical plane approach". In: *International Journal of Fatigue* 114 (Sept. 2018), pp. 282–288. DOI: 10.1016/j.ijfatigue.2018.04.015.

[90] D. Socie. "Multiaxial Fatigue Damage Models". In: *Journal of Engineering Materials and Technology* 109.4 (1987), p. 293. DOI: 10.1115/1.3225980.

[91] Darell F. Socie and Gary B. Marquis. *Multiaxial fatigue*. SAE International, 2000. ISBN: 9780768004533.

[92] Alan R. Kallmeyer, Ahmo Krgo, and Peter Kurath. "Evaluation of Multiaxial Fatigue Life Prediction Methodologies for Ti-6Al-4V". In: *Journal of Engineering Materials and Technology* 124.2 (Mar. 2002), pp. 229–237. DOI: 10.1115/1.1446075.

[93] IV Papadopoulos. "CRITICAL PLANE APPROACHES IN HIGH-CYCLE FATIGUE: ON THE DEFINITION OF THE AMPLITUDE AND MEAN VALUE OF THE SHEAR STRESS ACTING ON THE CRITICAL PLANE". In: *Fatigue & Fracture of Engineering Materials & Structures* 21.3 (1998), pp. 269–285. DOI: https://doi.org/10.1046/j.1460-2695.1998.00459.x. eprint: https://onlinelibrary.wiley.com/doi/pdf/10.1046/j.1460-2695.1998.00459.x. URL: https://onlinelibrary.wiley.com/doi/abs/10.1046/j.1460-2695.1998.00459.x.

[94] R.L. Graham. "An efficient algorith for determining the convex hull of a finite planar set". In: *Information Processing Letters* 1.4 (June 1972), pp. 132–133. DOI: 10.1016/0020-0190(72)90045-2.

[95] Pauli Virtanen et al. “SciPy 1.0: Fundamental Algorithms for Scientific Computing in Python”. In: *Nature Methods* 17 (2020), pp. 261–272. DOI: 10.1038/s41592-019-0686-2.

[96] Ky Dang Van. “Sur la résistance à la fatigue des métaux”. In: *Sciences Techniques Armement* (1973).

[97] I.V. Papadopoulos. “A new criterion of fatigue strength for out-of-phase bending and torsion of hard metals”. In: *International Journal of Fatigue* 16.6 (1994), pp. 377–384. ISSN: 0142-1123. DOI: https://doi.org/10.1016/0142-1123(94)90449-9. URL: https://www.sciencedirect.com/science/article/pii/0142112394904499.

[98] Hsi-Yung Feng et al. “An accurate and efficient algorithm for determining minimum circumscribed circles and spheres from discrete data points”. In: *Computer-Aided Design* 45.2 (2013). Solid and Physical Modeling 2012, pp. 105–112. ISSN: 0010-4485. DOI: https://doi.org/10.1016/j.cad.2012.07.014. URL: https://www.sciencedirect.com/science/article/pii/S0010448512001674.

[99] Henrik Svärd. “A branch and bound algorithm for evaluation of the Findley fatigue criterion”. In: *International Journal of Fatigue* 73 (Apr. 2015), pp. 27–38. DOI: 10.1016/j.ijfatigue.2014.11.008.

[100] Steven Diamond and Stephen Boyd. “CVXPY: A Python-embedded modeling language for convex optimization”. In: *Journal of Machine Learning Research* 17.83 (2016), pp. 1–5.

[101] The CGAL Project. *CGAL User and Reference Manual*. 5.2. CGAL Editorial Board, 2020. URL: https://doc.cgal.org/5.2/Manual/packages.html.

[102] David G. Luenberger and Yinyu Ye. *Linear and Nonlinear Programming*. Springer US, 2008. DOI: 10.1007/978-0-387-74503-9.

[103] A. Bernasconi and I.V. Papadopoulos. “Efficiency of algorithms for shear stress amplitude calculation in critical plane class fatigue criteria”. In: *Computational Materials Science* 34.4 (2005), pp. 355–368. ISSN: 0927-0256. DOI: https://doi.org/10.1016/j.commatsci.2005.01.005. URL: http://www.sciencedirect.com/science/article/pii/S0927025605000509.

[104] J.A. Araújo et al. “On the characterization of the critical plane with a simple and fast alternative measure of the shear stress amplitude in multiaxial fatigue”. In: *International Journal of Fatigue* 33.8 (2011). Multiaxial Fatigue Models, pp. 1092–1100. ISSN: 0142-1123. DOI: https://doi.org/10.1016/j.ijfatigue.2011.01.002. URL: http://www.sciencedirect.com/science/article/pii/S0142112311000041.

[105] B. Weber et al. “Improvements of multiaxial fatigue criteria computation for a strong reduction of calculation duration”. In: *Computational Materials Science* 15.4 (Nov. 1999), pp. 381–399. DOI: 10.1016/s0927-0256(98)00129-3.

[106] Rui Pereira et al. "Ranking programming languages by energy efficiency". In: *Science of Computer Programming* 205 (2021), p. 102609. ISSN: 0167-6423. DOI: https://doi.org/10.1016/j.scico.2021.102609. URL: https://www.sciencedirect.com/science/article/pii/S0167642321000022.

[107] Mr. E. M. Eden, Mr. W. N. Rose, and Mr. P. L. Cunningham. "The Endurance of Metals: Experiments on Rotating Beams at University College, London". In: *Proceedings of the Institution of Mechanical Engineers* 81.1 (1911), pp. 839–974. DOI: 10.1243/PIME_PROC_1911_081_017_02. URL: https://doi.org/10.1243/PIME_PROC_1911_081_017_02.

[108] G. A. Tomlinson. "The Rusting of Steel Surfaces in Contact". In: *Proceedings of the Royal Society of London A: Mathematical, Physical and Engineering Sciences* 115.771 (1927), pp. 472–483. ISSN: 0950-1207. DOI: 10.1098/rspa.1927.0104. eprint: http://rspa.royalsocietypublishing.org/content/115/771/472.full.pdf.

[109] G. A. Tomlinson, P. L. Thorpe, and H. J. Gough. "An Investigation of the Fretting Corrosion of Closely Fitting Surfaces". In: *Proceedings of the Institution of Mechanical Engineers* 141.1 (1939), pp. 223–249. DOI: 10.1243/PIME_PROC_1939_141_034_02. eprint: https://doi.org/10.1243/PIME_PROC_1939_141_034_02. URL: https://doi.org/10.1243/PIME_PROC_1939_141_034_02.

[110] E.J. Warlow-Davies. "Fretting Corrosion and Fatigue Strength: Brief Results of Preliminary Experiments". In: *Proceedings of the Institution of Mechanical Engineers* 146.1 (June 1941), pp. 32–38. DOI: 10.1243/PIME_PROC_1941_146_012_02. URL: https://doi.org/10.1243/PIME_PROC_1941_146_012_02.

[111] Kunio Nishioka and Kenji Hirakawa. "Fundamental Investigations of Fretting Fatigue : (Part 2, Fretting Fatigue Testing Machine and Some Test Results)". In: *Bulletin of JSME* 12.50 (1969), pp. 180–187. DOI: 10.1299/jsme1958.12.180.

[112] MH Attia and RB Waterhouse, eds. *Standardization of Fretting Fatigue Test Methods and Equipment*. ASTM International, Jan. 1992. DOI: 10.1520/stp1159-eb.

[113] R.W. Neu. "Progress in standardization of fretting fatigue terminology and testing". In: *Tribology International* 44.11 (Oct. 2011), pp. 1371–1377. DOI: 10.1016/j.triboint.2010.12.001.

[114] *Guide for Fretting Fatigue Testing*. DOI: 10.1520/e2789-10r15.

[115] D.A. Hills and D. Nowell. "What features are needed in a fretting fatigue test?" In: *Tribology International* 42.9 (2009). Special Issue: Fifth International Symposium on Fretting Fatigue, pp. 1316–1323. ISSN: 0301-679X. DOI: http://dx.doi.org/10.1016/j.triboint.2009.04.023. URL: http://www.sciencedirect.com/science/article/pii/S0301679X09000905.

[116] TC Lindley and KJ Nix. "Fretting Fatigue in the Power Generation Industry: Experiments, Analysis, and Integrity Assessment". In: *Standardization of Fretting Fatigue Test Methods and Equipment*. ASTM International, 1992, pp. 153–153–17. DOI: 10.1520/stp25828s.

[117] D.A. Hills and D. Nowell. "Mechanics of fretting fatigue-Oxford's contribution". In: *Tribology International* 76 (Aug. 2014), pp. 1–5. DOI: 10.1016/j.triboint.2013.09.015.

[118] M. Sabsabi, E. Giner, and F.J. Fuenmayor. "Experimental fatigue testing of a fretting complete contact and numerical life correlation using X-FEM". In: *International Journal of Fatigue* 33.6 (2011), pp. 811–822. ISSN: 0142-1123. DOI: https://doi.org/10.1016/j.ijfatigue.2010.12.012. URL: https://www.sciencedirect.com/science/article/pii/S0142112310003130.

[119] "Critical issues in high cycle fatigue". In: *International Journal of Fatigue* 21 (1999), S221–S231. ISSN: 0142-1123. DOI: https://doi.org/10.1016/S0142-1123(99)00074-2. URL: http://www.sciencedirect.com/science/article/pii/S0142112399000742.

[120] Patrick J. Golden. "Development of a dovetail fretting fatigue fixture for turbine engine materials". In: *International Journal of Fatigue* 31.4 (Apr. 2009), pp. 620–628. DOI: 10.1016/j.ijfatigue.2008.03.017.

[121] J.-J. Chen et al. "Experimental and numerical investigation on crack initiation of fretting fatigue of dovetail". In: *Fatigue & Fracture of Engineering Materials & Structures* 41.6 (Feb. 2018), pp. 1426–1436. DOI: 10.1111/ffe.12787.

[122] Shouyi Sun et al. "Fretting fatigue failure behavior of Nickel-based single crystal superalloy dovetail specimen in contact with powder metallurgy pads at high temperature". In: *Tribology International* 142 (Feb. 2020), p. 105986. DOI: 10.1016/j.triboint.2019.105986.

[123] G. Bradski. "The OpenCV Library". In: *Dr. Dobb's Journal of Software Tools* (2000).

[124] EJ Berger. "Friction modeling for dynamic system simulation". In: *Applied Mechanics Reviews* 55.6 (Nov. 2002), pp. 535–577. DOI: 10.1115/1.1501080.

[125] Z.R. Zhou and L. Vincent. "Mixed fretting regime". In: *Wear* 181-183 (1995). 10th International Conference on Wear of Materials, pp. 531–536. ISSN: 0043-1648. DOI: https://doi.org/10.1016/0043-1648(95)90168-X. URL: https://www.sciencedirect.com/science/article/pii/004316489590168X.

[126] N Banerjee and D. A Hills. "Analysis of stick–slip and contact-edge behaviour in a simplified fretting fatigue test". In: *The Journal of Strain Analysis for Engineering Design* 41.3 (2006), pp. 183–192. DOI: 10.1243/03093247JSA83. eprint: https://doi.org/10.1243/03093247JSA83. URL: https://doi.org/10.1243/03093247JSA83.

[127] A. Klarbring, M. Ciavarella, and J.R. Barber. "Shakedown in elastic contact problems with Coulomb friction". In: *International Journal of Solids and Structures* 44.25 (2007), pp. 8355–8365. ISSN: 0020-7683. DOI: https://doi.org/10.1016/j.ijsolstr.2007.06.013. URL: https://www.sciencedirect.com/science/article/pii/S002076830700251X.

[128] James R. Barber, Anders Klarbring, and Michele Ciavarella. "Shakedown in frictional contact problems for the continuum". In: *Comptes Rendus Mécanique* 336.1 (2008). Duality, inverse problems and nonlinear problems in solid mechanics, pp. 34–41. ISSN: 1631-0721. DOI: https://doi.org/10.1016/j.crme.2007.10.013. URL: https://www.sciencedirect.com/science/article/pii/S1631072107001957.

[129] C.M. Churchman and D.A. Hills. "Slip zone length at the edge of a complete contact". In: *International Journal of Solids and Structures* 43.7-8 (Apr. 2006), pp. 2037–2049. DOI: 10.1016/j.ijsolstr.2005.06.099.

[130] R. D. Mindlin. "Compliance of Elastic Bodies in Contact". In: *Journal of Applied Mechanics ASME* 16 (1949), pp. 259–268.

[131] Kris De Moerlooze, Farid Al-Bender, and Hendrik Van Brussel. "A Generalised Asperity-Based Friction Model". In: *Tribology Letters* 40.1 (June 2010), pp. 113–130. DOI: 10.1007/s11249-010-9645-x.

[132] James R. Rice, Nadia Lapusta, and K. Ranjith. "Rate and state dependent friction and the stability of sliding between elastically deformable solids". In: *Journal of the Mechanics and Physics of Solids* 49.9 (2001). The JW Hutchinson and JR Rice 60th Anniversary Issue, pp. 1865–1898. ISSN: 0022-5096. DOI: https://doi.org/10.1016/S0022-5096(01)00042-4. URL: https://www.sciencedirect.com/science/article/pii/S0022509601000424.

[133] Jim Woodhouse, Thibaut Putelat, and Andrew McKay. "Are there reliable constitutive laws for dynamic friction?" In: *Philosophical Transactions of the Royal Society A: Mathematical, Physical and Engineering Sciences* 373.2051 (Nov. 2015), p. 20140401. DOI: 10.1098/rsta.2014.0401.

[134] K Popp, N Hinrichs, and M Oestreich. "Dynamical behaviour of a friction oscillator with simultaneous self and external excitation". In: *Sadhana* 20.2-4 (Apr. 1995), pp. 627–654. DOI: 10.1007/bf02823210.

[135] A. Papangelo et al. "Multiple spatially localized dynamical states in friction-excited oscillator chains". In: *Journal of Sound and Vibration* 417 (2018), pp. 56–64. ISSN: 0022-460X. DOI: https://doi.org/10.1016/j.jsv.2017.11.056. URL: https://www.sciencedirect.com/science/article/pii/S0022460X17308520.

[136] J. M. Carlson and J. S. Langer. "Mechanical model of an earthquake fault". In: *Phys. Rev. A* 40 (11 Dec. 1989), pp. 6470–6484. DOI: 10.1103/PhysRevA.40.6470. URL: https://link.aps.org/doi/10.1103/PhysRevA.40.6470.

[137] R. Burridge and L. Knopoff. "Model and theoretical seismicity". In: *Bulletin of the Seismological Society of America* 57.3 (June 1967), pp. 341–371. ISSN: 0037-1106.

[138] Brittany A. Erickson, Björn Birnir, and Daniel Lavallée. "Periodicity, chaos and localization in a Burridge-Knopoff model of an earthquake with rate-and-state friction". In: *Geophysical Journal International* 187.1 (Aug. 2011), pp. 178–198. DOI: 10.1111/j.1365-246x.2011.05123.x.

[139] K. Y. Sanliturk, D. J. Ewins, and A. B. Stanbridge. "Underplatform Dampers for Turbine Blades: Theoretical Modeling, Analysis, and Comparison With Experimental Data". In: *Journal of Engineering for Gas Turbines and Power* 123.4 (Nov. 1998), pp. 919–929. DOI: 10.1115/1.1385830.

[140] D.M. Mulvihill et al. "Investigation of non-Coulomb friction behaviour in reciprocating sliding". In: *Wear* 271.5 (2011), pp. 802–816. ISSN: 0043-1648. DOI: https://doi.org/10.1016/j.wear.2011.03.014. URL: https://www.sciencedirect.com/science/article/pii/S004316481100189X.

[141] Yu. I. Shalapko and T. V. Tarasova. "Processes of dynamics of surface layers during low-amplitude fretting". In: *Journal of Friction and Wear* 34.3 (May 2013), pp. 166–174. DOI: 10.3103/s1068366613030124.

[142] Kjetil Thøgersen et al. "History-dependent friction and slow slip from time-dependent microscopic junction laws studied in a statistical framework". In: *Physical Review E* 89.5 (May 2014), p. 052401. DOI: 10.1103/physreve.89.052401.

[143] John F. Hall. "Problems encountered from the use (or misuse) of Rayleigh damping". In: *Earthquake Engineering & Structural Dynamics* 35.5 (2006), pp. 525–545. DOI: https://doi.org/10.1002/eqe.541. eprint: https://onlinelibrary.wiley.com/doi/pdf/10.1002/eqe.541. URL: https://onlinelibrary.wiley.com/doi/abs/10.1002/eqe.541.

[144] R.I. Leine et al. In: *Nonlinear Dynamics* 16.1 (1998), pp. 41–54. DOI: 10.1023/a:1008289604683.

[145] H. Poincaré and R. Magini. "Les méthodes nouvelles de la mécanique céleste". In: *Il Nuovo Cimento* 10.1 (July 1899), pp. 128–130. DOI: 10.1007/bf02742713.

[146] Matthew P. Szolwinski and Thomas N. Farris. "Mechanics of fretting fatigue crack formation". In: *Wear* 198.1-2 (Oct. 1996), pp. 93–107. DOI: 10.1016/0043-1648(96)06937-2.

[147] J. C. Butcher. *Numerical Methods for Ordinary Differential Equations*. John Wiley & Sons, Ltd, July 2016. DOI: 10.1002/9781119121534.

Appendix A

Appendices

A.1 Paper I

A review of theories and methodologies used on fretting fatigue with special attention to applicability to engineering applications.

International Journal of Fatigue 117 (2018) 314–326

Contents lists available at ScienceDirect

International Journal of Fatigue

journal homepage: www.elsevier.com/locate/ijfatigue

Predicting fretting fatigue in engineering design

Steffen Loen Sunde*, Filippo Berto, Bjørn Haugen

Norwegian University of Science and Technology (NTNU), Department of Mechanical and Industrial Engineering, Norway

ARTICLE INFO

Keywords:
Fretting
Fretting fatigue
Crack initiation
Contact mechanics
Fretting maps
Critical plane
Crack analogue
Notch analogue
Asymptotic methods

ABSTRACT

The progress in fretting fatigue understanding and predictability is reviewed, with engineering applications in mind. While industrial assessments often relies on simple empirical parameters, research in fretting fatigue should allow the design engineer to improve confidence in the fretting fatigue analysis.

Fretting fatigue cracks often form in multiaxial stress fields with severe gradients under the contact area, and are inherently difficult to predict.

By describing the fretting stress gradients using comparisons with the mechanical fields surrounding cracks and notches, crack nucleation threshold conditions and finite life can efficiently be determined. Also, non-local stress intensity multipliers provide promising tools for the industrial finite element analysis, often involving complex geometries and loading conditions.

The use of multiaxial fatigue criteria to determine fretting fatigue nucleation life is also reviewed. Researchers have shown that critical plane calculations with some stress-averaging method can predict fretting fatigue crack initiation. However, the frictional interface causes non-proportional loading paths, and the application of critical plane methods is not straight forward.

1. Introduction

Fretting is the phenomenon in which contacting surfaces subjected to oscillatory relative movement experience surface damage. Over time, cracks form at the surface and result in *fretting fatigue* related failures. Fretting can greatly reduce the fatigue life of the contacting parts.

Although the mechanisms of fretting have been studied for over a century, its exact nature and behaviour is still not well understood [1–3]. As early as in 1911, "fretting" was mentioned in relation with the formations of debris in plain fatigue tests [4], interpreting it as *surface wear*. Later, the term fretting fatigue arose, as researches started acknowledging its negative effect on fatigue life [5,6]. It became apparent during the following decades that fretting fatigue was indeed a complicated phenomenon; Collins [7] proposed dependence on more than 50 parameters. However, due to the difficulties involved in accurately controlling and monitoring different parameters during fretting fatigue tests, early experiments and discussions were questionable [8]. The phenomena involved are also known to be interconnected, and Collins suggested that the parameters could be narrowed down into eight broader categories: Amplitude of relative slip, magnitude and distribution of the contact pressure, the local state of stress, number of cycles, material and surface conditions, cyclic frequency, temperature, and environments surrounding the surfaces [7]. Further complications are realised as the length scales involved in fretting fatigue are often on the same order of magnitude as material microstructural features [9] and surface features [10].

Fretting fatigue have mainly been studied for metallic alloys and ceramics used in engineering. In bearings, loss of clearance may be caused by fretting wear, but also jamming due to debris [11]. In biomaterials, debris formations induces inflammations in the host tissue [12,13]. Highly loaded components like turbine blades [14,1] and axle press-fits [15–17] may catastrophically fail due to fretting initiated cracks being driven to propagate into the substrate. Other examples are spline couplings, keyed joints, flexible marine risers and pipe fittings [18–21].

2. Mechanisms of fretting fatigue

The fretting fatigue process is usually separated into different stages. The initial phase is often concerned with wearing off the oxide layer on the surfaces. After the oxide layer is worn off, cold-welds form at the surface asperities, increasing the coefficient of friction. Subsequent loading of the surfaces then cause these micro-welds to break, forming wear debris [22]. This wear debris can work as an abrasive medium, but can also form a protective third body layer reducing wear [11]. Additional loading cycles may introduce plastic

* Corresponding author.
E-mail address: steffen.sunde@ntnu.no (S.L. Sunde).

https://doi.org/10.1016/j.ijfatigue.2018.08.028
Received 19 April 2018; Received in revised form 14 August 2018; Accepted 17 August 2018
Available online 20 August 2018
0142-1123/

Nomenclature

$2N_f$	number of cycles for fatigue failure
ΔK_{th}	threshold stress intensity factor range
δ	relative slip
$\Delta\epsilon$	strain range
$\Delta\gamma$	shear strain range
$\Delta\sigma_1$	plain fatigue limit
ϵ_f'	fatigue ductility coefficient
γ'	shear fatigue ductility coefficient
ν	Poisson's ratio
σ_f'	fatigue strength coefficient
σ_T	stress in tangential direction of contact
σ_y	yield stress
τ	contact shear stress
τ_a	shear stress amplitude
τ_f'	shear fatigue strength coefficient
a	contact semi-width
a_0	El Haddad intrinsic length parameter
b	fatigue strength exponent
b_0	shear fatigue strength exponent
c	fatigue ductility exponent
c_0	shear fatigue ductility exponent
E	Young's modulus
f	coefficient of friction
G	shear modulus
g_{max}	maximum gap of contacting profile (unloaded)
k	Findley's influence factor
P	contact normal force
Q	contact sliding force
Y	LEFM Geometrical factor

deformation and microcracks to the surfaces, which cause additional wear debris and the potential of further propagating cracks into the material. These cracks eventually grow out of the contact stress fields and becomes dominated by the far-field stresses, if present.

In *partial slip* conditions, the friction is high enough to restrict the surfaces from global sliding and there is only a very small amount of local sliding between the generally adhered surfaces. These conditions are the most prone to fretting fatigue [23,24]. The competing effects of *tribologically transformed structure* [25], particle detachment and nucleation of fatigue cracks [26] makes a quantitative prediction for a given material and given operating conditions very difficult. The crack initiation process is highly dependent on the material microstructure [27,28].

Wear is often neglected in fretting fatigue analysis, but is reported to sometimes affect the fretting fatigue life [27,29,30]. The exact reasons for the underlying phenomena are still debated, but it is likely depending on material combination and loading conditions. Material removal due to surface wear may eliminate nucleating cracks at the surface. Wear also redistributes the contacting pressure [31], even in the partial slip regime as studied by Shen et al. [23]. They concludes that the wear could not be neglected. However, as other researchers have reported, wear in partial slip conditions is minor [27] and can in many cases be neglected for small values of slip. Frictional contacts are also known to sometimes *shake down*, i.e. residual shearing tractions building up and restricting further sliding, eventually leading to a steady state response being notionally adhered [2,32].

The fretting problem is quite different, depending on whether the contact is *complete* or incomplete. For incomplete contact, at least one of the mating surfaces is of convex shape and the contact area is related to the load. For complete (conforming or flat) however, notionally sharp corners introduce stress singularities. For tangentially loaded incomplete contact, there is no frictional shakedown effect, and some local sliding will always occur. Thus, incomplete contacts are more prone to partial slip fretting fatigue.

3. Fretting maps

Various visual descriptions of fretting have been researched using fretting loops or fretting maps to characterise the fretting problem and to separate the regimes involved. Fretting loops plot the relation between friction force and displacement amplitude, sometimes along a third, temporal axis. Fretting loops form the basis for many fretting maps [33].

The slip amplitude was early identified as one of the most defining parameters for fretting. Vingsbo and Söderberg [24] introduced the concept of fretting maps with three different regimes of sliding conditions.

1. *Stick regime* with low sliding action and low surface damage (oxidation and wear). Low fretting damage.
2. *Mixed stick-slip regime* had fretting fatigue with small amounts of wear. Accelerated crack growth rate reduced fatigue life.
3. *Gross slip regime* showed severe damage due to wear but crack formations were limited. In the gross slip regime, the wear coefficient increased by several orders of magnitude.

Hence, this fretting map could be used to determine the fretting regimes for a set of conditions. Fig. 1 illustrates the different regimes. Fretting maps was an important development in the work of fretting assessment. Today they are used to describe the overall fretting behaviour, including contact conditions, fretting regime, wear mechanism, crack nucleation and propagation [33].

Some years after Vingsbo and Söderberg, Zhou and Vincent [26,34] proposed to separate the problem using two different types of fretting maps, *running condition fretting map* (RCFM) and *material response fretting map* (MRFM). RCFM distinguished between partial slip regime, mixed fretting regime and slip regime, and is in some ways quite similar to Vingsbo and Söderberg. It is however, maybe more correct in unifying the stick and partial-slip regimes, since in reality there will always be some local sliding. The material response fretting map was related to the *post hoc* degradation analysis of the specimen.

Different maps related to the number of cycles have also been proposed [35]. In 2006 Zhoul et al. [36] reviewed the progress in fretting maps and covered additional proposals, but arrives to the

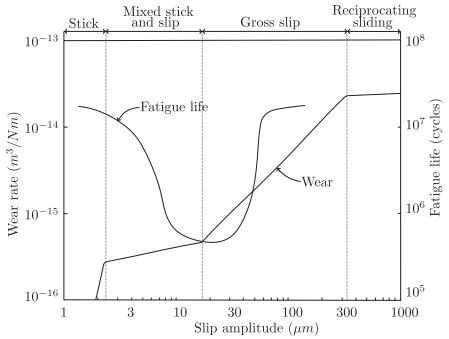

Fig. 1. Relating the slip amplitude to fretting regime, as proposed by Vingsbo and Söderberg [24].

conclusion that further work is needed to quantify the competing effects in fretting fatigue, especially in mixed regime.

In 2015 Pearson and Shipway [33] investigated the paper of Vingsbo and Söderberg on fretting maps and criticised their suggestion that the wear coefficient was strongly dependent on displacement amplitude. They point out that in general, fretting research at that time had two limitations: Firstly, many researchers used far-field displacement amplitudes and not the actual slip for the contact thus also including the compliance of the test rig. Secondly, research has also shown that there appears to be a threshold below which wear does not occur. The errors related to not recognising these effects grows as the slip amplitude becomes smaller, where the relative difference between the displacement amplitude and *slip* amplitude is bigger.

The different fretting maps proposed serves well as graphical demonstrations of the competing mechanisms usually involved in fretting and is useful for the engineer in the early design phase, especially when considering to apply surface treatment, etc. [37,36]. Very quantitative predictions for fretting fatigue are, however, difficult to achieve using maps only. *Computational fretting maps* may also be used in parametric numerical fretting fatigue studies [38,39].

4. Design parameters

In aerospace, nuclear and other safety-critical industries, much effort have been put into predicting fretting fatigue through knockdown factors and different design parameters. These parameters are often easily computed and may serve as a first step in the design process. Collins [7] early identified the usefulness of quantitative factors in the fretting fatigue design phase.

The first attempts to mathematically relate the contact stress fields with fatigue damage was Ruiz et al. [14]. They investigated fretting fatigue life of turbine blade dovetail joints and proposed a design parameter, "fretting damage" (FD), by multiplying the highest surface tangential stress with the maximum frictional work ($\tau\delta$):

$$FD = (\sigma_T)_{max} \cdot (\tau\delta)_{max} \tag{1}$$

However, as the maximum tangential stress may occur at a different location than the maximum frictional work, it is numerically awkward. A second parameter was obtained by simply maximising the product of tangential stress σ_T, surface shear stress τ and relative slip (Eq. (2)). This "fretting fatigue damage" (FFD) parameter was reported to predict the location of crack, but failed to predict the number of cycles to crack initiation or crack growth [40]. The parameters proposed by Ruiz et al. have nonetheless been extensively used, mainly due to their simplicity and the fact that it may predict crack initiation probability [27].

$$FFD = \sigma_T \cdot \tau \cdot \delta \tag{2}$$

For more recent variations and extensions to the Ruiz parameters, see e.g. [41,42]. These critera combines the frictional power or frictional work with multiaxial fatigue parameters.

More recently, Varenberg et al. [43,44] proposed a dimensionless *slip index* aiming to distinguish between the fretting regimes in a more unified and rigorous way than the classical use of fretting maps. By using dimensional analysis they derived an expression for the slip ratio which is governed by the dimensionless parameter $\delta = A_d S_c/N$, with A_d being the imposed displacement amplitude, S_c the slope of the friction loop and N is the normal load. Applied to fretting experiments, the different regimes were separated. Partial slip exists for $0.5 \leqslant \delta < 0.6$ and gross slip for $\delta > 0.6$.

In 2015 Li et al. [3] noted that there is still no satisfactory fretting fatigue damage criterion and they proposed a parameter for fretting fatigue life predictions, by expressing the "fretting related damage parameter" (FRD) as

$$FRD = \alpha + \beta\sqrt{\frac{Q}{fP}} \tag{3}$$

The FRD parameter was related to the plain fatigue methods as a knock-down factor to determine the number of cycles to failure and thus making full use of already existing plain fatigue data. Q is the sliding force, P is the normal load, f coefficient of friction α and β are fitting coefficients.

5. Critical plane methods

More extensive parameters for fretting fatigue have been proposed by making use of the different plain fatigue parameters. Due to the multiaxial nature of the stresses, particularly critical plane-based methods have been attempted to determine the fretting fatigue limit. Empirical combinations of stresses and strains are assumed to drive the cracks to initiate and grow in certain material planes. Applied to the stress gradients of fretting fatigue, the critical plane methods usually considers a point at a critical distance or in an averaged sense, and searches for the material plane orientation having the most damaging parameter. Thus, often *cracking direction* is also obtained. In general, these methods can be divided into stress-based, strain-based and energy-based parameters. Numerous parameters for fatigue have been applied to the fretting case, and the following list is by no means exhaustive.

Szolwinski and Farris [22] used the Smith-Watson-Topper (SWT) [45] to find the initiation location and life. It may be given by

$$SWT = \sigma_{max}\frac{\Delta\,\epsilon}{2} \tag{4}$$

As SWT was extended to be used in a critical plane method [46], this would mean finding the material plane maximising the product of normal strain range and maximum tensile stress on that plane during the loading cycle (i.e. *strain energy density*). Combining Eq. (4) with Basquin's law and Coffin-Manson, the SWT critical plane parameter may be expressed as [47]:

$$SWT = \frac{(\sigma_f')^2}{E}(2N_f)^{2b} + \sigma_f'\,\epsilon_f'\,(2N_f)^{b+c} \tag{5}$$

σ_f' and b are the material fatigue strength and exponent, ϵ_f' and c are the fatigue ductility coefficient and exponent respectively. E is the modulus of elasticity and N_f is the number of cycles to initiate a crack with a given length. Making use of Eq. (5), the life of the component may be estimated by finding the critical SWT and comparing with fully reversed uniaxial test data. The SWT is found either by evaluating Eq. (5) on the plane experiencing the largest range of principal strain, or by searching for the plane with maximum SWT [46].

Fatemi and Socie (FS) [48] proposed a strain based critical plane parameter for shear dominated cracks, studying the effects of out-of-phase loading. It has also been applied to fretting fatigue [47,40,9]. Using the FS criterion, the material plane having the maximum shear strain is considered the critical plane, with the influence of opening mode included through the material parameter α. It can be expressed as

$$FS = \frac{\Delta\gamma}{2}\left(1 + \alpha\frac{\sigma_{max}}{\sigma_y}\right) = \frac{\tau_f'}{G}(2N_f)^{b_0} + \gamma_f'(2N_f)^{c_0} \tag{6}$$

where $\Delta\gamma$ is the shear strain range during the cycle, σ_{max} maximum normal stress, σ_y is the yield stress, G is the shear modulus and α, τ_f', γ_f' are material related parameters. b_0 and c_0 are the shear fatigue strength exponent and shear fatigue ductility exponent respectively. Thus, the critical plane is found by maximising Eq. (6), where the shear strain range is evaluated as the difference between the largest and smallest shear strain during the cycle [49]. Eq. (6) can alternatively be related uniaxial data using the following relations derived from von Mises' criterion [50].

$$\tau_f' = \frac{\sigma_f'}{\sqrt{3}}, \quad \gamma_f' = \sqrt{3}\,\epsilon_f', \quad b_0 = b, \quad c_0 = c, \quad G = \frac{E}{2(1+\nu)} \tag{7}$$

Shear based parameters work better for ductile materials and tensile criteria work better for brittle materials. The dominant mode of initiation is often not known *a priori*, which makes the decision of which criterion to apply difficult. As Araújo and Nowell [47] suggests, a possible, conservative approach may be to simply calculate both FS and SWT parameters - and then use the worst case. Averaging methods were shown to reveal a contact size effects in Al-4%Cu and Ti-6Al-4V samples, but concerns about assuming the averaging parameters to be material constant are raised.

Lykins et al. [40] found SWT to be effective for predicting initiation life and location for Ti-6Al-4V, and noted the FS parameter to be effective for initiation location. The *Maximum strain amplitude* was concluded to be important in the fretting crack initiation for the Ti–6Al–4V alloy. Araújo [9] found SWT to predict crack direction for AISI 1034 and 35NCD16 samples, using averaged stresses over a characteristic length along the crack direction.

The stress parameter proposed by Findley (FP) [51] in the sixties combines the shear loads with the normal loads. More specifically, the critical plane is defined as the material plane experiencing the maximum combination of shear stress amplitude and maximum normal stress over a stabilized cycle. Thus, maximising Eq. (8) yields the critical plane.

$$FP = \tau_a + k\sigma_{max} \tag{8}$$

where k is a parameter describing the material crack growth sensitivity to normal stresses, and is determined based on experimental data. Higher values of k can be interpreted as higher sensitivity to *opening mode* effects on the shear cracks. k is therefore normally lower for shear dominated (ductile materials) than for brittle materials. Socie [50] propose to use 0.1–0.2 for ductile materials. In terms of the number of cycles to failure it may be expressed as [52]:

$$FP = \tau_a + k\sigma_{max} = \tau_f'(2N_f)^{b_0} \tag{9}$$

Namjoshi et al. [53] tested the Findley criteria for fretting fatigue crack initiation of different pad geometries on Ti-6Al-4V "dog bone" specimens for a variety of stress levels. The Findley parameter (and SWT) was found to be effective in finding the location but not the orientation of cracks. They proposed the modified shear stress range critical plane parameter, having four curve fitting constants. The researchers argue that the criterion is thus less influenced by pad geometry, and that it would be successful in finding the crack orientation and initiation life.

Most studies on using critical plane parameters to quantify fretting fatigue have considered convex contact geometries and in-phase loading. Recently, Bhatti and Wahab [54] found a number of parameters to be appropriate for different cases of phase-shifted loading conditions. Foletti et al. [55] applied the (mesoscopic) *Dang Van* [56] and Liu–Mahadevan [57] criteria to fretting fatigue in railway axle press-fits. Chakherlou et al. [58] compared seven different critical plane criteria for life estimations on different models e.g. with aluminium plate joint with pre-tensioned bolts and residual stresses due to cold expansion. They conclude that no criterion is universally accurate, but SWT parameter was within a factor of two for most specimens.

The stress based fatigue parameters neglects plastic effects. Since for higher contact loads, micro plasticity is expected to occur, the stress based parameters might be less reliable than the strain based parameters. However, the different criteria used for different materials have shown reasonable accuracy for specific sets of experimental data, and is less accurate in the general sense. In general it is noted that due to the stress gradients involved in fretting fatigue, some non-local approach must be used in addition [59,49,47]. Thus, averaging the stress over some material dependent critical distance becomes necessary.

Some researchers have used stress-invariant criteria and thus avoiding the computationally expensive critical plane method. Ferré et al. [60] averaged the Crossland criterion over a critical area and achieved <10% error for nucleation endurance for titanium samples. Fouvry et al. [61] achieved 12% error for steel specimen. The Dang Van criterion is often used as comparison with other methods [62,63]. The stress-invariant methods are considerably easier to implement, compared with critical plane methods, but at the cost of accuracy. Also, by assuming stress-invariance, the potential information about initial cracking direction is lost.

6. Analytical methods

The analytical studies of contact started in the 1880s by Hertz [64] who first studied the stresses in spherical bodies in contact. His theories was restricted to frictionless contact between linear elastic bodies, proving the *Hertzian* pressure distribution. He also restricted his study to non-conforming contact for which the contact area was *small* compared to the bodies, i.e. *half-space theory*. Since Hertz, numerous researchers have put efforts into extending the theory and its become a useful tool in fretting analysis, especially for closed form comparisons with experiments.

Bradley [65] showed that contacting spheres share adhesive forces when put into contact and Johnson, Kendall and Roberts [66] (JKR) extended the Hertzian contact for elastic bodies subjected to small contact loads to include adhesive forces associated with the free surface energies. The JKR theory introduced a singularity at the contact boundary and a *separation force* to the problem, which effectively increases the contact area. Derjaguin, Muller, and Toporov (DMT) [67] proposed an adhesive law based on the undeformed Hertzian profile, thus avoiding the JKR singularity. More recently, adhesion was introduced to models to introduce stress singularities in rounded contact fatigue problems [68].

6.1. Sliding contact

Cattaneo [69] extended the Hertzian contact problem to include tangential loads experiencing interfacial partial slip. The normal load was held constant, whilst monotonically increasing the tangential load. The partial slip conditions were described by superimposing the full sliding terms with a correction related to the contacting pressure coming from the normal contact. Independently, Mindlin [70] studied the same type of solution but with some generalisations to the loading path. Further generalisations to the *Cattaneo-Mindlin problem (CM)* followed [71,72].

The CM case also became a popular setup for experimental testing of fretting fatigue, though the shear tractions in the fretting tests differ from the CM solution due to the bulk stresses. The plane strain approximation is usually assumed for the cylinder-on-plane case. Nowell and Hills demonstrated in 1987 the effect of bulk tension on the stress distributions for the CM case [73] by perturbing the Mindlin solution on integral form. It was shown that the bulk stresses in the specimen introduces an *eccentricity* to the contact stick zone due to strain mismatch. The use of the Mindlin solution with the eccentricity is shown to be a good approximation except for near the contact center. The half-plane stresses were thus found for the case where the bulk stresses are *in-phase* with the tangential load and they argue that the Mindlin case is reasonable approximate.

Ciavarella [74] and Jäger [75] independently extended the CM problem to more general geometries, and this generalisation is often referred to as the *Ciavarella-Jäger theorem (CJ)*. The theorem holds for two-dimensional contact, but for 3D only in the unrealistic case of vanishing Poisson ratio, otherwise only in approximate sense. This limitation also applies to the original CM solution [1], and may not always be neglected [76].

Barber et al. [32] applied periodic tangential loads and periodic normal loads to the CJ case. The uncoupled contact problem (vanishing Dundur's constant) was studied with the loads in PQ-space being bounded by $Q = \mu P$ so that gross slip would not occur. They conclude that the extent of the *permanent stick zone* during steady state, was

independent of loading path. The interior traction distributions, however, are depending on loading path. By extending the methods of Jäger and Ciavarella to cyclic tangential loading, they show that the frictional system reaches a steady state after the first cycle. The paper conclude that the system will shakedown to a steady state independent of transient conditions, with a given permanent stick zone.

Ciavarella and Demelio [1] reviewed in 2000 some of the efforts made to the analytical approaches to fretting fatigue, again by considering the case of elastically similar half-planes where the normal and shearing tractions are uncoupled. They considered constant normal load and oscillating tangential load for indenters ranging from the Hertzian to flat indenters (complete contact) with increasingly sharply rounded corners. The analytical solutions are combined with the classical fretting damage parameters of slip amplitude and frictional slip energy [14] and stress intensity factors for cracking. For increasingly sharp indenter, tensile stresses at surface increases, but also becomes more localised. Thus, the stress intensity factor (K_I) rapidly decrease, and cracks have greater chance of self-arresting. However, only opening mode (K_I) is considered. The authors point out the possibilities to separate the stress concentration effect and frictional damage for further testing, which can help to understand the complexities involved. According to the authors, it is not entirely clear if there is an "optimal" corner radius on the rounded indenter. A simple expression for the relative microslip at onset of *full sliding* was given as

$$\delta_{max} = fg_{max} \tag{10}$$

where f is the coefficient of friction and g_{max} is the maximum gap of the contacting profiles before loading.

The Cattaneo-Mindlin problem was revisited by Etsion [77] and its assumptions were validated. Experimental evidence show that the contact does change when tangential forces are applied, a phenomena coined "junction growth" by Tabor [78]. The problem is to assume a local Coloumb friction law because when friction and contact pressure are high, unrealistically high contact stresses may occur, exceeding yield. By relating the incipient sliding to *plastic failure*, these assumptions were relaxed, suggesting a model for the other end of the scale with respect to actual plasticity in the given contact situation. Wang et al. [79] studied partial slip conditions for elastically dissimilar materials by coupling the normal and tangential loads using constraint equations on the slip in the contact plane. Other, *semi-analytical* methods for solving partial slip cases are also proposed [80,81].

Davies et al. [82] considered the CJ theorem and extended it for loading with varying normal load. The evolution of the stick-slip zones were determined, still limiting the analysis to contact profiles satisfying half-plane theory and by avoiding gross slip in the P-Q space. The authors are mainly interested in determining the energy dissipation in the system, but argues that fretting crack nucleation can be assumed to coincide with the point of maximum dissipation. Along with the paper, a Mathematica code was given for researchers to further study stick-slip evolutions.

The analytical and semi-analytical models are important tools for fretting and provides mathematical ground for researchers to study fretting fatigue. They are also useful for comparing with experimental results and parameter studies [83], even though the exact fretting conditions are hard to control. By adjusting the parameters involved, these methods can be used to simulate the stress fields in the real component. However, quite significant size effect have been reported [47], which puts limitations to this method. Also, numerical methods such as finite element, are becoming increasingly used, allowing for more complex geometry, material models, loading histories, etc. In general, when half-plane theory is violated, more elaborate numerical methods are needed.

7. Asymptotic methods

The stress concentrations in fretting fatigue can also be studied using asymptotic analysis, leading to an analogy with cracks in fracture mechanics. As the contact edges become increasingly sharp, Hertzian stress analysis fail. For sharp, (complete) contact, stress singularities arise and asymptotes can be applied [84–86]. In these methods, the stress fields are matched with truncated asymptotic expansions, and one enters the discussion on the *order of singularity* of the stress field and its spatial range of validity. In reality, of course, there always exists some rounding of the corners, but notionally complete contact occur in engineering situations [2] and the asymptotic methods can be suitable approximations. Also, in rough contacting surfaces, local singularities may occur due to adhesion [11].

Williams [87] developed a framework for analysing singular stress fields in wedges by expressing the stresses as functions of wedge angle in a polar coordinate system (r, θ) with its origin in the singular point. Using the biharmonic equation, the solutions for the stresses and displacements are expanded as an asymptotic series in powers of r (Eq. (11)), and non-trivial solutions are obtained for certain eigenvalues λ.

Following Williams method, the stress field surrounding the apex can be expressed on the form [84]

$$\sigma_{ij}(r,\theta) = K_I r^{\lambda_I - 1} f_{ij}^{I}(\theta) + K_{II} r^{\lambda_{II}(\theta) - 1} f_{ij}^{II}(\theta) + \text{higher order terms} \tag{11}$$

where for a mode $n \in \{1, 2\}$, K_n is the stress intensity function, λ_n is the eigenvalue and $f(\theta)$ is the corresponding eigenfunction. Thus, sufficiently close to the singularity, the stress field is dominated by the lowest eigenvalue, and the environment for crack nucleation in this critical region may be quantified. For wedge angle of $\theta = 360°$ the solution for a crack is obtained with its lowest, and hence dominant eigenvalue being 0.5. This solution is important in the fields of fracture mechanics and contact mechanics. See e.g. Mugadu et al. [84] for considering the edges of contact in a spline coupling. Note however, that the Williams solution considers elastically similar bodies [88] and solutions for elastically dissimilar contact exists, see Bogy et al. [89–91].

Though being quite mathematical, these serves as foundation for useful tools for engineers encountering singularities such as in sharp edge contact. For a more thorough description, the reader is referred to published literature [92,93].

Sackfield et al. [94] applied asymptotic expressions to the mathematical description of a rigid punch pressed into a half-plane substrate. For flat punch they assumed *small* rounded corners so that the stress at the corners were dominated by the singular term (generalised stress intensity factor K^*) in the stress expansion. The stresses were matched with the corresponding sharp edged indenter, and thus relies on the radius to be small compared with the indenter dimensions. This is beneficial in cases where the sharp edge solutions exist and can be used for indenters with small radii, which in finite elements solutions often requires very fine element mesh to resolve.

The asymptotic analysis was then used for *incomplete* contact in partial slip by Dini and Hills in 2004 [86] and compared with the classical Cattaneo-Mindlin solution. They argue that the stress expansion from the local singularity is impractical for sliding contact, but for partial slip the stick-slip interface is a natural location for crack nucleation. The stress intensity factors K_I and K_{II} serves as scaling parameters for the normal and shear forces respectively, and characterises the contact. Thus it provides a means to simply obtain the stress characterisation to evaluate the fretting fatigue. Good agreement for the stresses is only expected close to the contact corners, which anyways are the most likely locations for crack nucleation. By evaluating the contact situation in such a local manner permits one to recreate the fretting problem of a prototype to a simple laboratory test setup [95,96,2].

The asymptotic solution of complete contact between elastically dissimilar bodies was investigated by Churchman et al. [91]. Whether failure is most likely to happen at the leading or the trailing edge depends on the slip direction, but for the fretting case of oscillating punch,

the problem is symmetric.

Hills and Dini [2] reviewed in 2016 the efforts on using asymptotic forms to describe the stress fields for fretting fatigue, pointing out the fundamentally different nature of incomplete and complete contact. For incomplete contact, they argue that the local fields (stress and slip) are determined by the two stress intensity factors and the friction coefficient. Hence, the fields can be used to model and replicate the situation for complex prototypes. For complete contact however, slip will be contained inside the contact area, limiting the sliding motion to very small values. The authors thus claim that fretting fatigue, in its traditional sense, should not occur for complete contact. In their approach the normal load is held constant and the case of oscillating normal load is retained for further studies. Contact of parts of conforming geometry ("punch on punch") and "receding" contact is only mentioned and points out that the research in these types of contact is lacking. It is also remarked that the contact stress intensity factors are only valid near the contact edge and hence it is useful for nucleation criteria, but not necessarily crack growth as the crack grows farther away from the edge. Plots of *total* fretting fatigue life versus the crack nucleation fields are as such not entirely accurate.

Since the stick-slip situation for incomplete contact can be described by the three parameters K_T, K_N and μ, laboratory experiments can be made into replicating the situation for complex prototypes. For complete contact however, the use of asymptotic solutions can demonstrate that fretting fatigue should not occur in complete contacts: For high enough coefficients of friction, the contact is in an *adhered* state, and for lower coefficients, frictional shakedown will cause the steady-state slip values to be very small [97]. Given that the nonlinear (process) zone is small, the strain energy should be characterised by the asymptotes. Further studies to be made are to account for oscillating normal load, and to match the asymptotic methods to rounded contact.

Recently, Fleury et al. [98] used asymptotic methods for the incomplete contact subjected to more complex loading histories, with varying normal and shear load (in-phase). The slip zone size and amount of slip are found through the two stress intensity factors K_T and K_N (see Fig. 2), and the fretting damage may then be found e.g. using the energy dissipation. This asymptotic formulation gives good approximations when the slip zone is small compared with the contact size, but at decreasing accuracy for larger variations in normal load.

Asymptotic methods are useful for fretting fatigue because it provides means for characterising the most detrimental fields (surrounding the contact edges) from which cracks nucleate, circumventing the need to analyse the entire contact. Thus, the local stress fields may be matched with those in experiments and as such be used to quantify fretting fatigue strength. The methods are however limited to (local) half-plane idealisation [98], decoupling tangential and normal stresses. Examples of asymptotic matching is presented in the literature for simple contacts with closed-form solutions, but for complex cases, numerical methods like the finite element can be used to find the generalised intensity factors, see e.g. Montebello et al. [99].

8. Crack initiation and growth

Whereas the asymptotic methods can permit the fretting fatigue conditions to be described without the need for explicit modelling of the micromechanics by locally matching the necessary fields with experiments, other methods attempts to micromechanically describe the fretting fatigue cracking process.

The mechanisms involved have been extensively researched for metallic contacts, but initiation of fretting fatigue cracks is still an elusive problem. Usually, the fatigue life is split into nucleation and propagation phases, but the relative importance of one phase over the other have been debated. Fig. 3 shows the fracture surface from a fretted titanium specimen by Araújo and Nowell [47]. Navarro et al. [59] noted that the relative importance of initiation versus propagation may depend on the fatigue criterion used, the loading conditions, material, geometry, etc. and thus one cannot *a priori* know to which phase the majority of life is.

Despite the advancements in characterising the fretting fields of stresses and strains, resolving the crack nucleation driving forces continues to be a target of research [2,84]. As nucleation criteria in fretting fatigue, mainly three different methodologies have been used: *short crack methodologies*, multiaxial fatigue criteria and fretting specific parameters (Ruiz, etc.). Recently, the use of *continuum damage mechanics* have also been applied to fretting fatigue. The short crack methods uses threshold curves for the stress intensity factors to determine whether a crack will arrest after initiation, and uses normally either Kitagawa-Takahashi diagram or El-Haddad curves [100–102]. The critical plane methods usually assumes the fatigue crack to form along *persistent slip bands* in the material crystals, and uses empirical parameters to determine the most detrimental plane orientation.

Szolwinski and Farris [22] attempted to quantitatively model the nucleation life for fretting fatigue experiments and noted that characterising the stresses alone was not sufficient. They turned to the Smith-Watson-Topper model and used Westegaard's method for characterising the stress distribution. Fortran routines were written to find the plane having the largest damage parameter defined in Eq. (4) which they used to find the crack origin and orientation, in what they called the Γ-model. The nucleation life was taken to be the number of cycles needed to form a crack of 1 mm length, and Paris law was used to propagate the crack to failure. The life estimates provided was within the scatter of the data from experiments.

Araújo and Nowell discussed in their 2002 paper [47] the size effects in fretting fatigue. For incomplete contact, they performed experimental and analytical analysis, and varied the contact size whilst holding the same levels of stress on the contact surface. They show that two different critical plane criteria (SWT and FS) are overly conservative for smaller contacts. For smaller contacts, the stresses at the surface are the same, however with a more rapid decay beneath the surface. Hence, for smaller contacts, the driving forces for crack growth are less severe than for larger ones, and the point-based (local) critical plane criteria does in general not account for this gradient. They proposed averaging over a characteristic volume or depth. This depth or volume was found to be on the same scale as microstructural parameters, essentially meaning that accurate predictions needs to include features of material microstructure.

For determining the orientations of early cracks, Araújo et al. [9] proposed a method where the normal and shearing driving forces were averaged over a line of characteristic length and then used in different critical plane algorithms. Thus, the critical plane calculations is not necessary at each integration point. As the steep stress gradients related to fretting fatigue can cause small-scale crack reorientations, an incremental approach should be used. Continuum elasticity is assumed, which is regarded as an engineering approximation due to microstructural effects playing a role in the real case. FS, SWT and *Modified Wöhler Curve Method* (MWCM) were used and only SWT was successful in predicting the orientations of the cracks, although, not accurately.

The Dang Van criterion [56] has also been used in attempts to

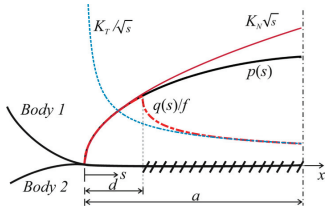

Fig. 2. Matching the stress fields with edge asymptotes [98].

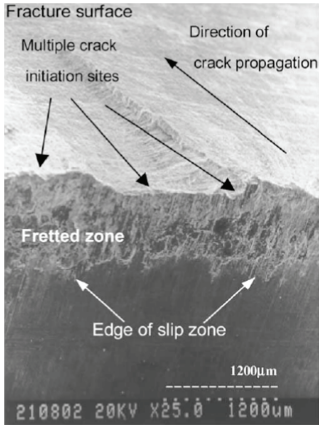

Fig. 3. Scanning electron micrograph of a fretting crack surface [47].

describe nucleation [63,103]. Fouvry et al. [63] compared it with other classical multiaxial parameters. Under partial slip conditions, the coefficient of friction was confirmed to be important and the crack nucleation conditions were accurately quantified. Tests were performed on steel specimen with a titanium nitride coating. It was found that with the compressive stresses introduced, the coating greatly reduced the cracking nucleation risk.

Lykins et al. [40] tested the Ruiz parameters and a number of fatigue criteria to predict fretting fatigue crack initiation in titanium alloy. The Ruiz parameters were deemed ineffective, but improved when corrections for contact effects and mean stress ratio were included. Fretting fatigue nucleation was shown to have the same trends in the Wöhler-diagrams. The crack initiation locations found in the experiments were shown to coincide with the maximum strain amplitude.

Navarro et al. [104] proposed the method they called the *variable initiation length model* in which the number of cycles for crack nucleation was calculated for material points along the crack path. For these points, the crack growth rate was computed both for initiation using Basquin's equation and for propagation force using *Linear Elastic Fracture Mechanics (LEFM)*. The depth at which the LEFM driving forces surpassed the driving forces representing the initiation mechanisms was taken to be the initiation length. Thus the total life is obtained by adding the number of cycles to initiation at this depth and the number of cycles to propagate the crack until failure.

Bhatti and Wahab [54] studied fretting fatigue for 2024-T351 Aluminium using for different phase angles between the axial load and tangential load. Finite element models of three different combinations of boundary conditions with three different phase angles were considered: 0 deg, 90 deg and 180 deg. Results were compared with literature [105]. They conclude that the location of crack initiation for fretting damage is highly dependent on the phase angle, but the Ruiz parameter and SWT multiaxial fatigue criterion was reported to show good correlation with the results of Szolwinski and Farris. Initiation life is shortest for 180 deg phase shift and longest for the 90 deg case.

The determination of crack growth in uniform stress fields is fairly established today, e.g. using Paris law. In fretting fatigue however, the non-proportional mixed-mode stress fields close to the contact significantly complicates the matter [106,47,59]. Recently Baietto et al. [107] coupled experimental fretting results with a numerical model to model fretting fatigue mixed mode crack initiation and growth. However, Faanes [108] found fretting cracks to be notably affected by Mode II only in the short initial stage.

In continuum damage mechanics (CDM) an accumulating damage variable is used to describe material degradation and was introduced to fatigue by Lemaitre [109]. This damage parameter $0 \leqslant D < 1$ (scalar for isotropic damage) is used to define the *effective stress* which may be given as

$$\tilde{\sigma} = \frac{\sigma}{1-D} \tag{12}$$

Zhang et al. [110] used CDM in a three dimensional finite element model with multiaxial fatigue calculations. They used a nonlinear damage accumulation and compared the results with the SWT parameter for notched and unnotched plain fatigue as well as fretting. In an effort to do lifetime predictions for different values of slip amplitude, the results were compared with published data. The model is successful in suggesting the reduction in fretting fatigue life for increasing relative slip in the partial slip regime. Also, the predicted life increases slightly in the gross slip regime. For low amplitudes of slip in the partial slip regime life predictions were non-conservative, and the researchers argues this may be explained due to not including wear. The study was later followed up by including wear [23].

Hojjati-Talemi and Wahab [111] also found CDM to give accurate predictions for experimental data found in the literature, and concludes that the method is appropriate for the multiaxial stress state.

Implementing damage evolution concepts to the finite element analysis provides an efficient tool for predicting fretting fatigue damage. In safe-life design, the application of short crack methodologies to determine the cracking risk is appropriate. The critical plane methods are computationally expensive, having to evaluate the different parameters for a range of possible plane orientations, but permits estimating the crack initiation angle. The need for non-local methods, however, can introduce somewhat arbitrary length parameters to the problem (e.g. the critical distance).

9. Notch analogue model

Researchers in fretting fatigue have attempted to draw the very useful parallel to the theory of notch fatigue, thus possible making use of the extensive research on stress raisers in notches. Giannakopoulos et al. [85] drawed the analogy between fretting fatigue for rounded flat punches and (blunt) notch fatigue. By recognising that stress gradients and multiaxiality are important in fatigue for both notches and fretting contact, the analogy is clear. The most highly stressed point in the case of incomplete contact is the surface point at the edge of contact. Here, the normal and shear stresses will reach zero and the stress field might be assumed to be uniaxial [101]. In this case, multiaxial parameters might be avoided. It is generally believed, however, that initiation and early growth is mixed mode dominated and stress multiaxiality becomes important [112].

A method to account for the size effects in fretting fatigue is the classical *hot spot* method. However, studies have shown that the hot-spot method tends to be overly conservative [62]. More promising is using the *Theory of Critical Distances* (TCD), where the stresses are averaged in some sense. In the *point method* the stress is considered at a certain distance to the stress raiser, the *Line Method* averages the stresses over a line of certain length and in the *Area Method* the stresses are averaged over an area [113]. Researchers have successfully used TCD combined with different multiaxial criteria to determine fretting fatigue threshold conditions [112]. In general, TCD method can work well for determining orientations of Mode I dominated long cracks, but for initial crack orientation the approximation made by using volume averaging methods fail [114].

Fouvry et al. [115] conducted fretting fatigue tests under partial slip conditions of a sphere on plane and recorded normal force, tangential force and displacement. The results were compared with the predictions

made by describing the loading conditions using Mindlin and Hamilton [116] formulations with the Dang Van criterion. A volume-averaging method was used to account for the size effect and came to the conclusion that crack nucleation can be predicted by finding the size of the material intrinsic critical volume.

Araújo et al. [112] used MWCM [117,118] with the TCD method and compared with experimental data for cylinder-on-plane contact fatigue tests. The critical length L, was taken to be given by the material intrinsic "transition crack size" separating the short and long cracks regimes [119], see Eq. (14). The method was reported to correctly predict failures in the medium-cycle regime and for the high cycle regime within an error of ± 20 %, and also captured the size effect. The method is simple to implement as a post-processing step for linear elastic analysis, but relies on the fatigue crack formation processes to be confined in the critical volume. The size of this volume for a given material is however not dependent on geometrical features [120].

Santus [21] applied the MWCM with TCD to study fretting fatigue of steel-to-aluminium threaded pipe connections used in a corrosive environment. This method was mapped together with a slip-based parameter from which a fatigue limit was deduced based on experimental results from full scale tests. The slip parameter was used simply as a means of incorporating the competing effects of fretting wear and crack nucleation in the partial slip regime.

Ferré et al. [121] used different combinations of local and non-local multiaxial fatigue approaches to study the stress gradient effect on fretting crack nucleation. They performed cylinder-on-plane contact tests for Ti-6V-4V specimens in *low cycle fatigue loading* for three different cylinder radii and evaluated the different fatigue predictions for a range of stress gradients. Assessments were made using a local stress approach, volume-averaging approach, critical distance, and a weighted function approach based on work by Papadopoulos [122]. In general all the non-local approaches performed well, so they preferred the volume-averaging method for being practical.

For materials with large defects, cast iron, high strength steels, etc. probabilistic methods might also be useful methods to model the size effects [123,124]. Probabilistic methods for fretting fatigue is in general less researched than its deterministic counterparts, even though fretting fatigue is essentially a random process [125].

10. Crack analogue model

Related to the asymptotic methods for characterising the local fields surrounding the contact edges, a *crack analogue* for fretting fatigue have emerged, comparing the contact stress singularities with the stresses for cracks, essentially inferring the order of singularity to be square root bounded. The crack growth in fretting fatigue can then be viewed as a branching crack from the primary crack represented by the contact interface.

Giannakopoulos et al. [126] presented in 1998 a study in which the stress and strain fields of contact mechanics were matched with fracture mechanics solutions, see Fig. 4. They proposed to use the asymptotic field descriptions in linear elastic fracture mechanics (LEFM) as means to predict fretting fatigue life using the classical Paris law. Using the LEFM concept of T-stress, bulk cyclic stress, surface treatment residual stresses, etc. could be included. The *local* crack driving forces k_1 and k_2 were described using two coupled equations with the *remote* stress intensity factors K_I and K_{II}. The angle of initiation was found by assuming the crack to initiate along the direction for which the local mode II intensity factor vanishes ($k_2 = 0$), governed by the contact load P and tangential load Q. As the crack grows into the substrate however, the crack reorients to having the applied cyclic bulk stress σ_{app} as opening mode. The total life is thus modelled as two separate stages; The first stage for which the contact loads initiates and drives the crack to grow to a critical distance from the surface. Depending on the applied loads, the crack then either arrests or is driven further in Mode I govern by the cyclic bulk stress σ_{app}.

By quantitatively comparing with data found in the literature, Giannakopoulos et al. [126] found their results to agree with 15 fretting experiments from different studies. The limitations are however clear, inheriting the small-scale yielding limits from LEFM. The punch is also assumed to be rigid in this study, but the researchers refers to the work of Dundurs [127] and his material parameters for elastic bodies in contact. Crack initiation is assumed to be driven solely by the mechanical effects of the contact, thus surface roughness, wear, lubrication, etc. are neglected. Though the stress fields are not always square-root singular, these solutions are expected to be at least approximately valid for many combinations of materials and geometries [126].

This crack analogue model was also generalised to rounded contact where the stress singularities are induced from adhesion [68]. The stick/slip conditions were classified using the notion of strong and weak adhesion for static and dynamic friction. The three different modes of stress intensity factors were found at the stick-slip boundary and compared with material fatigue thresholds using an empirical relation between the adhesion and friction as derived by McFarlane and Tabor in 1950 [128]. Correlations were found for the crack initiation angle and threshold, but deviations were expected due to the stick-slip zone sizes in many cases being comparable with material grain size.

Inspired by the "crack analog", Fouvry and Berthel [61] recently used the width of the *partial slip sliding zone* as a length scale parameter in their crack analogue parameter. By multiplying the maximum shear stress with the square root of the sliding zone width, the fretting crack nucleation was represented without the need for very fine contact mesh in the FEM analysis.

Recently, researchers have put effort into systematising stress intensity factor computations for fretting fatigue [129–131].

Montebello et al. [99] proposes a method that is based on characterising the mechanical fields surrounding the contact by the *velocity field*. In this way, by using non-local stress intensity factors, comparing loading conditions does not require a full finite element simulation with extremely fine element meshes. This is an interesting approach and a possibly very useful method for industrial applications. It is expected that more research will look into the use of non-local stress intensity factors to account for the gradient effects.

10.1. Unified crack-notch model

Atzori and Lazzarin [132,133] unified the notch sensitivity and defect (crack) sensitivity in fatigue by defining a transition size a^* for which the "crack like notch" starts to behave like a "large blunt notch". They used a material intrinsic parameter to separate the classical notch mechanics regime with its peak stress criteria, and the fracture mechanics regime in which stress field criteria are used. The idea is that small contact area problems are described by a crack analogue where the fatigue threshold is not dependant on the crack geometry. But above a certain size, the notch analogue model becomes applicable, in which stress concentrations are accounted for. Ciavarella applied this method to the fretting problem [134,135], thus unifying the crack analogue with the notch analogue. When applied to the fretting test results by

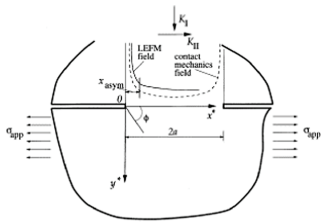

Fig. 4. Comparing the stress fields of contact with LEFM [126].

Araújo and Nowell [100,62], the method correctly separated the failed specimens from the run-outs.

The *Crack-Like Notch Analogue Model* (CLNA) uses the fatigue knock-down factor introduced by Ciavarella [134] on the fretting fatigue problem.

The Atzori-Lazzarin criterion can be mathematically expressed as

$$K_f = \min\left(\sqrt{1 + Y^2\frac{a}{a_0}}, K_t\right) \tag{13}$$

where a is half the crack width for an internal crack and the crack width for an edge crack. a_0 is the El Haddad crack length parameter [119] which is used to describe the transition from a "short crack" to a "long crack", together with the geometrical factor Y. The intrinsic property a_0 is given by

$$a_0 = \frac{1}{\pi}\left(\frac{\Delta K_{th}}{\Delta\sigma_1}\right)^2 \tag{14}$$

where ΔK_{th} is the threshold stress intensity factor range and $\Delta\sigma_1$ is the plain specimen fatigue limit.

The infinite-life predictions of the CLNA model were compared with Hertzian experiments and experiment data available from Araújo and Nowell [100] and others. In general, the model predicted failures and run-outs correctly. Ciavarella argues that, at least within the conditions described in [134], the parameters for multiaxiality were not necessary. Araújo et al. notes [112], the CLNA method is extremely efficient, but the application of this method on engineering applications is questionable, since it's based on 2D convex contact with constant normal load and in-phase oscillating bulk and tangential loads. However, due to its simplicity, it is excellent for early-stage design and planning experiments. Ciavarella and Berto [136] also contributed to the CLNA methods by further extending the methods to incorporate varying normal load.

As noted recently by Antunes et al. [129], there is lack of general expressions for stress intensity factors for cracks originating from bodies in contact under fretting conditions, and they seek to relieve this deficiency. They argue that a problem with CLNA method and analytical SIF in general, is neglecting non-linear effects. For estimating fretting fatigue life they used the Topper-El Haddad [137] notion of a crack tip stress raiser, calling it *Stress Gradient Factor (SGF)* as it modifies the reference stress intensity factor.

11. Wear

Fretting is in general referring to bodies in contact subjected to small sliding, and is not to be confused with the more specific terms *fretting corrosion*, *fretting wear* and *fretting fatigue*.

In tribology, fretting involves questions around friction, surface roughness, lubrication effects, wear debris formation and ejection, etc. [11]. The tribologically transformed structure and particle formation in fretting was studied by Sauger et al. [138]. Velocity accommodation effects may also be important [29] in some cases. However, it may be argued that many cases of *fretting fatigue* is negligibly affected by some tribological phenomena due to very small values of slip. Nonetheless, there is an increasing interest in incorporating wear into the fretting fatigue cracking analysis [139].

An energy description of the wear process was proposed by Fouvry et al. [25] using the interfacial shear work and considering situations where debris ejection was unrestricted. Thus, the frictional energy is related to the "contact endurance" and they proposed using Energy density-N diagrams as analogue to the S-N fatigue curves. This can be used e.g. to determine life time of the surface treatments for partial and gross sliding. The energy-based wear has been proven superior to the Archard model for sliding contact, unifying the wear over a range of sliding regimes [140].

Madge et al. [141] were among the first to try to numerically combine wear mechanisms with fatigue cracking analysis, attempting to relate the reduction in fatigue life with increasing slip amplitude which is reported in literature. They found that the pressure redistributing effect of material removal was critical in the driving forces for cracks. As material removal shifts the fretting fatigue damage evolution from the contact edge to the stick-slip boundary, a critical (*optimal*) value for wear coefficient can be found that increases fatigue life by spreading the fatigue damage over a larger area.

In gross slip, initial surface roughness plays an important role for the friction coefficient and wear [142]. Paggi et al. [143] derived a linear relationship between the tangential force and the stick contact area for the Greenwood-Williams contact with a rough surface described by an exponential probability distribution of the asperities. They used the generalised superpositioned principles of Ciavarella [74] and Jäger [75]. The probability distribution function of the surface (height distribution) were shown to only very weakly affect the results.

Yue and Wahab recently [144] considered the cylinder-on-flat geometry and studied the effect of variable coefficient of friction on the fretting wear on a range of sliding conditions. For gross sliding conditions, little difference was found, but for partial slip they found increasingly accurate measures of wear volume compared with experimental results previously reported. A finite element model was used with the energy based wear rates defined using a polynomial relation of coefficient of friction with the number of cycles.

12. Finite element methods

Today, numerical analysis of contact problems using the finite element method (FEM) is well established using either Lagrangian multipliers, augmented Lagrangian multipliers or the penalty method. For accurate descriptions of stick-slip in fretting contact however, additional computational costs involved with high number constraints for the Lagrangian multipliers might be necessary. Various methods are researched for modelling fretting fatigue using FEM including wear [141,144,140], plasticity [131], crack growth [145].

Continuum damage mechanics may be used in the FEM code to model the damage evolution and crack initiation [110]. Goh et al. (2003) studied microstructural effects on fretting fatigue by using a crystal plasticity model to describe the inherent material heterogeneity [146].

The *Extended Finite Element method* (XFEM) can be seen as the a natural extension to the standard finite element method (FEM), but with additional functions *enriching* the solution. Through the principle of partition of unity, discontinuous basis functions can be added to the solution space of FEM and provide capabilities to capture local and discontinuous effects like cracks, material interfaces, etc. Möes, Dolbow and Belytschko [145] introduced in 1999 the methods as a means for modelling cracks in the finite element framework without the need for remeshing.

Martínez et al. [147] used the XFEM implementation introduced by Giner et al. [148] in an attempt to predict cracking trajectory in railway axles under bending. *Crack closure* effects were considered by introducing restrictions to the appropriate nodes using truss elements. Using *the minimum shear stress range* as crack propagation criteria produced the most accurate results when compared with the real railway axle, but neglecting variations in the crack growth rate.

Nesládek and Španiel [149] recently initiated a project for developing a software tool to predict fretting fatigue. In engineering applications with complex model geometries, both fretting fatigue and plain fatigue often co-exist. Therefore, a plugin for Abaqus finite element software was proposed, attempting to unifying the assessments. The plugin is integrated in the graphical user interface and permits using multiaxial fatigue criteria in a post-processing step. TCD is used for the fretting stress gradients.

An interesting direction for further development in terms of the finite element modelling method is developing element formulations and

incorporating asymptotic descriptions. This could permit the singular and near singular fields to be calculated without the need for very fine meshes, and thus make it more useful in an engineering context. It may also serve as a platform for further studying microstructural effects on fretting fatigue crack nucleation [150]. Giner et al. [151] used singular expressions for complete contact as enrichment functions in the finite element formulation and found good estimates of stress intensity factors with relatively coarse meshes. Recently Cardoso et al. [152] applied singular enrichment functions to *incomplete* contact. Non-local intensity factors [99] was used to track the contact edges, hence, identifying the nodes to be enriched. Increased accuracy for coarse mesh.

In general, the FEM analysis has become an important tool for engineers, but for detailed contact analysis, FEM often require very fine meshes. Contact elements of size less than 10 μm are not uncommon. Thus, for larger models and for complex loading histories, the computational costs may not be justified, w.r.t. the accuracy and predictability actually gained. Sub-modelling techniques can be used to separate the contact problem from the structural analysis, thus avoiding the need for fine contact mesh in the global solution. Also, the use of non-local stress intensity factors is very useful for sub-modelling techniques [151,99,152].

13. Some comments on fretting fatigue testing

Given the complex nature of fretting fatigue, testing is in some cases *necessary* to obtain predictive confidence. A review of the methods and equipment used in testing probably deserves a whole separate treatment and is only shortly mentioned here. A number of different methods and test rigs are devised in the literature and in 1992 there was an attempt to start standardisation of the fretting fatigue test [153]. However, there is still no accepted generic standard [154]. The recent ASTM E2789 standard [155] provides only guidelines and general requirements for conducting a fretting fatigue test program. While it provides definitions and terminology for fretting fatigue testing, it does not propose a specific test configuration.

Hills and Nowell summarized in 2009 [156] the most important features with fretting fatigue testing. They argue that the standardisation of fretting fatigue test geometries will alleviate the comparison of different sets of results, but standardisation can also restrict the diversity of test results and hence make them less helpful for understanding fretting fatigue as a whole.

Early fretting fatigue tests made use of single-actuator test rigs where pads, usually of “bridge” type where clamped onto the specimen using e.g. a proving ring [157]. The clamping force was therefore constant as long as the wear was negligible. The Japanese standard *JSME S 015-2002* uses this test configuration [154]. More advanced, biaxial test rigs permits the cyclic load to be controlled independently from the contact loading. Early fretting tests at Oxford University used the fretting bridge on dogbone specimen, but during the end of 60s, they developed a test rig using Hertzian contact and electromagnetic resonance to generate the shear forces [158]. With this, the contact stresses, slip and displacements were known. These tests had a high degree of repeatability. Further generelisation was made that permitted independent control of shear and bulk forces in the specimen. This was also tested for *complete contact* with a self-aligning property avoiding rotation of the shear forces. The new arrangement have three independent actuators for the normal, shearing and bulk loads.

Other interesting developments in fretting fatigue testing include the use of *digital image correlation* (DIC) method to resolve the contact situation during the experiment [159,160].

14. Conclusions

Over a century after the first studies, researchers and engineers are still interested in and concerned with fretting fatigue. This article has attempted to review the progress in fretting fatigue understanding and predictions, with the engineering applications in mind. Fretting fatigue assessments in the industry are often very simple and relies on unsophisticated parameters. Comparing these parameters with company internal empirical data and experience the overall risk of fretting is determined, i.e. designing for “infinite life”. However, research in fretting and fretting fatigue have increased the understanding of the underlying phenomena and improvements have been made into determining fretting fatigue life. It is therefore argued that more elaborate analysis may be appropriate in many engineering applications.

It is clear that fretting and *fretting fatigue* are indeed complex problems, and for the practical engineering case not all contributing phenomena are important. The integrity of an engineering component is evaluated according to its intended requirements and operating conditions, and the design engineer must carefully identify the fretting regimes and choose the appropriate analysis. Some sliding motion are in many engineering cases inevitable, and partial slip conditions are common, promoting fretting fatigue. In other cases, fretting wear is more critical. Thus, the use of fretting maps is a valuable tool for the design engineer to predict the fretting regime and to visually reason about the mechanisms involved.

For more quantitative predictions of fretting fatigue, simple parameters like Ruiz (FD and FRD) give the engineers the possibility to numerically evaluate their design, however purely empirical. The Ruiz-parameters are widely used in the industry, mainly due to being accessible.

Drawing analogies to notches and cracks can be a great improvement in the predictability of fretting fatigue. These methods are easily applied to engineering cases to predict cracking risk and thereby designing for infinite life. The practicality of asymptotic methods in engineering applications may not seem obvious at first. However, the fact that the crack nucleation risk in critical regions surrounding contact edges can be matched to a small laboratory test may provide very useful tools. Most analyses are restricted by half-plane theory and small scale plasticity. For cases of varying contact normal load however, the asymptotic methods are difficult to use due to the moving contact edges.

For predicting fretting fatigue damage nucleation, multiaxial fatigue methods might be used, but with the amount of uncertainty involved, it most likely requires high safety-factors. Applying critical plane calculations as a post-processing step in elastic FEM analysis is a practical, but sometimes computationally costly approach. Sub-modelling techniques and non-local stress intensity factors are promising methods and may alleviate the problems with computational costs.

References

[1] Ciavarella M, Demelio G. A review of analytical aspects of fretting fatigue, with extension to damage parameters, and application to dovetail joints. Int J Solids Struct 2001;38(10):1791–811. https://doi.org/10.1016/S0020-7683(00)00136-0.
[2] Hills DA, Dini D. A review of the use of the asymptotic framework for quantification of fretting fatigue. J Strain Anal Eng Des 2016;51(4):240–6. https://doi.org/10.1177/0309324716638968.
[3] Li X, Zuo Z, Qin W. A fretting related damage parameter for fretting fatigue life prediction. Int J Fatigue 2015;73(Supplement C):110–8. https://doi.org/10.1016/j.ijfatigue.2014.12.003.
[4] Eden MEM, Rose MWN, Cunningham MPL. The endurance of metals: experiments on rotating beams at university college, London. Proc Inst Mech Eng 1911;81(1):839–974. https://doi.org/10.1243/PIME\PROC\1911\081\017\02.
[5] Tomlinson GA, Thorpe PL, Gough HJ. An investigation of the fretting corrosion of closely fitting surfaces. Proc Inst Mech Eng 1939;141(1):223–49. https://doi.org/10.1243/PIME\PROC\1939\141\034\02.
[6] Warlow-Davies E. Fretting corrosion and fatigue strength: brief results of preliminary experiments. Proc Inst Mech Eng 1941;146(1):32–8. https://doi.org/10.1243/PIME\PROC\1941\146\012\02.
[7] Collins JA. Fretting-fatigue damage-factor determination. J Eng Indust 1965;87(3):298–302. https://doi.org/10.1115/1.3670822.
[8] Beard J. An investigation into the mechanisms of fretting fatigue [Ph.D. thesis]. University of Salford; 1982.
[9] Araújo J, Almeida G, Ferreira J, da Silva C, Castro F. Early cracking orientation under high stress gradients: the fretting case. Int J Fatigue 2017;100:611–8. https://doi.org/10.1016/j.ijfatigue.2016.12.013.

[10] Golden PJ, Hutson A, Sundaram V, Arps JH. Effect of surface treatments on fretting fatigue of Ti-6Al-4V. Int J Fatigue 2007;29(7):1302–10. https://doi.org/10.1016/j.ijfatigue.2006.10.005.

[11] Berthier Y, Vincent L, Godet M. Fretting fatigue and fretting wear. Tribol Int 1989;22(4):235–42. https://doi.org/10.1016/0301-679x(89)90081-9.

[12] Teoh S. Fatigue of biomaterials: a review. Int J Fatigue 2000;22(10):825–37. https://doi.org/10.1016/s0142-1123(00)00052-9.

[13] Hoeppner D, Chandrasekaran V. Fretting in orthopaedic implants: a review. Wear 1994;173(1-2):189–97. https://doi.org/10.1016/0043-1648(94)90272-0.

[14] Ruiz C, Boddington PHB, Chen KC. An investigation of fatigue and fretting in a dovetail joint. Exp Mech 1984;24(3):208–17. https://doi.org/10.1007/BF02323167.

[15] Ekberg A. Fretting fatigue of railway axles—a review of predictive methods and an outline of a finite element model. Proc Inst Mech Eng Part F: J Rail Rapid Transit 2004;218(4):299–316. https://doi.org/10.1243/0954409043125905.

[16] Gürer G, Gür C. Failure analysis of fretting fatigue initiation and growth on railway axle press-fits. Eng Fail Anal 2018;84:151–66. https://doi.org/10.1016/j.engfailanal.2017.06.054.

[17] Gutkin R, Alfredsson B. Growth of fretting fatigue cracks in a shrink-fitted joint subjected to rotating bending. Eng Fail Anal 2008;15(5):582–96. https://doi.org/10.1016/j.engfailanal.2007.04.003.

[18] O'Halloran S, Harte A, Shipway P, Leen S. An experimental study on the key fretting variables for flexible marine risers. Tribol Int 2018;117:141–51. https://doi.org/10.1016/j.triboint.2017.07.032.

[19] Ding J, Leen SB, Williams EJ, Shipway PH. Finite element simulation of fretting wear-fatigue interaction in spline couplings. Tribol Mater Surf Interfaces 2008;2(1):10–24. https://doi.org/10.1179/175158308x320791.

[20] Sum W, Williams E, Leen S. Finite element, critical-plane, fatigue life prediction of simple and complex contact configurations. Int J Fatigue 2005;27(4):403–16. https://doi.org/10.1016/j.ijfatigue.2004.08.001.

[21] Santus C. Fretting fatigue of aluminum alloy in contact with steel in oil drill pipe connections, modeling to interpret test results. Int J Fatigue 2008;30(4):677–88. https://doi.org/10.1016/j.ijfatigue.2007.05.006. URL <http://www.sciencedirect.com/science/article/pii/S0142112307001740>.

[22] Szolwinski MP, Farris TN. Mechanics of fretting fatigue crack formation. Wear 1996;198(1–2):93–107. https://doi.org/10.1016/0043-1648(96)06937-2.

[23] Shen F, Hu W, Voyiadjis GZ, Meng Q. Effects of fatigue damage and wear on fretting fatigue under partial slip condition. Wear 2015;338–339:394–405. https://doi.org/10.1016/j.wear.2015.07.012.

[24] Vingsbo O, Söderberg S. On fretting maps. Wear 1988;126(2):131–47. https://doi.org/10.1016/0043-1648(88)90134-2.

[25] Fouvry S, Liskiewicz T, Kapsa P, Hannel S, Sauger E. An energy description of wear mechanisms and its applications to oscillating sliding contacts. Wear 2003;255(1–6):287–98. https://doi.org/10.1016/s0043-1648(03)00117-0.

[26] Zhou Z, Vincent L. Mixed fretting regime. Wear 1995;181–183:531–6. https://doi.org/10.1016/0043-1648(95)90168-x.

[27] Nowell D, Hills D. Crack initiation criteria in fretting fatigue. Wear 1990;136(2):329–43. https://doi.org/10.1016/0043-1648(90)90155-4.

[28] McCarthy O, McGarry J, Leen S. Microstructure-sensitive prediction and experimental validation of fretting fatigue. Wear 2013;305(1-2):100–14. https://doi.org/10.1016/j.wear.2013.05.012.

[29] Berthier Y, Vincent L, Godet M. Velocity accommodation in fretting. Wear 1988;125(1–2):25–38. https://doi.org/10.1016/0043-1648(88)90191-3.

[30] Blanchard P, Colombie C, Pellerin V, Fayeulle S, Vincent L. Material effects in fretting wear: application to iron, titanium, and aluminum alloys. Metall Trans A 1991;22(7):1535–44. https://doi.org/10.1007/bf02667367.

[31] Faanes S. Distribution of contact stresses along a worn fretting surface. Int J Solids Struct 1996;33(23):3477–89. https://doi.org/10.1016/0020-7683(95)00190-5.

[32] Barber J, Davies M, Hills D. Frictional elastic contact with periodic loading. Int J Solids Struct 2011;48(13):2041–7. https://doi.org/10.1016/j.ijsolstr.2011.03.008.

[33] Pearson S, Shipway P. Is the wear coefficient dependent upon slip amplitude in fretting? Vingsbo and Söderberg revisited. Wear 2015;330–331:93–102. https://doi.org/10.1016/j.wear.2014.11.005.

[34] Zhou Z, Fayeulle S, Vincent L. Cracking behaviour of various aluminium alloys during fretting wear. Wear 1992;155(2):317–30. https://doi.org/10.1016/0043-1648(92)90091-l.

[35] Jin O, Mall S. Effects of slip on fretting behavior: experiments and analyses. Wear 2004;256(7–8):671–84. https://doi.org/10.1016/s0043-1648(03)00510-6.

[36] Zhou Z, Nakazawa K, Zhu M, Maruyama N, Kapsa P, Vincent L. Progress in fretting maps. Tribol Int 2006;39(10):1068–73. https://doi.org/10.1016/j.triboint.2006.02.001.

[37] Fu Y, Wei J, Batchelor AW. Some considerations on the mitigation of fretting damage by the application of surface-modification technologies. J Mater Process Technol 2000;99(1–3):231–45. https://doi.org/10.1016/s0924-0136(99)00429-x.

[38] Alquezar M, Arrieta V, Constantinescu A, Flandi L, Maitournam MH, Wackers P. Computational fretting fatigue maps for different plasticity models. Fatigue Fract Eng Mater Struct 2014;37(4):446–61. https://doi.org/10.1111/ffe.12130.

[39] Garcin S, Fouvry S, Heredia S. A FEM fretting map modeling: effect of surface wear on crack nucleation. Wear 2015;330–331:145–59. https://doi.org/10.1016/j.wear.2015.01.013.

[40] Lykins CD, Mall S, Jain V. An evaluation of parameters for predicting fretting fatigue crack initiation. Int J Fatigue 2000;22(8):703–16. https://doi.org/10.1016/S0142-1123(00)00036-0. URL <http://www.sciencedirect.com/science/article/pii/S0142112300000360>.

[41] Vidner J, Leidich E. Enhanced Ruiz criterion for the evaluation of crack initiation in contact subjected to fretting fatigue. Int J Fatigue 2007;29(9–11):2040–9. https://doi.org/10.1016/j.ijfatigue.2007.02.010.

[42] Ding J, Houghton D, Williams E, Leen S. Simple parameters to predict effect of surface damage on fretting fatigue. Int J Fatigue 2011;33(3):332–42. https://doi.org/10.1016/j.ijfatigue.2010.09.008.

[43] Varenberg M, Etsion I, Halperin G. Slip index: a new unified approach to fretting. Tribol Lett 2004;17(3):569–73. https://doi.org/10.1023/b:tril.0000044506.98760.f9.

[44] Varenberg M, Etsion I, Altus E. Theoretical substantiation of the slip index approach to fretting. Tribol Lett 2005;19(4):263–4. https://doi.org/10.1007/s11249-005-7442-8.

[45] Smith K, Watson P, Topper T. Stress- strain function for the fatigue of metals. J Mater 1970;5(4):767–78. cited By 1301. URL <https://www.scopus.com/inward/record.uri?eid=2-s2.0-00148901048&partnerID=40&md5=9381f9c5e7de03987a62416d0faf5ea7>.

[46] Socie D. Multiaxial fatigue damage models. J Eng Mater Technol 1987;109(4):293. https://doi.org/10.1115/1.3225980.

[47] Araújo J, Nowell D. The effect of rapidly varying contact stress fields on fretting fatigue. Int J Fatigue 2002;24(7):763–75. https://doi.org/10.1016/S0142-1123(01)00191-8. URL <http://www.sciencedirect.com/science/article/pii/S0142112301001918>.

[48] Fatemi A, Socie DF. A critical plane approach to multiaxial fatigue damage including out-of-phase loading. Fatigue Fract Eng Mater Struct 1988;11(3):149–65. https://doi.org/10.1111/j.1460-2695.1988.tb01169.x.

[49] Araújo JA, Nowell D, Vivacqua RC. The use of multiaxial fatigue models to predict fretting fatigue life of components subjected to different contact stress fields. Fatigue Fract Eng Mater Struct 2004;27(10):967–78. https://doi.org/10.1111/j.1460-2695.2004.00820.x.

[50] Socie DF, Marquis GB. Multiaxial fatigue. SAE International; 2000.

[51] Findley WN. A theory for the effect of mean stress on fatigue of metals under combined torsion and axial load or bending. Engineering Materials Research Laboratory, Division of Engineering, Brown University; 1958.

[52] Park J. Evaluation of an energy-based approach and a critical plane approach for predicting constant amplitude multiaxial fatigue life. Int J Fatigue 2000;22(1):23–39. https://doi.org/10.1016/s0142-1123(99)00111-5.

[53] Namjoshi SA, Mall S, Jain VK, Jin O. Fretting fatigue crack initiation mechanism in Ti-6Al-4V. Fatigue Fract Eng Mater Struct 2002;25(10):955–64. https://doi.org/10.1046/j.1460-2695.2002.00549.x.

[54] Bhatti NA, Wahab MA. Finite element analysis of fretting fatigue under out of phase loading conditions. Tribol Int 2017;109:552–62. https://doi.org/10.1016/j.triboint.2017.01.022.

[55] Foletti S, Beretta S, Gurer G. Defect acceptability under full-scale fretting fatigue tests for railway axles. Int J Fatigue 2016;86:34–43. https://doi.org/10.1016/j.ijfatigue.2015.08.023.

[56] Dang-Van K. Macro-micro approach in high-cycle multiaxial fatigue. In: Advances in multiaxial fatigue. ASTM International. p. 120–120-11. https://doi.org/10.1520/stp24799s.

[57] Liu Y, Mahadevan S. Multiaxial high-cycle fatigue criterion and life prediction for metals. Int J Fatigue 2005;27(7):790–800. https://doi.org/10.1016/j.ijfatigue.2005.01.003.

[58] Chakherlou TN, Abazadeh B. Estimation of fatigue life for plates including pre-treated fastener holes using different multiaxial fatigue criteria. Int J Fatigue 2011;33(3):343–53. https://doi.org/10.1016/j.ijfatigue.2010.09.006.

[59] Navarro C, Muñoz S, Domínguez J. On the use of multiaxial fatigue criteria for fretting fatigue life assessment. Int J Fatigue 2008;30(1):32–44. https://doi.org/10.1016/j.ijfatigue.2007.02.018.

[60] Ferré R, Fouvry S, Berthel B, Amargier R, Ruiz-Sabariego J. Prediction of the fretting fatigue crack nucleation endurance of a Ti-6V-4Al/Ti- 6V-4Al interface: influence of plasticity and tensile/shear fatigue properties. Procedia Eng 2013;66:803–12. https://doi.org/10.1016/j.proeng.2013.12.134.

[61] Fouvry S, Berthel B. Prediction of fretting-fatigue crack nucleation using a surface shear – sliding size crack analog parameter. Procedia Eng 2015;133:179–91. https://doi.org/10.1016/j.proeng.2015.12.649.

[62] Araújo J, Susmel L, Taylor D, Ferro J, Ferreira J. On the prediction of high-cycle fretting fatigue strength: theory of critical distances vs. hot-spot approach. Eng Fract Mech 2008;75(7):1763–78. https://doi.org/10.1016/j.engfracmech.2007.03.026. critical Distance Theories of Fracture. URL <http://www.sciencedirect.com/science/article/pii/S0013794407001506>.

[63] Fouvry S, Kapsa P, Vincent L. Quantification of fretting damage. Wear 1996;200(1–2):186–205. https://doi.org/10.1016/s0043-1648(96)07306-1.

[64] Hertz H. Ueber die berührung fester elastischer körper. J für die reine und angewandte Mathematik 1882;92:156–71. URL <http://eudml.org/doc/148490>.

[65] Bradley MA RS. LXXIX. The cohesive force between solid surfaces and the surface energy of solids. Lond Edinburgh Dublin Philos Mag J Sci 1932;13(86):853–62. https://doi.org/10.1080/14786449209461990.

[66] Johnson KL, Kendall K, Roberts AD. Surface energy and the contact of elastic solids. Proc Roy Soc Lond Math Phys Eng Sci 1971;324(1558):301–13. https://doi.org/10.1098/rspa.1971.0141. URL <http://rspa.royalsocietypublishing.org/content/324/1558/301>.

[67] Derjaguin B, Muller V, Toporov Y. Effect of contact deformations on the adhesion of particles. J Colloid Interface Sci 1975;53(2):314–26. https://doi.org/10.1016/0021-9797(75)90018-1.

[68] Giannakopoulos A, Venkatesh T, Lindley T, Suresh S. The role of adhesion in contact fatigue. Acta Mater 1999;47(18):4653–64. https://doi.org/10.1016/s1359-6454(99)00312-2.

[69] Cattaneo C. Sul contatto di due corpi elastici: distribuzione locale degli sforzi.

Rend Accad Naz Lincei 1938;27(6):342–8.
[70] Mindlin RD. Compliance of elastic bodies in contact. J Appl Mech ASME 1949;16:259–68.
[71] Mindlin R, Deresiewicz H. Elastic spheres in contact under varying oblique forces. J Appl Mech 1953;20:327–44.
[72] Hamilton GM, Goodman LE. The stress field created by a circular sliding contact. J Appl Mech 1966;33(2):371–6. https://doi.org/10.1115/1.3625051. URL <http://appliedmechanics.asmedigitalcollection.asme.org/article.aspx?articleid=1397631>.
[73] Nowell D, Hills D. Mechanics of fretting fatigue tests. Int J Mech Sci 1987;29(5):355–65. https://doi.org/10.1016/0020-7403(87)90117-2. URl <http://www.sciencedirect.com/science/article/pii/0020740387901172>.
[74] Ciavarella M. The generalized Cattaneo partial slip plane contact problem. I—theory. Int J Solids Struct 1998;35(18):2349–62. https://doi.org/10.1016/S0020-7683(97)00154-6.
[75] Jäger J. A new principle in contact mechanics. J Tribol 1998;120(4):677–84. https://doi.org/10.1115/1.2833765.
[76] Munisamy RL, Hills DA, Nowell D. Static axisymmetric hertzian contacts subject to shearing forces. J Appl Mech 1994;61(2):278. https://doi.org/10.1115/1.2901441.
[77] Etsion I. Revisiting the Cattaneo-Mindlin concept of interfacial slip in tangentially loaded compliant bodies. J Tribol 2010;132(2):020801. https://doi.org/10.1115/1.4001238.
[78] Tabor D. Junction growth in metallic friction: the role of combined stresses and surface contamination. Proc Roy Soc A: Math Phys Eng Sci 1959;251(1266):378–93. https://doi.org/10.1098/rspa.1959.0114.
[79] Wang Z-J, Wang W-Z, Wang H, Zhu D, Hu Y-Z. Partial slip contact analysis on three-dimensional elastic layered half space. J Tribol 2010;132(2):021403. https://doi.org/10.1115/1.4001011.
[80] Li J, Berger EJ. A semi-analytical approach to three-dimensional normal contact problems with friction. Comput Mech 2003;30(4):310–22. https://doi.org/10.1007/s00466-002-0407-y.
[81] Kogut L, Etsion I. A semi-analytical solution for the sliding inception of a spherical contact. J Tribol 2003;125(3):499. https://doi.org/10.1115/1.1538190.
[82] Davies M, Barber J, Hills D. Energy dissipation in a frictional incomplete contact with varying normal load. Int J Mech Sci 2012;55(1):13–21. https://doi.org/10.1016/j.ijmecsci.2011.11.006.
[83] Fouvry S, Kapsa P, Vincent L. Analysis of sliding behaviour for fretting loadings: determination of transition criteria. Wear 1995;185(1–2):35–46. https://doi.org/10.1016/0043-1648(94)06582-9.
[84] Mugadu A, Hills D, Limmer L. An asymptotic approach to crack initiation in fretting fatigue of complete contacts. J Mech Phys Solids 2002;50(3):531–47. https://doi.org/10.1016/s0022-5096(01)00091-6.
[85] Giannakopoulos, Suresh, Chenut. Similarities of stress concentrations in contact at round punches and fatigue at notches: implications to fretting fatigue crack initiation. Fatigue Fract Eng Mater Struct 2000;23(7):561–71. https://doi.org/10.1046/j.1460-2695.2000.00306.x.
[86] Dini D, Hills DA. Bounded asymptotic solutions for incomplete contacts in partial slip. Int J Solids Struct 2004;41(24–25):7049–62. https://doi.org/10.1016/j.ijsolstr.2004.05.058.
[87] Williams ML. Stress singularities resulting from various boundary conditions in angular corners of plates in extension. J Appl Mech 1952;4(19):526–34.
[88] Flicek R, Hills D, Dini D. Sharp edged contacts subject to fretting: a description of corner behaviour. Int J Fatigue 2015;71:26–34. https://doi.org/10.1016/j.ijfatigue.2014.02.015.
[89] Bogy DB. Edge-bonded dissimilar orthogonal elastic wedges under normal and shear loading. J Appl Mech 1968;35(3):460. https://doi.org/10.1115/1.3601236.
[90] Dundurs J, Lee MS. Stress concentration at a sharp edge in contact problems. J Elast 1972;2(2):109–12. https://doi.org/10.1007/bf00046059.
[91] Churchman C, Mugadu A, Hills D. Asymptotic results for slipping complete frictional contacts. Eur J Mech A Solids 2003;22(6):793–800. https://doi.org/10.1016/s0997-7538(03)00074-3.
[92] Johnson K. Contact mechanics. Cambridge University Press; 1985. URL <http://app.knovel.com/hotlink/toc/id:kpCM000008/contact-mechanics/contact-mechanics>.
[93] Barber J. Elasticity. 3rd ed. Springer; 2010. URL <https://www.springer.com/gp/book/9789048138081>.
[94] Sackfield A, Mugadu A, Barber J, Hills D. The application of asymptotic solutions to characterising the process zone in almost complete frictionless contacts. J Mech Phys Solids 2003;51(7):1333–46. https://doi.org/10.1016/s0022-5096(03)00020-6.
[95] Hills DA, Dini D. A new method for the quantification of nucleation of fretting fatigue cracks using asymptotic contact solutions. Tribol Int 2006;39(10):1114–22. https://doi.org/10.1016/j.triboint.2006.02.041.
[96] Hills D, Thaitirarot A, Barber J, Dini D. Correlation of fretting fatigue experimental results using an asymptotic approach. Int J Fatigue 2012;43:62–75. https://doi.org/10.1016/j.ijfatigue.2012.02.006.
[97] Churchman C, Hills D. Slip zone length at the edge of a complete contact. Int J Solids Struct 2006;43(7–8):2037–49. https://doi.org/10.1016/j.ijsolstr.2005.06.099.
[98] Fleury R, Hills D, Ramesh R, Barber J. Incomplete contacts in partial slip subject to varying normal and shear loading, and their representation by asymptotes. J Mech Phys Solids 2017;99:178–91. https://doi.org/10.1016/j.jmps.2016.11.016.
[99] Montebello C, Pommier S, Demmou K, Leroux J, Meriaux J. Analysis of the stress gradient effect in fretting-fatigue through nonlocal intensity factors. Int J Fatigue 2016;82:188–98. https://doi.org/10.1016/j.ijfatigue.2015.02.009.
[100] Araújo J, Nowell D. Analysis of pad size effects in fretting fatigue using short crack arrest methodologies. Int J Fatigue 1999;21(9):947–56. https://doi.org/10.1016/S0142-1123(99)00077-8. URL <http://www.sciencedirect.com/science/article/pii/S0142112399000778>.
[101] Nowell D, Dini D, Hills D. Recent developments in the understanding of fretting fatigue. Eng Fract Mech 2006;73(2):207–22. https://doi.org/10.1016/j.engfracmech.2005.01.013. advanced Fracture Mechanincs for Life Safety Assessments.
[102] Fouvry S, Nowell D, Kubiak K, Hills D. Prediction of fretting crack propagation based on a short crack methodology. Eng Fract Mech 2008;75(6):1605–22. https://doi.org/10.1016/j.engfracmech.2007.06.011.
[103] Lehtovaara A, Rabb R. A numerical model for the evaluation of fretting fatigue crack initiation in rough point contact. Wear 2008;264(9–10):750–6. https://doi.org/10.1016/j.wear.2006.12.083.
[104] Navarro C, García M, Domínguez J. A procedure for estimating the total life in fretting fatigue. Fatigue Fract Eng Mater Struct 2003;26(5):459–68. https://doi.org/10.1046/j.1460-2695.2003.00647.x.
[105] Szolwinski MP, Farris TN. Observation, analysis and prediction of fretting fatigue in 2024-t351 aluminum alloy. Wear 1998;221(1):24–36. https://doi.org/10.1016/s0043-1648(98)00264-6.
[106] Lamacq V, Dubourg MC, Vincent L. Crack path prediction under fretting fatigue—a theoretical and experimental approach. J Tribol 1996;118(4):711. https://doi.org/10.1115/1.2831599.
[107] Baietto M, Pierres E, Gravouil A, Berthel B, Fouvry S, Trolle B. Fretting fatigue crack growth simulation based on a combined experimental and XFEM strategy. Int J Fatigue 2013;47:31–43. https://doi.org/10.1016/j.ijfatigue.2012.07.007.
[108] Faanes S. Inclined cracks in fretting fatigue. Eng Fract Mech 1995;52(1):71–82. https://doi.org/10.1016/0013-7944(94)00331-b.
[109] Lemaitre J. Coupled elasto-plasticity and damage constitutive equations. Comput Methods Appl Mech Eng 1985;51(1–3):31–49. https://doi.org/10.1016/0045-7825(85)90026-x.
[110] Zhang T, McHugh P, Leen S. Finite element implementation of multiaxial continuum damage mechanics for plain and fretting fatigue. Int J Fatigue 2012;44:260–72. https://doi.org/10.1016/j.ijfatigue.2012.04.011.
[111] Hojjati-Talemi R, Wahab MA. Fretting fatigue crack initiation lifetime predictor tool: using damage mechanics approach. Tribol Int 2013;60:176–86. https://doi.org/10.1016/j.triboint.2012.10.028.
[112] Araújo J, Susmel L, Taylor D, Ferro J, Mamiya E. On the use of the theory of critical distances and the modified Wöhler curve method to estimate fretting fatigue strength of cylindrical contacts. Int J Fatigue 2007;29(1):95–107. https://doi.org/10.1016/j.ijfatigue.2006.02.041. URL <http://www.sciencedirect.com/science/article/pii/S0142112306000776>.
[113] Taylor D. Geometrical effects in fatigue: a unifying theoretical model. Int J Fatigue 1999;21(5):413–20. https://doi.org/10.1016/s0142-1123(99)00007-9.
[114] Susmel L, Taylor D. Non-propagating cracks and high-cycle fatigue failures in sharply notched specimens under in-phase mode i and II loading. Eng Fail Anal 2007;14(5):861–76. https://doi.org/10.1016/j.engfailanal.2006.11.038.
[115] Fouvry S, Kapsa P, Vincent L. Multiaxial fatigue analysis of fretting contact taking into account the size effect. In: The 2nd international symposium on fretting fatigue: current technology and practices, no. 1367 in 2; 2000. p. 167–82.
[116] Hamilton GM. Explicit equations for the stresses beneath a sliding spherical contact. Proc Inst Mech Eng Part C: J Mech Eng Sci 1983;197(1):53–9. https://doi.org/10.1243/PIME\PROC\1983\197\076\02.
[117] Susmel L, Lazzarin P. A biparametric Wöhler curve for high cycle multiaxial fatigue assessment. Fatigue Fract Eng Mater Struct 2002;25(1):63–78. https://doi.org/10.1046/j.1460-2695.2002.00462.x.
[118] Susmel L, Taylor D. Two methods for predicting the multiaxial fatigue limits of sharp notches. Fatigue Fract Eng Mater Struct 2003;26(9):821–33. https://doi.org/10.1046/j.1460-2695.2003.00683.x.
[119] Haddad ME, Topper T, Smith K. Prediction of non propagating cracks. Eng Fract Mech 1979;11(3):573–84. https://doi.org/10.1016/0013-7944(79)90081-X. URL <http://www.sciencedirect.com/science/article/pii/001379447990081X>.
[120] Susmel L. A unifying approach to estimate the high-cycle fatigue strength of notched components subjected to both uniaxial and multiaxial cyclic loadings. Fatigue Fract Eng Mater Struct 2004;27(5):391–411. https://doi.org/10.1111/j.1460-2695.2004.00759.x.
[121] Ferré R, et al. Stress gradient effect on the crack nucleation process of a Ti-6Al-4V titanium alloy under fretting loading: comparison between non-local fatigue approaches. Int J Fatigue 2013;54(Supplement C):56–67. https://doi.org/10.1016/j.ijfatigue.2013.03.005. URL <http://www.sciencedirect.com/science/article/pii/S0142112313000844>.
[122] Papadopoulos Ioannis V, Panoskaltsis Vassilis P. Invariant formulation of a gradient dependent multiaxial high-cycle fatigue criterion. Eng Fract Mech 1996;55(4):513–28. https://doi.org/10.1016/S0013-7944(96)00047-1. URL <http://www.sciencedirect.com/science/article/pii/S0013794496000471>.
[123] Chantier, et al. A probabilistic approach to predict the very high-cycle fatigue behaviour of spheroidal graphite cast iron structures. Fatigue Fract Eng Mater Struct 2000;23(2):173–80. https://doi.org/10.1046/j.1460-2695.2000.00228.x.
[124] Luu DH, Maitournam MH, Nguyen QS. Formulation of gradient multiaxial fatigue criteria. Int J Fatigue 2014;61:170–83. https://doi.org/10.1016/j.ijfatigue.2013.11.014.
[125] Enright MP, Chan KS, Moody JP, Golden PJ, Chandra R, Pentz AC. Probabilistic fretting fatigue assessment of aircraft engine disks. J Eng Gas Turbines Power 2010;132(7):072502. https://doi.org/10.1115/1.4000130.
[126] Giannakopoulos A, Lindley T, Suresh S. Aspects of equivalence between contact mechanics and fracture mechanics: theoretical connections and a life-prediction

methodology for fretting-fatigue. Acta Mater 1998;46(9):2955–68. https://doi.org/10.1016/S1359-6454(98)00011-1.
[127] Dundurs J. Discussion: “edge-bonded dissimilar orthogonal elastic wedges under normal and shear loading” (Bogy, D.B., 1968, ASME J. Appl. Mech. 35, pp. 460–466). J Appl Mech 1969;36(3):650. https://doi.org/10.1115/1.3564739.
[128] McFarlane JS, Tabor D. Adhesion of solids and the effect of surface films. Proc Roy Soc A: Math Phys Eng Sci 1950;202(1069):224–43. https://doi.org/10.1098/rspa.1950.0096.
[129] Antunes Marcelo Avelaer, et al. Stress intensity factor solutions for fretting fatigue using stress gradient factor. Eng Fract Mech 2017;186:331–46. https://doi.org/10.1016/j.engfracmech.2017.10.031.
[130] de Pannemaecker A, et al. Numerical methods for stress intensity factor δk calculations of fretting cracked interface. Tribol Int 2018;119:389–403. https://doi.org/10.1016/j.triboint.2017.10.029. URL <http://www.sciencedirect.com/science/article/pii/S0301679X17304954>.
[131] Gandiolle Camille, Fouvry Siegfried. Experimental analysis and modeling of the crack arrest condition under severe plastic fretting fatigue conditions. Procedia Eng 2013;66:783–92. https://doi.org/10.1016/j.proeng.2013.12.132.
[132] Atzori Bruno, Lazzarin Paolo. Notch sensitivity and defect sensitivity under fatigue loading: two sides of the same medal. Int J Fract 2001;107(1):1–8. https://doi.org/10.1023/A:1007686727207.
[133] Atzori B, Lazzarin P, Meneghetti G. Fracture mechanics and notch sensitivity. Fatigue Fract Eng Mater Struct 2003;26(3):257–67. https://doi.org/10.1046/j.1460-2695.2003.00633.x.
[134] Ciavarella M. A ‘crack-like’ notch analogue for a safe-life fretting fatigue design methodology. Fatigue Fract Eng Mater Struct 2003;26(12):1159–70. https://doi.org/10.1046/j.1460-2695.2003.00721.x.
[135] Ciavarella M. Some observations on the CLNA model in fretting fatigue. Tribol Int 2006;39(10):1142–8. https://doi.org/10.1016/j.triboint.2006.02.032. the Fourth International Symposium on Fretting Fatigue.
[136] Ciavarella M, Berto F. A simplified extension of the crack analogue model for fretting fatigue with varying normal load. Theoret Appl Fract Mech 2017. https://doi.org/10.1016/j.tafmec.2017.03.011.
[137] El Haddad MH, Topper TH, Topper TN. Fatigue life predictions of smooth and notched specimens based on fracture mechanics. J Eng Mater Technol 1981;103(2):91. https://doi.org/10.1115/1.3224996.
[138] Sauger E, et al. Tribologically transformed structure in fretting. Wear 2000;245(1–2):39–52. https://doi.org/10.1016/s0043-1648(00)00464-6.
[139] Madge JJ, et al. Contact-evolution based prediction of fretting fatigue life: effect of slip amplitude. Wear 2007;262(9–10):1159–70. https://doi.org/10.1016/j.wear.2006.11.004.
[140] Zhang T, McHugh PE, Leen SB. Computational study on the effect of contact geometry on fretting behaviour. Wear 2011;271(9-10):1462–80. https://doi.org/10.1016/j.wear.2010.11.017.
[141] Madge JJ, Leen SB, Shipway PH. The critical role of fretting wear in the analysis of fretting fatigue. Wear 2007;263(1–6):542–51. https://doi.org/10.1016/j.wear.2006.11.021.
[142] Pawlus Pawel, et al. The effect of random surface topography height on fretting in dry gross slip conditions. Proc Inst Mech Eng Part J: J Eng Tribol 2014;228(12):1374–91. https://doi.org/10.1177/1350650114539467.
[143] Paggi Marco, Pohrt Roman, Popov Valentin L. Partial-slip frictional response of rough surfaces. Sci Rep 2014;4(1). https://doi.org/10.1038/srep05178.
[144] Yue Tongyan, Wahab Magd Abdel. Finite element analysis of fretting wear under variable coefficient of friction and different contact regimes. Tribol Int 2017;107:274–82. https://doi.org/10.1016/j.triboint.2016.11.044.
[145] Moës N, Dolbow J, Belytschko T. A finite element method for crack growth without remeshing. Int J Numer Meth Eng 1999;46(1):131–50. https://doi.org/10.1002/(sici)1097-0207(19990910)46:1<131::aid-nme726>3.0.co;2-j.
[146] Goh C-H, Neu R, McDowell D. Influence of nonhomogeneous material in fretting fatigue. In: Fretting fatigue: advances in basic understanding and applications. ASTM International. p. 183–183-23. https://doi.org/10.1520/stp10760s.
[147] Martínez JC, Useche LVV, Wahab MA. Numerical prediction of fretting fatigue crack trajectory in a railway axle using XFEM. Int J Fatigue 2017;100:32–49. https://doi.org/10.1016/j.ijfatigue.2017.03.009.
[148] Giner E, Sukumar N, Tarancón J, Fuenmayor F. An Abaqus implementation of the extended finite element method. Eng Fract Mech 2009;76(3):347–68. https://doi.org/10.1016/j.engfracmech.2008.10.015.
[149] Nesládek M, Španiel M. An Abaqus plugin for fatigue predictions. Adv Eng Softw 2017;103:1–11. https://doi.org/10.1016/j.advengsoft.2016.10.008.
[150] Hills D, Ramesh R, Fleury R, Parel K. A unified approach for representing fretting and damage at the edges of incomplete and receding contacts. Tribol Int 2017;108:16–22. https://doi.org/10.1016/j.triboint.2016.08.026.
[151] Giner E, Sukumar N, Fuenmayor FJ, Vercher A. Singularity enrichment for complete sliding contact using the partition of unity finite element method. Int J Numer Meth Eng 2008;76(9):1402–18. https://doi.org/10.1002/nme.2359.
[152] Cardoso Raphael Araújo et al. An enrichment-based approach for the simulation of fretting problems. In: Computational mechanics; May 2018. https://doi.org/10.1007/s00466-018-1577-6.
[153] Attia MH, Waterhouse RB, editors. Standardization of fretting fatigue test methods and equipment ASTM International; 1992. https://doi.org/10.1520/stp1159-eb.
[154] Neu RW. Progress in standardization of fretting fatigue terminology and testing. Tribol Int 2011;44(11):1371–7. https://doi.org/10.1016/j.triboint.2010.12.001.
[155] Guide for fretting fatigue testing. https://doi.org/10.1520/e2789-10r15.
[156] Hills D, Nowell D. What features are needed in a fretting fatigue test? Tribol Int 2009;42(9):1316–23. https://doi.org/10.1016/j.triboint.2009.04.023 special Issue: Fifth International Symposium on Fretting Fatigue.
[157] Lindley TC, Nix KJ. Fretting fatigue in the power generation industry: experiments, analysis, and integrity assessment. Standardization of fretting fatigue test methods and equipment ASTM International; 1992. p. 153-153-17. https://doi.org/10.1520/stp25828s.
[158] Hills DA, Nowell D. Mechanics of fretting fatigue – oxford’s contribution. Tribol Int 2014;76:1–5. https://doi.org/10.1016/j.triboint.2013.09.015.
[159] Kartal ME, Mulvihill DM, Nowell D, Hills DA. Determination of the frictional properties of titanium and nickel alloys using the digital image correlation method. Exp Mech 2010;51(3):359–71. https://doi.org/10.1007/s11340-010-9366-y.
[160] Juoksukangas J, Lehtovaara A, Mäntylä A. Applying the digital image correlation method to fretting contact for slip measurement. Proc Inst Mech Eng Part J: J Eng Tribol 2016;231(4):509–19. https://doi.org/10.1177/1350650115601695.

A.2 Paper II

Investigating efficiency of shear stress-based critical plane methods for general three-dimensional stress cycles.

International Journal of Fatigue 134 (2020) 105448

Contents lists available at ScienceDirect

International Journal of Fatigue

journal homepage: www.elsevier.com/locate/ijfatigue

Efficient implementation of critical plane for 3D stress histories using triangular elements

Steffen Loen Sunde*, Filippo Berto, Bjørn Haugen

Norwegian University of Science and Technology (NTNU), Department of Mechanical and Industrial Engineering, Norway

ARTICLE INFO

Keywords:
Critical plane
Multiaxial fatigue
Computation
Findley criterion
Fatigue crack initiation

ABSTRACT

Multiaxial fatigue and the application of critical plane criteria are briefly reviewed. Methods to increase the efficiency of such criteria are discussed. A simple methodology is also presented where the critical plane search space is discretised using triangular elements and adaptively refined. It is shown to increase accuracy in the damage search with fewer candidate plane evaluations, useful for large 3D models. Parallel computations are also leveraged.

1. Introduction

In engineering practice, fatigue assessments often involve large 3D models of complex geometry subjected to multiaxial stresses. In many cases, the loads are also non-proportional [1,2], which greatly complicates the fatigue evaluation.

It is a well-observed phenomenon that cracks form and grow in preferential material planes [3,4], the orientation of which depends on the loading and the material. This fact, combined with multiaxial stresses, have caused critical plane (CP) criteria to be a popular method for many researchers [5–9]. These criteria are concerned with searching for the material plane orientation having the largest fatigue damage and thus have a physical foundation. Critical plane criteria are, however, known to be computationally expensive, having to evaluate the fatigue damage on a large number of candidate material planes. For real-world engineering cases, finite element models often have hundreds of thousands or millions of elements subjected to complex load histories and critical plane fatigue assessment can become too expensive, especially in the early design iteration stage. By accelerating the critical plane computational effort, higher analysis throughput will allow for a more efficient design iteration process. In these cases, early identification of critical areas and hot-spots can be important.

This paper describes a numerical implementation of a critical plane analysis for multiaxial fatigue and considers several methods to accelerate the analysis. Multiaxial fatigue is quickly reviewed with special regards to its relation with critical plane analysis for fatigue assessments. Shear stress-dominated fatigue is considered, and some improvements to the critical plane implementation are investigated.

The main aim of this paper is to survey the efficiency of critical plane analysis applications to engineering models. An adaptive implementation of the critical plane search is described and its effectiveness is demonstrated. Some of the points raised are applicable to certain classes of critical plane models but do not apply in general.

2. Critical plane approach to multiaxial fatigue

Fatigue is often heuristically divided into low-cycle fatigue (LCF) and high-cycle fatigue (HCF) due to the dominating mechanisms being distinct. In LCF plasticity plays an important role, but in HCF, plasticity is usually of negligible importance. LCF analyses are concerned with loading in the range of $1 - 10^4$ cycles whereas HCF is often in the range of $10^4 - 10^8$ cycles. Some applications are even concerned with very high-cycle fatigue (VHCF) regimes ($>10^8$) [10]. Engineers often design for loads in HCF and VHCF ranges but damaging events (shocks etc.) belonging to the LCF regimes may occur [11]. The loading regime is an important factor when choosing a critical plane criterion; whereas for HCF stress-based criteria are often used, for problems involving plasticity, strain-based criteria are often used.

For fatigue assessments involving variable amplitude loading, popular methods reduces the multiaxial stress history into an equivalent (*invariant*) stress history on which damage is counted and accumulated. Among the most popular, classical criteria using stress invariants are

Abbreviations: 2D, two-dimensional; 3D, three-dimensional; CH, convex hull; CP, critical plane; CPU, central processing unit; HCF, high-cycle fatigue; JIT, just-in-time; LC, longest chord; LCF, low-cycle fatigue; LP, longest projection; MCC, minimum circumscribed circle; MRH, maximum rectangular hull; SWT, Smith-Watson-Topper criterion; VHCF, very high-cycle fatigue

* Corresponding author.
E-mail address: steffen.sunde@ntnu.no (S.L. Sunde).

https://doi.org/10.1016/j.ijfatigue.2019.105448
Received 6 September 2019; Received in revised form 18 December 2019; Accepted 19 December 2019
Available online 10 January 2020
0142-1123/

Nomenclature

(ϕ^c, θ^c)	tuple of angles representing the critical plane
τ^*	centre of MCC
τ	shear stress
τ_m	mean shear stress
τ_{t_i}	shear stress at timet_i
$\mathbf{n}$	unit normal vector
$\mathbf{t}$	traction vector
δ	phase difference
γ_a	shear strain amplitude
λ	frequency ratio
ω	orientation of shear path for MRH
ϕ	normal vector azimuth
π	candidate material plane
Ψ	shear path in material plane
σ	Cauchy stress tensor
σ_n	normal stress
σ_y	material yield stress
$\sigma_{n,max}$	maximum normal stress during a cycle
$\sigma_{xx,a}$	normal stress amplitude
$\sigma_{xx,m}$	mean normal stress
$\sigma_{xy,a}$	shear stress amplitude
$\sigma_{xy,m}$	mean shear stress
τ_a	equivalent shear stress amplitude
τ_i	shear vector in candidate plane at time t_i
θ	normal vector inclination
$a_{1,2}$	sides of the MRH
k_{Fn}	Findley material constant
k_{FS}	material constant
N	total number of candidate planes
P	time period
p	material point
t	time instant
k	number of points in hemisphere
l	refinement threshold
m	subset size
n	subset reduction factor

the Sines [12] and Crossland [13]. It is clear, however, that these methods will not correctly account for phase- and frequency differences, and that they exclude the load signs of the different stress components ("channels"). This makes them only suitable for simple proportional load histories. For variable amplitude loading, it is especially important with a proper cycle counting method to account for all damaging events.

Uniaxial and equivalent stress histories are one-dimensional and therefore popularly counted using traditional *Rainflow counting* [14] or one of its derivatives. For non-proportional multiaxial fatigue, however, the single-channel counting algorithms fail due to neglecting reversals on more than one stress component. Attempts to perform multiaxial cycle counting have been made by applying Rainflow counting on each projected material plane [15]. Other methodologies executes the counting on *relative quantities* of the stress invariants. Wang and Brown [16] performed counting on relative von Mises strains to overcome the problem of load sign loss in the stress invariants. Meggiolaro and de Castro [17] proposed a modification to avoid the largest load range to be missed. Anes et al. [18] proposed a "stress scale factor" between the shear and axial stresses on which counting was performed. Weighted averages and statistical parameters are also used [19].

The additional complexity of non-proportional loads is important due to the stress tensors having components that individually may change throughout the load history. If all the oscillating stress components are in-phase, the principal direction of the stress is constant, and the load is classified as proportional. In non-proportional loading, however, the stress components change in a non-proportional fashion with each other, and thus the principal direction of stress rotates. Consequently, the orientation of the material plane experiencing the most damaging stress is not known *a priori*. With non-proportional cyclic stresses, the material may experience additional hardening due to non-planar slip bands, which can greatly reduce the fatigue life [20]. Sensitivity to non-proportional loading varies from material to material, depending on its microstructure, hardness etc. [2]. Many steels have been found to experience non-proportional hardening, while e.g. aluminium alloys are less affected [21]. In general, non-proportional loading is known to be at least as damaging as proportional loading and should be incorporated in the fatigue model [22]. This suggests that fatigue damage accumulates on different material planes independently and that critical plane models are physically ground. Recently, significant attention has been paid to the effects of non-proportionality on the fatigue analysis [23–25].

3. Critical plane analysis

In the following, the material is assumed to be isotropic undergoing small deformations. Combinations of stresses and strains are assumed to drive the cracks to initiate and grow in certain material planes. These driving forces are evaluated at material points, thought to represent small, homogeneous volumes of material. Consider a material point p in a coordinate frame $Oxyz$ being subjected to stress given by the tensor σ. Its components can be expressed by the symmetric matrix

$$\sigma = \begin{bmatrix} \sigma_{xx} & \sigma_{xy} & \sigma_{xz} \\ \sigma_{xy} & \sigma_{yy} & \sigma_{yz} \\ \sigma_{xz} & \sigma_{yz} & \sigma_{zz} \end{bmatrix}$$

i.e. with six independent components which in general can be its own function of time.

Consider now a *candidate* material plane π centered in this point and with its orientation given by the unit normal vector $\mathbf{n}$. The orientation is alternatively expressed by the two angles ϕ and θ. The traction stress vector $\mathbf{t}$ acting on this plane is given by Cauchy's stress theorem and obtained by

$$\mathbf{t} = \sigma \cdot \mathbf{n} \tag{1}$$

From the traction vector, the normal stress *scalar* σ_n and shear stress *vector* τ acting in the material plane π can subsequently be obtained by the vector dot product

$$\sigma_n = \mathbf{t} \cdot \mathbf{n} \tag{2}$$

and

$$\tau = \mathbf{t} - \sigma_n \mathbf{n} \tag{3}$$

Now, a load history can be discretised by a set of stress tensors acting on the material point throughout the loading sequence. This loading history, or more specifically, its projected shear stresses and normal stresses are driving force for the fatigue damage in the material plane. The direction of the normal stress is given by the plane normal vector, but the shear stress history, being a vector acting in the material plane, can be thought to describe a two-dimensional path Ψ in π. For a proportional load cycle, this path is represented by a straight line, but for a non-proportional cycle, the path can be a complex 2D shape, see Fig. 1.

In terms of calculating the fatigue damage in a candidate plane, most criteria depend on *amplitude* values of the load. Determining the normal stress amplitude acting on the plane is trivial. The shear path is generally a two-dimensional shape, and determining amplitude and mean values is therefore nontrivial. There is extensive research focused

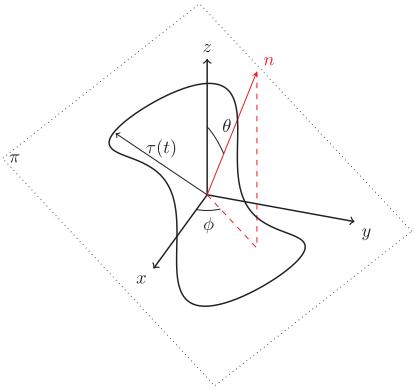

Fig. 1. Shear stress acting in the candidate plane π.

on this specific problem, and only a brief review of the methodologies is considered in the here.

First, some relevant critical plane criteria are considered for context.

The Findley critical plane parameter [26] can be expressed as a linear combination of the shear stress amplitude and the maximum normal stress. The orientation of the critical plane can be expressed mathematically by

$$(\phi^c, \theta^c)\colon \max_{\phi,\theta}\{\tau_a(\phi, \theta) + k_{Fn}\sigma_{n,max}(\phi, \theta)\} \tag{4}$$

where τ_a is the shear stress amplitude and $\sigma_{n,max}$ is the maximum normal stress acting on the plane during the cycle. k is a material parameter that often ranges between 0.1 and 0.2 [27]. As highlighted by Papadopoulos [22], the Findley criterion predicts a dependence on mean shear stress, which is found to be negligible in many HCF studies [28]. The criterion is popular nonetheless and shown to work for titanium, steel, and aluminium, among others. For small values of k, the effects of static shear are also negligible.

Analogously, the multiaxial fatigue damage can be defined through a *strain*-based parameter, often applied to LCF and ductile materials. Fatemi et al. [6] found the critical plane to be at or near the plane of maximal shear strain amplitude. In this case, the critical plane can be described by

$$(\phi^c, \theta^c)\colon \max_{\phi,\theta}\left\{\gamma_a\left(1 + k_{FS}\frac{\sigma_{n,max}}{\sigma_y}\right)\right\} \tag{5}$$

where γ_a is the shear strain amplitude and $\sigma_{n,max}$ is the largest normal stress on the critical plane. σ_y is the yield stress and k_{FS} is a material constant.

Implicit relation for the fatigue life can then be expressed and related to relevant fatigue parameters by combining the damage parameter for the critical plane with Basquin and Coffin-Manson laws [29]. Subsequently, for life predictions, the number of cycles are solved for using e.g. Newton-Raphson iterations.

Other shear based critical plane parameters are the Modified Wöhler Curve Method [30], Matake [31], McDiarmid [32] and more recently a class of extensions to the classical energy-based criterion by Smith, Watson and Topper (swt) [33,34,24].

3.1. Equivalent shear amplitude

The aforesaid complexities related to the shear-based fatigue criteria are now addressed. As the shear stress history is a vector history, there is no immediate amplitude value given for the non-proportional load history. For criteria based on shear amplitude quantities, a scalar-valued function is needed to transform the vector history into an *equivalent amplitude*. A large amount of research has been put into these functions, and a number of two-dimensional geometric projection methods have been proposed. The two most simple methods are the *longest chord* (LC) and *longest projection* (LP) methods, for which the shear path is projected onto a single line in the candidate plane. LC method searches for the largest distance between two points on the path. The amplitude is the half-length of the line connecting these two points and the mean is its midpoint. In the LP method however, the path points are projected onto all lines in the candidate plane running through the origin. The amplitude is half-length of the extreme points on this projection and the mean is its center. The problem with LC and LP is that for some load paths, the definitions of the mean and amplitude are ambiguous.

Minimum Circumscribing circle (MCC) was proposed by Dang Van [35] in the 90s and is often used [36]. A circle is found to cover the shear path. The center of the circle is taken as the mean shear value and the radius represents the shear stress amplitude. The problem of finding the MCC can be expressed as [22]

$$\tau_m\colon \min_{\tau^*}\{\max_{t_i}||\tau(t_i) - \tau^*||\} \tag{6}$$

where τ_m is the mean shear, $\tau(t_i)$ is the shear vector tip at time t_i and τ^* is the vector position of the circle center.

The MCC problem as stated above is mathematically well-defined as it can be shown that this circle is unique. A brute-force solution solves the problem in $O(n^4)$ time where n is the number of history points, and may therefore be quite time consuming for longer time histories. There are, however, algorithmic solutions of *linear* time complexity [36,37] and iterative methods converge quickly. Nonetheless, as remarked by some authors, a problem with the MCC method is its inability to distinguish between some proportional and non-proportional histories [9,38].

3.2. Maximum rectangular hull

Araújo et al. [9] proposed to calculate the equivalent shear stress by using the maximum rectangular hull (MRH). This rectangle is found by simply rotating the shear path $\omega \in [0, \pi/2]$ and finding its longest projection along two perpendicular axes, expressed as a_1 and a_2 in the equations below. The mean shear stress can then be evaluated as the centre of the rectangle and the amplitude is the half the rectangle diagonal. For proportional loading histories, MRH provides the same result as the longest projection. However, by taking its maximum projection over the possible rotations of the path, MRH correctly predicts larger equivalent amplitudes for non-proportional paths. Therefore, the Maximum Rectangular Hull provides an improvement over MCC, LC and LP wrt. differentiating proportional and non-proportional loads.

$$\tau_a = \max_{\omega}\sqrt{a_1^2(\omega) + a_2^2(\omega)},\ 0 \le \omega \le \pi/2 \tag{7}$$

where the sides of the rectangle a_1 and a_2 are given by

$$a_i(\omega) = \frac{1}{2}[\max_t \tau_i(\omega, t) - \min_t \tau_i(\omega, t)],\ i = 1, 2 \tag{8}$$

Thus, the equivalent shear stress is found by rotating the projected shear path (Ψ) for a pre-determined resolution of angles ω and finding its maximum bidirectional projection in the candidate plane. See Fig. 2 for a comparison of the MRH and MCC.

3.3. Convex hull

Dealing with discrete shear paths Ψ_i as two-dimensional polygons, the field of computational geometry has provided some potentially useful algorithms. The convex hull (CH) of a set of points in the two-

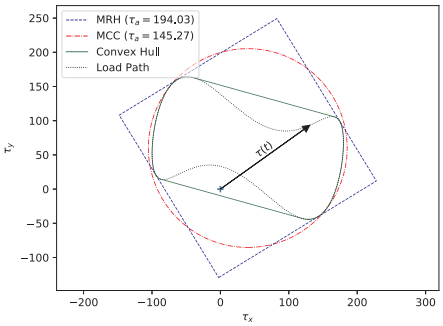

Fig. 2. Comparing MRH and MCC equivalent shear stress amplitude for a fictitious shear stress history in the candidate material plane.

dimensional plane is the (unique) smallest polygon containing all the points. It can be shown that the ch of a set of points will be entirely contained within its enclosing surface (MRH, MCC etc.). For longer load histories (i.e. many points) the CH can greatly reduce the the number of points considered for the shear stress path, essentially assuming that the interior loading points do not contribute to fatigue damage. A number of algorithms exists for computing the ch. In this paper the *Graham Scan* algorithm is used, introduced by Graham [39] in 1972. Whilst a brute force search for the convex hull is $O(n^3)$, the Graham Scan is $O(n \log n)$ where n is the number of points in the original path.

3.4. Critical plane search space

It is convenient to describe the orientation of the candidate plane normal vector in a spherical coordinate frame (r, θ, ϕ) where r is the radial distance, θ is the inclination and ϕ is the azimuth. Since the material normal vector is of unit length, the search space is effectively described by a unit sphere. By using the fact that negating the normal vector describes the same plane, the search space is reduced to a *hemisphere*.

In theory the hemisphere describes an infinite set of material plane orientations. A naive (brute-force) procedure of discretising this hemisphere is by using a pre-determined angular increment for the inclination and azimuth (henceforth referred to as *angle grid*). This however, will not guarantee to find the critical plane, and the accuracy of the solution depends on the resolution of the angle grid. Also, this discretisation provides a non-uniform partition of the hemisphere due to the semi-circumferences being divided into equally many points [40]. Thus, poles becomes more dense than around the equator. Using a pre-determined grid of angles is inefficient, due to having to evaluate the fatigue criteria in a large set of sub-critical candidate planes.

By instead discretising the hemisphere using triangular cells allows for a much more uniform spacing [36], see Fig. 4. The hemisphere is divided into triangular cells where each corner point represents the unit

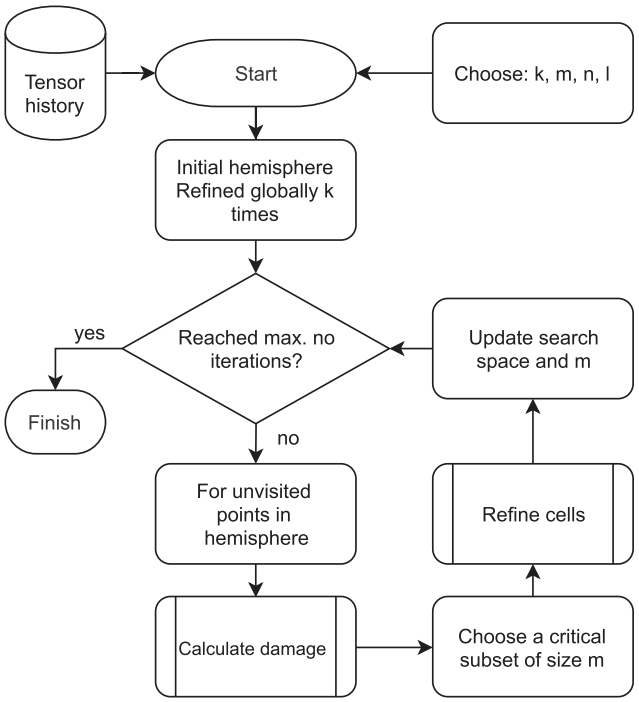

Fig. 3. Flowchart for a simple adaptive implementation of critical plane search.

normal for a candidate plane. Triangular cells are also trivial to recursively partition into new, smaller (children) cells. An iterative scheme can start of by an initial (coarse) set of material plane orientation. Then, after each round of fatigue damage evaluations, the most critical cells are refined and the damage is computed for the new set of points.

The simplest adaptive scheme uses a pre-determined number of iterations and refines a subset of cells for each iteration. Thus, the convergence for a given load history will depend on the initial set of points and on the size of subsets. For a fixed subset size, the total number of orientations can grow quite large. More elaborate refinement schemes are possible [41]. Svärd [36] used a *branch and bound* method for the cp search for the Findley criterion and showed its convergence to be guaranteed. In general, objective functions represented by fatigue criterion evaluation are non-convex functions and guaranteed convergence is not possible.

Here, a simple adaptive scheme is demonstrated, where for each iteration, a subset of points is chosen based on their computed value (damage) during the previous iteration. The cells connected to this subset are refined. The subset size is lowered for each iteration until a threshold condition is met. Initial size (k), its the subset threshold (m) and its reduction factor (n) are chosen by the user. A cell is only refined if its value represented an increase in damage wrt. its parent cell. The adaptive scheme is shown in the flowchart in Fig. 3.

Fig. 4 shows the resulting hemisphere discretisation from the adaptive refinement for the simple case of uni-axial loading.

3.5. Model validation and results

To validate the method of using triangular elements with adaptive refinement, fatigue damages are compared with the "correct" solution of 180x180 angles, and a number of grid refinement levels used in practice [9,21,27]. Comparisons are made for a series of experimental results found in the literature [22,9,42,43] (see Table 1–3), and $2{\cdot}10^6$ pseudo-random load histories consisting of three or four history points.

The referenced load histories are bi-axial, synchronous and asynchronous bending and torsion, i.e. they can be expressed as

$$\sigma(t) = \begin{bmatrix} \sigma_{xx}(t) & \sigma_{xy}(t) & 0 \\ \sigma_{xy}(t) & 0 & 0 \\ 0 & 0 & 0 \end{bmatrix} \tag{9}$$

where

$$\sigma_{xx}(t) = \sigma_{xx,a}\sin\left(\frac{2\pi t}{P}\right) + \sigma_{xx,m} \tag{10}$$

and

$$\sigma_{xy}(t) = \sigma_{xy,a}\sin\left(\lambda\frac{2\pi t}{P} + \delta\right) + \sigma_{xy,m} \tag{11}$$

Shear stress amplitude is used as damage measure (Findley $k = 0.0$) on the bi-axial load cases for comparison with the sources. To determine the shear amplitude, the MRH method is used. As noted by Petrucci [38], MRH has some of the same problems as LC in that there are cases where the mean shear is not always unique. But as highlighted by Papadopoulos [22] the mean shear effect is negligible, and therefore is of small concern in many cases. The authors of MRH found the rectangular hull to converge for only five rotations (ω in equation 3.2). Here, MRH was tested on the 2 million pseudo-random histories for angle increments of 1 and 10 degrees and the maximum difference was found to be 0.4% (around 0.1% on average).

Fig. 5 shows an example of a non-proportional bi-axial load history for a material point and the resulting equivalent shear stress amplitude as a function of material plane orientation. As mentioned in Section 2, special care must be taken for non-proportional histories to properly identify the load reversals and account for damaging cycles.

Note in Fig. 5b that there are more than one direction where the equivalent shear stress are equally critical in terms of its amplitude. For unambiguous direction, a choice of critical plane can be made e.g. by choosing the plane experiencing the largest normal stress [9].

Comparing different angle grid refinements with the "correct" damage (equivalent shear amplitude denoted τ_a) for the histories in Tables 1 and 2 shows that the error is quite low for relatively coarse grids. The

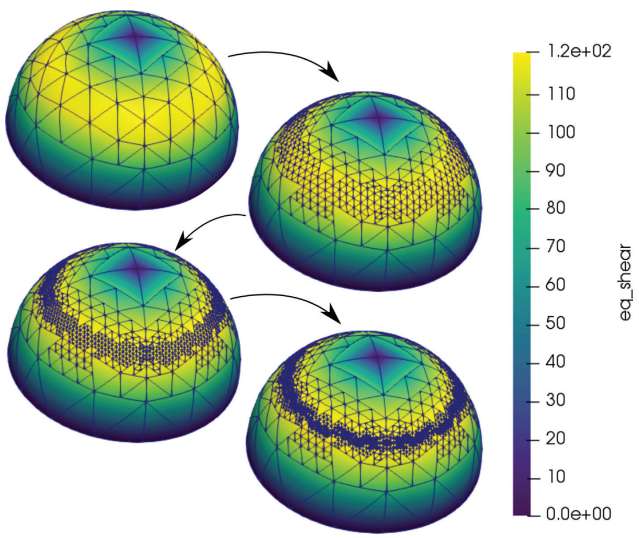

Fig. 4. Adaptive refinement illustrated by the simple case of cyclic push-pull loading, $\sigma_{yy}(t) = 242\sin t$.

Table 1
Synchronous experimental data ($\lambda = 1$).

Case	No.	$\sigma_{xx,a}$	$\sigma_{xx,m}$	$\sigma_{xy,a}$	$\sigma_{xy,m}$	δ	τ_a
		MPa	MPa	MPa	MPa	deg	MPa
a	0	138.1	0.0	167.1	0.0	0.0	180.8
	1	140.4	0.0	169.9	0.0	30.0	180.8
	2	145.7	0.0	176.3	0.0	60.0	180.5
	3	150.2	0.0	181.7	0.0	90.0	181.7
	4	245.3	0.0	122.7	0.0	0.0	173.4
	5	249.7	0.0	124.8	0.0	30.0	170.5
	6	252.4	0.0	126.2	0.0	60.0	159.7
	7	258.0	0.0	129.0	0.0	90.0	161.2
	8	299.1	0.0	62.8	0.0	0.0	162.2
	9	304.5	0.0	63.9	0.0	90.0	158.9
b	10	328.0	0.0	157.0	0.0	0.0	227.0
	11	286.0	0.0	137.0	0.0	90.0	175.8
	12	233.0	0.0	224.0	0.0	0.0	252.5
	13	213.0	0.0	205.0	0.0	90.0	205.2
	14	266.0	0.0	128.0	128.0	0.0	184.6
	15	283.0	0.0	136.0	136.0	90.0	174.2
	16	333.0	0.0	160.0	160.0	180.0	230.9
	17	280.0	280.0	134.0	0.0	0.0	193.8
	18	271.0	271.0	130.0	0.0	90.0	166.7
b	19	314.0	0.0	157.0	0.0	0.0	222.0
	20	315.0	0.0	158.0	0.0	60.0	199.6
	21	316.0	0.0	158.0	0.0	90.0	197.5
	22	315.0	0.0	158.0	0.0	120.0	199.6
	23	224.0	0.0	224.0	0.0	90.0	224.0
	24	380.0	0.0	95.0	0.0	90.0	201.9
	25	316.0	0.0	158.0	158.0	0.0	223.4
	26	314.0	0.0	157.0	157.0	60.0	198.7
	27	315.0	0.0	158.0	158.0	90.0	197.1
	28	279.0	279.0	140.0	0.0	0.0	197.6
	29	284.0	284.0	142.0	0.0	90.0	177.5
	30	355.0	0.0	89.0	178.0	0.0	198.6
	31	212.0	212.0	212.0	0.0	90.0	212.0
	32	129.0	0.0	258.0	0.0	90.0	258.0
d	33	485.0	0.0	280.0	0.0	0.0	370.4
	34	480.0	0.0	277.0	0.0	90.0	319.9
	35	480.0	300.0	277.0	0.0	0.0	366.5
	36	480.0	300.0	277.0	0.0	45.0	339.3
	37	470.0	300.0	270.0	0.0	60.0	318.2
	38	473.0	300.0	273.0	0.0	90.0	315.3
	39	590.0	300.0	148.0	0.0	0.0	330.0
	40	565.0	300.0	141.0	0.0	45.0	302.3
	41	540.0	300.0	135.0	0.0	90.0	286.9
	42	211.0	300.0	365.0	0.0	0.0	379.9

Table 2
Asynchronous experimental data.

Case	No.	$\sigma_{xx,a}$	$\sigma_{xx,m}$	$\sigma_{xy,a}$	$\sigma_{xy,m}$	δ	λ	τ_a
		MPa	MPa	MPa	MPa	deg		MPa
e	43	263.0	0.0	132.0	0.0	0.0	4.00	222.9
f	44	186.0	0.0	93.0	0.0	0.0	0.25	158.3
	45	185.0	0.0	93.0	0.0	0.0	4.00	156.9
g	46	285.0	0.0	285.0	0.0	0.0	0.25	352.7
	47	290.0	0.0	290.0	0.0	0.0	4.00	367.5
h	48	259.5	0.0	150.0	0.0	0.0	2.00	215.6
	49	266.0	0.0	153.6	0.0	0.0	3.00	225.6
i	50	210.0	0.0	105.0	0.0	0.0	0.25	178.7
	51	220.0	0.0	110.0	0.0	0.0	2.00	169.3
	52	242.0	0.0	121.0	0.0	90.0	2.00	164.2
	53	196.0	0.0	98.0	0.0	0.0	8.00	170.7

maximum error for angle steps of 10, 9, 7.5 and 6 are 0.9%, 1.2%, 0.8% and 0.4% respectively.

Now comparing the damage obtained by using the adaptive scheme described in previous section. The initial hemisphere consists of 41 points and subjected to different levels of initial refinement thresholds. Using threshold of 0.05, an average of 164 planes was investigated, resulting in maximum error of 0.5%. For thresholds of e.g. 0.075, 0.1 and 0.125, maximum error all converged to 0.02%, with average

Table 3
Material data for the load cases.

Case	Material	f_{-1}	t_{-1}	Source
		MPa	MPa	
a	Hard steel	313.9	196.2	McDiarmid et al. [44]
b	42CrMo4 steel	398.0	260.0	Lempp 1985, reported in [42]
c	34Cr4 steel	410.0	256.0	Zenner et al. [42]
d	30NCD16 steel	660.0	410.0	Froustey and Lasserre [43]
e	34Cr4 steel	415.0	259.0	Heidenreich et al. [45]
f	GGG60	275.0	249.0	Susmel et al. reported in [22]
g	30NCD16 steel	585.0	405.0	Froustey et al. reported in [9]
h	39NiCrMo3 steel	585.0	405.0	Froustey et al. reported in [9]
i	25CrMo4 steel	340.0	228.0	Kaniut et al. reported in [9]

around $5{\cdot}10^{-3}$ %. The number of candidate planes using these threshold were 241, 327 and 418 respectively. The time saved depends on details of the implementation. The computational overhead associated with the refinement process was found to be small. An illustration of the process for load case 52 can be seen in Fig. 6. Notice how all four peaks are identified.

The resulting number of candidate planes N_{planes} for the adaptive method depends on the load history. For the "correct" brute force method, a very fine angular step is used, $\Delta\phi = \Delta\theta = 1^{\circ}$, i.e. 32400 orientations. In most cases though, this level of refinement is excessive, depending on the behaviour of the damage function and of the desired accuracy. See more about this in Section 4.

All load histories were implemented with 100 stress tensors, which means that the time steps were different for the asynchronous histories. Across the data set reported in Tables 1 and 2, the use of the convex hull reduced the number of shear points in the candidate plane by around 55%. The overall effectiveness of CH depends on the load however; only interior points on the shear path are removed. Consider as an example the special case where the shear path in the candidate plane is described by a circle. In this case, all the points in the shear path are also points on the convex hull. Thus, no points are discarded and computation is wasted. Recall that the time complexity of the convex hull (using Graham Scan) is $O(n \log n)$ and the MRH algorithm is linear in n where n is the number of points. Hence, the gain by first computing the CH reduces as the number of points in the load history increases. Using convex hull resulted in 24% reduced computation time for 100 history points, but this reward is steadily decreased as the number of history points increases. For around 400 points, the effect was negligible.

The adaptive scheme is also demonstrated using the Findley criterion on a set of $2{\cdot}10^{6}$ pseudo-random stress histories consisting of three or four time steps. Findley criterion is chosen due to its simplicity and due to it demonstrating dependence on both shear and normal quantities in the candidate plane. In general, convergence is more challenging for these objective functions, compared with the well-behaving damage functions produced from harmonic time series, see e.g. Fig. 7. Correspondingly, coarse angle grids may potentially under-estimate damages. Using angle increments of 10, 9, 7.5 and 6 resulted in largest underestimation of fatigue damage of 1.8%, 1.5%, 1.0% and 0.7% respectively.

Here the initial hemisphere consists of 145 points ($k = 3$) and reduction factor 2. For subset a size of 0.05, error was 1.2% and resulted in 241 candidate planes on average. For 0.075, 0.1 and 0.125, the maximum error had converged to 0.5%. The average number of candidate planes were 280, 333 and 377, respectively.

The algorithms were implemented in Python 3.7 using *numpy* numerical library and in C++ using *Eigen3* template library. As expected, the runtime using a high-level language (Python) is considerably longer than the lower-level, compiled language C++. On average, Python ran almost two orders of magnitude slower to compute full 180x180 grid searches compared with the single-threaded C++ version. By making use of Just-in-time (JIT) compilation support for numpy arrays using

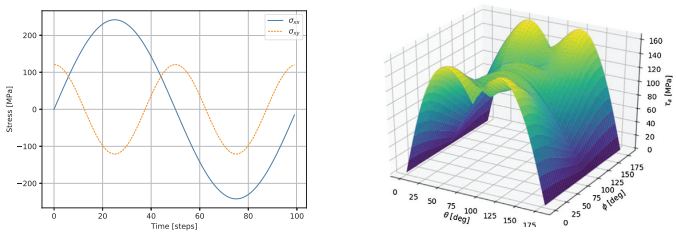

(a) Stress cycle for load case 52 in table 2. (b) Equivalent shear stress amplitude.

Fig. 5. Load cycle and resulting damage surface for load case 52 (see Table 2).

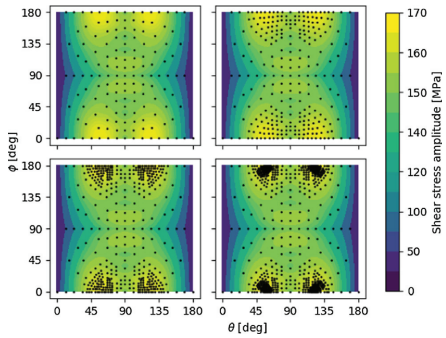

Fig. 6. A 2-dimensional representation of an adaptive scheme searching for the critical plane for case 52.

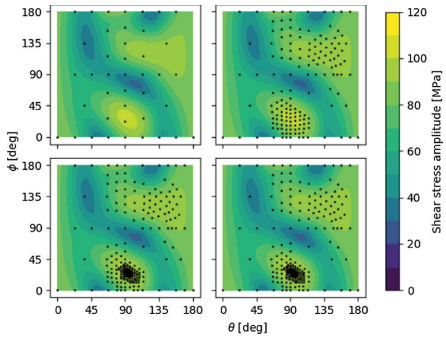

Fig. 7. Demonstration of an adaptive scheme and brute force damages for a stress cycle consisting of only three time steps.

the *numba* library [46], the Python programs can be accelerated considerably. By using JIT compilation, the python code is automatically translated into optimized low-level machine code.

To further accelerate the C++ critical plane search, the multi-threading library *OpenMP 4.5* [47] was used. The total search space is simply divided into blocks, one for each thread. Once each thread has finished its search for the maximum damage, the candidate planes for each block are compared and the global critical plane is found. By using e.g. 6 CPU cores (Intel Xeon 3.3 GHz) the multi-threaded version ran on average 5.6 times faster.

4. Discussion

A short discussion on the accuracy of the critical plane methods is appropriate. The accuracy of critical plane analysis and the computational cost generally is a trade-off. Investigating more candidate planes increases the chance of finding the maximum fatigue damage, and conservative analyses are preferred. Nonetheless, due to the inherent, large scatter and uncertainty in fatigue, most analyses require large safety factors anyways, especially for life predictions. Less underestimation is, however, always better, e.g. for hot-spot identification in engineering components.

The damage surface (see e.g. Fig. 5) of many combinations of load histories and fatigue criteria are relatively well-behaving. For such cases, small differences are often found for relatively coarse angle grids. Damage underestimation can still occur if maxima happens to occur in between grid points. Notice, e.g. how the maximum error increased when the angle grid was refined from 10 to 9 degree angular increment for the referenced load histories. This is why relatively fine grids (5–8 degree increments) are recommended for the fatigue damage to converge to “reasonable high” and stable values. Evaluation of the fatigue criteria on all points of such fine grids are expensive for large models and this is where an adaptive scheme can be of aid. The adaptive method demonstrated lower fatigue damage underestimation for comparably fewer candidate planes. Such a simple refinement scheme is easy to implement and can apply to a large class of critical plane criteria. It should however, be used with caution and not without verification. An adaptive scheme also introduces complications for the damage summation process for non-proportional load histories where damage is to be accumulated on each material plane. Lastly, more specific refinement schemes can be implemented, especially tailored for different fatigue criteria, see e.g. [36].

5. Conclusions

In this work, some aspects of critical plane analysis of multiaxial fatigue was considered. Methods to accelerate the search for the maximum fatigue damage using critical plane criteria were addressed, and in particular using triangular discretisation of the search space with an adaptive refinement. A very naive refinement rule is shown to give more accurate damage predictions for fewer fatigue criterion evaluations. It was tested on experimental data found in literature and two million pseudo-random load histories. Single-threaded C++ code was found to be around two orders of magnitude faster than the Python version, and multi-threading was found to scale well.

Declaration of Competing Interest

The authors declare that they have no known competing financial interests or personal relationships that could have appeared to influence the work reported in this paper.

References

[1] Zerres P, Vormwald M. Review of fatigue crack growth under nonproportional mixed-mode loading. Int J Fatigue 2014;58:75–83. https://doi.org/10.1016/j.ijfatigue.2013.04.001.

[2] Nima Shamsaei and Ali Fatemi. Effect of microstructure and hardness on non-proportional cyclic hardening coefficient and predictions. Mater Sci Eng, A May 2010;527(12):3015–24. https://doi.org/10.1016/j.msea.2010.01.056.

[3] Yingyu Wang and Luca Susmel. “Critical plane approach to multiaxial variable amplitude fatigue loading”. In: Fracture and Structural Integrity 9.33 (June 2015). Rainflow, linear Miner-Palmgren, Modified Manson Coffin Curve Method, Maximum variance method, issn: 1971-8993. doi: 10.3221/IGF-ESIS.33.38.

[4] Sum WS, Williams E, Leen S. Finite element, critical-plane, fatigue life prediction of simple and complex contact configurations. Int J Fatigue Apr. 2005;27(4):403–16. https://doi.org/10.1016/j.ijfatigue.2004.08.001.

[5] Liu Y, Mahadevan S. Multiaxial high-cycle fatigue criterion and life prediction for metals. Int J Fatigue July 2005;27(7):790–800. https://doi.org/10.1016/j.ijfatigue.2005.01.003.

[6] Fatemi Ali, Socie Darrell F. A critical plane approach to multiaxial fatigue damage including out-of-phase loading. Fatigue Fract Eng Mater Struct Mar. 1988;11(3):149–65. https://doi.org/10.1111/j.1460-2695.1988.tb01169.x.

[7] Carpinteri A, Spagoli A. Multiaxial high-cycle fatigue criterion for hard metals. Int J Fatigue 2001;23(2):135–45. https://doi.org/10.1016/s0142-1123(00)00075-x.

[8] Vantadori Sabrina, et al. Early fretting crack orientation by using the critical plane approach. Int J Fatigue Sept. 2018;114:282–8. https://doi.org/10.1016/j.ijfatigue.2018.04.015.

[9] Araújo JA, Dantas AP, Castro FC, Mamiya EN, Ferreira JLA. On the characterization of the critical plane with a simple and fast alternative measure of the shear stress amplitude in multiaxial fatigue. Int J Fatigue 2011;33(8):1092–100. https://doi.org/10.1016/j.ijfatigue.2011.01.002.

[10] Pyttel B, Schwerdt D, Berger C. Very high cycle fatigue – Is there a fatigue limit? Int J Fatigue Jan. 2011;33(1):49–58. https://doi.org/10.1016/j.ijfatigue.2010.05.009.

[11] Dal Cero Coelho F, Vu QH, Halm D, Nadot Y. Fatigue life modelling under variable amplitude multiaxial loading: Comparison between fatigue criterion and incremental modelling. Int J Fatigue 2018;117:461–70. https://doi.org/10.1016/j.ijfatigue.2018.08.013.

[12] G. Sines. Failure of materials under combined repeated stresses with superimposed static stresses. Tech. rep. NACA-TN-3495, 1955.

[13] Crossland B. Effects of large hydrostatics pressures on the torsional fatigue strength of an alloy steel. Proc. int. conf. on fatigue of metals. 1956.

[14] Matsuishi M, Endo T. Fatigue of metals subjected to varying stress fatigue lives under random loading. Proc. Kyushu District Meeting, JSEM 1968.

[15] Anes Vitor, et al. New cycle counting method for multiaxial fatigue. Int J Fatigue Oct. 2014;67:78–94. https://doi.org/10.1016/j.ijfatigue.2014.02.010.

[16] Wang CH, Brown MW. Life prediction techniques for variable amplitude multiaxial Fatigue—Part 1: theories. J Eng Mater Technol 1996;118(3):367. https://doi.org/10.1115/1.2806821.

[17] Meggiolaro Marco Antonio, de Castro Jaime Tupiassú Pinho. An improved multiaxial rainflow algorithm for non-proportional stress or strain histories – Part I: Enclosing surface methods. Int J Fatigue 2012;42:217–26. https://doi.org/10.1016/j.ijfatigue.2011.10.014.

[18] Anes V, et al. New approach for analysis of complex multiaxial loading paths. Int J Fatigue May 2014;62:21–33. https://doi.org/10.1016/j.ijfatigue.2013.05.004.

[19] Tao Z-Q, et al. Life prediction based on weight-averaged maximum shear strain range plane under multiaxial variable amplitude loading. Fatigue Fract Eng Mater Struct Feb. 2016;39(7):907–20. https://doi.org/10.1111/ffe.12417.

[20] Meggiolaro MA, de Castro JT, Wu H. On the use of tensor paths to estimate the nonproportionality factor of multiaxial stress or strain histories under free-surface conditions. Acta Mechanica. 2016;227(11):3087–100.

[21] Socie D. Critical Plane Approaches for Multiaxial Fatigue Damage Assessment. In: McDowell DL, Ellis JR, editors. Advances in Multiaxial Fatigue. 100 Barr Harbor Drive, PO Box C700, West Conshohocken, PA 19428-2959: ASTM International; 1993. p. 7–7-30. 10.1520/STP24793S.

[22] Papadopoulos I. A comparative study of multiaxial high-cycle fatigue criteria for metals. Int J Fatigue Mar. 1997;19(3):219–35. https://doi.org/10.1016/s0142-1123(96)00064-3.

[23] Liao Ding, Zhu Shun-Peng, Qian Guian. Multiaxial fatigue analysis of notched components using combined critical plane and critical distance approach. Int J Mech Sci Sept. 2019;160:38–50. https://doi.org/10.1016/j.ijmecsci.2019.06.027.

[24] Zhu Shun-Peng, et al. Evaluation and comparison of critical plane criteria for multiaxial fatigue analysis of ductile and brittle materials. Int J Fatigue July 2018;112:279–88. https://doi.org/10.1016/j.ijfatigue.2018.03.028.

[25] Zheng Hu, et al. Comparison of TCD and SED methods in fatigue lifetime assessment. Int J Fatigue June 2019;123:105–34. https://doi.org/10.1016/j.ijfatigue.2019.02.009.

[26] Nicholas Findley W. A theory for the effect of mean stress on fatigue of metals under combined torsion and axial load or bending. Engineering Materials Research Laboratory, Division of Engineering, Brown University; 1958.

[27] Socie Darell F, Marquis Gary B. Multiaxial fatigue. SAE International; 2000.

[28] Davoli P. Independence of the torsional fatigue limit upon a mean shear stress. Int J Fatigue June 2003;25(6):471–80. https://doi.org/10.1016/s0142-1123(02)00174-3.

[29] J. A. Araujo and D Nowell. “The effect of rapidly varying contact stress fields on fretting fatigue”. In: International Journal of Fatigue 24.7 (2002), pp. 763 –775. issn: 0142-1123. doi: https://doi.org/10.1016/S0142-1123(01) 00191 - 8. url: http: //www.sciencedirect.com/science /article/pii/S0142112301001918.

[30] J. A. Araujo et al. “On the use of the Theory of Critical Distances and the Modified W¨ohler Curve Method to estimate fretting fatigue strength of cylindrical contacts”. In: International Journal of Fatigue 29.1 (2007), pp. 95 –107. issn: 0142-1123. doi: https: //doi. org/10. 1016/j.ijfatigue. 2006. 02. 041. url: http: //www. sciencedirect. com/science/article/pii/S0142112306000776.

[31] Matake Tomokazu. An explanation on fatigue limit under combined stress. Bulletin of JSME 1977;20(141):257–63. https://doi.org/10.1299/jsme1958.20.257.

[32] McDiarmid DL. A general criterion for high cycle multiaxial fatigue failure. Fatigue Fract Eng Mater Struct Apr. 1991;14(4):429–53. https://doi.org/10.1111/j.1460-2695.1991. tb00673.x.

[33] K.N. Smith, P. Watson, and T.H. Topper. “Stress- strain function for the fatigue of metals”. In: J Mater 5.4 (1970). cited By 1301, pp. 767–778. url: https: //www.scopus. com/inward/record. uri ? eid = 2 - s2. 0 - 0014890104&partnerID = 40&md5 = 9381f9c5e7de03987a62416d0faf5ea7.

[34] Jiang. A fatigue criterion for general multiaxial loading. Fat Frac Eng Mat Struct 2000;23(1):19–32. https://doi.org/10.1046/j.1460-2695.2000.00247.x.

[35] Van K Dang, Le Douaron A, Lieurade HP. Multiaxial Fatigue Limit: A New Approach. Fracture 84. Elsevier; 1984. p. 1879–85. 10.1016/B978-1-4832-8440-8.50185-X.

[36] Svärd Henrik. A branch and bound algorithm for evaluation of the Findley fatigue criterion. Int J Fatigue 2015;73:27–38. https://doi.org/10.1016/j.ijfatigue.2014.11.008.

[37] Megiddo Nimrod. Linear-time algorithms for linear programming in R3 and related problems. In: 23rd Annual Symposium on Foundations of Computer Science (sfcs 1982). IEEE; 1982. doi: 10. 1109/sfcs. 1982.24.

[38] Petrucci Giovanni. A critical assessment of methods for the determination of the shear stress amplitude in multiaxial fatigue criteria belonging to critical plane class. Int J Fatigue 2015;74:119–31. https://doi.org/10.1016/j.ijfatigue.2015.01.001.

[39] Graham RL. An efficient algorith for determining the convex hull of a finite planar set. Informat. Process. Lett. June 1972;1(4):132–3. https://doi.org/10.1016/0020-0190(72)90045-2.

[40] Weber B, et al. Improvements of multiaxial fatigue criteria computation for a strong reduction of calculation duration. Comput Mater Sci Nov. 1999;15(4):381–99. https://doi.org/10.1016/s0927-0256(98)00129-3.

[41] Wentingmann M, Noever-Castelos P, Balzani C. An adaptive algorithm to accelerate the critical plane identification for multiaxial fatigue criteria. Proceedingsof 6th European Conference on Computational Mechanics. 2018.

[42] Zenner H, Heidenreich R, Richter I. Dauerschwingfestigkeit bei nichtsynchroner mehrachsiger Beanspruchung. Materialwiss Werkstofftech Mar. 1985;16(3):101–12. https://doi.org/10.1002/mawe. 19850160310.

[43] Froustey C, Lasserre S. Multiaxial fatigue endurance of 30NCD16 steel. Int J Fatigue May 1989;11(3):169–75. https://doi.org/10.1016/0142-1123(89)90436-2.

[44] McDiarmid DL. Fatigue under out-of-phase bending and torsion. Fatigue Fract Eng Mater Struct June 1987;9(6):457–75. https://doi.org/10.1111/j.1460-2695.1987.tb00471.x.

[45] Heidenreich R, Richter I, Zenner H. Schubspannungsintensit¨atshypothese - Weitere experimentelle und theoretische Untersuchungen. Konstruktion Jan. 1984;36(3):99–104.

[46] Lam Siu Kwan, Pitrou Antoine, Seibert Stanley. Numba Press; 2015. https://doi.org/10.1145/2833157.2833162.

[47] OpenMP 4.5 specification. OpenMP Architecture Review Board, Nov. 2015. url: https://www.openmp.org/wp- content/uploads/openmp 4.5.pdf.

A.3 Paper III

Brief overview of fretting analyses relevant for medium speed reciprocating engines.

Received: 2 July 2020 | Revised: 21 July 2020 | Accepted: 26 July 2020
DOI: 10.1002/mdp2.201

SPECIAL ISSUE ARTICLE

WILEY

Fretting in medium-speed reciprocating engines—Comments on practices and opportunities

Steffen Loen Sunde | **Filippo Berto** | **Bjørn Haugen**

Department of Mechanical and Industrial Engineering, Norwegian University of Science and Technology, Trondheim, Norway

Correspondence
Steffen Loen Sunde, Norwegian University of Science and Technology, Department of Mechanical and Industrial Engineering, Trondheim, Norway.
Email: steffen.sunde@ntnu.no

Abstract
Fretting and fretting fatigue are important considerations to be made in the design and development of medium-speed reciprocating engines. Predictive capabilities for safe-life design often rely on very simple empirical parameters and experience. Practices are briefly reviewed, and opportunities for more sophisticated methodologies are highlighted. It is concluded that more research into fretting fatigue with complex load sequences are needed.

KEYWORDS
fretting fatigue, Ruiz, reciprocating engines

1 | INTRODUCTION

Fretting is a term for surface damage occurring between contacting bodies with microscopic relative motion. The actual manifestation of fretting damage varies and depends on up to 50 factors[1,2] but most important are probably material bulk and microscopic properties, loading conditions, contact geometry, surface roughness, and surface hardness.[3–7] Large contact pressures cause local plastic flow on asperity level, and with sliding motion (slip), adhesion detaches particles from the surfaces, subsequently promoting abrasive wear. For smaller values of relative sliding motion, typically less than 50-μm, stress concentrations at stick–slip interfaces initiates surface cracks. In some cases, competitive processes can arise, where surface wear removes surface micro-cracks before they are allowed to propagate. However, if bulk stresses are high enough, fretting-initiated cracks propagate and ultimately cause failure by *fretting fatigue*.

Fretting fatigue is of major concern in medium-speed reciprocating engines.[8–11] Here, complex components in contact are subjected to large dynamic loads and excited by vibrations with a wide spectrum of frequencies. Materials are usually cast iron and steels. Full-scale testing is expensive but sometimes necessary, either by class rules or by general verification. During the design stages and due to continuous improvements, predictive capabilities are very useful as it allows for fretting to be avoided at an early stage, thus reducing costs. Moreover, with the accompanying experimental testing, correlations with predictive analyses can be very beneficial for increasing knowledge of the mechanisms involved. However, due to the complex and non-linear nature of fretting fatigue, combined with long service lives, prediction is a very difficult task. Wear is known to cause friction to increase,[12] effectively reducing relative slip. Loss of bolt pre-tension due to wear, on the contrary, can increase slip. Hence, even non-critical contacts can slowly change fretting regime and generate unpredictable results. Engines are designed to operate reliably for extremely long lives and the number of loading cycles for certain components range in the very high-cycle regimes and beyond ($>10^7 - 10^9$ cycles).

2 | DYNAMIC ANALYSIS

For some cases of fretting contact, forced dynamic response of the engine may be required. Three-dimensional computer models are the basis for design and production, accompanied with extensive analyses using finite element (FE) methods. Large geometries with small but important details like contact and fillets result in complex models with millions of degrees of freedom (DOFs) as shown in Figure 1. Performing forced dynamic analysis on such large models becomes computationally infeasible, and specialized software and methodologies are employed. By using *model order reduction* (MOR) techniques, the FE solution space is reduced to a very small subset of DOFs. FE *superelements* are pre-computed using methods of condensation, usually based on a combination of static and modal DOFs.[13] This reduces the solution space according to a given set of DOFs up to a maximum modal frequency. The condensed models (engine block, crankshaft, connecting rods, etc.) are then fed into multi-body dynamic (MBD) software and treated as separate elastic components, linked with forces and connectors. Non-linear effects like hydrodynamic bearings and gear meshing are included but detailed contact analysis with stick–slip still requires a densely meshed FE model. Therefore, the global dynamics are solved in MBD and the resulting loads are applied to a contact model as boundary conditions. Stresses, strains, and contact slip are post-processed to finally evaluate fretting fatigue using appropriate criteria.

Examples of critical engine components wherein fretting fatigue is known to cause problems are the connecting rod,[11] main bearing caps, and crankshaft counterweights.[9] The connecting rod is responsible for transmitting the linear combustion forces to the rotating crankshaft. Consequently, it is subjected to large gas forces and inertial forces. Usually, the connecting rod has a bolted split around the bearing shells, and the mating split surfaces are susceptible to fretting.[11] Main bearing caps support the crankshaft bearings to the engine block. Wear potentially cause material removal to reduce bolt pre-tension and bearing clearances, subsequently increasing the danger of bearing failure. Since mating surfaces are in *complete contact*, material removal and debris ejection are somewhat restricted for smaller values of slip. Moreover, reduced pre-tension in the bolts can enable fretting fatigue to occur in the bolt threads, as shown in Figure 2. As fretting wear gradually causes bolt pre-tension to decrease, slip rates can rise during operations. The bolt failed from fretting fatigue initiated in the first loaded thread.

3 | FRETTING FATIGUE CRITERIA

In the field of fretting, it was early recognized that slip amplitudes were among the most important parameters governing fretting performance.[14] The most basic fretting assessment relies simply on comparing relative slip amplitudes with threshold values from previous experience. Often, slip values are to be minimized and kept below 10 μm.

The classical Ruiz parameters have long been used as a simple means of quantifying fretting. Ruiz et al.[15] studied fretting in dovetail joints and suggested that the intensity of the surface damage to be governed by the frictional work ( ). They included the surface tangential stress as surface crack driving force and thus proposed

$$k = \quad _t \tag{1}$$

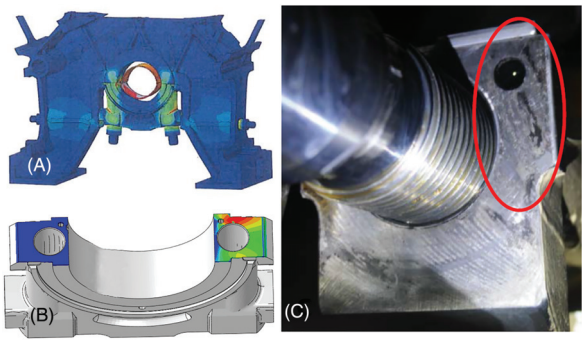

FIGURE 1 Slip analyses of engine main bearing cap. (A) Assembly in engine cross-section. (B) Resulting slip values. (C) Inspection of bearing cap after approximately 15k running hours

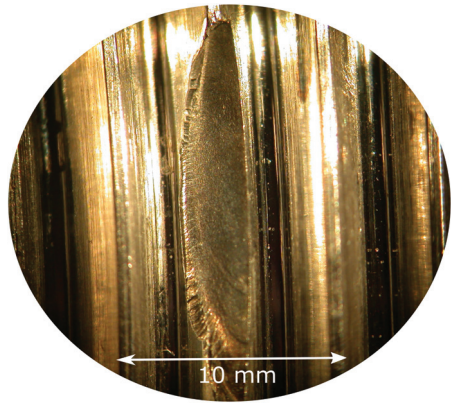

FIGURE 2 Fretting-initiated crack in connecting rod stud bolt after approx. 45k running hours

as a parameter, henceforth for simplicity abbreviated FFDP (fretting-fatigue damage parameter). $_t$ is the stress component acting parallel to the surface, is the shear stress, and is the relative slip. Modern implementations of this parameter integrate the shear work over the fretting cycle $t \in [0,T]$ to obtain a physical value for the specific frictional work (W),[16] hence

$$k = {}_1 \cdot W = {}_1 \int \cdot d\boldsymbol{s} = {}_1 \int_0^T \cdot \dot{\boldsymbol{s}} dt, \tag{2}$$

where is the shear stress vector and $\boldsymbol{s}$ is the slip vector. Tangential stress $_t$ is here swapped with *maximum principal stress* $_1$ to overcome the unidimensional nature of the original Ruiz parameter. Numerically, the shear work can be calculated using the midpoint rule as

$$W = \sum_{n=1}^{N} \frac{{}_{n-1} - {}_n}{2} \cdot (\boldsymbol{s}_n - \boldsymbol{s}_{n-1}), \tag{3}$$

where $n \in [1, N]$ is the discrete time step. Note however, the lack of physical interpretation of the FFDP. It is simply an empirical, "composite" parameter obtained by multiplying the surface damage (via shear work) with the crack driving force (via the normal stress). Nowell and Hills[17] found 1 to correlate with fretting cracks and that there seems to be a threshold value. It was recently suggested to use the frictional power instead of the frictional work, as the intensity of energy dissipation should affect crack initiation.[18] Also note that the value of FFDP in 2 vanishes as slip work approaches zero.

More elaborate criteria are in some cases warranted. Many researchers suggest using multiaxial fatigue parameters and critical plane formulations to predict fretting fatigue initiation.[19–21] Compared with maximum principal stress used in 2, critical plane parameters can better account for the non-proportional cycles experienced in near-contact stresses. Vidner and Leidich[18] suggested extensions to the Ruiz parameter where critical plane-based parameters to be used in place of maximum principal stress. Direct use of multiaxial fatigue parameters combined with the theory of critical distances have also been shown to effectively predicting fretting fatigue.[22–26]

Methodologies based on crack arrest are also appropriate, as they aim to predict whether a fretting-initiated crack will grow or arrest, thus predicting safe life.[27,28] Many relevant engineering applications have nominally flat contacts and by asymptotic expansion of the edge stress fields, threshold conditions can be analyzed using stress intensity factors.[29–31] They allow for rapid assessment of the behavior of fretting cracks and could serve as an engineering approach alongside wear analyses. The singular stress fields can be asymptotically matched with small-scale testing.

However, the assumptions of half-plane theory do not always hold, and the effects of complex loads (e.g., varying contact pressure) are still a topic for research.[32]

4 | CONCLUSIONS

Fretting fatigue is an important part of infinite-life design of medium-speed reciprocating engines. Bolted joints are used extensively and when subjected to complex dynamic forces, a complete fretting assessment is difficult. The large number of contributing factors in fretting fatigue, where many of which are inter-dependent, makes the synthesis of fretting almost chaotic in nature and very hard to predict. In engineering, holistic approaches are often favored, providing a safe-life prediction capability for a wide range of relevant conditions.

While research into fretting fatigue is dominated by multiaxial fatigue, asymptotic methods, and so forth (see, e.g., Bhatti and Wahab[33] for an excellent overview), engineering practices often rely on empirical, slip-based parameters like Ruiz and its descendants (FFDP). With recent developments in fretting fatigue knowledge, computational power, and modeling techniques, there are indeed opportunities to extend the predictive capabilities with more sophisticated methods. Life predictions can permit more carefully controlled service intervals and detailed cracking models can assist in fault-tolerant analysis.

Many researches show that the Ruiz parameters work well to provide cracking locations but are less trustworthy in regards with life estimation and threshold (safe-life) identification. Industrial practices often use FFDP in the early design stages, and when coupled with experience and in-house data, these parameters work quite well as "composite" parameters, accounting for both wear and fretting fatigue.

There is (and probably always will be) need for more research into fretting and fretting fatigue in components subjected to complicated load sequences. Testing components where fatigue load, contact pressure, and shear forces can be controlled independently would give insight into the mechanisms that play important roles to the fretting fatigue performance. Fretting fatigue size-effects complicates the application of small-scale laboratory testing to engineering industrial components. Additionally, there is comparatively lacking experimental results of fretting fatigue in cast iron.

CONFLICT OF INTEREST

The authors declare that they have no conflicts of interest.

ORCID

Steffen Loen Sunde https://orcid.org/0000-0001-6671-387X
Filippo Berto https://orcid.org/0000-0001-9676-9970

REFERENCES

1. Collins JA. Fretting-fatigue damage-factor determination. *J Ind Eng*. June 1965;87(3):298-302. https://doi.org/10.1115/1.3670822
2. Berthier Y, Vincent L, Godet M. Fretting fatigue and fretting wear. *Tribol Int*. Aug. 1989;22(4):235-242. https://doi.org/10.1016/0301-679x(89)90081-9
3. Cheng W, Cheng HS, Mura T, Keer LM. Micromechanics modeling of crack initiation under contact fatigue. *J Tribol*. 1994;116(1):2-8. https://doi.org/10.1115/1.2927042
4. Hills DA. Mechanics of fretting fatigue. *Wear*. June 1994;175(1–2):107-113. https://doi.org/10.1016/0043-1,648(94)90173-2
5. Nowell D, Dini D, Hills DA. Recent developments in the understanding of fretting fatigue. *Eng Fract Mech*. 2006;73(2):207-222. issn: 0013–7944. https://doi.org/10.1016/j.engfracmech.2005.01.013
6. Lemm JD, Warmuth AR, Pearson SR, Shipway PH. The influence of surface hardness on the fretting wear of steel pairs—its role in debris retention in the contact. *Tribol Int*. 2015;81:258-266. https://doi.org/10.1016/j.triboint.2014.09.003
7. V'azquez J, Navarro C, Dom'inguez J. Analysis of the effect of a textured surface on fretting fatigue. *Wear*. 2013;305(1–2):23-35. https://doi.org/10.1016/j.wear.2013.05.003
8. Chao J. Fretting-fatigue induced failure of a connecting rod. *Eng Fail Anal*. 2019;96:186-201. https://doi.org/10.1016/j.engfailanal.2018.10.006
9. Antti M. ¨antyl¨a and Conrad L¨onnqvist. "Fretting simulation for crankshaft-counterweight contact". 2009.
10. Pujatti M, Suhadolc M, Piculin D. Fretting-initiated fatigue in large bore engines connecting rods. *Procedia Eng*. 2014;74:356-359. https://doi.org/10.1016/j.proeng.2014.06.279
11. Son JH, Ahn SC, Bae JG, et al. Fretting damage prediction of connecting rod of marine diesel engine. *J Mech Sci Tech*. 2011;25(2):441-447. https://doi.org/10.1007/s12206-010-1,206-6

12. Fouvry S, Du'o P, Perruchaut P. A quantitative approach of Ti6Al-4 V fretting damage: friction, wear and crack nucleation. *Wear*. Nov. 2004;257(9–10):916-929. https://doi.org/10.1016/j.wear.2004.05.011
13. Ma MT, Offner G, Loibnegger B, Priebsch HH, McLuckie IR. A fast approach to model hydrodynamic behaviour of journal bearings for analysis of crankshaft and engine dynamics. *Tribology Series*. 2003;43:313–327. https://doi.org/10.1016/S0167-8922(03)80059-7
14. Vingsbo O, S¨oderberg S. On fretting maps. *Wear*. Sept. 1988;126(2):131-147. https://doi.org/10.1016/0043-1648(88)90134-2
15. Ruiz C, Boddington PHB, Chen KC. An investigation of fatigue and fretting in a dovetail joint. *Exp Mech*. 1984;24(3):208-217. issn: 1741–2765. https://doi.org/10.1007/BF02323167
16. Ziaei M. "Analytical study of noncircular profile families and numerical optimization of standardised polygon profiles for shaft–hub connections." Professorial dissertation, Chemnitz University of Technology [in German]. 2002.
17. Nowell D, Hills DA. Crack initiation criteria in fretting fatigue. *Wear*. Mar. 1990;136(2):329-343. https://doi.org/10.1016/0043-1,648(90)90155-4
18. Vidner J, Leidich E. Enhanced Ruiz criterion for the evaluation of crack initiation in contact subjected to fretting fatigue. *Int J Fatig*. 2007;29(9–11):2040-2049. https://doi.org/10.1016/j.ijfatigue.2007.02.010
19. Fouvry S, Kapsa P, Vincent L. "Multiaxial fatigue analysis of fretting contact taking into account the size effect". The 2nd International Symposium on Fretting Fatigue: Current Technology and Practices. 21,367. 2000, pp. 167–182.
20. Ara'ujo JA, Nowell D, Vivacqua RC. The use of multiaxial fatigue models to predict fretting fatigue life of components subjected to different contact stress fields. *Fatig Fract Eng Mater Struct*. Oct. 2004;27(10):967-978. https://doi.org/10.1111/j.14602695.2004.00820.x
21. Navarro C, M´unoz S, Dom'ınguez J. On the use of multiaxial fatigue criteria for fretting fatigue life assessment. *Int J Fatig*. Jan. 2008;30(1):32-44. https://doi.org/10.1016/j.ijfatigue.2007.02.018
22. Sum WS, Williams E, Leen S. Finite element, critical-plane, fatigue life prediction of simple and complex contact configurations. *Int J Fatig*. Apr. 2005;27(4):403-416. https://doi.org/10.1016/j.ijfatigue.2004.08.001
23. Ara'ujo JA et al. On the prediction of high-cycle fretting fatigue strength: theory of critical distances vs. hot-spot approach. *Eng Fract Mech*. 2008;75(7):1763-1778. issn: 0013–7944. https://doi.org/10.1016/j.engfracmech.2007.03.026
24. Vantadori S, Almeida GMJ, Fortese G, Pessoa GCV, Araújo JA. Early fretting crack orientation by using the critical plane approach. *Int J Fatig*. 2018;114:282-288. issn: 0142–1123. https://doi.org/10.1016/j.ijfatigue.2018.04.015
25. Adriano VSR, Martínez JMG, Ferreira JLA, Araújo JA, da Silva CRM. The influence of the fatigue process zone size on fatigue life estimations performed on aluminum wires containing geometric discontinuities using the theory of critical distances. *Theor Appl Fract Mech*. 2018;97:265-278. issn: 0167–8442. https://doi.org/10.1016/j.tafmec.2018.09.002
26. Araújo JA, Castro FC, Matos IM, Cardoso RA. Life prediction in multiaxial high cycle fretting fatigue. *Int J Fatig*. 2020;134:105504. issn: 0142–1123. https://doi.org/10.1016/j.ijfatigue.2020.105504
27. Ciavarella M. A 'crack-like' notch analogue for a safe-life fretting fatigue design methodology. *Fatig Fract Eng Mater Struct*. 2003;26(12):1159-1170. issn: 1460–2695. https://doi.org/10.1046/j.1460-2695.2003.00721.x
28. Cardoso RA, Campos ERFS, Ferreira JLA, Wang D, Araújo JA. A crack arrest methodology based on Bazant's parameter to fretting fatigue. *Theor Appl Fract Mech*. 2018;95:208-217. issn: 0167–8442. https://doi.org/10.1016/j.tafmec.2018.03.001
29. Giannakopoulos AE, Lindley TC, Suresh S. Aspects of equivalence between contact mechanics and fracture mechanics: theoretical connections and a life-prediction methodology for fretting-fatigue. *Acta Materialia*. 1998;46(9):2955-2968. issn: 1359–6454. https://doi.org/10.1016/S1359-6454(98)00011-1
30. Mugadu A, Hills DA, Limmer L. An asymptotic approach to crack initiation in fretting fatigue of complete contacts. *J Mech Phys Solid*. Mar. 2002;50(3):531-547. https://doi.org/10.1016/s0022-5,096(01)00091-6
31. Hills DA, Dini D. A review of the use of the asymptotic framework for quantification of fretting fatigue. *J Strain Anal Eng Des*. 2016;51(4):240-246. https://doi.org/10.1177/0309324716638968
32. Ciavarella M, Berto F. A simplified extension of the crack analogue model for fretting fatigue with varying normal load. *Theor Appl Fract Mech*. 2017;91:37-43. issn: 0167–8442. https://doi.org/10.1016/j.tafmec.2017.03.011
33. Bhatti NA, Wahab MA. Fretting fatigue crack nucleation: a review. *Tribol Int*. May 2018;121:121-138. https://doi.org/10.1016/j.triboint.2018.01.029

How to cite this article: Sunde SL, Berto F, Haugen B. Fretting in medium-speed reciprocating engines—Comments on practices and opportunities. *Mat Design Process Comm*. 2020;e201. https://doi.org/10.1002/mdp2.201

A.4 Paper IV

Demonstrates the use of a new fretting fatigue test fixture.

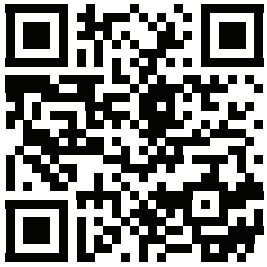

International Journal of Fatigue 143 (2021) 106011

Contents lists available at ScienceDirect

International Journal of Fatigue

journal homepage: www.elsevier.com/locate/ijfatigue

Experimental and numerical fretting fatigue using a new test fixture

Steffen L. Sunde *, Bjørn Haugen, Filippo Berto

Norwegian University of Science and Technology, Dept. of Mech. and Industrial Engineering, Trondheim, Norway

ARTICLE INFO

Keywords:
Fretting fatigue
Critical plane
TCD
Ruiz
Ti-6Al-4V

ABSTRACT

A unique dovetail-based test fixture for fretting fatigue was designed and is demonstrated with a combined experimental and numerical campaign. Fretting fatigue damage is analysed and correlated with numerical analyses using a modern Ruiz formulation and Findley critical plane parameter with the Theory of Critical Distances. Initial test results show that a simple critical plane model correlates life and cracking directions with experiments; however, the Ruiz parameter only serves as a hot-spot indicator. The fixture is designed to permit testing in submerged conditions and to allow additional loads to the specimens by using a multi-axial fatigue machine.

1. Introduction

Fretting is a concern arising from metallic components in contact, subjected to oscillating forces. Highly localized contact stresses and small relative movements cause surface damage and if the bulk stresses are high enough, fretting cracks propagate and cause *fretting fatigue*.

The features of fretting fatigue are quite complex with numerous interconnected parameters [1,2]. Most importantly are the conditions of the contacting surfaces, material properties and multi-axial non-proportional stress variations with steep gradients. Although fretting and fretting fatigue has been studied for over a century, it is still not fully understood. The chaotic synthesis of all the involved mechanisms makes the assessment very difficult, both in terms of analysis and in terms of experimental testing.

When analysing and predicting fretting fatigue, engineers are often faced with large geometries subjected to complex loads. Complete fretting assessments are next to impossible, because it would require considering a large array of different mechanisms in combination. Hence, simple assumptions are made and only a few key mechanisms are included in the analysis to make the problem practical. With respect to physical testing of fretting, careful control and monitoring the different mechanisms are difficult, and to isolate contact features for the analysis is challenging.

A number of different fretting fatigue test configurations have been devised throughout the years, starting from quite simple fatigue machines with "bridge-type" contact pads [3] to general fretting machines with multiple actuators and load cells capable of varying the fatigue loads, contact pressure and sliding force independently [2]. The most "classical" geometry for fretting fatigue is, perhaps, the dovetail joint studied by Ruiz et al. [4] and followed by many others [5–8]. Fretting fatigue in the dovetail joints of aircraft turbine blades is an important application and has been the target for much research. This test configuration is also quite popular due to its simplicity; there is no need for a specialized multi-actuator fatigue machine. A simple pulling action is used to simulate the centripetal forces acting on the turbine blade during operations. Optionally, additional actuators or shakers can used to apply the vibrational excitations from structure, aerodynamics, etc. [9].

In this work, yet another test fixture based on the dovetail joint is presented. This is the starting initiative for a new test program being developed, aiming at numerical and experimental investigations of fretting fatigue conditions relevant for engineering. The fixture presented here has some interesting additions when compared to previously developed dovetail test fixtures, as will be described in the following section. The main aim of this paper is to demonstrate the use of this new fixture, prove its usefulness in studying fretting fatigue and to address its potential to study a wide range of contact conditions. A long-term goal is to provide with useful experimental data and, with its accompanying numerical analysis, to permit scaled-down tests to apply to engineering components.

2. Experimental testing

The main advantages of the dovetail joint as a test setup for fretting fatigue is that it is easy to arrange and does not require special fatigue machines. The *disadvantage* is that there is much less control of the

* Corresponding author.
E-mail address: steffen.sunde@ntnu.no (S.L. Sunde).

https://doi.org/10.1016/j.ijfatigue.2020.106011
Received 31 July 2020; Received in revised form 17 October 2020; Accepted 20 October 2020
Available online 7 November 2020

contact pressure and shear stress, compared to bi-axial fretting rigs [10,11]. Several additions are introduced to the fixture shown in this work, see Fig. 1. Due to high stiffness of the lower fixture flange, a wide range of loads and specimen sizes are permitted. As the tension on the specimens increases, so does the wedge opening effect on the gripping mechanism, increasing the contact angle and altering the contact tractions. The width of the lower flange provide a possible additional source of excitation when using a multiaxial fatigue machine; By having two specimens with a *radial offset*, as shown in Fig. 1, a small torque can be applied to the specimens. The added force come, however, at the cost of some contact edge-effects as the contact pressure will vary over the specimen width.

The contact pads are slid into carefully machined slots. This allows for easily interchangeable contact pads and consequently permits testing with different contact geometries, surface treatments, material combinations, etc.

The lower gripping flange front and back sides can be enclosed, enabling submerged contact conditions. The rig is small enough to fit inside the temperature chamber for testing in elevated temperatures which is relevant for turbine blade dovetail joints. If the lower gripping flange is not enclosed, contact slip conditions and specimen strain can be analysed using *Digital Image Correlation* (DIC) techniques as performed in previous studies, see e.g. [12–14].

One of the main difficulties with the dovetail configuration is determining the appropriate loading conditions. A numerical analysis for each test program is necessary to determine the contact conditions and slip regimes for the given loads and geometry. For sharp-edged contact pads, the specimen can experience local plasticity even though the bulk loads are too small for fretting cracks to propagate. A large unknown in all types of fretting tests is the coefficient of friction (COF), which determines the contact conditions. The COF value is a *system* parameter and depends on not only material combination but loading, roughness, hardness, environment, sliding distance, geometry, etc.

A set of specimens is made in Grade 5 Ti-6Al-4V titanium alloy (see Tables 1 and 2) which is a commonly used alloy for fretting fatigue studies. The combination of low density, high strength and excellent heat resistance and bio-compatibility makes the alloy useful for aviation applications and orthopedic implants, among other fretting-critical fields. The geometrical details of the dovetail specimen and the contact pad is shown in Fig. 2. Note that the contact pads in this particular study have rounded contact profile.

The chemical composition of specimens material prior to machining is given in Table 2.

The material is rolled and cut using EDM wire machine and the specimen sides were machined flat. Rolled titanium is highly anisotropic with elongated grains and EDM wire cutting produces a surface with melted particles, micro-cracks and altered hardness. In other words,

Table 1
Mechanical material parameters from material certificate in accordance with ASTM E8/E8M-15a.

Tensile str. MPa	Yield str. (0.2%) MPa	Hardness HV	Ra μm
920	838	301	$\leqslant 3.2$

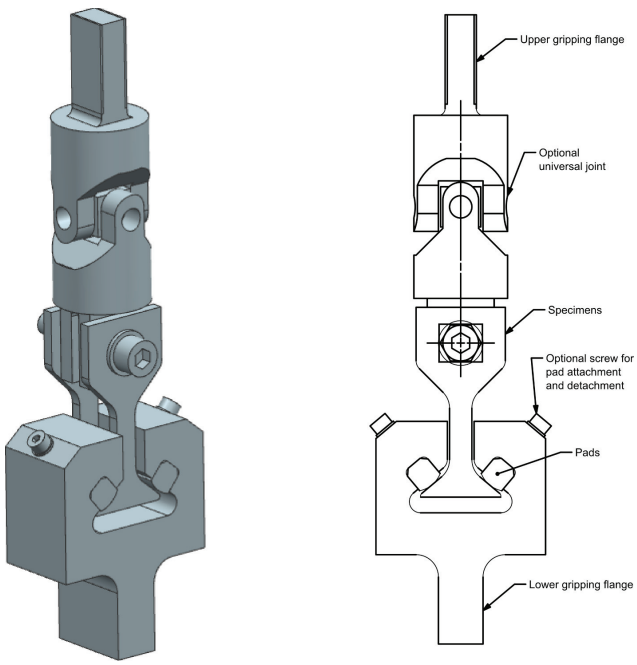

Fig. 1. Dovetail fixture arrangement. A universal joint is used to make the test rig self-align when the axial loads are applied, providing symmetric loads to the specimens.

Table 2
Chemical composition of specimens according in accordance with ASTM B348-13, forged annealed and peeled.

Al	Fe	C	N	O	H	V
6.23	0.03	0.01	<0.01	0.13	0.003	4.1

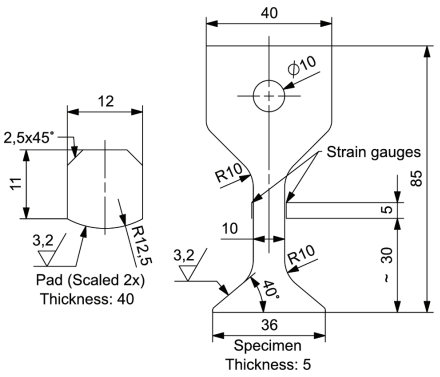

Fig. 2. Geometric details of the specimen and contact pad used in this paper. General tolerances are in accordance with ISO 2768-m. Units are in millimetres.

there are factors of uncertainty related to the material and specimen surfaces. For many engineering applications, EDM wire cutting is an appropriate manufacturing method due to its efficiency and precision. Consequently, fretting fatigue performance of such surfaces are of interest despite its inherent uncertainty.

Hardness of the contacting surfaces was tested using pyramid diamond indenter with 1 kg force for four seconds. The hardness of the EDM wired surfaces was found to be approx. 300 HV1 and the machined surfaces were around 350 HV1. Fig. 10 shows a Scanning Electron Microscope (SEM) picture of the surface where quite irregular surfaces can be seen with round, melted drops. The edges of the samples were deburred by grinding, causing potential crack initiation points and some uncertainties for the contact area. Specimens were cleaned using ethanol immediately before testing.

A *MTS 809 Axial/Torsional test system* fatigue machine was used to apply uniaxial fretting load to a single specimen at a time (see Fig. 3). A universal joint was used to avoid over-constrained specimens to be loaded asymmetrically. A Peak-Valley compensator in the test controller was used, allowing for testing at higher frequencies whilst maintaining full load ranges. Load and displacement were recorded during testing and a pre-determined stopping criterion was assigned to the displacement signal so that the test would stop when a crack had caused the sample to elongate. A subset of samples were also equipped with strain gauges on both flanks in order to more accurately record specimen behaviour during the test (see Fig. 2). Load and displacement data were logged at 50 Hz using the built-in load cell in the fatigue machine. FLAB-5-11 strain gauges (TOKYO Sokki Kenkyujo Co. Ltd.) were recorded using a HBM MX1615B amplifier at 300 Hz, resulting in large amounts of data.

3. Numerical modelling

A series of 2D finite element analyses (FEA) were performed to evaluate the design and to compare numerical predictions of fretting fatigue performance with experimental results. FEA is often the preferred method of solving fretting fatigue contact, providing accurate contact stresses and strains. For the case of uni-axially loaded specimen, symmetry conditions permit the FE model to be halved, see Fig. 4. Reference points are used as control nodes in top and bottom of the model and kinematic couplings are used to attach the model degrees of freedom to boundary conditions and loads. Abaqus 2017 FE software

Fig. 3. Fixture mounted in multiaxial fatigue machine with a single Ti-6Al-4V specimen instrumented with strain gauges on both flanks.

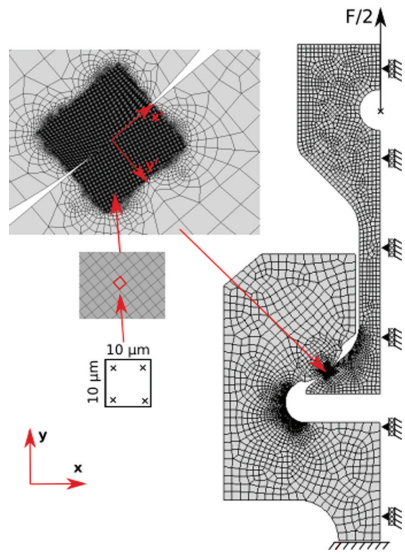

Fig. 4. 2D Finite element model. Symmetry conditions ($u_x = r_y = r_z = 0$) is applied along the centreline and bottom are fixed ($u_y = 0$). Contact and subsurface area are meshed with structured bi-linear elements.

package was used to solve for the stresses and strains. Python was used to extract results and parallelised C++ was used to perform critical plane computations.

Four-noded (bi-linear) plane strain elements were used due to spatially small stress gradient compared to specimen width. Approximate global element size for the fixture is 2 mm and refined in critical areas according to a thorough stress convergence study. Element size in the chamber fillet is approximately 0.125 mm. For the specimens 1 mm elements were used globally and refined to 0.25 mm at the fillet. Mesh was allowed to be unstructured for the majority of the model, but structured mesh is used for the subsurface material (see Fig. 4). For accurate contact slip and stresses, a very fine mesh of 10 μm was required in areas surrounding the contact. Due to the severe stress gradients and micro-sliding, a highly refined mesh is necessary. It is not uncommon with element sizes in fretting studies to be in the ranges of 10–50 μm and even down to 2–5 μm [15]. Here, contact stresses converge rather quickly but for accurate values of relative movement (slip) a fine mesh is important. A high resolution of subsurface stresses is also useful for the critical plane post-processing stage when averaging techniques are used, see Section 3.3. Material elasticity parameters for Ti-6Al-4V used here are as were Young's modulus of 115 GPa and Poisson's ratio of 0.32 [1].

Contact analyses are performed using Coloumb friction with two different values for COF. To ensure accurate contact solutions, the fretting interface is modelled using Lagrangian multipliers for normal and tangential behaviour. Lagrangian multipliers introduces extra degrees of freedom to accurately solve the frictional sliding between the master and slave body, pad and specimen respectively. Whilst a "penalty" formulation is much simpler numerically, and sufficiently accurate for contact stress analysis in many cases, the Lagrangian multipliers are used if the contact slip conditions are important. "Hard" normal conditions will cause FE solver iterations to enforce that no slave surface nodes penetrate master surface elements. In some cases hard contact makes convergence more difficult, but will provide more accurate results. A precise value for the COF is difficult to obtain, even through extensive testing. Here, COF is not measured explicitly but numerical simulations are performed with two different values, 0.55 borrowed from [1] and one higher value of 0.70 [16]. Although often simplified as being dependant only on the two materials in contact, COF is a systems property and is depending on numerous factors, e.g. contact pressure, surface roughness, environmental conditions, etc. Therefore, it is reasonable to think that the COF itself will change throughout the fretting life, particularly if frictional wear or plastic deformation alter the contact conditions. Friction is known to be especially difficult to represent in fretting fatigue, and is often reported to increase during fretting life [17,16,18].

As the stress state in the contact area is assumed to be in plane strain, the stress tensor is on the form

$$\boldsymbol{\sigma}(t) = \begin{bmatrix} \sigma_{xx}(t) & \sigma_{xy}(t) & 0 \\ \sigma_{xy}(t) & \sigma_{yy}(t) & 0 \\ 0 & 0 & \sigma_{zz}(t) \end{bmatrix} \tag{1}$$

That is, the stress is three-axial with an out-of-plane z-component owing to the material contraction due to the Poisson effect. It can be shown to be reduced to a 2D problem, but is here solved using a general three-dimensional post-processing code [19]. A separate, rotated coordinate system is placed in the center of contact, as shown in Fig. 8. The stresses are solved for at the element integration points and extrapolated to the element nodes. They are then averaged for each connected element to obtain the global nodal values. Subsequently, stresses are transformed to the local contact coordinate system and extracted for a subset of elements beneath the contact surface as shown in Fig. 4.

3.1. Contact analysis

Since contact normal load and tangential load for the dovetail in general vary proportionally, a Hertzian (cylinder on plane) type of contact forms and grows in magnitude as axial load is increased. When the load is released, shear instantly changes direction at the outer edges of contact where the local frictional resistance is low. Now a partial slip conditions appears, qualitatively comparable with the classical Cattaneo-Mindlin (CM) solution [20,21]. In the CM solution however, normal load is constant as the tangential load is gradually applied and kept within frictional load.

Initially, during ramp loading, contact is in gross slip conditions, as can be seen in Fig. 5. During the cyclic loading however, partial slip is seen with the boundary between stick and slip changes continuously. Therefore, a quite large area becomes severely fretted, causing multiple potential sites for crack initiation. The value of Q/P is usually lower than the average coefficient of friction, except during the ramping step.

The classical works by Ruiz et al. [4] presented two different mathematical parameters specific to fretting and fretting fatigue. The first parameter (here denoted k_1 to meet the original notation) was obtained by simply multiplying the largest tangential stress by the maximised frictional work, thus being expressed as

$$k_1 = (\sigma_{xx})_{max} \cdot (\tau\delta)_{max} \tag{2}$$

where σ_{xx} is the stress component acting parallel to the contact surface, τ is the shear stress and δ is the relative slip. Previous studies, such as [22,19] notes that this parameter is slightly inconvenient due to the maximum frictional work and maximum tangential stress potentially occurring at different locations. Thus obviously not being physically sound. Ruiz et al. [4] also noted that, although they found reasonable agreement with experiments performed for dovetail specimens, k_1 did not indicate *cracking location* particularly accurate. An alternative, empirical parameter was therefore proposed,

$$k_2 = \sigma_{xx} \cdot \tau\delta \tag{3}$$

Thus, fretting fatigue damage is quantified by the product of shear work ($\tau\delta$) and stress component acting parallel to the contact surface. Numerically, the parameter k_2 is evaluated by integrating the specific shear work over the fretting cycle, like in more recent versions of the Ruiz criterion [23–25]. A considerable advantage of this parameter over k_1 is that its local and can that it can easily be integrated over the fretted surface (see Fig. 6). However, it is clear that, the Ruiz' parameters lack in terms of physical interpretation [5,2]. Regarding k_2 and as material parameters is somewhat artificial, but nonetheless serves as a means of comparison and is widely used in engineering practice [26,27]. Also note that the parameters k_1 and k_2 are one-dimensional in this form but can be extended to use for 3D models [25,28].

3.2. Critical plane analysis

As indicated in the previous section, simple fretting parameters like Ruiz and its derivatives are very accessible and sometimes useful for qualitative comparisons of different fretting situations. These parameters can provide hot-spot indications but for more quantitative analyses like life predictions, more thorough analysis is required and physical criteria are preferred. Fretting fatigue crack nucleation in mixed and partial slip regimes is commonly evaluated by using multiaxial fatigue methods [29–33].

Here, stresses are extracted for eight time steps of the loading cycle, for a node set representing the specimen subsurface and stored in separate files. A critical plane post-processing procedure is then carried out using the Findley parameter [34] for a variety of conditions. Since the coefficient of friction is not known accurately for the actual system, the critical plane analysis is made for a set of different values of COF (see Fig. 14).

The multi-axial fatigue parameter proposed by Findley in the sixties combines the shear loads with the normal loads. More specifically, the critical plane is defined as the candidate material plane (π) experiencing

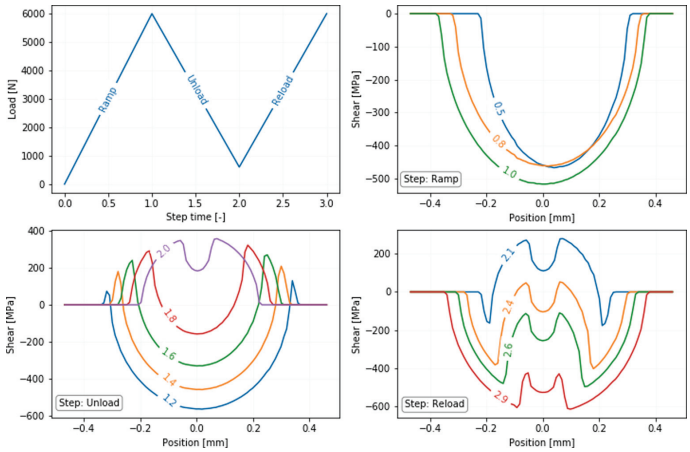

Fig. 5. Contact shear evolution for test case 6 (T6), see Table 3.

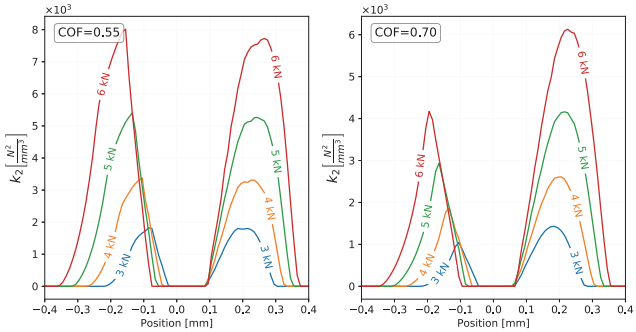

Fig. 6. Ruiz FFD parameter. The left and right peaks in each plot are the leading and trailing edges, respectively.

the maximum combination of shear stress amplitude and maximum normal stress over a stabilized cycle. Accordingly, maximising Eq. (4) yields the critical plane. Findley damage parameter is here denoted as F and may be expressed in a general three dimensional critical plane context as

$$F_{max} = \max_{\phi,\theta}\{F\} = \max_{\phi,\theta}\{\tau_a(\phi,\theta) + k\sigma_{n,max}(\phi,\theta)\} \quad (4)$$

where θ and ϕ are the first and second angular coordinates in a spherical coordinate system centered in the material point, see Fig. 7. k is a material parameter describing the material cracking sensitivity to normal stresses, and is determined based on experimental data. Higher values of k can be interpreted as increased sensitivity to *opening mode* effects on the shear cracks. k is therefore normally lower for shear dominated (ductile materials) than for brittle materials. Socie [35] propose to use 0.1–0.2 for ductile materials and Kallmeyer et al. [36] found 0.35 to give best correlation with uni-axial and bi-axial data for Ti-6Al-4V. A value of 0.35 was found to work well in this study. The damage function (F) in Eq. (4) can be thought of as the objective function to be maximised over

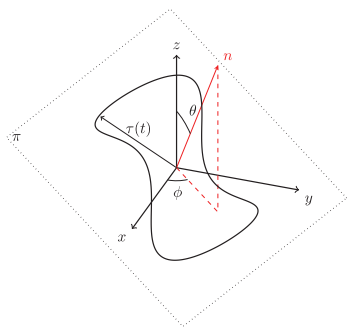

Fig. 7. Shear stress acting in the candidate plane π.

the space of possible material plane orientations and is visualized in Fig. 13. The damage F is plotted as a function of material plane orientation (θ, ϕ), but as the stress histories obtained from FEA in reality is a two-dimensional, critical plane needs only to be searched for over the angle ϕ. For the general 3D critical plane analysis using shear-based criteria, additional complexity is related to the problem of defining and computing *resolved shear stress amplitudes*. The shear stress history is a two-dimensional path in the candidate plane [37,38], as illustrated in Fig. 7. A very fine grid of angles (θ, ϕ) is obtained with angular increments of 1 degree. The resolved shear stress amplitudes used to compute the damage 13 are *computed with the maximum rectangular hull* (MRH) as demonstrated by Araújo et al. [38]. This algorithm calculates the shear amplitude by halving the largest diagonal of all rectangles enclosing the shear stress path in the candidate plane. Rectangles are computed by projecting the shear stress history on to a set of rotated coordinate axes in π. It has computational advantages over the more popular method of *minimum circumscribed circle* and handles non-proportionality better.

In terms of the number of cycles to initiate a crack, fatigue damage be expressed as [39]:

$$F_{max} = \tau_f^{'}(2N_f)^{b_0} \tag{5}$$

where $\tau_f^{'}$ is the shear stress fatigue strength, N_f is the number of cycles to initiate a crack and b_0, is the fatigue strength exponent. Material fatigue parameters were borrowed from [1]. The shear fatigue strength was calculated by

$$\tau_f^{'} = \frac{\sigma_f^{'}}{\sqrt{3}} \tag{6}$$

where $\sigma_f^{'}$ is the material uniaxial fatigue strength coefficient.

3.3. Theory of critical distances

It is well known that hot-spot fatigue evaluation over-estimate fatigue damage when steep stress gradients are present. This is indeed the case for fretting fatigue, where the subsurface stresses are high at the contact edges due to contact pressure and discontinuities in shear traction. A very steep stress gradient is clearly visible in Fig. 12, where fatigue damages are plotted for the specimen sub-surface. The peaks in shear stress at the slip edges are seen in Fig. 5. Using the *Theory of Critical Distances* (TCD), a material characteristic length (or depth) is used to evaluate a *process zone* in which the stresses are averaged by a certain criterion; using the *Point Method* the fatigue damage is calculated at the center of the process zone and for the *Volume Method* the stresses are averaged over the volume [1,40]. Here, the critical plane analyses are performed using both the Point Method and Volume Method. More specifically, the point method is implemented such that the fatigue life is evaluated at the critical point, defined as the material point at a distance $L/2$ from the hot-spot *along the hot-spot cracking direction*. Refer to Fig. 8. For the volume method, the fatigue damage is averaged over a ball (a circle in 2D case) of radius $L/2$ centered in the critical point.

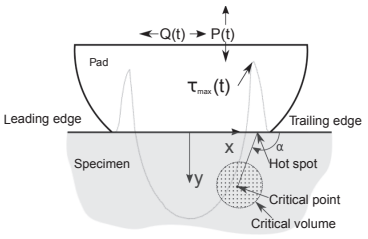

Fig. 8. Terminology for critical plane analysis using TCD. Note that the size and position of the critical volume is not necessarily in scale; in many cases it will reach the surface.

The numerical value of L is often related to the threshold stress intensity factor of the material from LEFM [41,42,29]

$$L = \frac{1}{\pi}\left(\frac{\Delta K_{th}}{\Delta \sigma_0}\right)^2 \tag{7}$$

where ΔK_{th} is the threshold stress intensity factor for crack fatigue growth and σ_0 is the plain fatigue limit [42]. Here, the value is calculated using material parameters from Dowling [43]. With $\Delta K_{th} = 5.5\ \text{MPa}\sqrt{\text{m}}$ and $\sigma_0 = 583\ \text{MPa}$ the critical distance L becomes approximately 28 μm. This value is in range of values used in [1] for the same material.

4. Results

Experimental results are shown in Table 3. A total of 15 tests, T1 through T15, were run until a stopping criterion was met or until run-out limit, which was set to two million cycles. The loads followed a sine-wave function with loading ratio $R = 0.1$ at 20 Hz. The loads in Table 3 are the peak (maximum) load for each specimen.

The two lowest loaded specimens were run-outs, see Fig. 14. All remaining specimens failed due to fretting fatigue, with cracks initiating from the near-center towards the trailing edge of contact and growing at an angle 50–60 degrees from the surface as seen in Fig. 9. Initiation angles seemed to be steeper for some samples as can be seen in Fig. 9b, however, comprehensive study of the crack initiation site proved to be difficult; cyclic contact pressure is still exerted on the fretted surface after the crack has been initiated, causing some small damage to the initiation sites. One can probably reduce this effect by defining more strict stopping criteria in the test configuration. Additionally, the latency introduced by peak-valley compensation caused some small damage to the initiation site.

Fractography using scanning electron microscope (SEM) confirmed that in general, cracks formed under the contact inside the slip region near the theoretical point of initial contact (see Fig. 10b). As can be seen in Fig. 10a, the EDM wired surface is very irregular and rough, with melted drops and potential surface defects. The melted drops are vulnerable to plastic flow as the pad comes into contact with the specimen and are probably subjected to plowing during early sliding, as can be observed as furrows in Fig. 10a around the edge of contact. Since the contact is cylindrical in profile, particle ejection is mostly unhindered, promoting wear. Debris particles caused by wear are seen on the fretted surface and at the edge of contact.

A subset of specimens were equipped with strain gauges on each side, as illustrated in Fig. 2. An example of the monitored strains are post-processed and plotted in Fig. 11 for T12. Here, peaks and troughs are extracted from the continuous signal and shown as separated lines for each side. Notice how the strain range is slightly higher on the left side of the specimen even though the opposite side is the one to experience the fretting fatigue crack. Peak strains on the right side is slowly decreasing from early on, even though the left strain is fairly constant until around $8.5{\cdot}10^5$. Then, as the crack grows, strains quickly change. Peaks and troughs are also shown for the overall displacement of specimen during its lifetime. The transient response during the first few cycles after loading is first probably dominated by fluid film effects in the U-joint followed by some small contact plastic flow. The contact eventually reaches elastic shakedown after which the response is relatively stable, until sudden crack growth and failure. Displacements are slowly increasing during the first few 100 k cycles until it stabilizes. This can be due to increased wear and easy particle ejection during the early fretting life, when the unworn Hertzian profile cause high contact stresses and wear. By evaluating the increase in displacements, the onset of crack

Table 3
Experimental test results. Samples marked with * were run-outs.

Test	T1	T2*	T3	T4	T5*	T6	T7	T8
Load [kN]	5.00	3.00	4.00	4.50	3.50	6.00	3.75	4.25
Cycles	377972	2e6	1869836	952207	2e6	313831	1016966	1648296
Test	T9	T10	T11	T12	T13	T14	T15	
Load [kN]	6.50	5.00	5.50	4.00	4.80	4.20	5.20	
Cycles	284403	624729	590233	1025609	722932	1293027	724374	

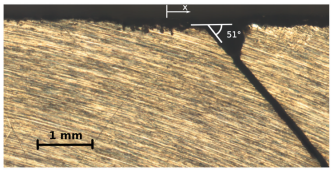

(a) Cracking direction for sample T6.

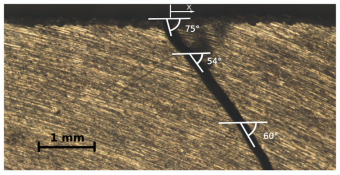

(b) Cracking direction for sample T9.

Fig. 9. Two typical cracking angles. Contact center and positive sliding direction is annotated by the arrow. The visible textures on the specimen sides are due to being machined flat.

failure is demonstrated by dotted lines and found in general to be 90–95% of overall specimen life.

Separating fretting fatigue crack initiation life from the overall fatigue life is in general an elusive problem. The definition of defect size for which the transition from initiation phase to growth phase is not unequivocally defined. Additionally, the relative importance of one phase over the other is in general not known. As noted by Navarro et al. [44], this transition may depend upon the fatigue criterion used, loading condition, material, geometry, etc. and cannot be known *a priori*. If the crack growth phase was to be significant, a modelling technique from *Linear-Elastic Fracture Mechanics* (LEFM) could be used to subtract the long crack growth regime. Here however, the fretting crack nucleation/initiation life is assumed to be 90% of overall specimen fatigue life. This is obviously a generalisation, but is perhaps somewhat justified by the recorded "fretting maps" (see Fig. 11). Also, previous researchers have reported initiation life in fretting fatigue of 85–95% [45–47].

4.1. Numerical post-processing

From the FE analysis, stresses and strains are extracted for a subset of 20,000 material points representing the specimen subsurface. By post-processing the FE results using the Findley critical plane parameter, the entire load history is conveniently transformed to a vector field representing fatigue damage. The length of each vector represents the fatigue damage in the material point and the angle represents the cracking direction. Fig. 12 demonstrates the subsurface fatigue damage for test cases T2 and T6 for two different values of COF. The hot-spot is marked with its cracking direction vector by an arrow. The figure clearly shows the steep gradients in the surface region, and highlights the edges of contact as being the critical areas. Generally, trailing edge ($x = 0.45$) of contact is found to be the hot-spot, as expected. The shapes of the critical areas at contact edges are elongated due to the slip interface changing throughout the loading cycle, thus "smearing" fatigue damage.

Findley fatigue damage parameter can also be plotted for single material points as a function of 3D material plane orientation (θ, ϕ), see Fig. 13. Here, the damage is calculated for a grid of 180x180 different material plane orientations for the hot-spot and critical point for load case T2. Due to the FE assumption of plane strain in the contact area, one only need to search through one dimension of angles. Note the symmetry of the damage parameter around $\theta = 90°$.

Negative values of the Findley parameter are due to small values for the resolved shear amplitude and with negative (compressive) normal stresses acting on the plane. Recall Eq. (4). Numerical simulations show that the Findley parameter is very sensitive to coefficient of friction for this geometry. Larger friction force gives higher shear stresses near the surface.

The experimental results is plotted with a set of numerical predictions in Fig. 14. The effect of increasing COF is unsurprising. Life predictions made without TCD are obviously over-conservative, however by using a critical distance found based on El Haddad [41],

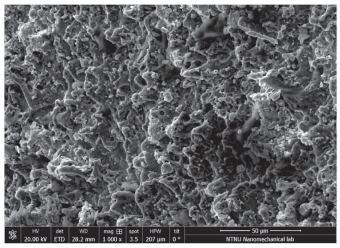

(a) EDM wired surface.

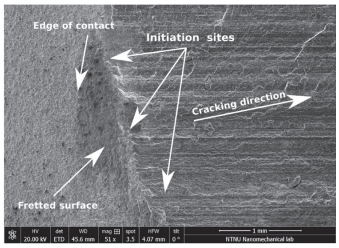

(b) Fretted surface meets crack surface

Fig. 10. Scanning electron microscope image of fractured surface.

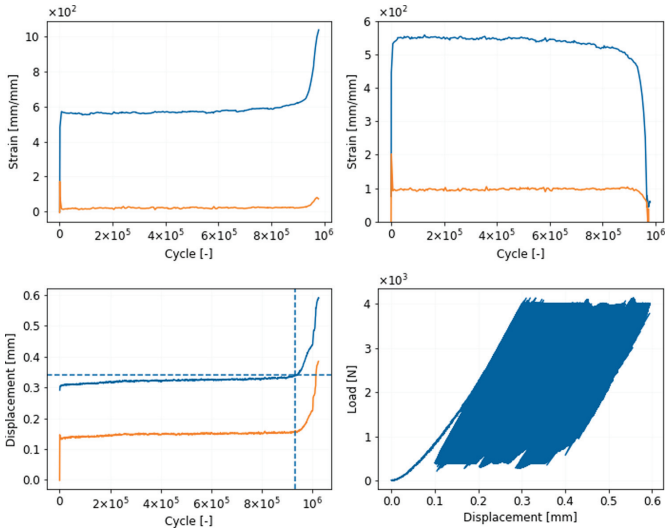

Fig. 11. *In-situ* monitoring specimen behaviour (test T12).

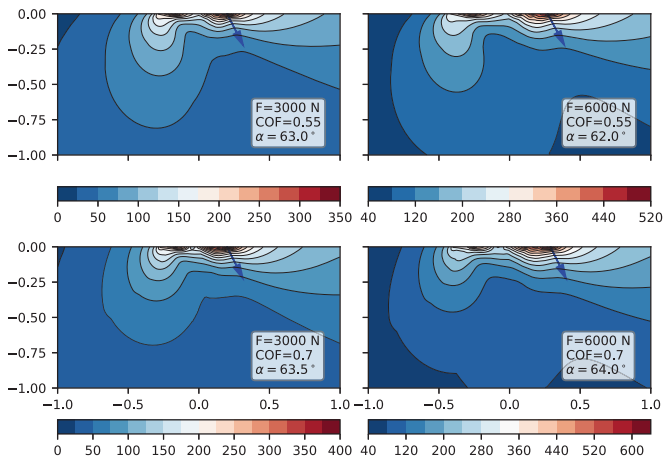

Fig. 12. Subsurface Findley damage parameter with hot-spot cracking direction indicated by arrow.

predictions are significantly improved. It is clear, however, that the slopes seen in the experimental results are different from the numerical predictions and so the inaccuracy increase as the loads are reduced. With respect to wear, this is slightly unexpected as wear often is thought to wipe out potential initiation sites, resulting in longer lives. The abrupt change in life prediction using the point method shows how evaluation of fatigue life at a single point is somewhat sensitive to spatial perturbations.

5. Discussion

The demonstrated test-rig is inspired by the classical dovetail fixture designs and its many descendants; however, it has a number of small additions which makes it capable of testing and comparing a wide range of fretting fatigue conditions. The width of the gripping mechanism permits specimens of different sizes to be tested. Additionally, the possibility of enclosing the lower gripping flange enable tests to be run in submerged conditions. In a multi-axial test machine with combined

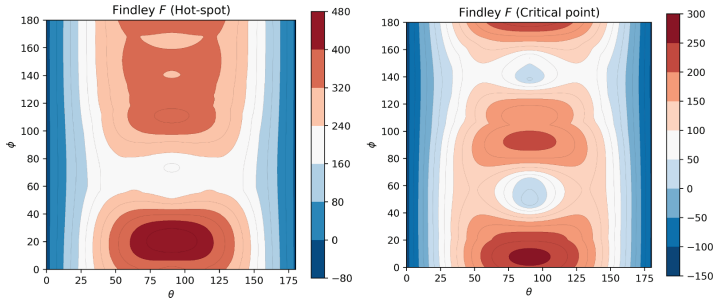

Fig. 13. Comparing candidate plane fatigue damage for the hot-spot (left) and at critical distance (right). Notice how the symmetries reveal the two-dimensional nature of the FE model.

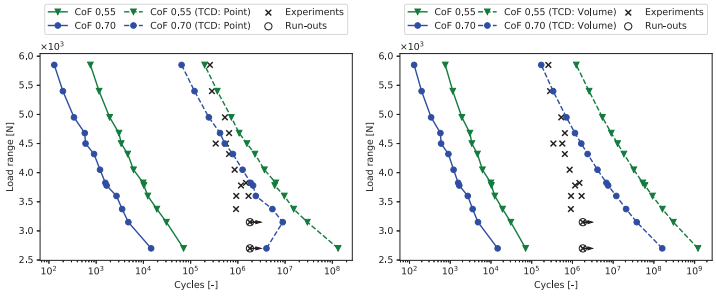

(a) Load-life using Point method. (b) Load-life using Volume method.

Fig. 14. Experimental results with numerical predictions using Findley criterion and TCD. Notice the "kink" in predicted life using the point method. This shows the potential instability when evaluating fatigue damage at a single point for very steep stress gradients.

tension-torsion actuators, additional excitation can be exerted on the specimens. In this study however, only single specimens were tested in dry conditions in room temperature.

A total of 15 EDM wired Ti-6Al-4V specimens were tested using the new rig resulting in fatigue failure initiated from the contact. To accompany the experimental data, numerical simulations were performed using finite element methods. Linear-elastic stress results were post-processed using Ruiz parameters and critical plane using the Findley criterion. In general, Ruiz provided insights into the critical areas, but failed to give meaningful life-predictions. The Findley criterion proved to be reasonable accurate in predicting crack angle and life when combined with the Theory of Critical Distances and length parameter based on LEFM.

Specimens were monitored during testing using strain gauges collecting large amounts of data. Post-processing the running data collection can potentially give valuable insights into fretting fatigue using appropriate data analysis.

The numerical model used to correlate life predictions with experimental results is evidently simplified. Like in many engineering applications, the analyses relied on bulk material properties, technical standards and assumptions made for contact friction. One potential next development step for the numerical model is to include wear analyses, but as noted by [29], the added computational cost is not always justified. Specimens in this test program were mostly in mixed regime between partial slip and gross slip. It is hypothesised that the inclusion of wear in the numerical model presented here will improve accuracy. Plasticity effects are not accounted for either, but was only observed in small, localized amounts related to the rough surfaces from the EDM wiring process. Work is initiated to add routines to handle plasticity and wear to the numerical model.

The new test rig demonstrated in this works has thus far only been used in its most simple configuration: Dry contact and uniaxially loaded specimens with cylindrical (Hertzian) contact pads. A planned advancement experimentally is to apply additional excitations to the specimens using the torsion actuators. Also of interest is to enclose the dovetail chamber and test specimens in submerged conditions. Changing the contact geometry to complete or rounded-flat will increase the resemblance with actual dovetail joints, increase contact stick and change the surface stress concentrations.

6. Conclusion

A combined experimental and numerical study has been conducted, using a new fretting fatigue test rig based on the classical dovetail joint. The main aim of this project is to initiate a new capacity for performing fretting fatigue experiments and associated numerical analysis. The project provides groundwork for future fretting fatigue test programs and parameter studies. The test setup has been demonstrated on a set of EDM-wired specimens in an engineering context, using bulk material properties and assumptions made for the coefficient of friction. The test

rig is concluded to be appropriate for detailed studies of fretting fatigue where material properties are of interest. This relies on explicit measurements of the system coefficient of friction and carefully controlled material properties and contact surfaces.

Declaration of Competing Interest

The authors declare that they have no known competing financial interests or personal relationships that could have appeared to influence the work reported in this paper.

Acknowledgements

xxx

References

[1] Araújo JA, Nowell D. The effect of rapidly varying contact stress fields on fretting fatigue. Int J Fatigue 2002;24(7):763–75. https://doi.org/10.1016/S0142-1123(01)00191-8. ISSN: 0142-1123. URL: http://www.sciencedirect.com/science/article/pii/S0142112301001918.

[2] Nowell D, Dini D, Hills DA. Recent developments in the understanding of fretting fatigue. Eng Fract Mech 2006;73(2):207–22. https://doi.org/10.1016/j.engfracmech. 2005.01.013. Advanced Fracture Mechaninc for Life Safety Assessments. ISSN: 0013-7944. URL: http://www.sciencedirect.com/science/article/pii/S0013794405001803.

[3] Lindley TC, Nix KJ. Fretting fatigue in the power generation industry: experiments, analysis, and integrity assessment. In: Standardization of fretting fatigue test methods and equipment. ASTM International; 1992. p. 153–17. doi: 10.1520/stp25828s.

[4] Ruiz C, Boddington PHB, Chen KC. An investigation of fatigue and fretting in a dovetail joint. Exp Mech 1984;24(3):208–17. https://doi.org/10.1007/BF02323167. ISSN: 1741-2765.

[5] Ciavarella M, Demelio G. A review of analytical aspects of fretting fatigue, with extension to damage parameters, and application to dovetail joints. Int J Solids Struct 2001;38(10):1791–811. https://doi.org/10.1016/S0020-7683(00)00136-0. ISSN: 0020-7683. URL: http://www.sciencedirect.com/science/article/pii/S0020768300001360.

[6] Conner BP, Nicholas T. Using a dovetail fixture to study fretting fatigue and fretting palliatives. J Eng Mater Technol 2006;128(2):133. https://doi.org/10.1115/1.2172272.

[7] Golden Patrick J. Development of a dovetail fretting fatigue fixture for turbine engine materials. Int J Fatigue 2009;31(4):620–8. https://doi.org/10.1016/j.ijfatigue.2008.03.017.

[8] Chen J-J, et al. Experimental and numerical investigation on crack initiation of fretting fatigue of dovetail. Fatigue Fract Eng Mater Struct 2018;41(6):1426–36. https://doi.org/10.1111/ffe.12787.

[9] Rajasekaran R, Nowell D. Fretting fatigue in dovetail blade roots: Experiment and analysis. Tribol Int 2006;39(10):1277–85. https://doi.org/10.1016/j.triboint.2006.02.044.

[10] Hills DA, Nowell D. What features are needed in a fretting fatigue test? In: Tribology International 42.9. Special Issue: Fifth International Symposium on Fretting Fatigue; 2009. p. 1316–23. https://doi.org/10.1016/j.triboint.2009.04.023. ISSN: 0301-679X. URL: http://www.sciencedirect.com/science/article/pii/S0301679X09000905.

[11] Hills DA, Nowell D. Mechanics of fretting fatigue-Oxford's contribution. Tribol Int 2014;76:1–5. https://doi.org/10.1016/j.triboint.2013.09.015.

[12] Kartal ME, et al. Determination of the frictional properties of titanium and nickel alloys using the digital image correlation method. Exp Mech 2010;51(3):359–71. https://doi.org/10.1007/sll340-010-9366-y.

[13] De Pauw J, et al. On the use of digital image correlation for slip measurement during coupon scale fretting fatigue experiments. Int J Solids Struct 2014;51(18):3058–66. https://doi.org/10.1016/j.ij solstr.2014.05.002.

[14] Juoksukangas J, Lehtovaara A, Mantyla A. Applying the digital image correlation method to fretting contact for slip measurement. Proc Inst Mech Eng Part J: J Eng Tribol 2016;231(4):509–19. https://doi.org/10.1177/1350650115601695.

[15] Kyvia Pereira et al. On the convergence of stresses in fretting fatigue. In: Materials 9.8; July 2016. p. 639. DOI: 10.3390/ma9080639.

[16] Fouvry S, Duo P, Perruchaut Ph. A quantitative approach of Ti-6A1-4V fretting damage: friction, wear and crack nucleation. Wear 2004;257(9–10):916–29. https://doi.org/10.1016/j.wear.2004.05.011.

[17] Suh Nam P, Sin H-C. The genesis of friction. In: Wear 69.1; June 1981. p. 91–114. DOI: 10.1016/0043-1648(81)90315-x.

[18] Yue Tongyan, Wahab Magd Abdel. Finite element analysis of fretting wear under variable coefficient of friction and different contact regimes. Tribol Int 2017;107:274–82. https://doi.org/10.1016/j.triboint.2016.11.044.

[19] Sunde Steffen Loen, Berto Filippo, Haugen Bjorn. Efficient implementation of critical plane for 3D stress histories using triangular elements. Int J Fatigue 2020;134:105448. https://doi.org/10.1016/j.ijfatigue.2019.10544.

[20] Mindlin RD. Compliance of Elastic Bodies in Contact. J Appl Mech ASME 1949;16:259–68.

[21] Ciavarella M. Transition from stick to slip in Hertzian contact with Griffith friction: The Cattaneo-Mindlin problem revisited. J Mech Phys Solids 2015;84:313–24. https://doi.org/10.1016/j.jmps.2015.08.002.

[22] Lykins Christopher D, Mall Shankar, Jain Vinod. An evaluation of parameters for predicting fretting fatigue crack initiation. Int J Fatigue 2000;22(8):703–16. https://doi.org/10.1016/S0142-1123(00)00036-0. ISSN: 0142-1123. URL: http://www.sciencedirect.com/science/article/pii/S0142112300000360.

[23] Ziaei M. Analytical study of noncircular profile families andnumerical optimization of standardised polygon profiles for shaft-hub connections. Professorial Dissertation; 2002.

[24] Ding J, Leen SB, McColl IR. The effect of slip regime on fretting wear-induced stress evolution. Int J Fatigue 2004;26(5):521–31. https://doi.org/10.1016/j.ijfatigue.2003.09.001. ISSN: 0142-1123. URL: http://www.sciencedirect.com/science/article/pii/S0142112303002032.

[25] Vidner J, Leidich E. Enhanced Ruiz criterion for the evaluation of crack initiation in contact subjected to fretting fatigue. Int J Fatigue 2007;29(9-11):2040–9. https://doi.org/10.1016/j.ij fatigue.2007.02.010.

[26] Sunde SL, Berto F, Haugen B. Predicting fretting fatigue in engineering design. Int J Fatigue 2018;117:314–26. https://doi.org/10.1016/j.ijf atigue.2018.08.028.

[27] Strozzi A, et al. A repertoire of failures in connecting rods for internal combustion engines, and indications on traditional and advanced design methods. Eng Fail Anal 2016;60:20–39. https://doi.org/10.1016/j.engf ailanal. 2015.11.034.

[28] Ding J, et al. Simple parameters to predict effect of surface damage on fretting fatigue. Int J Fatigue 2011;33(3):332–42. https://doi.org/10.1016/j.ijf atigue. 2010. 09. 008.

[29] Araujo JA, et al. Life prediction in multiaxial high cycle fretting fatigue. Int J Fatigue 2020;134:105504. https://doi.org/10.1016/j.ij fatigue.2020.105504.

[30] Nowell D, Hills DA. Crack initiation criteria in fretting fatigue. Wear 1990;136(2):329–43. https://doi.org/10.1016/0043-1648(90) 90155-4.

[31] Fouvry Siegfried, Kapsa Philippe, Vincent Leo. Quantification of fretting damage. Wear 1996;200(1–2):186–205. https://doi.org/10.1016/s0043-1648(96)07306-l.

[32] Vantadori Sabrina, et al. Early fretting crack orientation by using the critical plane approach. Int J Fatigue 2018;114:282–8. https://doi.org/10.1016/j.ijfatigue.2018.04.015.

[33] Sum WS, Williams E, Leen S. Finite element, critical-plane, fatigue life prediction of simple and complex contact configurations. Int J Fatigue 2005;27(4):403–16. https://doi.org/10.1016/j.ijfatigue.2004.08.001.

[34] Nicholas Findley W. A theory for the effect of mean stress on fatigue of metals under combined torsion and axial load or bending. Engineering Materials Research Laboratory, Division of Engineering, Brown University; 1958.

[35] Socie Darell F, Marquis Gary B. Multiaxial fatigue. SAE International: Marquis. Multiaxial fatigue; 2000. ISBN: 9780768004533.

[36] Kallmeyer Alan R, Krgo Ahmo, Kurath Peter. Evaluation of multiaxial fatigue life prediction methodologies for Ti-6A1-4V. J Eng Mater Technol 2002;124(2):229–37. https://doi.org/10.1115/1.1446075.

[37] Papadopoulos IV. Critical plane approaches in high-cycle fatigue: on the definition of the amplitude and mean value of the shear stress acting on the critical plane. Fatigue Fract Eng Mater Struct 1998;21(3):269–85. https://doi.org/10.1046/j.1460-2695.1998.00459.x.

[38] Araujo JA, et al. On the characterization of the critical plane with a simple and fast alternative measure of the shear stress amplitude in multiaxial fatigue. Int J Fatigue 2011;33(8):1092–100. https://doi.org/10.1016/j.ijfatigue.2011.01.002. Multiaxial Fatigue Models, . ISSN: 0142-1123. URL: http://www.sciencedirect.com/science/article/pii/S0142112311000041.

[39] Park J. Evaluation of an energy-based approach and a critical plane approach for predicting constant amplitude multiaxial fatigue life. Int J Fatigue 2000;22(1):23–39. https://doi.org/10.1016/s0142-1123(99)00111-5.

[40] Susmel Luca, Taylor David. Non-propagating cracks and high-cycle fatigue failures in sharply notched specimens under in-phase Mode I and II loading. Eng Fail Anal 2007;14(5):861–76. https://doi.org/10.1016/j.engfailanal.2006.11.038.

[41] El Haddad MH, Smith KN, Topper TH. Fatigue crack propagation of short cracks. J Eng Mater Technol 1979;101(1):42. https://doi.org/10.1115/1.3443647.

[42] Taylor D. Geometrical effects in fatigue: a unifying theoretical model. Int J Fatigue 1999;21(5):413–20. https://doi.org/10.1016/s0142-1123(99)00007-9.

[43] Dowling Norman E. Mechanical behaviour of materials. Pearson Education Limited; 2013.

[44] Navarro C, Muñoz S, Dominguez J. On the use of multiaxial fatigue criteria for fretting fatigue life assessment. Int J Fatigue 2008;30(1):32–44. https://doi.org/10.1016/j.ijfatigue.2007.02.018.

[45] Szolwinski Matthew P, Farris Thomas N. Mechanics of fretting fatigue crack formation. Wear 1996;198(1–2):93–107. https://doi.org/10.1016/0043-1648(96)06937-2.

[46] Lykins C. Combined experimental-numerical investigation of fretting fatigue crack initiation. Int J Fatigue 2001;23(8):703–11. https://doi.org/10.1016/s0142-1123(01)00029-9.

[47] Shi Liang, et al. An investigation of fretting fatigue in a circular arc dovetail assembly. Int J Fatigue 2016;82:226–37. https://doi.org/10.1016/j.ijfatigue.2015.07.025.

Some very simple code snippets are included here to demonstrate the application of three different languages used in this thesis, see Section 2.8. Since the code given in these appendices are included for demonstration purposes, they are not necessarily optimised and tested with full coverage.

Convex Hull

The Convex hull is a central algorithm used in this project to calculate the equivalent shear stress amplitude in the candidate critical plane (See Section 2.7). In this section, a simple implementation in C++ is shown. It calculate the two-dimensional convex hull using only standard features.

```
#include <vector>
#include <iostream>
#include <optional>
#include <cassert>
#include <execution>

struct Point {
    double x;
    double y;

    constexpr bool operator==(Point const& rhs)
    {
        return (std::abs(x-rhs.x) < 1e-12) && (std::abs(y-rhs.y) < 1e-12);
    };
};

enum class Turn {
    CW,     // Clockwise
    CCW     // Counter-clockwise
};

/// Determines the orientation of three concecutive points.
/// Returns None for co-linear points.
constexpr auto orientation(
    Point const& a,
    Point const& b,
    Point const& c,
    double const& eps=1e-6)
-> std::optional<Turn>
{
    double cross_product = (b.x - a.x)*(c.y - b.y)
                         -(b.y - a.y)*(c.x - b.x);
    if (cross_product < -eps) {
        return Turn::CW;
    } else if (cross_product > eps) {
        return Turn::CCW;
    }
    return std::nullopt;
}

/// Sorts the list of points first in x and then in y.
auto lexicographical_sort(
    std::vector<Point> points)
-> std::vector<Point>
{
```

```
    constexpr auto lexicographical_order = [](
        Point const& a, Point const& b) -> bool {
        if (a.x < b.x) {
            return true;
        } else if (a.x > b.x) {
            return false;
        }
        return (a.y < b.y);
    };

    // Remove execution policy if compile problems
    std::sort(std::execution::par_unseq, points.begin(), points.end(),
lexicographical_order);
    return points;
}

/// Computes the convex hull using Graham Scan algorithm.
/// Time complexity O(nlogn) due to the sorting step.
auto convex_hull(
    std::vector<Point> points)
-> std::vector<Point>
{
    size_t num_points = points.size();
    if (num_points < 2) return points;
    points = lexicographical_sort(points);

    std::vector<Point> upper{points[0], points[1]};
    upper.reserve(num_points);
    for (size_t i = 2; i < num_points; ++i) {
        size_t pos = 0;
        while (upper.size() - pos >= 2) {
            size_t length = upper.size();
            auto turn = orientation(upper[length-pos-2],
                                    upper[length-pos-1],
                                    points[i]);
            if (turn && turn.value() == Turn::CW) {
                pos++;
            } else {
                upper.erase(upper.end()-pos-1);
            }
        }
        upper.push_back(points[i]);
    }

    std::vector<Point> lower{points[num_points-1], points[num_points-2]};
    lower.reserve(num_points);
    for (size_t i = num_points-3; i-- > 0; ) {
        size_t pos = 0;
        while (lower.size() - pos >= 2) {
            size_t length = lower.size();
            auto turn = orientation(lower[length-pos-2],
                                    lower[length-pos-1],
                                    points[i]);
            if(turn && turn.value() == Turn::CW) {
```

```
                pos++;
            } else {
                lower.erase(lower.end()-pos-1);
            }
        }
        lower.push_back(points[i]);
    }

    if (lower.size() > 2) {
        upper.insert(upper.end(), lower.begin()+1, lower.end()-1);
    }

    return upper;
}

int main()
{
    // Simple test case
    std::vector<Point> const input = {
        {3,6}, {5,2}, {4,4}, {2,3}, {1,1},
        {4,3}, {3,4}, {0,5}, {3,5}, {4,1}
    };

    std::vector<Point> const correct = {
        {0,5}, {3,6}, {5,2}, {4,1}, {1,1}
    };

    std::vector<Point> answer = convex_hull(input);
    assert(answer.size() == correct.size());
    for(size_t i = 0; i < correct.size(); ++i) {
        assert(answer[i] == correct[i]);
    }
    return 0;
}
```

Convex hull

A simple demonstrator showing the use of pure Python to compute the convex hull.

In [1]:

```
from typing import List, Tuple
```

In [2]:

```
def convex_hull(points: List[Tuple[float, float]]) -> List[Tuple[float, float]]:
    num_points = len(points)
    points = sorted(points)
    if num_points < 3:
        return points

    is_clockwise = lambda a, b, c: (b[0] - a[0])*(c[1] - b[1]) \
                                 - (b[1] - a[1])*(c[0] - b[0]) < 0
    def traverse(points, direction="forward"):
        if direction == "backward":
            indices = iter(range(len(points)-1, -1, -1))
        else:
            indices = iter(range(0, len(points)))

        hull = [points[next(indices)], points[next(indices)]]
        for i in indices:
            pos = 0
            while len(hull) - pos >= 2:
                if is_clockwise(hull[-pos-2], hull[-pos-1], points[i]):
                    pos += 1
                else:
                    del hull[-pos-1]
            hull.append(points[i])
        return hull

    upper_hull = traverse(points)
    lower_hull = traverse(points, "backward")

    return upper_hull + lower_hull[1:len(lower_hull)-1]
```

Visual example

In [3]:

```
from random import uniform
import matplotlib.pyplot as plt
```

In [4]:

```
test_points = [(uniform(-1, 1), uniform(-1, 1)) for _ in range(100)]
ch = convex_hull(test_points)
ch.append(ch[0])  # Make hull close on itself
```

In [5]:

```
fig, ax = plt.subplots()
ax.scatter(*zip(*test_points), label="Points")
ax.plot(*zip(*ch), label="Convex Hull")
plt.show()
```

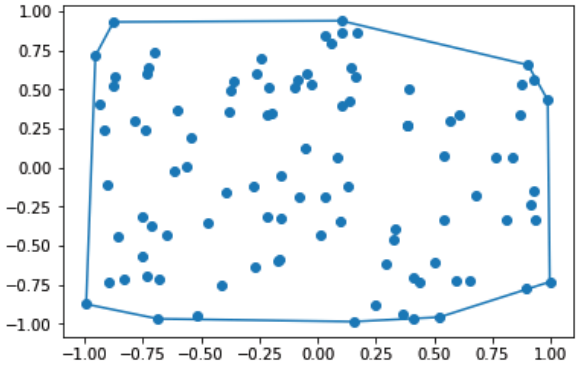

Convex hull in Rust

Rust is a young language compared with C/C++ and Python and is growing in popularity in software development but also in numerical and scientific computing. In this thesis, Rust was used e.g. to calculate the convex hull, see Section 2.7.4. Here, the Graham Scan algorithm for calculating the convex hull is shown. The algorithm is implemented for natural numbers to avoid rounding errors, NaNs etc.

```
#[derive(Debug, PartialEq, Eq, PartialOrd, Ord, Clone, Copy)]
pub struct Point {
    x: i32,
    y: i32
}
```

Here the compiler is told to automatically implement traits derived using the #[derive] attribute.

- Deriving Debug let's us easily print the struct through {:?} formatter
- Deriving PartialEq and Eq makes the type comparable by eqivalence
- PartialOrd makes our type ordered so that it can be sorted
- Ord: All struct fields are Ord. struct becomes lexicographically ordered
- Clone is required for struct to be Copy.
- Copy because all fields are trivially and inexpensively copyable.

Finally, the Point struct is made public as is needed by the caller of the convex hull function.

```
println!("{:?}", Point{x: 10, y: 20});
```

```
Point { x: 10, y: 20 }
```

Construction of objects are usually preferred in rust using the builder-pattern, and naming a zero cost constructor using function named new().

```
impl Point {
    fn new(x: i32, y: i32) -> Self {
        Self {x, y}
    }
}
```

Graham Scan

The idea of the algorithm is to traverse the sorted list of points and simply discarding the points that does not form a **right turn**. The points are first sorted lexicographically and are then traversed twice; once left

to right for forming the upper part of the hull and once right to left for the lower part. The two parts are then combined so that the points of the convex hull are given uniquely starting from the lexicographically lowest point and following the hull in counter-clockwise fashion.

```
#[derive(Debug)]
enum Turn {
    CW,   // Clockwise
    CCW,  // Counter-clockwise
}
```

```
/// Returns the orientation of three consecutive points in the 2D plane.
fn orientation(a: &Point, b: &Point, c: &Point) -> Option<Turn> {
    let crossprod = (b.x - a.x)*(c.y - b.y) - (b.y - a.y)*(c.x - b.x);
    if crossprod < 0 {
        Some(Turn::CW)
    } else if crossprod > 0 {
        Some(Turn::CCW)
    } else {
        None
    }
}
```

```
println!("{:?}", orientation(&Point{x: 0, y: 0}, &Point{x: 1, y: 0},
&Point{x: 1, y: 1}));
println!("{:?}", orientation(&Point{x: 0, y: 0}, &Point{x: 0, y: 1},
&Point{x: 1, y: 1}));
println!("{:?}", orientation(&Point{x: 0, y: 0}, &Point{x: 1, y: 1},
&Point{x: 2, y: 2}));
```

```
Some(CCW)
Some(CW)
None
```

The sorted points are traversed twice, once from each end. We can therefore abstract over the traversing algorithm and for this, the very useful `Either<L, R>` sum type is used from the external crate `either`. We also use a simple sum type `Direction` to denote the direction of traversion.

```
:dep either
use either::Either;
```

```
```

```
enum Direction {
    Forward,
    Backward
}
```

```
fn traverse(points: &[Point], dir: Direction) -> Vec<Point> {
    let iterator = match dir {
          Direction::Forward => Either::Left(points.iter()),
          Direction::Backward => Either::Right(points.iter().rev()),
    };

    let mut hull = Vec::new();
    iterator.for_each(|p| {
        let mut pos = 0;
        loop {
            let len = hull.len();
            if pos + 2 > len {
                break;
            }

            match orientation(&hull[len-pos-2], &hull[len-pos-1], &p){
                Some(Turn::CW) => pos += 1,
                _ => { hull.remove(len-pos-1); }
            }
        }
        hull.push(*p);
    });

    hull
}
```

Finally, the public function `convex_hull`.

```
/// Calculates the convex hull usin Graham Scan algorithm
pub fn convex_hull(points: &[Point]) -> Vec<Point> {
    let mut points = points.to_vec();
    points.sort();

    return if points.len() > 2 {
        let upper = traverse(&points, Direction::Forward);
        let lower = traverse(&points, Direction::Backward);
        [&upper[..], &lower[1..lower.len() - 1]].concat()
    } else {
        points
    }
}
```

Small test case

```
let points =vec![
    Point::new(3, 6),
    Point::new(5, 2),
    Point::new(4, 4),
    Point::new(2, 3),
    Point::new(1, 1),
    Point::new(4, 3),
    Point::new(3, 4),
    Point::new(0, 5),
    Point::new(3, 5),
    Point::new(4, 1)
];

println!("{:?}", convex_hull(&points));
```

```
[Point { x: 0, y: 5 }, Point { x: 3, y: 6 }, Point { x: 5, y: 2 }, Point {
x: 4, y: 1 }, Point { x: 1, y: 1 }]
```

Minimum circumscribed circle

A standard form of quadratic programming (QP) is

$$\begin{aligned} \min_{x} \quad & \frac{1}{2} x^T P x + q^T x \\ \text{s.t.} \quad & Gx \leq h \\ & Ax = b \end{aligned}$$

where x is a vector of (real) *variables*, G is an $m \times n$ matrix of constraints, h is a vector of coefficients, P is a symmetrix positive-semidefinite $n \times n$ matrix representing the quadratic objective function. G is a matrix representing the inequality constraints and A represents the equality constraints.

The minimum circumscribed circle

The minimum circumscribed circle (MCC) of a given set of n 2D points is the smallest circle to cover all points in each dimension (x and y)

$$\min_{x,y} \quad \max_{i} \{(x - u_i)^2 + (y - v_i)^2\}$$

Where u_i and v_i are the x and y components of the point i respectively. This can be rewritten as

$$\begin{aligned} \min_{x,y,z} \quad & x^2 + y^2 + z^2 \\ \text{s.t.} \quad & z \geq 2xu_i + 2yv_i + z \geq u_i^2 + v_i^2, \quad i = 1..n \end{aligned}$$

this is a convex quadratic programming (QP) problem with one linear constraint for each point (n). This is a well-studied problem in optimisation and can readily be solved using pre-existing solvers.

In the following, equation is solved using open-source python library *cvxopt*.

[1]:
```
# Import dependencies
from cvxopt import matrix, solvers
import numpy as np
from math import sqrt
import matplotlib.pyplot as plt
```

[2]:
```
# Define function to compute MCC using QP
def mcc_qp(points):
    """Computes the smallest circle completely enclosing the given list of 2D␣
 ↪points.

    Parameters
    ----------
    points : List of 2-dimensional points (x, y)

    Returns
    ----------
    center : Coordinates (x, y) for the circle center
```

```
    radius : Radius of circle

    """
    G = []
    h = []
    for p in points:
        G.append([-2*p[0], -2*p[1], -1.0])
        h.append(-p[0]**2 - p[1]**2)
    G = matrix(np.array(G), tc='d')
    h = matrix(np.array(h), tc='d')
    q = matrix(np.array([0,0,1]), tc='d')
    P = matrix(np.array([[1,0,0], [0,1,0], [0,0,0]]), tc='d')

    sol = solvers.qp(P, q, G, h)
    return (sol['x'][0], sol['x'][1]), sqrt(sol['x'][2])
```

[3]:
```
# Simple test-case
test_points = [(0, 0), (2, 3), (1,-4), (2,-2), (1,1), (-1, 3), (-4,2)]
center, radius = mcc_qp(test_points)
```

```
     pcost       dcost       gap    pres   dres
 0:  1.0737e+01  2.7930e+02  4e+02  7e-01  1e+02
 1:  1.9286e+01  1.2441e+01  7e+00  6e-03  8e-01
 2:  1.6776e+01  1.6412e+01  4e-01  2e-16  1e-15
 3:  1.6613e+01  1.6609e+01  4e-03  0e+00  9e-16
 4:  1.6611e+01  1.6611e+01  4e-05  2e-16  9e-16
 5:  1.6611e+01  1.6611e+01  4e-07  0e+00  2e-15
Optimal solution found.
```

[4]:
```
# Visualise the result for test-case
fig, ax = plt.subplots()
plt.scatter(*zip(*test_points))
circle = plt.Circle(center, radius, fill=False)
ax.add_artist(circle)
ax.set_aspect("equal", adjustable="box")
ax.set_xlim((-5, 5))
ax.set_ylim((-5, 5))
ax.grid()
plt.show()
```

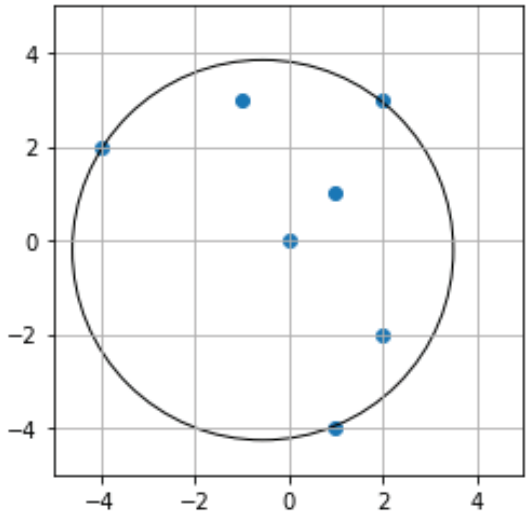
4
2
0
−2
−4
−4
−2
0
2
4

A.9 Fourth order Runge-Kutta

The classical fourth order Runge-Kutta scheme was used to integrate the friction systems in Section 4. This scheme can be written as

$$y_{n+1} = y_n + \frac{h}{6}\left(k_1 + 2k_2 + 2k_3 + k_4\right) \tag{A.1}$$

where the four slopes $k_{1..4}$ is defined by

$$k_1 = f\left(t_n, y_n\right) \tag{A.2}$$

$$k_2 = f\left(t_n + \frac{h}{2}, y_n + \frac{h}{2}k_1\right) \tag{A.3}$$

$$k_3 = f\left(t_n + \frac{h}{2}, y_n + \frac{h}{2}k_2\right) \tag{A.4}$$

$$k_4 = f\left(t_n + h, y_n + hk_3\right) \tag{A.5}$$

or by its Butcher tableau [147]

0				
1/2	1/2			
1/2	0	1/2		
1	0	0	1	
	1/6	1/3	1/3	1/6

ISBN 978-82-326-6612-6 (printed ver.)
ISBN 978-82-326-5195-5 (electronic ver.)
ISSN 1503-8181 (printed ver.)
ISSN 2703-8084 (online ver.)

NTNU

Norwegian University of
Science and Technology